UNIVERSITY OF SOUTHAMPTON

FACULTY OF NATURAL AND ENVIRONMENTAL SCIENCE

Ocean and Earth Science

Volume 1 of 1

BIOAVAILABILITY OF NITROGEN, PHOSPHORUS, IRON AND COBALT TO SURFACE WATER PLANKTONIC MICROBES IN THE LOW LATITUDE ATLANTIC OCEAN

by

Catherine Louise Burd

Thesis for the degree of Doctor of Philosophy

March_2018

UNIVERSITY OF SOUTHAMPTON

ABSTRACT

FACULTY OF NATURAL AND ENVIRONMENTAL SCIENCE

Ocean and Earth Science

Thesis for the degree of Doctor of Philosophy

BIOAVAILABILITY OF NITROGEN, PHOSPHORUS, IRON AND COBALT TO SURFACE WATER PLANKTONIC MICROBES IN THE LOW LATITUDE ATLANTIC OCEAN

by Catherine Louise Burd

The effects on bacterioplankton of very low concentrations of nitrogen and phosphorus/iron in the Atlantic were investigated using shipboard enrichment experiments. In the North Atlantic gyre, bacterioplankton abundance and amino acid uptake increased upon combined addition of ammonium and phosphate (9-42% and 120-880% increase, respectively). Outside the gyre, the requirement for phosphate additions was reduced. In the South Atlantic, ammonium additions generally caused an increase in bacterioplankton abundance (10-32% after 48 h) and amino acid uptake (20-300%), particularly in the gyre centre. Conversely, iron additions showed a negligible response. These results contribute towards understanding the effect of low nutrient concentrations on bacterioplankton. Reduced abundance or metabolic activity of bacterioplankton due to low nutrient concentrations may impact marine primary production and carbon fluxes, which is a particular concern due to the expansion of oligotrophic gyres as a result of climate change.

Iron and cobalt are essential micronutrients that are susceptible to forming particulate/insoluble species (e.g. via adsorption, oxidation, precipitation). These species can be lost from the surface ocean, thus reducing nutrient bioavailability. Therefore, mechanisms affecting their formation were also investigated. Cell surface iron adsorption was measured in the South Atlantic, with highest levels occurring in the gyre (~180-300 zmol Fe/cell, verses ~3-155 zmol Fe/cell in productive waters). This was hypothesised to be due to low ambient iron in the gyre, resulting in a larger free cell surface area for iron binding. Particulate cobalt formation was enhanced (>150%) in the presence of *Aurantimonas* (a manganese-oxidising bacteria), was generally elevated under higher manganese concentrations (e.g. ~13-60% increase upon adding $MnCl_2$ to manganese-poor cultures), but was slightly reduced in the presence of nickel (6.2±7.4% decrease) or copper (7.4±12.2% decrease). These results further understanding of factors influencing micronutrient speciation, which is especially important considering potential changes to ocean biogeochemistry as a result of anthropogenic activity.

Table of contents

List of tables

List of figures

DECLARATION OF AUTHORSHIP

I, Catherine Burd declare that this thesis and the work presented in it are my own and has been generated by me as the result of my own original research.

Title of thesis: Bioavailability of nitrogen, phosphorus, iron and cobalt to surface water planktonic microbes in the low latitude Atlantic Ocean.

I confirm that:

1. This work was done wholly or mainly while in candidature for a research degree at this University;
2. Where any part of this thesis has previously been submitted for a degree or any other qualification at this University or any other institution, this has been clearly stated;
3. Where I have consulted the published work of others, this is always clearly attributed;
4. Where I have quoted from the work of others, the source is always given. With the exception of such quotations, this thesis is entirely my own work;
5. I have acknowledged all main sources of help;
6. Where the thesis is based on work done by myself jointly with others, I have made clear exactly what was done by others and what I have contributed myself;
7. None of this work has been published before submission.

Signed: .....

Date: .....

Acknowledgements

Firstly, I would like to thank my supervisors Mike Zubkov and Eric Achterberg for this opportunity and for all the help they have provided. I would also like to thank my co-supervisors Phil Warwick and Ivo Tews. This project was funded by the Natural Environment Research Council (grant code: NE/K500938/1).

I would also like to thank all the officers and crew of the R.S.S. James Clark Ross, as well as NMFSS (especially Richie, Candice, Nick and John), and all the scientists of the AMT-24 and AMT-25 cruises. Additionally, I would like to thank Insa Rapp and Christian Schlosser for help with iron measurements. And of course, not forgetting Pri, Moritz and Sara!

A special thank you is extended to Manuela Hartmann who was always there to provide advice and support, no matter how small the problem!

And finally, a huge thanks to all my friends and family who supported me throughout the project, including all my office mates, housemates and netball team!

The first sight of land after weeks at sea! Falkland Islands, November 2014

Definitions and abbreviations

Abbreviations

AASW	aged Atlantic seawater
AMT	Atlantic Meridional Transect cruise programme
AMT-24	the 24th AMT cruise
AMT-25	the 25th AMT cruise
ASW	artificial seawater
ATP	adenosine triphosphate
Aur	*Aurantimonas* sp. (ATCC BAA-1229)
CPM	counts per minute
DIN	dissolved inorganic nitrogen
DIP	dissolved inorganic phosphorus
DOC	dissolved organic carbon
DOM	dissolved organic matter
DON	dissolved organic nitrogen
DOP	dissolved organic phosphorus
EDTA	ethylenediaminetetraacetate
FL1-3	fluorescent filters 530±15 nm (FL1), 585±21 nm (FL2) and >650 nm (FL3)
GAU	Geosciences Advisory Unit

Halo	*Halomonas*
HDPE	high density polyethylene
HNA	high nucleic acid
HNLC	High Nitrate/Nutrient Low Chlorophyll
JCR	R.R.S. James Clark Ross
L-HNA	large group of HNA bacteria
Leu	leucine
LDPE	low density polyethylene
LNA	low nucleic acid
LSC	liquid scintillation counter
Met	methionine
MnOx	manganese oxide, oxyhydroxide and hydroxide complexes
NAG	North Atlantic subtropical gyre
NMFSS	National Marine Facilities Sea Systems
NOCS	National Oceanography Centre Southampton
PC	polycarbonate
PFA	paraformaldehyde
PP	polypropylene
POM	particulate organic matter
PON	particulate organic nitrogen
POP	particulate organic phosphorus

PSU	practical salinity unit
PTFE	polytetrafluoroethylene
SAG	South Atlantic subtropical gyre
SML	surface mixed layer
SSC	side scatter
$TiCl_3$ buffer	Titanium(III), citrate, and EDTA buffer (Hudson and Morel, 1989)

Definitions

Bacterioplankton	The bacterial component of the plankton community
Diazotroph	Microorganisms capable of N_2 fixation
Macronutrient	Nutrients required by cells in large amounts (e.g. N, P)
Micronutrient	Nutrients required by cells in trace amounts (e.g. Fe, Co)
Oligotrophic	Environment featuring low nutrient concentrations
Particulate cobalt	Includes insoluble and particulate cobalt, formed either abiotically or biotically (e.g. via sorption, assimilation, oxidation, precipitation)
Phytoplankton	Photosynthetic plankton (including cyanobacteria and eukaryotes)
Plankton	Free-floating oceanic microorganisms
Zooplankton	Larger heterotrophic plankton and tiny animals (e.g. larvae)

Chapter 1: Introduction

The microorganisms of the surface ocean are essential to the global ecosystem, with photosynthetic plankton (phytoplankton) contributing to approximately half of global photosynthesis [1], and bacterial plankton (bacterioplankton) being heavily involved in the cycling of nutrients and organic matter [2,3]. In order to maintain growth and metabolism, plankton require a range of nutrients; however, large areas of the ocean (including the subtropical gyres) are oligotrophic, and consequently feature low productivity [4]. Therefore, this thesis aimed to examine the bioavailability of essential nutrients to bacterioplankton, with a view to increase understanding of the marine ecosystem, which influences global productivity and carbon fluxes.

The first part of this chapter provides background information and literature reviews, giving context to the project. The biological structure and processes of the surface ocean are initially introduced, highlighting the basic cycling of organic matter. The vertical structure of the upper ocean is then introduced, as it dictates the environment that the surface ocean plankton inhabit, including the vertical structure of the water column, and the formation of oligotrophic subtropical gyres, which are a key focus of this thesis. Due to their essential requirement for plankton growth, essential nutrients (i.e. nitrogen, phosphorus, iron, cobalt) in the surface ocean are then discussed, with reference to marine cycling and microbial bioavailability. Following on from this, nutrient limitation is discussed, with specific reference to the microorganisms that have adapted to survival in the oligotrophic subtropical gyres, and to which this thesis is orientated. Finally, the layout and specific aims of the project are presented.

1.1 The microbial loop

Organic matter

Plankton dominate the global oceans [2] and are the base of a balanced and complex ecosystem. Intrinsically linked to plankton is the dissolved organic matter (DOM) pool, which includes viruses, macromolecules, and colloidal gels [5]. The term DOM encompasses organic nutrients such as dissolved organic carbon, nitrogen and phosphorus (DOC, DON and DOP, respectively), with DOC acting as a major organic carbon source [6,7]. Labile DOM is readily available for biological assimilation and is key to the microbial loop [6-8]. It has a very short turnover time (hours - days), and does not accumulate in the water column [6-8]. Conversely, recalcitrant DOM is more resistant to biological degradation and is able to accumulate in the oceans [8]. Consequently, this can lead to the sinking of DOC to the deep ocean, thus contributing to the biological carbon pump [8]. Recalcitrant DOM has varying degrees of reactivity, with turnover times ranging from months (semi-labile DOM, more prevalent in the upper oceans) to thousands of years (refractory DOM, found equally throughout the water column) [6-8]. The biological conversion of labile DOC to recalcitrant DOC (e.g. release of macromolecules via viral lysis) is known as the microbial carbon pump [9].

Typically, organic material larger than 0.7 μm is classified as particulate organic matter (POM) [6], and includes both living plankton and cell detritus [6]. POM can be lost from the surface ocean through sinking (as part of the biological pump), and contributes to deep water sequestration of carbon [6].

The microbial loop

The interaction of organic matter and plankton is termed the 'microbial loop' (Figure 1.1) [10,11] and is a major influence on global carbon flux and primary production. Phytoplankton

(including picoeukaryotes and cyanobacteria) fix inorganic carbon in the surface ocean via photosynthesis, with approximately half of global net primary production occurring in the oceans [1]. This fixation makes organic matter (DOM and POM) available to other marine organisms via grazing (e.g. protists, zooplankton), excretion and shedding of small molecules, and cell death (e.g. viral lysis) [2,3,5,12, and references therein]. All plankton are capable of production of organic matter through cell death and excretion [2,3]. The released organic matter is primarily assimilated by bacterioplankton [2]. These cells dominate the surface oceans both in their abundance and contribution to biomass [2]; for example, Campbell *et al* (1994) noted that ≥80% of microbial biomass in the North Pacific was bacterial [13]. Bacterioplankton are also responsible for mineralization of organic nutrients back to an inorganic form for re-use by phytoplankton [3].

Archaea

Archaea, the third taxonomic domain (the other two being bacteria and eukaryotes), are also part of the oceanic microbial loop (Figure 1.1). They are prokaryotic and have distinct cell membrane ether lipids [2] that are more resistant to degradation than bacteria [14]. Until fairly recently, archaea were thought to only occupy extreme environmental niches (e.g. deep sea hydrothermal vents) [15,16]; however, through analysis of nucleic acid, DeLong (1992) noted the presence of marine archaea in coastal surface waters and Fuhrman *et al* (1992) reported them in the upper 500 m of the Pacific Ocean [14-17]. Archaea are now known to inhabit a significant portion of the marine environment [2,16], particularly in the deep ocean [2]. They are involved in the cycling of organic matter [5], with many also being capable of chemolithotrophy (e.g. fixation of CO_2 via ammonium oxidation) [2,14,18]. However, the distinction of archaea from bacteria via flow cytometry in this study, is not possible; therefore, any term referring to bacterioplankton (or the marine bacterial community) throughout this thesis must be read with the understanding that archaea may

form part of the community. This includes bacterioplankton deemed as either high nucleic acid (HNA) or low nucleic acid (LNA) bacteria.

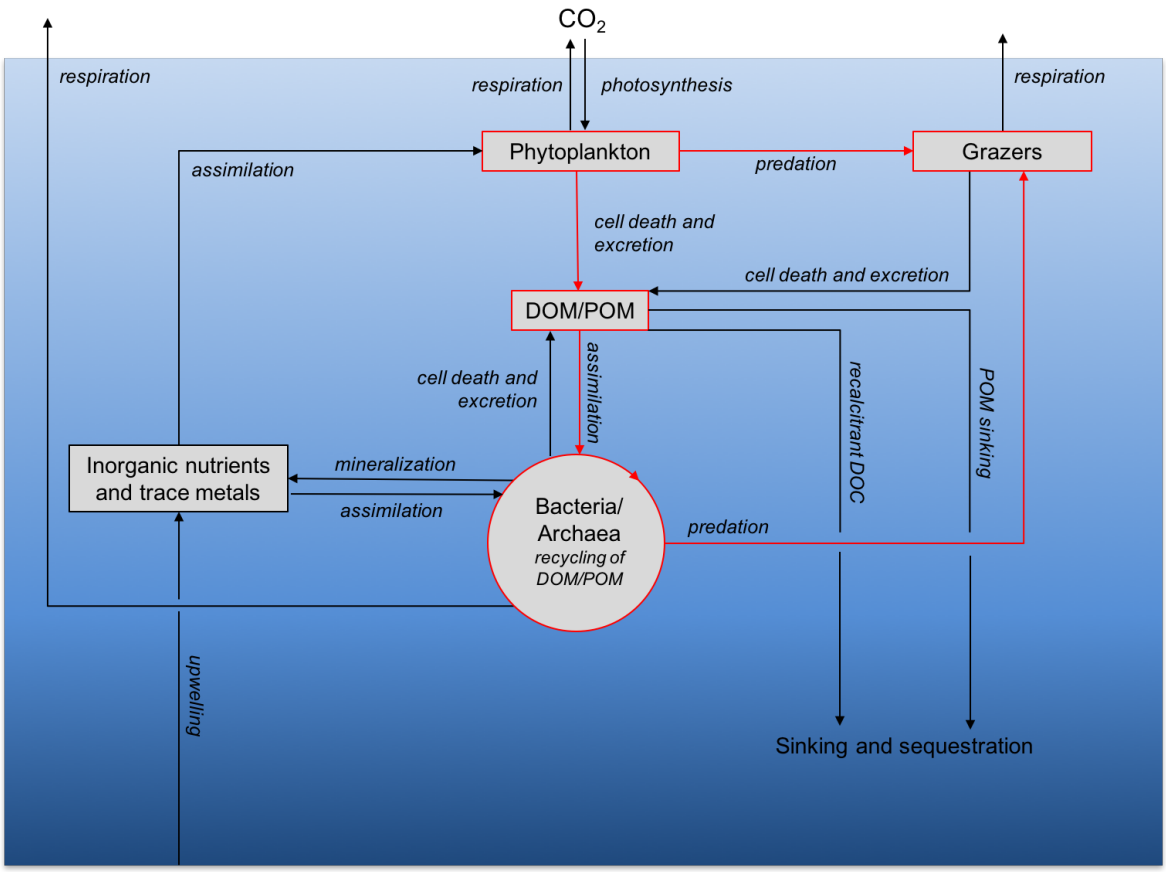

Figure 1.1: Cycling of organic material in the surface oceans
Figure adapted from Buchan et al (2014)[12], with additional information from Kirchman (2008) [2], Kirchman (2000) [3], and Azam & Malfatti (2007) [5]. The microbial loop is highlighted in red.

1.2 Vertical structure of the upper ocean

1.2.1 Stratification

When investigating biological oceanography, it is essential to understand the physical processes that influence the marine environment. The vertical structure of the water column is dictated by mixing and stratification, which consequently influences the plankton that inhabit the surface waters. The separation of water bodies and formation of layers

that are resistant to mixing is termed stratification [e.g. 19-21]. Stratification is influenced by parameters such as temperature, salinity and pressure, with the steep density gradient between ocean layers termed the pycnocline [22,23]. Due to the large amount of energy required to mix stratified waters, deep waters are prevented from mixing with the less dense surface waters [22-24]. The steep vertical gradient of temperature (due to adsorption of solar radiation) in the upper kilometre of the surface ocean is known as the thermocline [22,23]. As expected, the sea surface temperature is warmest in the tropics (annual average approximately 25-29ºC at the equator [25]) and coldest towards the polar regions (annual average approximately 0-4ºC at 60ºS [25]) [23]. As warmer water is less dense than cooler water, continued warming leads to a deeper pycnocline (and thus stronger ocean stratification) in the mid- and low- latitude oceans compared to higher latitudes [22,23]; for example, the approximate centre of the thermocline (based on a density anomaly in seawater of $\sigma = 26.5$) can be found at a depth of <100 m towards polar waters; however, this is located much deeper in the subtropical gyres (up to 500 m in the North Pacific) [23].

Salinity is higher in the subtropics due to increased levels of evaporation and glacial melt water, and is lower in the high latitude oceans due to higher levels of precipitation [23]. Although a higher salt content results in greater water density, the pycnocline is influenced more significantly by temperature in the open ocean, with salinity playing a minimal role [23,24]. Instead, the effects of salinity are more noticeable in the polar waters where fresh cold water (from glacial melting) is less dense than the warmer, saltier ocean waters [23], leading to salinity values as low as 28 psu (practical salinity unit) in the Arctic, compared to 35 psu in the tropics [26].

1.2.2 Critical depth

In the upper ocean, circulation from wind and heat convection mix the water, creating the surface mixed layer (SML) [23], where everything from heat content to nutrients to plankton are homogenously mixed vertically [22]. The thickness of the SML is generally 50-100 m, but can become deeper (e.g. up to 500 m) in high latitude oceans during winter months [23,27]. If the SML is thicker than the upper sunlit portion of the ocean (the euphotic zone: up to 150 m in subtropical waters [22]), then the photosynthetic microorganisms (phytoplankton) of the surface ocean will spend part of their life cycle in darkness, resulting in an overall lower rate of photosynthesis compared to that of respiration [4]. The depth whereby average primary production and loss (e.g. via respiration) is balanced is known as the critical depth, with loss exceeding primary production below this depth [4,28,29]. Critical depth has been linked to spring bloom events (e.g. such as that of the North Atlantic [28]), whereby upon shallowing of the SML to above the critical depth, there is increased phytoplankton irradiance and consequent primary production [4,28,29]. This can be demonstrated through the equation $r = \mu - (g + s + p + f) > 0$, where net growth ($r$) occurs when growth ($\mu$) exceeds total loss through grazing (g), sinking (s), viral lysis and parasites (p), and physical flushing (e.g. through vertical mixing) (f) [30 and references therein].

However, it should be noted that the original critical depth hypothesis [29] may not be fully comprehensive, with many studies observing bloom events that do not follow the traditional critical depth model, for instance the initiation of bloom events during winter, prior to spring stratification [30 and references therein]. As such, Behrenfeld (2010) proposed an alternative dilution-recoupling hypothesis for the North Atlantic that highlights the importance of phytoplankton grazing (and factors affecting grazing) in controlling bloom events; for example, dilution of grazers and grazing rates due to deepening of the mixed layer [30,31]. In contrast to the original model, Behrenfeld's results included an indication that phytoplankton loss was not constant, that maximum population levels were just as

likely to occur in winter as in spring, that bloom events are initiated in winter, and that both phytoplankton growth and loss increase during spring stratification [30].

1.2.3 Subtropical gyres and Atlantic oceanography

Oceanic currents are driven by wind, heat convection, rotation of the Earth (causing the Coriolis Effect), and placement of land masses [23]. Within these currents, closed cyclonic or anticyclonic circulating current systems form, which are termed gyres [23,32] and make up approximately 40% of the global ocean [e.g. 33]. Cyclonic systems result in surface water divergence and upwelling, which brings nutrients up from deeper waters [34]. Conversely, the anticyclonic system of a subtropical gyre results in surface water convergence and down-welling, and consequent nutrient removal from the upper ocean and suppression of nutrient-rich deep water upwelling [34]. Consequently, the SML (and vertical stratification) in the subtropical gyres is significantly deeper than in other oceanic waters [19].

Low nutrient supply, strong stratification and biological removal of nutrients before water enters the gyres, results in low-productivity oligotrophic subtropical gyral waters [4,19,33]. This can be observed through analysis of satellite data, which shows substantial areas of low chlorophyll concentration (and consequential low productivity), indicating the locations of the major oligotrophic gyres of the World's oceans (Figure 1.2). Significantly, climate change is resulting in the expansion of these regions due to rising sea temperatures that increase ocean stratification [35-38].

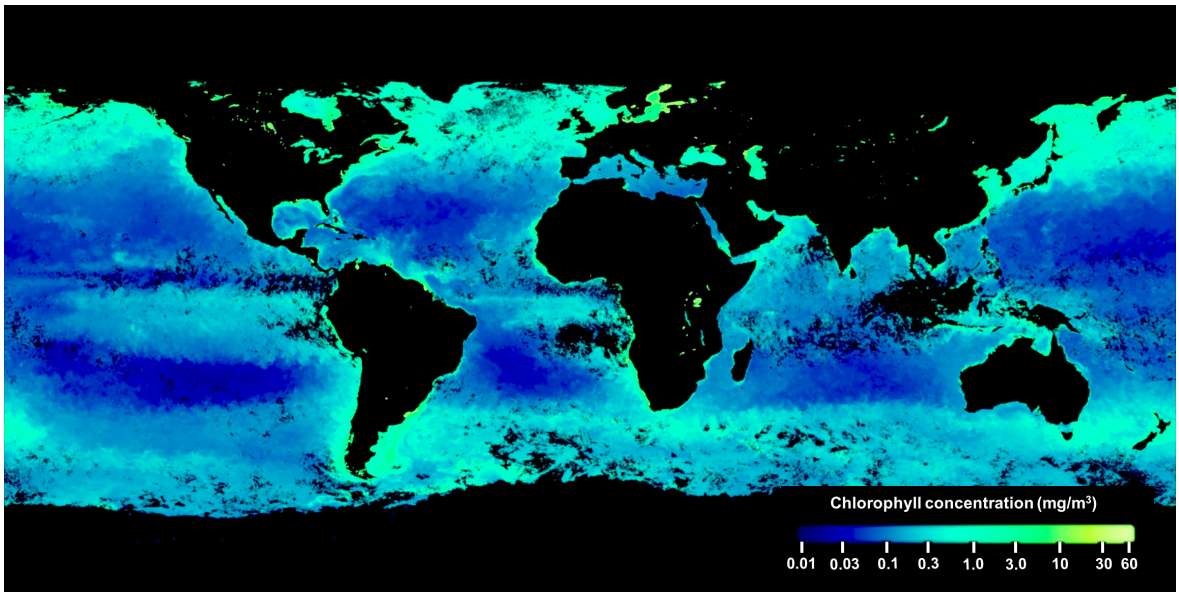

Figure 1.2: Global chlorophyll concentrations (October 2015)
The 5 major oligotrophic gyres are the North Pacific, North Atlantic, South Indian Ocean, South Pacific, and South Atlantic gyres, and can be visualized above by the low chlorophyll concentrations in these regions, indicating low productivity.
Image taken from NASA Earth Observations (neo.sci.gsfc.nasa.gov/). See full source in References, page 215 [39]. Slight colour adjustment was performed on the original image in order to make the colour gradient more defined.

Two of the 5 major oceanic gyres are found in the Atlantic Ocean, termed the North and South Atlantic subtropical gyres (NAG and SAG) (Figure 1.2). The World's oceans can be divided into separate biogeochemical provinces, known as Longhurst provinces (Figure 1.3), where Atlantic gyre provinces can be identified (i.e. Northwest Atlantic subtropical gyral province (NASW), the Northeast Atlantic subtropical gyral province (NASE), and the South Atlantic gyral province (SATL)). The NAG is dictated by the North Equatorial current to the south, the Gulf Stream to the west, the North Atlantic and the Azores currents to the north, and the Canary and Portugal currents to the east [23,40]. The SAG is bound by the South Equatorial current to the north, the Benguela current to the east, and the Brazil current to the west [23]. The South Atlantic current forms the southern boundary of the SAG and is influenced by the subtropical convergence zone formed where the Falkland and Brazilian currents meet [41,42].

Since 1995, the Atlantic Meridional Transect (AMT) cruise programme (www.amt-uk.org) has been running annually, providing an extensive dataset of biological, chemical and physical measurements, for more than two decades [43]. The cruise covers a range of

oceanic provinces across the Atlantic, including both subtropical gyres, equatorial waters, and temperate regions [43]. It provides a valuable insight into planktonic ecosystems and global carbon cycles [43]; as such, this study presents data gained from the participation of two AMT cruises (see Chapter 2).

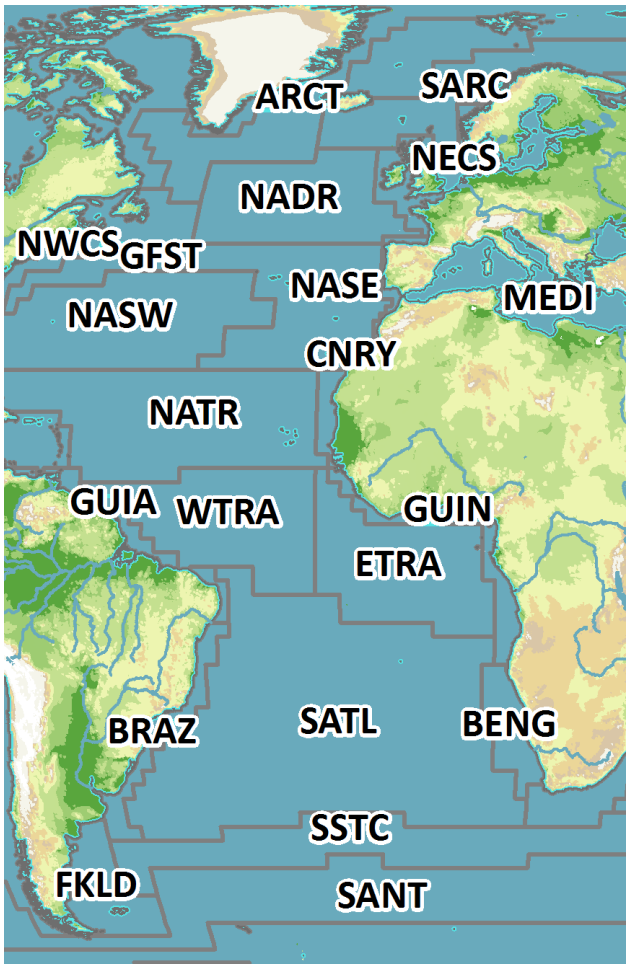

Figure 1.3: Longhurst provinces of the Atlantic Ocean and surrounding waters
Provinces shown on map: SARC (Atlantic sub-Arctic); ARCT (Atlantic Arctic); NECS (Northeast Atlantic shelves); NADR (North Atlantic Drift); NWCS (Northwest Atlantic shelves); GFST (Gulf Stream); NASE (Northeast Atlantic subtropical gyral); NASW (Northwest Atlantic subtropical gyral); CNRY (Canary current coast); MEDI (Mediterranean Sea); NATR (North Atlantic tropical gyral); GUIA (Guianas coast); WTRA (Western tropical Atlantic); GUIN (Guinea current coast); ETRA (Eastern tropical Atlantic); BRAZ (Brazilian current coast); SATL (South Atlantic gyral); BENG (Benguela current coast); SSTC (South subtropical convergence); SANT (Subantarctic water ring); FKLD (Southwest Atlantic Shelves).
Image taken (and then cropped) from: MarineRegions.org. See full source in References, page 215 [44]. Image licensed under a CC BY-NC-SA 4.0 license.

1.3 Nutrient cycling

A broad range of elements and nutrients are found within the water column, and their distributions are influenced by both geochemical and biological factors. Many of these nutrients are essential for plankton growth and metabolism, and thus require assimilation from the environment. The macronutrient elements nitrogen and phosphorus, as well as two trace metal micronutrients (iron and cobalt) are discussed subsequently, with reference to their role in cells and ocean cycling.

1.3.1 Nitrogen

Fixed nitrogen is a key macronutrient for all living organisms. With an average C:N Redfield ratio of 106:16 [45,46], nitrogen is essential for growth, is found in many key cellular components (e.g. proteins and nucleic acids), and can also be used as an energy source by some microorganisms [7]. including proteins and nucleic acids [47]. The cycling of nitrogen in the marine environment is depicted in Figure 1.4. The largest pool of nitrogen is that of dinitrogen (N_2); however, due to it being extremely inert, N_2 can only be utilized by a few specific microorganisms (diazotrophs), which carry out the energy expensive process of nitrogen fixation ($N_2 \rightarrow NH_3$) using the iron-containing enzyme nitrogenase [48].

Instead, plankton are able to access a number of other nitrogen sources in the marine environment, notably dissolved inorganic nitrogen (DIN) (i.e. ammonium (NH_4^+), nitrite (NO_2^-) and nitrate (NO_3^-)) [e.g. 7]. Physical inputs of dissolved inorganic nitrogen (DIN) into the marine environment include upwelling from deeper waters and aeolian dust transport [49,50], with biological transformations such as nitrification ($NH_3 \rightarrow NO_2^- \rightarrow NO_3^-$), reduction ($NO_3^- \rightarrow NH_3$) and anammox ($NH_4^+ + NO_2^- \rightarrow N_2 + 2H_2O$ [e.g. 51]) all working to cycle DIN [52].

Concentrations of nitrate are very low in surface waters of many low-latitude oceans [53], and are significantly lower than in coastal waters (e.g. 0.01 μM NO_3^- in Atlantic oligotrophic gyres, compared to 33 μM at the Benguela upwelling by the South African coast [54]), which benefit from continental inputs, coastal upwelling and shallower waters that prevent sinking [22]. The concentrations of NO_3^- increase with depth, away from the euphotic layer [49]. Conversely, ammonium and nitrite concentrations are maximal at the bottom of the euphotic zone, where formation from the regeneration of organic nitrogen (which consequently decreases in concentration with depth) and oxidation ($NH_3 \rightarrow NO_3^-$ + NO_2^-) is higher than plankton assimilation [49]. Interestingly, due to the very low concentration of nutrients in the surface ocean in subtropical waters, at the bottom of the euphotic zone there is a region of high chlorophyll concentration where cells reside in order to balance decreasing light levels with increasing nutrient levels (the deep chlorophyll maximum) [22]. Furthermore, regions of the ocean termed High Nitrate/Nutrient Low Chlorophyll (HNLC) regions (specifically the Southern Ocean, subarctic Pacific and the equatorial Pacific) have elevated surface concentrations of nitrate (e.g. >20 μM in the Southern Ocean, compared to an annual average of ≤0.25 μM in the subtropical Atlantic at approximately 30ºN [55]) but primary production is limited by low iron concentrations [56].

Despite its lower abundance in the surface ocean, ammonium is the preferred nitrogen source for most heterotrophic bacteria and phytoplankton, as nitrate utilization requires an additional energy-expensive reduction step and nitrite is only present at low concentrations (e.g. >5.9 μM, 0.2 μM, and <0.2 μM for NO_3^-, NO_2^- and NH_3, respectively in an eddy in the Atlantic Ocean, ca. 60ºN, 20ºW [57]) [3,49,50,54]. The majority of phytoplankton are still able to assimilate nitrate (and also consequently nitrite due to nitrification) [49]; although there are exceptions that cannot, including some strains of *Prochlorococcus* (e.g. strains MED4, MIT9301) [58,59].

DIN is assimilated into organic nitrogen by a wide range of cells [52]. These dissolved and particulate organic nitrogen (DON and PON) sources can be released via cell death and excretion, or can be converted back into NH_3 via ammonification for subsequent cellular use [52]. Additionally, there is increasing evidence for the utilization of DON (e.g. amino acids) in the marine environment by heterotrophic bacteria and some small phytoplankton [60].

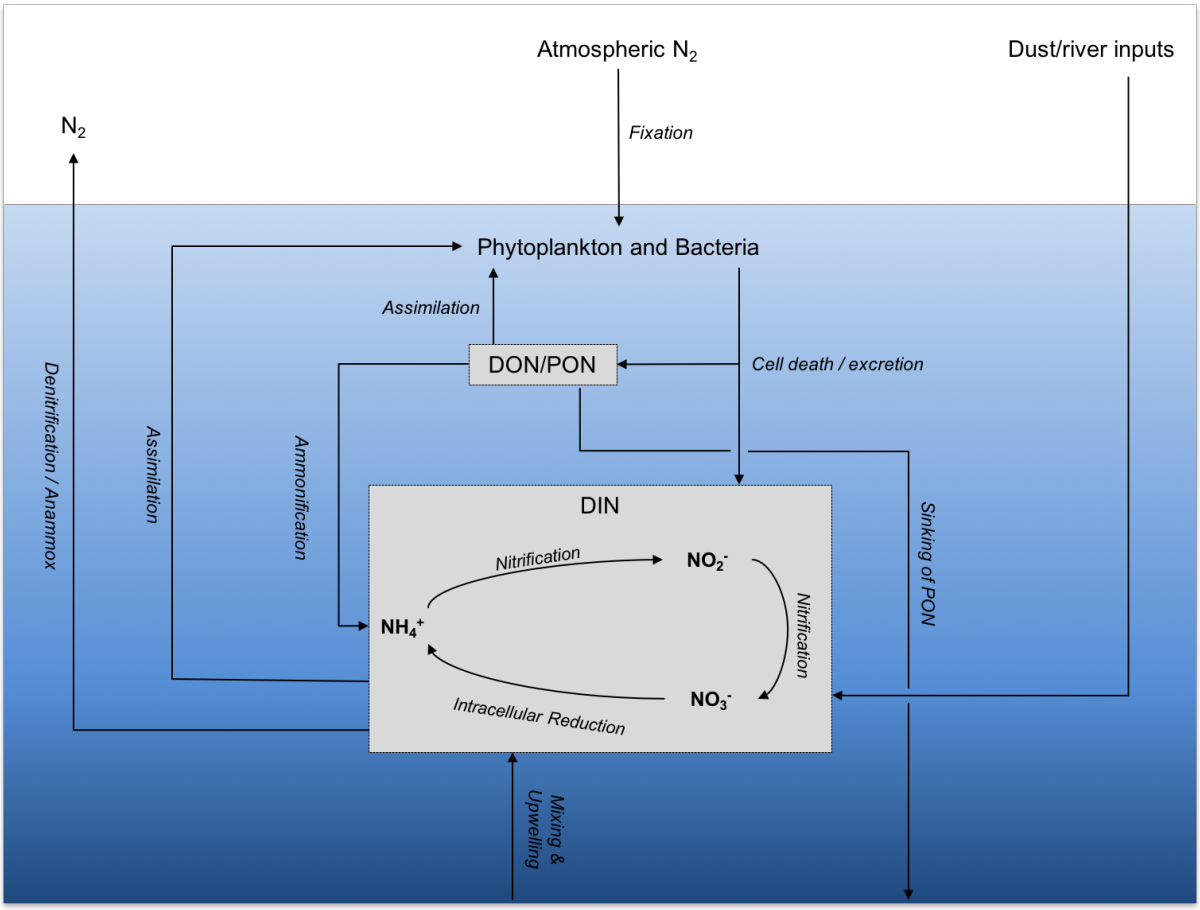

Figure 1.4: The oceanic nitrogen cycle
Figure adapted and legend information from: Capone (2000) [52], Zehr and Ward (2002) [50], Gruber (2008) [49], and Arrigo (2005) [61].

1.3.2 Phosphorus

Phosphorus is another key macronutrient for all living cells. It serves a role in energy storage and transformation (e.g. adenosine triphosphate, ATP), is a component of cellular

macromolecules (e.g. membrane phospholipids and nucleic acids) and is involved in key reactions such as photosynthesis [7,62]. Unlike nitrogen, phosphorus has one main inorganic form in the marine environment: phosphate (PO_4^{3-}) [3].

The major input of phosphorus to the ocean is via riverine and atmospheric transport of eroded rocks, with volcanic eruptions providing inputs to specific areas, and upwelling bringing inorganic phosphate to the surface ocean [62,63]. Low concentrations of phosphorus occurs in the surface ocean due to rapid biological uptake, with concentrations increasing with depth due to regeneration of dissolved organic phosphorus species (DOP) to PO_4^{3-}, as well as reduced microbial assimilation [64]. Conversely, DOP concentrations in the surface ocean are much higher and decrease with depth due to the increased regeneration [62]. Dissolved phosphorus cycles between inorganic (DIP) and DOP via the action of heterotrophic bacteria and phytoplankton [e.g. 62 and references therein]. Although inorganic phosphate assimilation is preferable, cells are also able to utilize DOP (via an additional conversion step to PO_4^{3-} by extracellular alkaline phosphatases), especially when concentrations of inorganic phosphorus are low [64 and references therein]. Indeed, in a study using radioactive dual labelling, Gómez-Pereira *et al* (2012) showed that molecules of adenosine-triphosphate were cleaved into phosphate and adenosine groups before cellular uptake [65]. Particulate organic phosphate (POP) is either microbially regenerated back to inorganic phosphate, or lost to the ocean via sinking and burial [62,63].

Across the global oceans, phosphate concentrations are lowest in subtropical oligotrophic gyres [53], with particularly low concentrations seen in the North Atlantic gyre (e.g. average values of 9 nM and 210 nM in the North and South Atlantic gyres, respectively) [66]. These unusually low concentrations are a consequence of increased iron inputs from Saharan dust, which increases nitrogen fixation by diazotrophs, and results in phosphate drawdown in the North Atlantic gyre [66]. As was described for nitrogen, HNLC regions

have high concentrations of surface phosphate (e.g. >1.5 μM in the Southern Ocean [55]), but low iron concentrations limit primary production [56].

1.3.3 Iron

Iron is an essential micronutrient for many metabolic reactions, functioning as an important cofactor in several key enzymes and proteins, such as those involved in nitrogen fixation and the removal of damaging reactive oxygen species (e.g. nitrogenases and superoxide dismutases) [67,68]. Most significantly, cellular iron is used within the cytochromes of the electron transport chain which are involved in photosynthesis and respiration [67]; indeed, an estimated 94% of all cellular iron in *E.coli* (a non-photosynthetic terrestrial bacterium) is found in the respiratory chain [69]. The only organism that appears to be able to survive without iron (or at least at severely reduced levels) is the Gram positive bacteria *Lactobacillus plantarum* [70]. Archibald (1983) hypothesised that this adaptation is linked to survival in high concentrations of hydrogen peroxide (through avoidance of free radical production via the Fenton reaction); thus, providing a competitive advantage in its natural habitat of decaying organic material [70].

Iron inputs to the marine environment are diverse and organisms rely on a mix of new and regenerated sources (Figure 1.5). The main source of new iron to the open ocean is aeolian dust transport [71]; for example, the supply of Saharan Desert dust to the North Atlantic [e.g. 72]. Other iron sources to the surface ocean include upwelling from the deep ocean, hydrothermal inputs, lateral mixing, as well as riverine and continental inputs to coastal waters, although this latter source is rapidly diminished by coastal plankton and particle scavenging processes before reaching the open ocean [71,73]. Globally, Fung *et al* (2000) estimated that plankton use 12 $x10^9$ mol Fe y^{-1} but are only supplied with new iron inputs of up to ~10 $x10^9$ mol Fe y^{-1}. Therefore, to make up the difference in supply and requirement, recycling of iron by plankton (e.g. via zooplankton grazing [74]) is an essential

process [71]. Removal of iron from the surface ocean occurs through biological uptake, as well as through formation of insoluble precipitates, and adsorption/scavenging onto particulate material [73,75-77]. As particulate iron sinks into the deeper ocean it is remineralized; thus, the concentrations of dissolved iron increase and particulate iron decrease with depth (below 250 m) [78 and references therein].

Under the current oxic conditions of the Earth, soluble ferrous iron (Fe(II)) is rapidly oxidised to its ferric form (Fe(III)); indeed, ferrous iron has a maximum half-life in seawater of only a few hours [79]. Photoreduction by solar UV light causes formation of ferrous iron, although it is quickly re-oxidized [79]. Ferric iron hydrolyses to stable oxyhydroxide species which will precipitate out of solution, thus reducing bioavailability to plankton [80]. Consequently, dissolved iron has a very short residence time in the surface ocean, persisting on a timescale of months [78,81]. This results in a significant pool of insoluble iron in the surface ocean, which is largely unavailable for biological uptake. The presence of marine ligands help maintain iron in solution (with >99% of dissolved iron bound by ligands) [82]. However, the combination of short residence time, limited solubility, biological removal and minimal inputs of new iron [71,73,79,80] results in surface open ocean concentrations of dissolved iron as low as 0.03-1.0 nM [73]. Higher surface iron concentrations may be found in coastal regions (including the Arctic due to the surrounding land mass), or in areas that receive high aeolian inputs (e.g. the North Atlantic) [73].

The illogically enhanced cellular requirement for such an unavailable element in the modern ocean stems from the early evolution of cells. Around 3.5-3.8 billion years ago, when the first signs of life were beginning to emerge [83,84], the reducing atmosphere and oceans of the Archean Earth meant that iron was abundant in its soluble ferrous form and thus readily available for cellular incorporation [85,86]. The unique properties of iron (i.e. multiple oxidation states that can easily undergo electron transfer, and a range of redox

potentials from differential ligand binding) as well as its high abundance (iron being the 4th most abundant element on the Earth's crust [e.g. 7]), made it a highly attractive cofactor for biochemical reactions [87], thus cellular incorporation of iron was a reasonable outcome.

Oceanic plankton have evolved several adaptations to cope with the low bioavailability of iron in modern oceans, including a much lower iron requirement compared to coastal species [88], a large surface area to volume ratio to maximise uptake potential [88], and the ability to make unavailable iron more bioavailable [89]. The latter adaptation is concerned with methods of iron assimilation. The most notable uptake mechanism is the production of high affinity iron chelating molecules known as siderophores. These molecules chelate ferric iron from minerals, existing complexes and particle-adsorbed iron in order to make iron soluble for biological uptake [67,90]. Iron acquisition genes (including siderophore production) is regulated by a Fur protein [91-93]. Under high concentrations of iron, a Fur Fe(II) complex will bind to a specific region of DNA (the Fur box), repressing iron acquisition gene expression [91]. Generally, marine siderophores fall into two main categories [91,94 and references therein]. The first group is photoreactive and contain an α-hydroxycarboxylic acid group (i.e. ß-hydroxyaspartic acid or citric acid), and include groups such as alterobactins and aerobactins [91,94 and references therein]. The second group is amphiphilic (such as, aquachelins, marinobactins and amphibactins) and contain a peptide head group to coordinate the iron, and a fatty acid tail that allows cell membrane attachment [91,94 and references therein].

However, this well evolved uptake mechanism can pose problems for plankton, primarily due to the diffusion of siderophores away from the cell following release [95,96]. This is not only a waste of energy by the cell, but also presents an opportunity for competing microorganisms to use the siderophores [67] . Although not all plankton can produce siderophores [97-99], some can still utilise siderophores that have been produced by other organisms, thus widening their capacity for iron acquisition [97,98,100]. An alternative uptake mechanisms is via a reductive pathway, which acquires iron through direct electron

transfer at the cell surface [97]. A reductive mechanism is likely to be more efficient as a large organic compound (i.e. a siderophore) does not need to be synthesised, and as reduction occurs at the cell surface, the risk of diffusion away from the cell is minimised

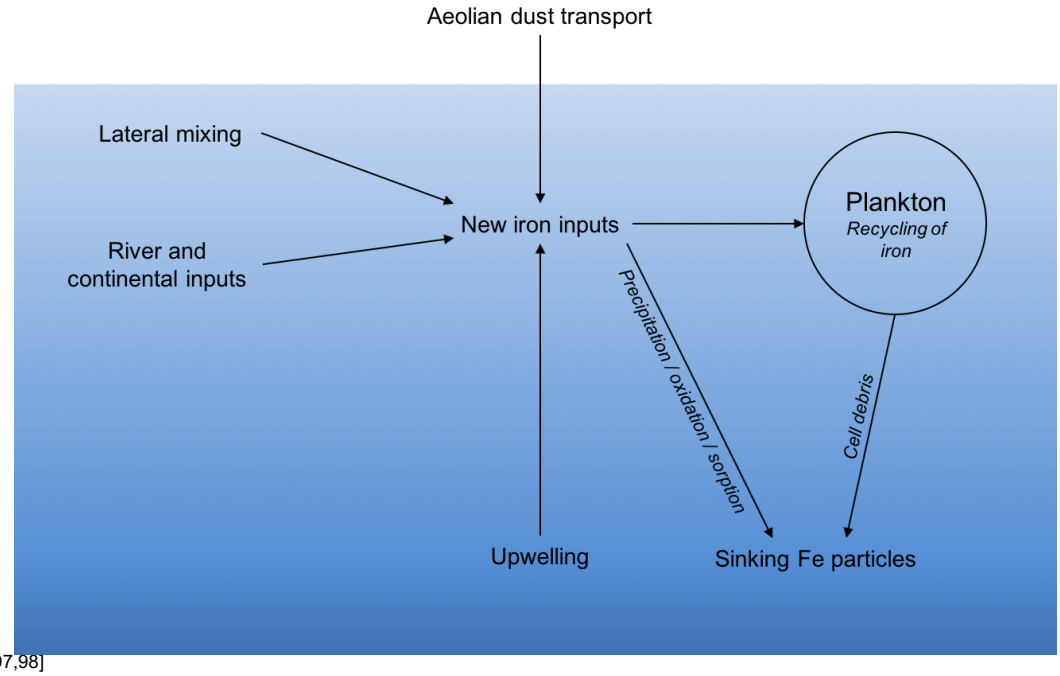

[97,98].

Figure 1.5: Basic oceanic iron cycle
Figure adapted and legend information from: de Baar and de Jong (2008) [73], and Fung et al *(2000) [71].*

1.3.4 Cobalt

Cobalt is another example of an essential trace micronutrient. The most significant use is in vitamin B12, which is required by multiple enzymes (e.g. methionine synthase and type II ribonucleotide reductase) [101,102] and has been shown to co-limit phytoplankton growth alongside iron [103]. Additionally, the involvement of cobalt and zinc in alkaline phosphatase has been noted [104], and cyanobacteria (namely *Prochlorococcus* and *Synechococcus*) have been shown to have a set requirement for cobalt [105]. Interestingly, studies have

shown the presence of biologically produced organic ligands that bind cobalt, with evidence for production by cyanobacteria, including *Prochlorococcus* [105,106, and 107 and references therein].

The cycling of cobalt in the marine environment is typical of a trace metal nutrient, with input sources coming from aeolian dust transport, lateral transfer, and upwelling of nutrients from the deep ocean [e.g. 108 and references therein]. Removal of cobalt from the surface ocean occurs predominantly through biological uptake and sinking of particulate material [e.g. 108 and references therein], with Bown *et al* (2011) noting in the South Atlantic/Southern Ocean that the largest input of cobalt to the ocean was lateral transfer, and the largest removal factor was from biological uptake [109]. Abiotic cobalt precipitation is a minimal removal factor in the marine environment; however, it is greatly enhanced by the presence of manganese oxidising microbes [e.g. 110,111]. The exact mechanism of formation of particulate and insoluble cobalt (termed particulate cobalt from here on) cobalt is disputed, being either a result of direct cell-surface pathway or an indirect result of biogenic manganese oxides formed by these specialised microbes [e.g. 112-114].

Concentrations of cobalt in the surface ocean are typically found in the picomolar range [109,115], with very low concentrations found in subtropical gyres (e.g. <6 pM in the SAG), which is low in comparison to elevated coastal concentrations (e.g. 200 pM by the Namibian coast) as a result of continental inputs [115]. Dissolved cobalt generally follows a typical nutrient like vertical profile in the open ocean, with low concentrations in the surface waters due to biological uptake, and an increasing concentration with depth following remineralization of particulates [109,115-117]. For example, Saito *et al* (2005) measured total dissolved cobalt concentrations of 93 pM at 90 m, but 45 pM at the surface of the Costa Rica upwelling dome [118]. However, vertical distributions of cobalt may differ according to the oceanic region [109,115]. In a study by Bown *et al* (2011), dissolved cobalt concentrations were elevated in polar surface waters, which was attributed to Patagonian dust transport and/or increased input from precipitation in the upper ocean, combined with

reduced biological uptake [109]. Additionally, cobalt concentrations decreased with depth, which was hypothesised to be due to increased scavenging [109]. Indeed, Saito and Moffett (2002) described cobalt as not conforming to the typical behaviour of a nutrient-type or a scavenging-type element (i.e. influenced by adsorption and precipitation) [116].

1.4 Nutrient limitation of bacterioplankton

All organisms require a wide range of nutrients, with the Redfield ratio setting out an average ratio of the key elements within a cell: 106:16:1 atoms of carbon, nitrogen and phosphorus [45,46], and later amendments showing that altered ratios can be accommodated by cells (e.g. ratios of N:P ranging from 5 to 34 in marine particulate matter [119]). Furthermore, the ratio can be extended in order to incorporate other elements, such as iron, again with ratios allowing for some variation between species (e.g. ratios of $(C_{124}N_{16}P_1)_{1000}Fe_{7.5}$ in eukaryotic phytoplankton [120] and $(C_{72}P_1)_{1000}Fe_{1.8}$ in diatoms and flagellates [121]).

Despite the essential cellular requirement, nutrients can often be found at very low concentrations across the global ocean, particularly in the oligotrophic gyres. These low nutrient concentrations occur when removal mechanisms (i.e. rapid cellular utilisation, as well as scavenging and sinking) are greater than input sources. This may result in limitation of plankton growth and/or metabolism, and can be demonstrated using nutrient enrichment studies [122], such as those of Moore *et al* (2008) [123] and Mills *et al* (2008) [124]. Plankton limitation may in turn have a knock-on effect on the marine (and indeed global) ecosystem through changes in carbon fluxes and a reduction in primary production.

Across the Atlantic, very low concentration of nitrogen in the surface ocean have been noted by many studies, with concentrations of ammonium and nitrate in the surface of the

open ocean on the order of 10-100 nM, compared to micromolar concentrations in more productive coastal waters (e.g. 14.7 μM by the Falkland Islands, 33.0 μM in the Benguela Upwelling) and beneath the surface ocean (e.g. >10 μM in the equatorial Atlantic below approximately 50 m) [54]. Similarly, very low phosphate concentrations have been observed in the NAG, which is believed to be due to high iron inputs from Saharan dust, causing increased nitrogen fixation and thus leading to phosphate drawdown [66]. Interestingly, dust deposition does not reach to the South Atlantic, due to the presence of the intertropical convergence zone, which impedes aerosol transport due to substantial rainfall [125]. Consequently, iron concentrations in the SAG are significantly lower than in the North Atlantic [e.g. 126,127]. Additionally, concentrations of the micronutrient cobalt are also lower in the Atlantic gyres in comparison to more productive coastal waters [e.g. 104,106,115,127].

DOC can limit bacterioplankton [e.g. 128], although surface concentrations across the North and South Atlantic gyres are higher in comparison to higher latitude waters [e.g. 129,130]. Indeed, most nutrient enrichment studies conducted in the NAG did not note primary carbon limitation of plankton [e.g. 124,131-133].

It should be noted that describing organisms as nutrient limited must be used with caution, as the term limitation can refer to multiple scenarios [53,122]. These can include co-limitation (i.e. an organisms is deficient in two or more nutrients/factors), physiological stress (i.e. a physiological response to a nutrient deficit), or stoichiometric deficiency (i.e. an imbalance in the ratio of one nutrient relative to another) [53]. For the purposes of this study, cells were described as nutrient limited if addition of the nutrient stimulated a positive cellular response (e.g. an increase in cell abundance or metabolic activity), a principle that has been previously used by several other studies [e.g. 123,131,134-136].

1.4.1 Oligotrophic micro-organisms

The very low concentration of biologically essential nutrients in subtropical gyres restricts the number of organisms that are able to survive in these waters. SAR-11 and *Prochlorococcus* are the two most noteworthy groups of microorganisms that have adapted to these conditions, and as a result dominate the global oceans [e.g. 137,138].

SAR-11 is a clade of heterotrophic alpha-proteobacteria (*Pelagibacter ubique*) identified in 1990 by Giovannoni *et al* through phylogenetic analysis of 16S rRNA clone libraries, and isolated through culturing by Rappé *et al* (2002) [139,140]. They are ubiquitous across the globe, with approximately 25% of microbes (~12% of prokaryotic biomass) in the world's oceans being SAR-11, equating to an estimated 2.4×10^{28} SAR-11 cells [137]. Due to their small size, SAR-11 can be defined as low nucleic acid (LNA) bacteria [141,142]. Nevertheless, despite their size, the high abundance of these cells means that they are of global importance and contribute to a significant proportion of DOM cycling in the marine environment [e.g. 142-145].

The bacteria that was to be later recognized as *Prochlorococcus* was initially noted by Johnson and Sieburth in 1979 [146] but was not properly identified until years later through flow cytometry and genomic analysis [138,147,148]. Despite being the smallest known photosynthetic bacterium [138], its preference for oligotrophic waters means it is highly abundant (approximate global population on the order of 10^{27} cells) and thus is a significant contributor to oceanic primary production, and indeed is the most abundant phytoplankton [138,149-154]. Furthermore, due to the existence of multiple strains that are adapted to different light levels, *Prochlorococcus* is able to populate the whole of the euphotic zone [e.g. 155, and 156 and references therein].

Another noteworthy picophytoplankton is the slightly larger (0.9 μm diameter [2]) *Synechococcus*, which was first identified in 1979 and contains the less common

phycoerythrin photosynthetic pigment [157]. *Synechococcus* are universally found across the global oceans, although its preference for nutrient rich waters means that it is only found in very low abundances in oligotrophic regions [158]. Nevertheless, its ubiquity means that the estimated global population is on the order of 10^{26} cells [151], thus it is also a significant contributor to global primary production [e.g. 159].

Together, *Prochlorococcus* and *Synechococcus* are estimated to contribute to approximately 25% of oceanic primary production [151]. Global distributions of these two cyanobacteria differ, with high concentration of *Prochlorococcus* found across the mid and low latitude oceans, but a marked decrease in abundance in high latitude oceans [151]. Conversely, *Synechococcus* are more ubiquitous across the World's oceans, although at lower concentrations [151]. In temperate and subtropical oligotrophic waters (e.g. in the North and South Atlantic subtropical gyres), the vertical profiles of these two cyanobacteria also vary, with the highest abundance of *Prochlorococcus* found at the bottom of the euphotic layer (just above the nutricline), but *Synechococcus* being equally distributed (albeit at low concentrations) across the same vertical profile [158]. Interestingly, Flombaum *et al* (2013), predicted an overall global increase in *Prochlorococcus* and *Synechococcus* cells due to rising sea surface temperatures as a result of climate change [151]. Such changes may cause large changes in species distribution (e.g. *Prochlorococcus* and *Synechococcus* populations shifting towards the poles [151]), as well as unknown feedback mechanisms and potential shifts in the whole ecosystem [156].

1.4.2 Oligotrophic adaptation

The main key to oligotrophic survival is minimalism. *Prochlorococcus* is the smallest known photosynthetic bacterium [138] (average diameter of 0.6 μm [160]) and SAR-11 (at just 0.37–0.89 μm in length, and 0.12–0.20 μm in diameter) are amongst the smallest free-living cells [140]. A small size results in a large surface area to volume ratio, making nutrient

acquisition and (for *Prochlorococcus*) light absorption much more efficient [e.g. 2,143,160-162]. Additionally, both *Prochlorococcus* and SAR-11 have a reduced genome (approximately 2 Mbp for *Prochlorococcus* and 1.3 Mbp for SAR-11), which means they have a reduced nutrient and metabolic requirement [138,143], relieving some of the strain of nutrient acquisition.

The ability to utilise a wide pool of nutrient sources (e.g. organic nitrogen uptake by *Prochlorococcus* [60] and a wide range of organic carbon molecules by SAR-11 [163]) provides an advantage over other cells that have a stricter nutrient range [60]. Indeed, Zubkov *et al* (2015) noted that *Prochlorococcus* and SAR-11 are able to store phosphate in an extracellular buffer, thus overcoming the limited storage capacity that results from their small size [164].

Furthermore, these cells have specific molecular adaptations that benefit oligotrophic living. For example, *Prochlorococcus* has a lowered phosphorus requirement [e.g. 165,166], due to its smaller genome (i.e. less phosphate required for the sugar-phosphate backbone of DNA) [166] and replacement of membrane phospholipids with sulpholipids [167]. Additionally, gene regulation pathways for the *Prochlorococcus* ammonium permease *amt1* are severely minimized, resulting in a constantly high level of ammonium uptake (bar under severely limited ammonium concentrations) [168,169]. SAR-11 also have a minimized regulatory network [170], as well as possessing proteorhodopsin, which occupies a substantial proportion (20%) of its membrane space [171]. Proteorhodopsin is a light driven proton pump that provides energy via production of a proton motive force, which helps cell survival under carbon limitation [170,171].

These adaptations for survival in such a huge ecological niche such as the oligotrophic gyres, means *Prochlorococcus* and SAR-11 are highly abundant, and thus globally dominant, bacterioplankton. It should be noted that although *Prochlorococcus* and SAR-11 are amongst the most well-adapted marine oligotrophs, other organisms can also

possess adaptations for survival in low nutrient environments. For example, oligotrophic *Synechococcus* species have adaptations that include: a reduced nutrient requirement, an increased surface area to volume ratio, and possession of high affinity transporters [172].

1.5 Summary

Oligotrophic gyres make up a significant proportion of the world's oceans; however, as a result of climate change, the gyres have been shown to be expanding [35-38]. Due to the substantial size of these regions, this expansion will consequently cause a major effect on the global ecosystem.

Within these gyres, communities of plankton are able to survive, with adaptation favouring minimalistic cells (notably, *Prochlorococcus* and SAR-11), and bacteria dominating microbial communities across the surface ocean [2]. Despite their small size, their sheer abundance means bacteria have a significant impact on the marine environment; and so, this study is primarily focused on bacterioplankton. Again, this is especially important considering the potential changes in species abundance and distribution (e.g. movement of *Prochlorococcus* and *Synechococcus* populations towards the poles [151]) that may occur due to climate change [e.g.151,156].

1.5.1 Research objectives and aims

To ensure successful cellular growth and to maintain the marine ecosystem, cells require a plethora of nutrients, including nitrogen, phosphorus, iron and cobalt. As such, the distribution and availability of these nutrients in the marine environment is critical, especially considering climate change may cause changes in marine chemistry [e.g. 173,174]. Very low concentrations of nitrogen have been observed across the majority of the

Atlantic Ocean [53], with very low concentrations of phosphate in the North and iron in the South also being reported [e.g. 66,126]. Additionally, factors controlling the distribution of biologically essential nutrients (such as through precipitation, adsorption and scavenging) is also major factor in determining the availability of these nutrients to plankton. For example, iron readily adsorbs to particulate matter (including cells) [e.g. 76,175], and particulate cobalt formation is significantly influenced by manganese (oxy)hydroxides and manganese-oxidising bacteria [e.g. 112-114].

The overarching aim of this thesis was to assess nutrient bioavailability. This was approached via two main objectives, each of which can be further sub-dived into more specific aims to tackle gaps in current knowledge:

- *Objective 1: Determination of the effect of low nutrient concentrations on bacterioplankton across the Atlantic Ocean using nutrient enrichment experiments.*

Many studies have addressed the low concentrations of nitrogen and phosphorus seen in the North Atlantic; however, the majority of these have not been conducted in the eastern North Atlantic or only examine phytoplankton [e.g. 128,132]. Therefore, Chapter 3 aimed to measure the responses of bacterioplankton to nitrogen and phosphorus additions in the central/eastern North Atlantic. Seawater samples were incubated on ship along a north-south transect, and changes in bacterioplankton abundance and metabolic activity was assessed upon nutrient additions. These responses were compared both inside and outside of the NAG.

Additionally, there are very few studies that have conducted nutrient enrichment experiments in the South Atlantic in order to assess the effect of the low concentrations of nitrogen and iron [176-179]. Therefore, Chapter 4 aimed to measure the responses of bacterioplankton abundance and metabolic activity to nitrogen and iron additions in the South Atlantic. As in Chapter 3, this was achieved through analysis of changes in bacterioplankton growth and metabolic activity upon nutrient addition, using seawater

samples analysed along a north-south transect. Due to the increasing understanding of oceanic iron limitation (i.e. in HNLC regions [e.g. 180 and references therein]), a particular focus was placed on determining potential iron stress of plankton within the gyre; therefore, nutrient enrichment experiments were supported with measurement of intracellular iron uptake rates. Finally, changes in cell abundance and metabolic activity, and iron uptake rates were compared inside and outside of the SAG.

- *Objective 2: Examination of factors affecting the formation of particulate/insoluble trace metal species in seawater, specifically the micronutrients iron and cobalt.*

Despite the influence of scavenging and sorption on metal distribution in the marine environment and the essential biological requirement of many trace metals, studies assessing cellular iron sorption are limited, especially in the South Atlantic, where iron concentrations are significantly lower than the North Atlantic [e.g. 126]. Therefore, Chapter 5 aimed to measure extracellular iron adsorption levels in the South Atlantic, with a view to compare adsorption levels inside and outside the SAG. Adsorption of iron to plankton (seawater samples, incubated on ship) was assessed using radiolabelled iron across a north-south transect in the South Atlantic. Adsorption levels were calculated on a per cell basis and compared inside and outside of the SAG. Additionally, iron adsorption in iron-replete laboratory cultures was used as a comparison to seawater samples.

Cobalt is another biologically essential nutrient; however, previous examinations of the mechanism of formation of particulate cobalt are not unified in their conclusions [e.g. 113,114], thus any additional data is beneficial to the field. Therefore, Chapter 6 aimed to examine the factors affecting formation of particulate/insoluble cobalt with a view to further understanding cobalt distribution in the marine environment. Formation of particulate cobalt by a laboratory culture of manganese-oxidising *Aurantimonas* was assessed using radiolabelled cobalt. The amount of particulate cobalt was compared when cultures were exposed to differing concentrations of manganese, as well as in the presence of

potentially competing transition metals (nickel, chromium and copper). Formation was also compared in non-manganese oxidising bacteria and in dead bacterial cultures.

1.5.2 Chapter 2

Before presenting results of this study, an introduction to the key methods is presented. Key theory and protocols are described, including flow cytometry, uptake of radiolabelled molecules (namely amino acids, but also iron and cobalt), seawater sampling and laboratory bacterial culturing. The aim of this chapter is to prevent repetition throughout the thesis, and to provide a platform for detailed description of specific methods.

Chapter 2: Introduction to key methodologies

2.1 Chapter Rationale

The following chapter provides detail on several pre-established methodologies that were frequently applied throughout this thesis. No original methods are presented in this chapter, simply background information and standard protocols for the key techniques. This chapter will serve to prevent unnecessary repetition of frequently used procedures in subsequent data chapters (Chapters 3-6) and will be referred to throughout the rest of the thesis. Chapters 3-6 will also contain information on the more specific protocols used to address the aims of the study.

Techniques presented in this chapter:

- water sampling during two research cruises
- flow cytometry
- amino acid uptake
- culturing of model laboratory bacteria

Unless stated otherwise, all chemicals were either from Sigma Aldrich, UK, or Fisher Scientific, UK. All deionized water used was MilliQ water, with a resistivity of 18.2 MΩcm (Millipore, UK). If required, pipette (Finnpipette) accuracy was checked through measurement of deionized water (based on 1µL of deionized water equalling 1 mg), such that the dispensed volume was within the accuracy range provided in the manufacturer's instructions.

2.2 Research cruises

A significant part of this research project was based around two major research cruises in the Atlantic Ocean. Both cruises were conducted as part of the Atlantic Meridional Transect (AMT) cruise programme on board the R.R.S. James Clark Ross (JCR), and ran from Immingham, UK to Stanley, Falkland Islands (Figure 2.1). These occurred on consecutive years from September to November 2014 (cruise AMT-24) and September to November 2015 (cruise AMT-25).

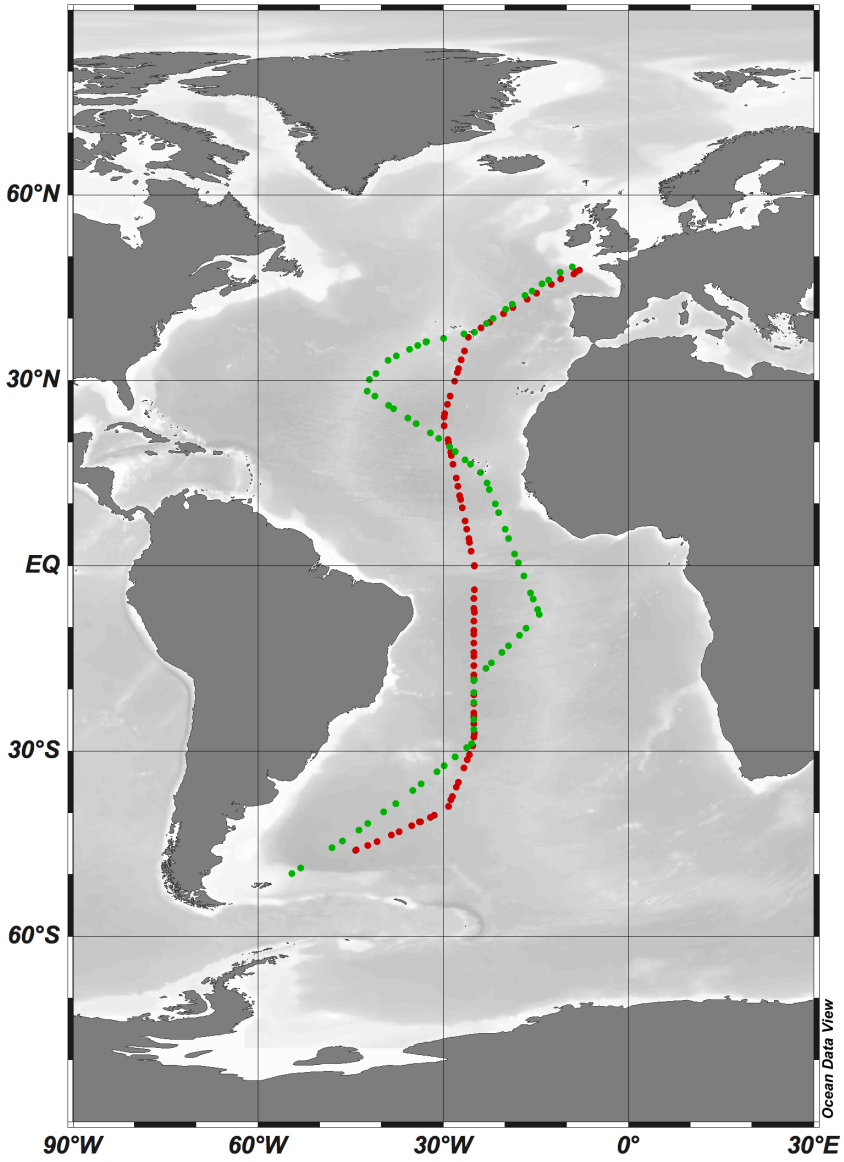

Figure 2.1: Profiles of the two research cruises attended during this project
Both cruises began in Immingham, UK and finished in Stanley, Falkland Islands. The red transect is that of AMT-24 from September to November 2014. The green transect is that of AMT-25 from September to November 2015. The map was created using Ocean Data View Software 4.7.10 [181].

2.2.1 Water sampling

For collection of seawater samples, a Go Flo bottle was the sampler of choice. It is more suited for trace metal clean work as it contains no metal parts, it can be deployed without use of a metal frame, and can remain closed until underwater. Additionally, it is small enough for only one user and can be easily transported to a clean environment before taking any water samples.

A 10-litre Go Flo (C-free model 130, OceanTest Equipment) (Figure 2.2) was used to collect all water samples [e.g. 182]. For experiments that required trace-metal conditions (i.e. work with iron), the Go Flo and all associated tubing and connectors, were cleaned prior to use (see 'Preparation of acid clean lab ware' below). Deployment of the Go Flo was conducted on the forecastle deck of the JCR, using a plastic-coated wire and weight, and a stainless-steel shackle. All samples were collected at approximately solar noon, from a depth of 20 or 30 m (AMT-24 and AMT-25, respectively), which was considered to be deep enough to avoid contamination from the boat, but still within the upper portion of the euphotic zone.

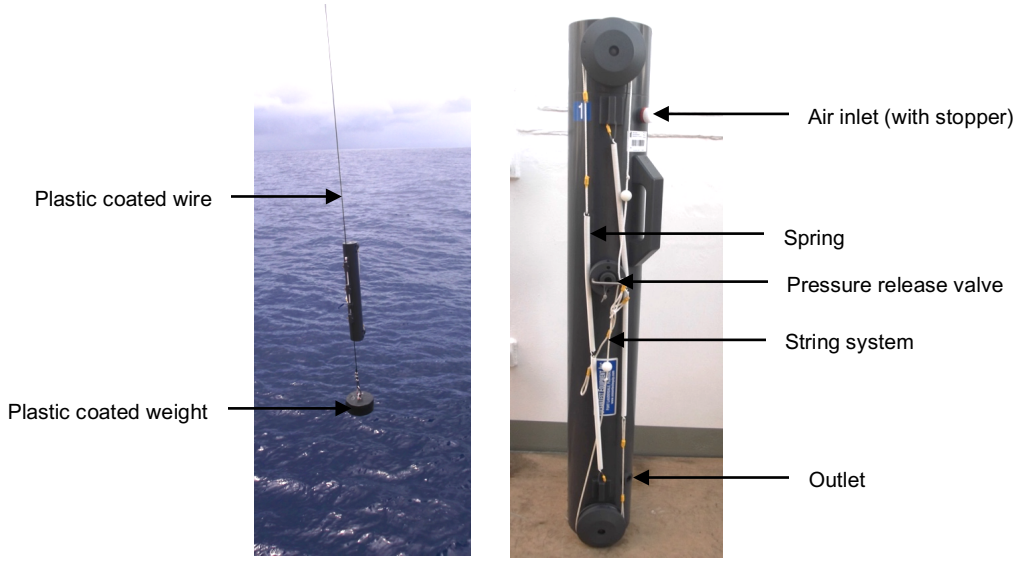

Figure 2.2: Labelled diagram of a 10L Go Flo water sampler
A Go Flo was the water sampler of choice for collection of seawater samples during AMT-24 and AMT-25. See text for description of deployment.
Go Flo: C-free model 130, OceanTest Equipment Ltd. Supplied by National Marine Facilities Sea Systems (NMFSS) based at the National Oceanography Centre Southampton (NOCS).

Go Flo deployment and seawater collection

Before use, an acid cleaned tap was attached to the Go Flo's outlet and a stopper was attached to the air inlet (Figure 2.2). The Go Flo was then primed for deployment by being held closed under tension using springs. The sampler was attached to a plastic-coated wire via clips on the back (Figure 2.2). A plastic-coated weight allowed the empty Go Flo to be lowered down into the water vertically. Once the Go Flo was beneath the surface of the water, a pressure release valve opened the Go Flo; however, the string system prevented the Go Flo closing. At the desired depth (20 or 30 m), a messenger weight was deployed down the wire to release the string system, closing the Go Flo. In order to reduce environmental contamination, a clean sterile sample bag immediately covered the outlet tap upon recovery (Figure 2.2). The unopened Go Flo was taken to a clean work area and secured adjacent to a laminar flow hood with a custom-made stand. An Acrovent 0.2 µm polytetrafluoroethylene (PTFE) filter (Pall Corporation) was attached to the top of the Go Flo via the air inlet (Figure 2.2) to prevent contamination from incoming air. Acid-clean tubing was attached to the outlet tap to allow for sample collection.

Preparation of acid clean lab ware

For experiments (both ship-board and on land) that worked with iron or cobalt, and so required trace metal clean conditions, all plasticware was acid-cleaned prior to use. For this, an acid bath was prepared using concentrated analytical grade hydrochloric acid, diluted to ~1 M with deionized water (resistivity >18.2 MΩcm). Plasticware was stored in the bath for approximately 24 h, before rinsing three times with either seawater (i.e. taken directly from the Go Flo), or deionized water. Plasticware that was not immediately used was stored in sealed plastic sample bags.

2.3 Flow cytometry

Flow cytometry is a technique used in microbiology (and other fields, such as haematology [e.g. 183]) that allows the enumeration and characterisation of cell cultures. It works by passing a steady stream of a cell suspension across a laser, whereby each particle crossing the light path will produce a specific refractive and fluorescence signal that is collected by electronic detectors [184]. Forward light scatter (refraction) allows assessment of cell size, with 90º side scatter (SSC) also providing an indication of a cell's surface characteristics [184]. Filters for specific wavelengths of light allow the filtration and detection of the various fluorescence signals emitted by different molecules [184]. Chlorophyll, for example, is identified by its red auto fluorescence between 670-685 nm [184-186] and the photosynthetic pigment phycoerythrin, found in *Synechococcus* [146,157], can be identified through its orange autofluorescence (560-600 nm) [184]. Furthermore, molecules that do not naturally fluoresce can be labelled to allow detection; for example, the DNA content of a cell can be determined through staining DNA with SYBR® Green, which will produce a detectable green fluorescence [149,187]. In this study, flow cytometry was used to enumerate and characterize laboratory cultures and seawater samples.

2.3.1 Sample preparation and measurement

Samples for analysis by flow cytometry were prepared following a standard procedure within the Microbial Plankton Group at the National Oceanography Centre Southampton (NOCS), and is described elsewhere (e.g. Olson *et al*., 1993; Zubkov *et al*., 1998, 2008; and Fuchs *et al*., 2005 [150,184,188,189]).

Briefly, 80 µL of 20% paraformaldehyde (PFA) was added to a 1.6 mL cell/seawater sample (1% final concentration) and incubated at room temperature for between 15 and

60 min. After fixation, 160 µL of ~0.3 M tri-potassium citrate (0.2 µm filter sterilized using disposable filters (Minisart)), and 16 µL of 1% SYBR® Green I were added to the sample [149,187] prior to incubation at room temperature for 30-60 min. Alongside the prepared samples, a blank was included that used deionized water in place of the cell suspension.

After incubation, 50-100 µL of a bead stock, which contained a known concentration of 0.5 µm and 1.0 µm fluorescent microbeads (Polysciences), was added to the sample [190]. The concentration of beads in the bead stock was pre-determined using a standard protocol (termed bead stock calibration) as described in Zubkov and Burkhill (2006) [190]. The sample was then placed into the flow cytometer and ran at a flow rate of 10-30 µL/min for 60-120 sec. This study used a FACSCalibur flow cytometer from Becton Dickinson, equipped with a 488 nm 20 mW laser, and 530±15 nm (FL1), 585±21 nm (FL2) and >650 nm (FL3) filters to allow for detection of green, orange and red fluorescence respectively (Table 2.1). The tubes used for measurement (polypropylene, VWR) had very specific dimensions (diameter of 75mm and length of 12 mm) in order to create an air-tight seal around the flow cytometer needle.

Table 2.1: Flow cytometric detectors and filters used in the FACSCalibur
The parameters used in this study to monitor cells are presented. Each detector or filter is identified with an ID (in brackets) and is shown alongside the characteristic it was used to measure.

Detector/Filter	Characteristic measured
90º Side Scatter detector (SSC)	Refraction of light to indicate cell size and surface characteristics
Filter for 530±15 nm light (FL1)	Green fluorescence signal (i.e. SYBR® Green stained DNA)
Filter for 585±21 nm light (FL2)	Orange fluorescence signal (i.e. phycoerythrin)
Filter for >650 nm light (FL3)	Red fluorescence signal (i.e. chlorophyll)

2.3.2 Data analysis

Cell concentration

Data were collected and analysed using Cell Quest Pro Software (Becton Dickinson), examples of which can be seen in Figures 2.3 and 2.4. In these images, each data point (or "event") refers to a particle passing across the laser light path. Clusters of events are seen to have similar characteristics and can be grouped ("gated") together for analysis.

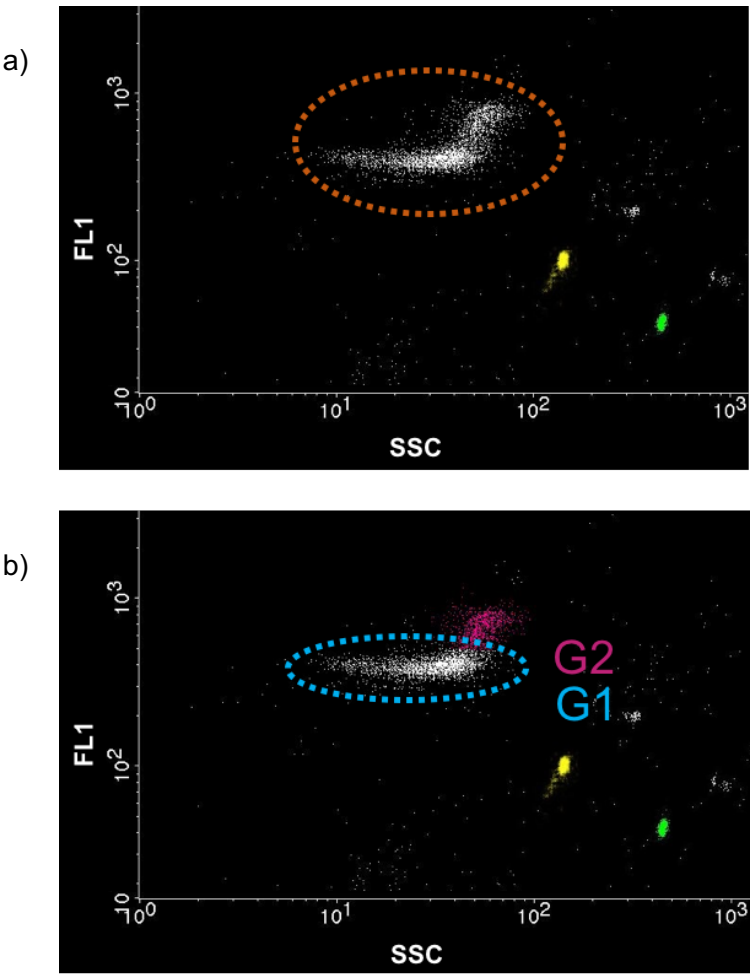

Figure 2.3: Example flow cytometric data file of a Halomonas culture
The plots show a typical profile from a laboratory culture of Halomonas. Green fluorescence (i.e. SYBR® Green stained DNA content, FL1) was plotted against side scatter (i.e. assessment of cell size, SSC). Plots were created in CellQuest Pro software (Becton Dickinson).
a) Circled in orange is the population of Halomonas cells. Highlighted in yellow and green are the 0.5µm and 1.0µm fluorescent beads, respectively. Above the beads are small clusters of bead doublets (i.e. multiple beads that have stuck together), which are not used for calculations or bead stock calibration.
b) The Halomonas population can be split into two stages of cell cycle (see text). G1 is circled in blue, and G2 phase (whereby the genome has replicated) is highlighted in pink.

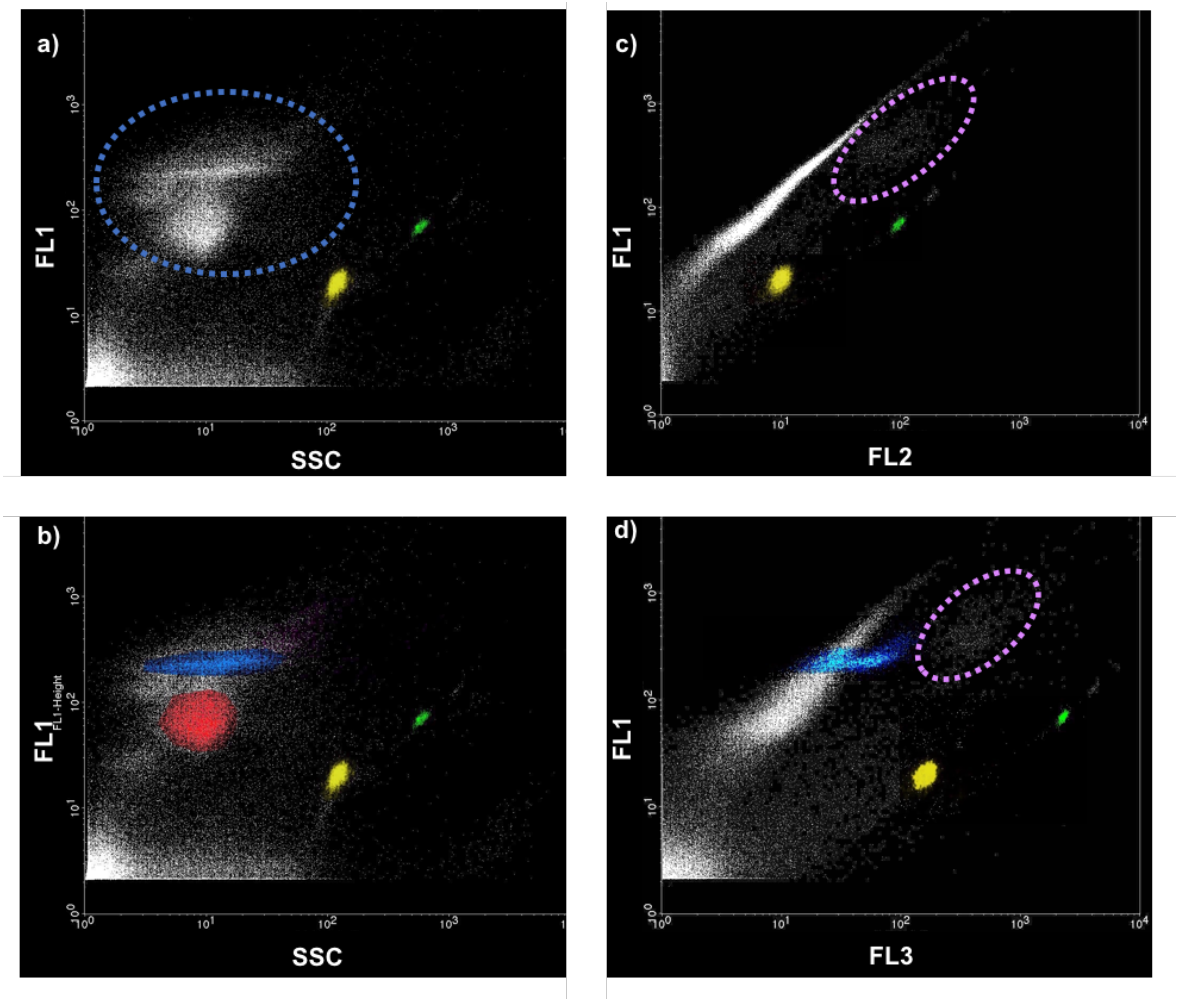

Figure 2.4: Example of flow cytometric data file of a typical bacterioplankton profile from seawater sample taken during an AMT cruise
Plots were created in CellQuest Pro software (Becton Dickinson).
a) *Plot of green fluorescence (FL1) (i.e. SYBR® Green stained DNA content) versus side scatter (SSC) (i.e. assessment of cell size). Circled in blue is the bacterioplankton community. Events below this can be considered noise [149,191], or could potentially indicate viruses [192].*
b) *This plot highlights specific populations seen in plot (a). The 0.5 µm and 1.0 µm beads are highlighted with yellow and green, respectively. Highlighted in pink is a clear population of smaller cells with a low DNA content, which can be identified as LNA bacteria. All other bacterioplankton can be considered as High Nucleic Acid (HNA) bacteria. Also, from plot (a), a denser band of cells can be seen in the centre of the bacterioplankton, highlighted in blue (plot (b)) and identified as Prochlorococcus (see plot (d)). Details of how these groups are identified is provided in the text.*
c) *Plot of green fluorescence (FL1) (i.e. SYBR® Green stained DNA content) versus orange fluorescence (FL2) (i.e. phycoerythrin content). Cells without phycoerythrin are shown in the main diagonal region and show a standard orange fluorescence:DNA ratio as determined from SYBR® Green staining alone. Synechococcus is distinguished as the population to the right of the main group and is circled in purple, with a higher orange fluorescence:DNA ratio due to the presence of phycoerythrin.*
d) *Plot of green fluorescence (FL1) (i.e. SYBR® Green stained DNA content) versus red fluorescence (FL3) (i.e. chlorophyll content). The main diagonal region shows a standard red fluorescence:DNA ratio as determined from SYBR® Green staining alone. Populations to the right of this have a higher red fluorescence:DNA ratio, indicating the presence of chlorophyll. Two groups are present here, with the lower but more dominant population representing Prochlorococcus (highlighted in blue), and the larger less abundant group representing Synechococcus (circled in purple).*

The 0.5 µm and 1.0 µm microbeads were used as internal standards for flow rate [190]. The number of events in each gate of 0.5 and 1.0 µm microbeads (Figures 2.3 and 2.4) could be compared to the known concentration of microbeads in the sample, thus providing the volume of sample analyzed (Equation 2.1).

Eq. 2.1 $$\frac{\textit{Number of microbead events}}{\textit{Concentration of microbeads in sample (beads/µL)}} = \textit{Volume analyzed (µL)}$$

Once the volume of sample analyzed was known, the concentration of cells in a sample could then be determined using the number of events in a cell gate (Equation 2.2) [193]. Accounting for dilution factors due to adding the bead stock, potassium citrate, PFA, and SYBR green to the flow cytometry sample, the concentration of cells in the original cell culture was determined (Equation 2.3).

Eq. 2.2 $$\frac{\textit{Number of cell events}}{\textit{Volume analyzed (µL)}} = \textit{Concentration of cells in analysed sample (cells/µL)}$$

Eq. 2.3 $$\frac{\textit{Original cell stock added to sample (µL)}}{\textit{Total volume of sample (µL)}} \times \textit{(Conc of cells in sample)} = \textit{Original cell stock conc (cells/µL)}$$

Cell cycle

Figure 2.3 shows the basic analysis of *Halomonas*, where stained DNA fluorescence is plotted against side scatter (FL1 vs SSC), thus providing an assessment of DNA content and cell size. Cells in different stages of their growth cycle may also be distinguished in this plot [194]. The *Halomonas* group can be split into two clusters. The cell size is similar (based on SSC), but they have different DNA contents (based on FL1). The upper G2

group has approximately double the DNA content of the lower G1 group, which is due to the genome replicating prior to cell division [194].

Seawater samples

Figure 2.4 shows a typical bacterioplankton profile of a seawater sample collected during the AMT cruises. Low Nucleic Acid (LNA) bacteria (dominated by SAR-11 [65,142]) are identifiable by their lower green fluorescence (i.e. lower DNA content) and side scatter (i.e. small cells) (Figure 2.4b) [142,189]. *Prochlorococcus* is identifiable due to a higher green fluorescence, side scatter, and red chlorophyll autofluorescence in comparison to heterotrophic bacteria (Figure 2.4d) [60,149]. *Synechococcus* can be separated from other cyanobacteria (i.e. *Prochlorococcus*) due to the presence of the photosynthetic pigment phycoerythrin, which is detected by its orange autofluorescence (Figure 2.4c) [60,150,189]. The remaining bacterioplankton population is termed high nucleic acid (HNA) bacteria, and may contain a wide range of species [189,195], which cannot be separated in this study by flow cytometry alone.

2.3.3 Calculation of cell concentration uncertainties

For laboratory cultures, multiple dilutions (e.g. x100 and x1000 dilutions) were made and analysed on the flow cytometer in order to produce replicate samples. Cell numbers were calculated for each replicate (accounting for dilutions), whereby an average and standard deviation for the sample was calculated. During AMT-24, triplicate flow cytometry samples were taken (no dilutions required for seawater samples) and the average and standard deviation was calculated.

For samples taken during AMT-25, uncertainties were calculated using the 0.5 and 1.0 μm microbeads (AMT-25 bead stocks calibrated by Priscila Lange, University of Oxford),

which worked as an internal standard. During any one run on the flow cytometer, multiple independent samples were analysed. As all of these samples used the same concentration of microbeads, differences in microbead event counts between these samples indicated the uncertainty of measurement. For each run on the flow cytometer, a coefficient of variance in microbead count was calculated, which was then used to determine uncertainty in individual samples. Table 2.2 below provides a worked example of this calculation.

Table 2.2: Worked example to calculate uncertainty in AMT25 cell counts
This example shows four different samples analysed consecutively, during the same flow cytometry run. Cell counts (in cells/mL) are already calculated and provided. As shown in the two 'Bead Events' columns, microbead counts vary from sample to sample, despite consistency in sample preparation and a theoretically equal microbead concentration. The average, standard deviation and coefficient of the difference in microbead events was calculated for the 0.5 µm and 1.0 µm microbeads (shown at the bottom of the table). The resulting two coefficients were averaged to produce an overall coefficient of variance for this run on the flow cytometer (0.0151). Finally, the error in cell concentration for each sample was calculated by multiplying the cell concentration with the average coefficient of variance (0.0151).

Sample	Cells/mL	Bead Events (0.5 µm)	Bead Events (1.0 µm)	Calculated error of cell count *(= cells/mL x 0.0151)*
1	857387	12751	4457	12959.8
2	1357031	13192	4389	20512.1
3	877681	12839	4318	13266.5
4	1546169	13078	4445	23371.0
average bead events ($\bar{x}$)		*12965.0*	*4402.3*	
standard deviation (σ^2)		*204.9*	*63.5*	
coefficient of variance ($\sigma^2/\bar{x}$)		*0.0158*	*0.0144*	
average coeff. of variance		***0.0151***		

2.4 Amino acid uptake

Amino acids form an important part of the dissolved organic matter pool in the marine environment [7]. In the marine environment, free amino acids are almost exclusively taken up by bacterioplankton [65,196]; for example, Gómez-Pereira *et al* (2012) showed no

statistical difference between methionine uptake in the total microbial community and bacterioplankton [65], and the same result was reported by Zubkov and Tarran (2008) for leucine and methionine uptake [196]. As amino acid uptake can be used as an assessment of protein synthesis [197], it can therefore be used as an indicator of the metabolic activity of bacterioplankton [e.g. 198].

Methods outlined in the following section are well-established protocols within the NOCS Microbial Plankton Group (e.g. Mary *et al* (2008), Hill *et al* (2011), Zubkov and Tarran 2005, Zubkov *et al* (2004, 2008) [188,198-201]). This project used amino acid uptake measurements in two ways: firstly, as a multi-concentration bioassay (termed 'Amino Acid Bioassay') during AMT-24 and AMT-25, and secondly in simple uptake measurements (termed 'Simple Amino Acid Uptake'), during laboratory and nutrient enrichment experiments.

2.4.1 Amino acid bioassay

The amino acid bioassay was carried out as described in previous studies (e.g. Wright and Hobbie (1966), Kirchman *et al* (1985), Mary *et al* (2008), Hill *et al* (2011), Zubkov and Tarran 2005, Zubkov *et al* (2004, 2008) [188,197-202]), with the basic principle being incubation of cells with various concentrations of an amino acid over various time periods. The bioassay allows calculation of amino acid uptake rate, as well as estimations of the concentration and total turnover time of ambient amino acid. In this project, two amino acids (whose uptake rates in plankton are strongly correlated [188]) were used: leucine (Leu) (during AMT-24) and methionine (Met) (during AMT-25). Leu is one of the most commonly found amino acids in cellular protein [203], thus should be readily assimilated by cells. Uniquely, Met contains a S atom, which can act as a reduced sulphur source for some bacterioplankton [204]. Additionally, a formylated version of Met is involved in bacterial protein synthesis initiation as the first amino acid of polypeptide chains [205]. Thus,

due to their abundance and importance, monitoring uptake of these amino acids provides a good indication of cellular protein synthesis. The procedure for measuring uptake of Leu and Met was broadly the same, although the high specific activity of Met meant that it had a marginally different setup to Leu. The following section describes a generic procedure for both amino acid bioassays, with a distinction between Met and Leu where appropriate.

An array of 24x 2 mL polypropylene (PP) tubes (Starlab) was set up as shown in Figure 2.5 for each assay. For the Met bioassay, (Figure 2.5a) 0.05 nM of radiolabelled Met (^{35}S-Met, Perkin Elmer, half-life 87 days) was added to each tube, as well as 0.1, 0.2, 0.4, 0.6, 0.8 or 1.0 nM of unlabelled ('cold') Met. For the Leu bioassay, (Figure 2.5b) 0.05, 0.1, 0.2, 0.4, 0.6, 0.8 or 1.00 nM of radiolabelled Leu (^{3}H-Leu, Hartmann Analytic, half-life 12.3 years) was added to each tube. A higher concentration of leucine was used compared to methionine due to the lower specific activity of ^{3}H compared to ^{35}S. Concentrations used were based on previous studies [e.g. 188,198], and were close to ambient concentrations in order to prevent the stimulation of low affinity transporters due to an artificially high amino acid concentrations [199]. To the amino acid, 1.6 mL of seawater sample was added to start the timed incubation. After approximately 10, 20, 30 and 40 min, each column of samples (Figure 2.5) was fixed with 80 µL of 20% PFA (final concentration 1%). Multiple time points (i.e. ~10, 20, 30, and 40 min) were used in order to allow calculation of uncertainty (Section 2.4.4).

Volumes of 10, 20, and 30 µL were taken from randomly selected samples that contained the highest concentration of amino acid (i.e. from tubes L22-24 or M22-24), and added to scintillation vials (20 mL, high-density polyethylene (HDPE), Meridian). These volumes were used to calculate radioactivity in the sample (Section 2.4.4), with the multiple volumes acting as replicates for uncertainty calculations (Section 2.4.4).

All fixed samples (including those samples that had 10/20/30 µL taken) were individually filtered (Section 2.4.3). The radioactivity maintained on the filters (i.e. retained within the cells) was measured, as described subsequently in Section 2.4.3.

a) ^{35}S-Met

	10min	20min	30min	40min	Cold Met
0.05nM	M1	M2	M3	M4	0.10nM
0.05nM	M5	M6	M7	M8	0.20nM
0.05nM	M9	M10	M11	M12	0.40nM
0.05nM	M13	M14	M15	M16	0.60nM
0.05nM	M17	M18	M19	M20	0.80nM
0.05nM	M21	M22	M23	M24	1.00nM

b) ^{3}H-Leu

	10min	20min	30min	40min
0.05nM	L1	L2	L3	L4
0.10nM	L5	L6	L7	L8
0.20nM	L9	L10	L11	L12
0.40nM	L13	L14	L15	L16
0.80nM	L17	L18	L19	L20
1.00nM	L21	L22	L23	L24

Figure 2.5: Experimental setup of the (a) Met and (b) Leu bioassay
Each grid represents a bioassay setup, whereby each square is an individually labelled sample tube. Values to the left of the grid show the concentration of radiolabelled amino acid added to the row. For the Met bioassay, the concentration of cold Met added is shown in green to the right of the grid. Approximate incubation times of each column are shown above each grid. The bioassay works so that each row receives an increasing concentration of amino acid and each column has an increasing incubation time; for example, the bottom right sample (M24/L24) will receive the highest concentration of amino acid and be incubated for the longest time period.

2.4.2 Simple amino acid uptake

This method was a streamlined version of the full bioassay. Instead of multiple concentrations, a single concentration of amino acid was added to cell samples. For the majority of laboratory-based experiments, ^{3}H-Leu was added to 2 mL PP tubes followed by 1.6 mL of cell culture, to give a final concentration of approximately 0.6 nM Leu. Nutrient addition experiments conducted during AMT-25 used 0.65 nM and 0.45 nM of Met (0.6 or 0.4 nM cold Met, plus 0.05 nM ^{35}S-Met, Chapters 3 and 4, respectively).

Samples were incubated between approximately 10-40 min before fixation with PFA, as described above. Samples of 10, 20 and 30 µL were taken from randomly selected samples and added to scintillation vials in order to determine the amount of radioactivity in each sample. Multiple time points (approximately 10, 20, 30, and 40 min) or volumes (10, 20, 30 µL) were taken to act as replicates to allow for calculation of uncertainty, as described in section 2.4.4. Finally, all samples were filtered and measured as described subsequently.

2.4.3 Filtration and measurement of samples

Once fixed with PFA, filtration of cells was the same for both the bioassay and the simple uptake experiment. A vacuum filtration manifold (DHI Lab Products) was set up as shown in Figure 2.6. Cellulose nitrate support filters (>0.45 µm pore size, 25 mm diameter, Whatman), wetted with deionized water, were placed on the filtration discs. A 0.2 µm, 25 mm, polycarbonate (PC) (Whatman) filter (again wetted with deionized water) was placed on top of the support filters. A pressure of approximately 0.4 bar [206] was maintained using the vacuum pump (Laboport, KNF) and a filter funnel was placed over each membrane. Samples were passed through the filters, and 2 x 3 mL deionized water was used to rinse the filter, washing away any unassimilated amino acid, meaning only intracellular radioactivity was measured. Once all liquid had passed through, the 0.2 µm PC filter membranes were removed and placed inside scintillation vials. Five mL of scintillation cocktail (Gold Star, Meridian) was added to all vials (including those with the 10, 20, and 30 µL volumes), before samples were counted using a Liquid Scintillation Counter (LSC) (Tri-Carb 3180 or Tri-Carb 2910, Perkin Elmer), using QuantaSmart software. Radioactive measurement using a LSC is dependent on the scintillation cocktail, which consists of an aromatic organic group and a light emitting scintillator [207]. Radioactive decay from the sample excites the aromatic group of the cocktail and transfers the energy to the

scintillator [207]. This energy is emitted as light energy, which can be quantifiably measured by a photomultiplier within the LSC [207]. Samples were counted for 2 min, using a counting window of 4-18.6 and 18.6-168 keV for ^{3}H-Leu and ^{35}S-Met, respectively, which were calculated based on the decay energy of the radionuclide. Radioactivity was measured in counts per minute (CPM). The LSC was calibrated using ^{3}H, ^{14}C and background standards (Perkin Elmer) and a pre-set protocol within the QuantaSmart software. All runs included a blank sample (a scintillation vial containing only scintillation cocktail), which was used to check background signal.

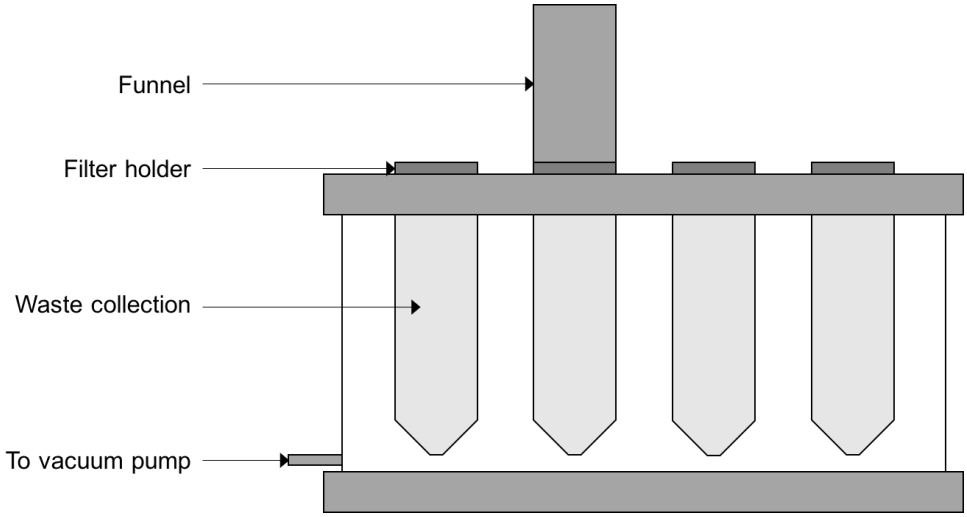

Figure 2.6: Diagram of the vacuum filtration manifold used to filter cell samples
Illustrative representation of the filtration manifold (side view) (DHI Lab Products). Wetted cellulose nitrate and PC filter membranes are placed onto the filter holders. A vacuum pump is used to maintain the pressure at approximately 0.4 bar. A funnel is placed on all filter holders (only one is represented in the figure) to allow easier filtration. Upon filtration of the cell sample, the cells are trapped in the filter membranes, and the liquid passes through into the waste, including unassimilated radionuclides. Up to 10 samples can be filtered at any one time using this manifold.

2.4.4 Data analysis

As described in Hill *et al* (2011) and Zubkov *et al* (2003) [60,198], linear regression analysis was used to determine the rate of amino acid uptake. In addition, the ambient amino acid concentration and turnover time was calculated for the bioassay experiments. In order to explain the analysis effectively, worked examples are explained in the following sections,

with an example dataset for the bioassay and simple amino acid uptake presented in Tables 1.2 and 1.3, respectively.

Table 2.3: Example dataset from a Leu bioassay
Provided is an example data set of a Leu bioassay conducted during AMT-24. Tubes are labelled according to the setup outlined in Figure 2.5. Samples in italics and highlighted in grey represent the volumes taken for radioactivity calculation. Equations or figures that relate to a column are identified in the column header. Note that the column header in italics (Actual Volume) refers to the radioactivity calculation, also in italics, and the 'Incubation Time' refers to all other non- italic values in the column.

Sample ID (Fig. 2.5)	**Leu in sample (nM)** (Fig. 2.5)	**Incubation time (min), or *Actual Volume (µL)***	**CPM assimilated**	**CPM in Tube** (Eq. 2.5 & 2.6)	**CPM/min** (Fig. 2.8)	**Uptake Time (hr)** (Eq. 2.9)
10 µL		*9.524*	*1091*			
20 µL	*1*	*19.048*	*2144*	180,800	-	-
30 µL		*28.571*	*3244*			
L1		11	500.5			
L2	0.05	20	935.5	9,040	38.7	3.9
L3		30	1067.5			
L4		40	1707.0			
L5		11	655.0			
L6	0.1	20	1292.5	18,080	54.4	5.5
L7		30	1481.0			
L8		40	2351.5			
L9		11	862.5			
L10	0.2	20	1577.0	36,160	81.2	7.4
L11		30	2176.5			
L12		40	3285.0			
L13		11	1067.5			
L14	0.4	20	2040.0	72,320	94.4	12.8
L15		30	2794.5			
L16		40	3869.0			
L17		11	1285.5			
L18	0.8	20	2228.0	144,640	113.6	21.2
L19		30	3324.5			
L20		40	4589.0			
L21		11	1307.5			
L22	1	20	2441.0	180,800	116.2	25.9
L23		30	3405.0			
L24		40	4745.0			

Table 2.4: Example dataset from a simple Leu uptake experiment
Provided is an example data set of a simple Leu uptake experiment. Samples in italics and highlighted in grey represent the volumes taken for radioactivity calculation. The radioactive concentration in this example is 88 CPM/µL, and for a sample volume of 1600 µL, this equates to 141917 CPM in each tube (Equation 2.5). The ratio of CPM:mol (Equation 2.7) allowed the measured CPM assimilated to be converted to fmol (Equation 2.8). Equations or figures related to a column are identified in the column header.

Sample ID	**Leu in sample (nmol)**	**Incubation time (min), or *Actual Volume (µL)***	**CPM assimilated**	**Leu assimilated (fmol)** (Equations. 2.7 and 2.8)
10 µL	*9.3E-04*	*9.524*	*860*	-
20 µL		*19.048*	*1852*	-
30 µL		*28.571*	*2539*	-
1	*9.3E-04*	11	15140	99
2		34.5	49045	320
3		49	56439	370
4		61.5	67963	450

Amount of radioactivity in a sample

The initial step for any amino acid uptake calculation was to determine the amount of radioactivity in any one sample tube. This used the 10, 20, 30 µL volumes that were taken from sample tubes. The actual volume of these samples was initially adjusted to account for the 80 µL of PFA added at the end of the incubation, which will have caused a minor dilution in the concentration of Leu/Met to which cells were originally exposed (Equation 2.4).

Eq. 2.4 $\textit{Volume pipetted} \times \frac{1600}{1680} = \textit{Actual Volume pipetted}$

e.g. Table 2.3, 10µL $10\ \mu L \times \frac{1600\ \mu L}{1680\ \mu L} = 9.524 \mu L$

These volumes were then plotted against measured radioactivity (count per minute, CPM). Example CPM values are provided in the top 3 rows of Table 2.3 and Table 2.4, and example data is plotted in Figure 2.7. The slope of the graph (Figure 2.7) provided the concentration of radioactivity in the tubes from which the 10, 20, 30 µL samples were taken, with the error of the slope accounting for uncertainty in sample measurement and pipetting accuracy (± 1.17 CPM/µL, see Equation 2.10 for calculation of error). Using this value (e.g. 113 CPM/µL for Table 2.3) the total radioactivity in these tubes was then calculated (Equation 2.5).

Eq. 2.5 *Radioactive conc. (CPM/µL) × Sample volume (µL) = CPM in tubes L22–24 or M22–24*

e.g. Table 2.3 *113 CPM/µL × 1600 µL = 180,800 CPM*

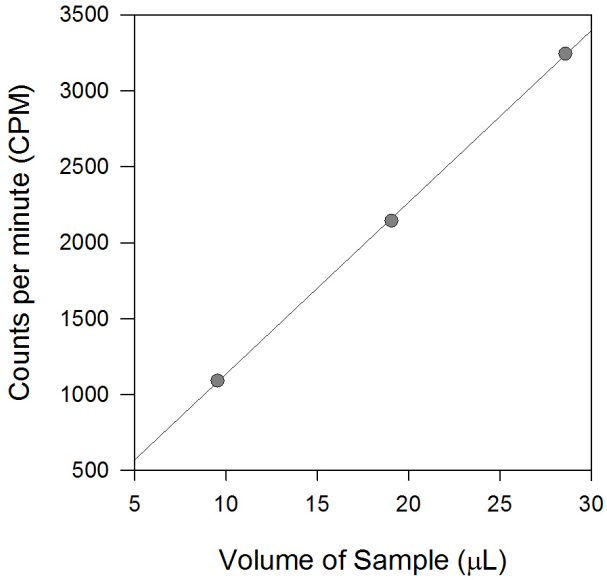

Figure 2.7: Determination of the radioactive concentration in sample measuring amino acid uptake
The CPM in each 10, 20, 30 µL sample is plotted against the adjusted volume (Equation 2.4). The slope of the graph provides the concentration of radioactivity in the tube. This example uses data from Table 2.3, and the concentration was calculated at 113 ± 1.17 CPM/µL. Using the sample volume (i.e. 1600 µL), the total amount of radioactivity added to the tube was then calculated (Equation 2.5).

For simple amino acid uptake, and for ^{35}S-Met bioassays, the amount of radioactivity added to different sample tubes did not change. However, the radioactivity concentration in L1-20 tubes will have differed as varying amounts of ^{3}H-Leu was added to these samples (Figure 2.5) (e.g. 0.05 nM in tubes L1-4); therefore, the CPM in each tube was adjusted accordingly (Equation 2.6)

Eq. 2.6 *CPM in first tube × Ratio of Leu = CPM in second tube*

e.g. 0.05 nM ^{3}H-Leu (Fig. 1.8, Table 2.3) $180{,}800\ CPM \times \frac{0.05\ nM}{1\ nM} = 9{,}040\ CPM$

If required, a ratio of CPM:mol was calculated (appropriate SI unit prefixes used, in this case CPM:nmol), which used the known concentration of amino acid added (e.g. 0.05 nM

Leu) to allow any measured CPM value to be converted to a mole value (Equations. 2.7 and 2.8).

Eq. 2.7 $\frac{\text{Total CPM in tube}}{\text{Total mol in tube}} = \text{Conversion Ratio (CPM/mol)}$

e.g. 0.05 nM Leu (Table 2.3) $\frac{9040\ \text{CPM}}{0.05\ \text{nM}} = 180{,}800\ \text{CPM/nmol}$

Eq. 2.8 $\frac{\text{Measured CPM}}{\text{Ratio (CPM/mol)}} = \text{Measured mol}$

e.g. Tube L3, Table 2.3 $\frac{1067.5\ \text{CPM}}{180800\ \text{CPM/nmol}} = 0.006\ \text{nmol}$

Amino acid bioassay

Once the amount of radioactivity in each tube was calculated, the uptake rate could be determined. For the bioassay, the original CPM values were used and not converted to moles. Assimilation rate (in CPM per minute) was established for each amino acid concentration by plotting CPM against incubation time, whereby the slope provided an uptake rate (CPM/min) (Figure 2.8) (Table 2.3). This was then used in combination with the total CPM in the sample tube to determine the time taken for the cells to take up all added amino acid in the tube for each concentration of amino acid (Equation 2.9) (Table 2.3).

Eq. 2.9 $\frac{\text{CPM in tube}}{\text{Uptake rate (CPM/min)} \times 60} = \text{Total uptake time of added Leu (h)}$

e.g. 0.05 nM ^{3}H-Leu (Table 2.3) $\frac{9040\ \text{CPM}}{\frac{38.7\ \text{CPM/min}}{60}} = 3.9\ \text{h}$

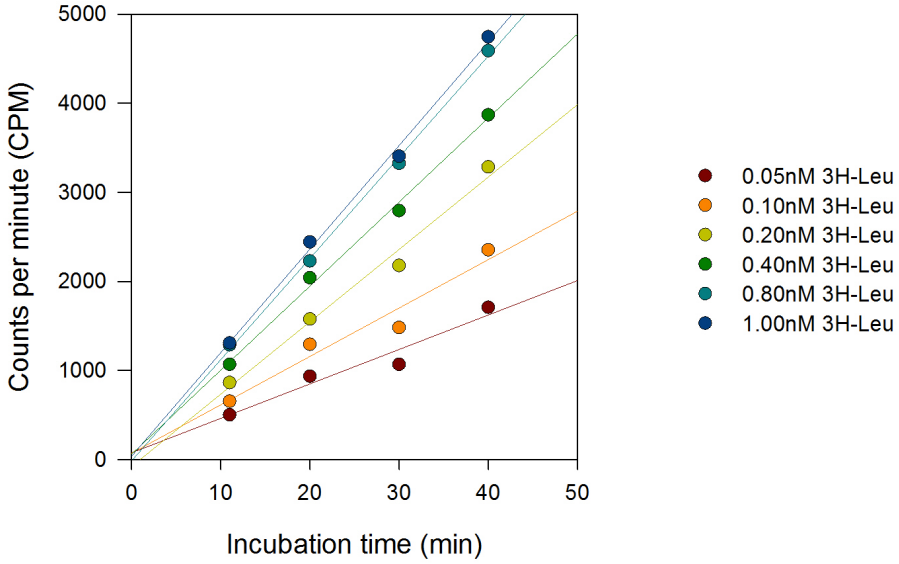

Figure 2.8: Individual uptake rates for each concentration of ^{3}H-Leu used in an example bioassay
For each concentration of ^{3}H-Leu, the radioactivity measured (CPM) was plotted against the incubation time, for which the slope provides an uptake rate in CPM/min. This plot shows the uptake rate for each concentration of ^{3}H-Leu, incrementally coloured as shown on the right.

These total uptake times were plotted against their respective concentration of Leu in each sample (Figure 2.9). The y-axis intercept indicated the turnover time of ambient Leu, with standard error of regression (calculated using the STEYX function in Microsoft Excel) used as the level of uncertainty [60,198]. The inverse of the slope indicated uptake rate (nM/hr), with the uncertainty of this measurement based on the error of the slope (Equation 2.10) [60,198]. Finally, the x-axis intercept provided an assessment of ambient Leu concentration, with uncertainty calculated from the error of propagation, using the uncertainties of the slope and y-intercept [60,198]. For all stages of calculation, outliers were eliminated based on being 3 standard deviations away from the mean.

Eq. 2.10
$$\frac{\textit{Standard error of regression}}{\textit{(standard deviation of x-values)} \times \sqrt{\textit{(number of x values)}}} = \textit{Error of slope}$$

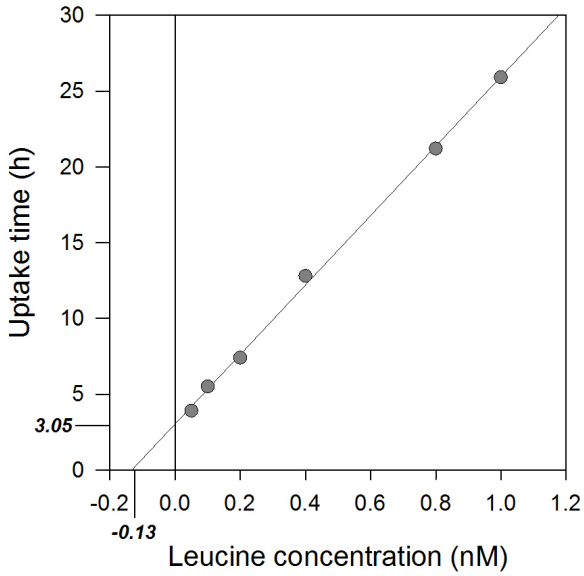

Figure 2.9: Leucine uptake rate, turnover time of leucine and ambient concentration of leucine from an example bioassay
Uptake time of each Leu concentration (Equation 2.9) is plotted against the concentration of Leu added to the samples. The inverse of the slope provides the uptake rate (0.044 ± 0.001 nM/h), the y-axis intercept shows turnover time of the ambient Leu (3.05 ± 0.37 h), and the x-axis intercept indicates the concentration of ambient Leu (0.13 ± 0.02 nM). The ambient concentration can also be calculated by multiplying the uptake rate by the turnover time.

Simple Leu uptake

As before, the radioactivity in each tube was initially calculated, and a CPM:mol ratio was determined (Equation 2.7). As only one concentration was used for simple uptake, the CPM in each experimental tube did not change. The CPM values measured in each filtered sample (i.e. the amount of Leu assimilated) was then converted to an amount in moles (Equation 2.8). Finally, uptake rate was calculated by plotting the amount of Leu assimilated against incubation time, whereby the slope represented the uptake rate in fmol/min (Figure 2.10), and the y-axis intercept shows any background adsorption. Uncertainty in uptake rate is calculated from the error of the slope (Equation 2.10).

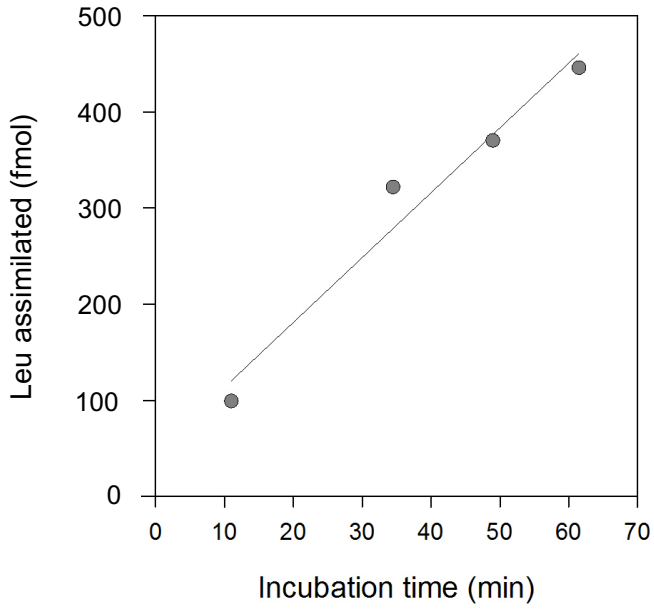

Figure 2.10: Determination of leucine uptake rate from an example simple uptake experiment
The plot shows the concentration of Leu assimilated versus incubation time, whereby the slope provides the uptake rate (6.7 ± 0.8 fmol/min), and uncertainty is calculated based on the error of the slope (Equation 2.10).

2.4.5 Uptake of radiolabeled iron and cobalt

In Chapters 4 and 5, iron assimilation was also assessed using radiolabelled iron (^{55}Fe or ^{59}Fe). Assimilation rates were calculated in the same manner as the simple amino acid uptake, whereby a single concentration of iron was incubated in multiple samples for an increasing incubation time (although on the scale of hours, not minutes to account for a slower cell assimilation rate of iron). Assimilation rates were based on linear regression of amount of assimilated iron against time, with the error of the slope providing the uncertainty in uptake. If there was no linear increase over time (i.e. radioactivity measurement remained constant), then rapid extracellular sorption was assumed; in these scenarios, the incubation times were disregarded and samples treated as replicates,

allowing the calculation of an average amount of sorbed iron per sample, and standard deviation used as the uncertainty.

Iron-59 was purchased from Perkin Elmer (1280.06 MBq/mL, 2727.16 MBq/mg). As it has a short half-life (44.6 days), experiments were done within 2.4 half-lives of delivery.

Iron-55 was commercially produced via proton bombardment at the University of Birmingham to the specifications set out by Geosciences Advisory Unit (GAU), Southampton. Two sources of ^{55}Fe were used in this study. Measurement and data analysis of these sources was conducted by Phil Warwick of GAU, using a LSC (Wallac Quantulus 1220) and mass spectrometer (Agilent 8800) to allow quantification of active and stable iron in each source (Table 2.5). Counts were performed in September 2014, and experiments were performed within one half-life (2.7 years) of this date. Known ratios of ^{55}Fe and stable iron (based on measurement, Table 2.5) allowed for the calculation of total iron added from the source.

Table 2.5: Concentration of iron in the two ^{55}Fe sources used in this study
For each source, the contribution of stable and active (^{55}Fe) iron is presented.

Source	Stable iron (nM)	Fe55 (nM)	Total Iron (nM)
A	940.10	17.24	957.35
B	259.65	31.30	290.95

For Chapter 6, the formation of particulate cobalt was assessed using radiolabelled cobalt (^{57}Co). These experiments, and subsequent data analysis, were normally conducted in the same manner as for iron, whereby a single concentration of cobalt was incubated in multiple replicates for an increasing time (exceptions discussed in Chapter 6). Co-57 was purchased from Perkin Elmer (3880.30 MBq/mL, 312.02 GBq/mg). Experiments were conducted within 6 months of purchase, which is within one half-life of ^{57}Co (271 days).

2.5 Cell culturing

2.5.1 Model bacteria

Halomonas

The majority of laboratory work used *Halomonas sp.* as the primary model bacteria. *Halomonas* are a genus of gammaproteobacteria, first characterised by Vreeland *et al* (1980) [208]. *Halomonas* are able to grow in salinities of approximately 3 to 20% [208,209], and at approximately 20 to 37ºC [209], although they have been stored successfully at temperatures as low as 4ºC [208]. They are also able to survive in a pH range between 5 and 9 [208]. The ease of laboratory culturing and ability to grow under conditions that can mimic the open ocean (i.e. ocean salinity is around 3.5% [210], and surface temperature of the majority of the ocean is ca. 5-30ºC [211]) made *Halomonas* an ideal model bacteria for this project.

Based on established protocols of the Microbial Plankton Group (NOCS) *Halomonas sp.* were grown on Difco marine agar (2216, BD) in petri dishes. Plates were prepared by dissolving 27 g of the dry marine agar in 500 mL deionized water before being autoclaved (210047, Prestige Medical) for 15 min at 121ºC and poured into petri dishes using aseptic technique (i.e. next to a Bunsen burner and under a biological safety cabinet (Herasafe)). Cultures were stored at 4ºC with sub-culturing onto a new agar plate every couple of weeks, again using aseptic technique. For each experimental run, a fresh agar plate was inoculated with *Halomonas* the day before and stored at room temperature. After an overnight incubation and working with aseptic technique as above, a swab of cells was collected from the agar using a sterile loop and re-suspended into either artificial seawater (ASW), or aged Atlantic seawater (AASW) that had been previously collected (in the middle of the North Atlantic subtropical gyre during the cruise D369 (R.R.S. Discovery) in

August-September 2011) by the Microbial Plankton Group, NOCS. The re-suspended cells were then filtered through a 1.0 µm PC filter (Whatman) to create a uniform cell suspension for use in experiments.

Aurantimonas

In addition to *Halomonas*, a second marine bacterial species was also used in specific experiments: *Aurantimonas sp.* (ATCC BAA-1229). *Aurantimonas*, is a genus of alphaproteobacteria found within the order *Rhizobiales*, and was first termed by Denner *et al* (2003) [212]. A noteworthy feature of *Aurantimonas* is that of its ability to stimulate manganese oxidation, converting Mn(II) to Mn(III/IV) [213,214]. Cells are able to grow at temperatures of 4-37ºC and at salinities of 0-15% [213], again allowing conditions of the open ocean (i.e. salinity of ~3.5% [210], temperature of ca. 5-30ºC [211]) to be simulated in the laboratory.

Aurantimonas media and cultures were prepared and maintained by Manuela Hartmann of the Microbial Plankton Group, NOCS. Cells were grown in media termed either 'manganese-replete', which was standard M media [215] or ATCC® 2584 media, or 'manganese-limited', which was altered M-media containing no manganese chloride, peptone or yeast (Appendix A). To prepare the cells for experimentation, the *Aurantimonas* culture was filtered through a 1.0 µm PC filter (Whatman) to remove cell aggregates and create a uniform cell suspension.

2.5.2 Artificial seawater

Based on the method of Wilson *et al* (1996), 25 g of sodium chloride was dissolved into ~900mL of deionized water. To this solution, a number of salts were added, achieving the following concentrations: 88 µM sodium nitrate, 98 µM magnesium chloride, 33.5 µM

potassium chloride, 22.5 µM calcium chloride, 0.142 mM magnesium sulphate, 49.94 µM Tris, and 0.43 mM dipotassium phosphate. The pH was adjusted to pH 8.0 using concentrated hydrochloric acid (Analytical grade) and the solution made up to 999 mL with deionized water. Finally, 1 mL of a trace metal stock solution (previously prepared by Manuela Hartmann) was added, providing 46.3 µM boric acid, 9.1 µM manganese chloride, 0.8 µM zinc chloride, 1.6 µM sodium molybdate, 32 nM copper sulphate, 0.2 µM cobalt nitrate, 11.1 µM iron chloride and 1.4 µM ethylenediaminetetraacetic acid disodium magnesium salt (final concentrations). The final seawater solution was then autoclaved at 121ºC for 15 min.

2.6 Statistical significance of data

In order to determine statistical significance between two data sets, a paired or unpaired (as appropriate for the data) Student's t-test (two-tailed) was performed, using a significance value of 0.05. A p value of less than 0.05 shows statistically significant difference between the two data sets analysed, whereas a p-value of more than 0.05 showed no statistical difference. If the normality check failed, then a Mann-Whitney rank sum test or a Wilcoxon signed rank test was performed for unpaired or paired data sets, respectively. All tests were performed using Sigma Plot 12.5 software.

Alongside the t-test, the variances of the two data sets was analysed using the F-test, whereby an F-value less than the critical value, indicated equality in variances between the two datasets (accept the null hypothesis). As two-tailed tests were performed, the critical F value was determined from a F-distribution chart using an alpha value of 0.025 (0.05 halved)

.

Chapter 3: Bacterioplankton response to inorganic nitrogen and phosphorus additions in the North Atlantic subtropical gyre

3.1 Introduction

Oligotrophic subtropical gyres have extremely low nutrient concentrations and yet comprise over 40% of the world's oceans [e.g. 33]. Due to the effects felt from climate change, increasing sea surface temperatures and ocean stratification are resulting in the expansion of these regions [35-38], with the North Atlantic Gyre (NAG) (see Chapter 1, Section 1.2.3, and Appendix B) proposed to be subject to the highest rate of expansion [37].

Bacterioplankton dominate oligotrophic waters [2,13], with the cyanobacteria *Prochlorococcus* and the heterotroph SAR-11 being the two most prevalent species [142,191]. For example, Campbell and Nolla (1994) showed that 31% of bacterioplankton counts in the upper 100 m of the North Pacific Ocean were *Prochlorococcus* [13], and Mary *et al* (2006) saw 36±6% of total bacterioplankton were LNA bacteria [142] (LNA bacteria primarily consist of SAR-11 [65,142]). The growth of a microbial population is controlled by top-down factors such as predation, and bottom-up mechanisms such as nutrient availability [7]; therefore, the reduced availability of biologically essential nutrients in oligotrophic gyres may limit plankton growth [7,53]. As the oceans contribute approximately 50% of global primary production, with higher production levels occurring out of the gyres [1], the potential expansion of these low nutrient waters and the consequent limitation of phytoplankton growth could be highly detrimental to the global ecosystem; indeed, ocean primary production has been suggested to have decreased by 6.3% since the 1980s [35].

In the surface NAG, concentrations of nitrogen and phosphorus, two key biological elements, are present at very low concentrations [53]. Low oceanic nitrogen availability appears to be a widespread phenomenon [53]. Nitrate concentrations in the oligotrophic surface ocean are typically <100 nM compared to micromolar concentrations in other oceanic regions (e.g. 1.5 μM in the Canary current coast province, see Figure 1.3; and 33 μM in the Benguela Upwelling [54]) [7,54]. This can also be seen in additional nutrient data provided by the British Oceanography Data Centre (contains data supplied by the Natural Environment Research Council) for AMT-25 (Appendix B), where most of the surface ocean (≤100 m) along the AMT-25 transect had a NO_3^- + NO_2^- concentration less than 0.02 μM. Additionally, ammonium concentrations in oligotrophic surface waters are generally <0.05 μM, compared to higher values (generally <0.5 μM) found in more productive waters (e.g. 0.3 μM in the Canary current coast province, see Figure 1.3; and 5.2 μM in the Benguela Upwelling [54]) [7,54].

Phosphorus concentrations are also very low in the NAG [e.g. 66,216]. As discussed in Chapter 1, poor nutrient supply and strong stratification contribute to low nutrient concentrations in the gyres [e.g. 4,19,33]. However, the concentration of phosphate in the NAG is very low in comparison to the South Atlantic gyre (SAG) (see Appendix B). This has been proposed to be a consequence of iron inputs from desert dust [66,217,218], which leads to an increased level of nitrogen fixation [134], resulting in phosphorus drawdown relative to nitrogen, and the bioavailable pool of phosphate being rapidly diminished [66,216,217]. As a result, phosphate concentrations in the NAG are significantly lower (<9 nM) in comparison to the South Atlantic gyre [66,216] (e.g. 210 nM PO_4^{3-} in the South Atlantic gyre [66]).

Nutrient enrichment bioassays can be used as a method to indicate nutrient limitation, providing all other variables are unchanged [122]. Upon nutrient addition, an increase in a parameter (such as cell growth or primary production) may signify limitation. For example, Rivkin and Anderson (1997) proposed phosphorus limitation of bacterial growth in the Northwest Atlantic due to an increase in growth upon addition of phosphate (either alone

or in combination with glucose or ammonium) [135]. Several such studies have been conducted in the NAG in an attempt to determine whether the low concentrations of nitrogen and phosphorus limit the growth or physiology of bacterioplankton. The western North Atlantic has been extensively studied [e.g. 128,131-133,135,219], leaving the east under-represented; therefore, to address this, this study conducted nutrient enrichment experiments in the central-eastern North Atlantic. The north-south AMT transect analyzed in this study is of particular interest as it passes through the centre of the NAG, and covers the more productive waters on either side; thus, allowing a direct comparison between cells both inside and outside of the NAG. Furthermore, this investigation was conducted in September and October, after the boreal spring bloom when the concentration of nutrients in the surface ocean are very low [153,220]. Therefore, the temporal and seasonal features of this study makes it distinct from the majority of other studies that have assessed nitrogen and phosphorus additions in alternative seasons [e.g. 123,124,136] and locations [e.g. 221, and studies in the western North Atlantic], thus providing information on potential nutrient limitation in an under-studied region of the ocean and expanding the understanding of the effects of low nutrient concentrations across the whole of the North Atlantic. Additionally, this study focuses on the total bacterioplankton population (including heterotrophic and photosynthetic bacteria) in the central-eastern North Atlantic, which is underrepresented in comparison to studies on phytoplankton in the same area [e.g. 134,177,221].

The effects of inorganic nutrient additions have been assessed in heterotrophic bacteria [e.g. 124], phytoplankton [e.g. 123,132,134,136,221] and the total bacterial community [e.g. 128,131-133,135,219]. However, total bacterioplankton abundance should be assessed in combination with analysis of individual groups that may respond differently to the community, perhaps reflecting adaptation for survival in the NAG. Mills *et al* (2008), for example, observed different responses to nutrient additions in two different groups of bacterioplankton [124]. Flow cytometry was chosen for this study to measure changes in bacterioplankton, as it has been demonstrated to be an ideal tool for ship board enumeration [222], thus allowing

changes in abundance to be monitored after incubation with added sources of nitrogen and phosphorus. Additionally, flow cytometry allows the characterisation of specific bacterial groups, based on their relative size and fluorescence properties [60,142,189], with the key groups analysed being: *Prochlorococcus*, *Synechococcus*, small heterotrophic low nucleic acid (LNA) bacteria (primarily consisting of SAR-11 cells [65,142]), and heterotrophic high nucleic acid (HNA) bacteria. As an additional measure, changes in methionine (Met) uptake rate were also monitored. Met uptake is almost entirely carried out by bacterioplankton [65,196,201]. For example, Gómez-Pereira *et al* (2012) noted there was no statistical difference (t-test, p-value = 0.17) between total microbial methionine uptake and bacterioplankton methionine uptake (bacterioplankton separated from total via flow cytometric sorting) [65]. Thus, methionine uptake can be used as a proxy for bacterioplankton metabolic activity by assessing protein synthesis [197].

As the preferred sources of nitrogen and phosphorus for bacterioplankton [223-225], ammonium (NH_4^+) and phosphate (PO_4^{3-}) were added to seawater samples before a 2-day incubation, a duration that was in line with times used by previous studies [e.g. 123,124,133,221]. Indeed, Cotner *et al* (1997) noted the maximum response of bacterioplankton to nutrient additions was between 24 and 48 h [133]. Additionally, a short-term incubation period (2-3.5 h) was used as a control to indicate if addition of synthetic ammonium and phosphate negatively affected cell abundance or metabolic activity.

This study aimed to examine the effect of NH_4^+ and PO_4^{3-} additions on bacterioplankton in the oligotrophic North Atlantic, which has been shown to have very low concentrations of nitrogen and phosphorus [7,53,54,66,216]. Cell growth and metabolic activity (using radiolabeled amino acids) were monitored, whereby an increase in these parameters would indicate a positive response to the nutrient enrichments and thus potentially indicate limitation. In addition to total community analysis, individual bacterioplankton groups were assessed for changes in cell abundance, including *Prochlorococcus*,

Synechococcus and heterotrophic bacteria, to assess potential differences in responses to nutrient additions.

3.2 Methods

3.2.1 Seawater sample collection

This study was conducted during the 25th Atlantic Meridional Transect (AMT-25) cruise aboard the R.R.S. James Clark Ross (JCR) in September and October 2015. Seawater samples were routinely collected, along a north south transect (Figure 3.1 and Table 3.1), using a 10 L Go Flo bottle (Ocean Test Equipment), deployed to a depth of 30m using a plastic-coated wire, at approximately solar noon. The Go Flo bottle was then transferred to a laboratory container and secured adjacent to a laminar flow hood. Seawater was collected from the bottom of the bottle using acid cleaned tubing (Chapter 2, Section 2.2.1), with a Acrovent 0.2 µm filter (Pall Corporation) attached to an inlet at the top to prevent particulate contamination from the air (Chapter 2, Section 2.2).

A small water sample (<100 mL) was collected for initial on-ship analysis of cell abundance and identification of major cell populations, via a well-established flow cytometric protocol [e.g. 150,184,188,189]. A detailed description of this method is covered in Chapter 2 (Section 2.3). Additionally, a Met bioassay was conducted on this sample, which assessed Met uptake rate, ambient Met and total turnover time of Met, as described in Chapter 2 (Section 2.4) and outlined in previous studies [e.g. 188]. The remaining water was then used for the nutrient addition experiments.

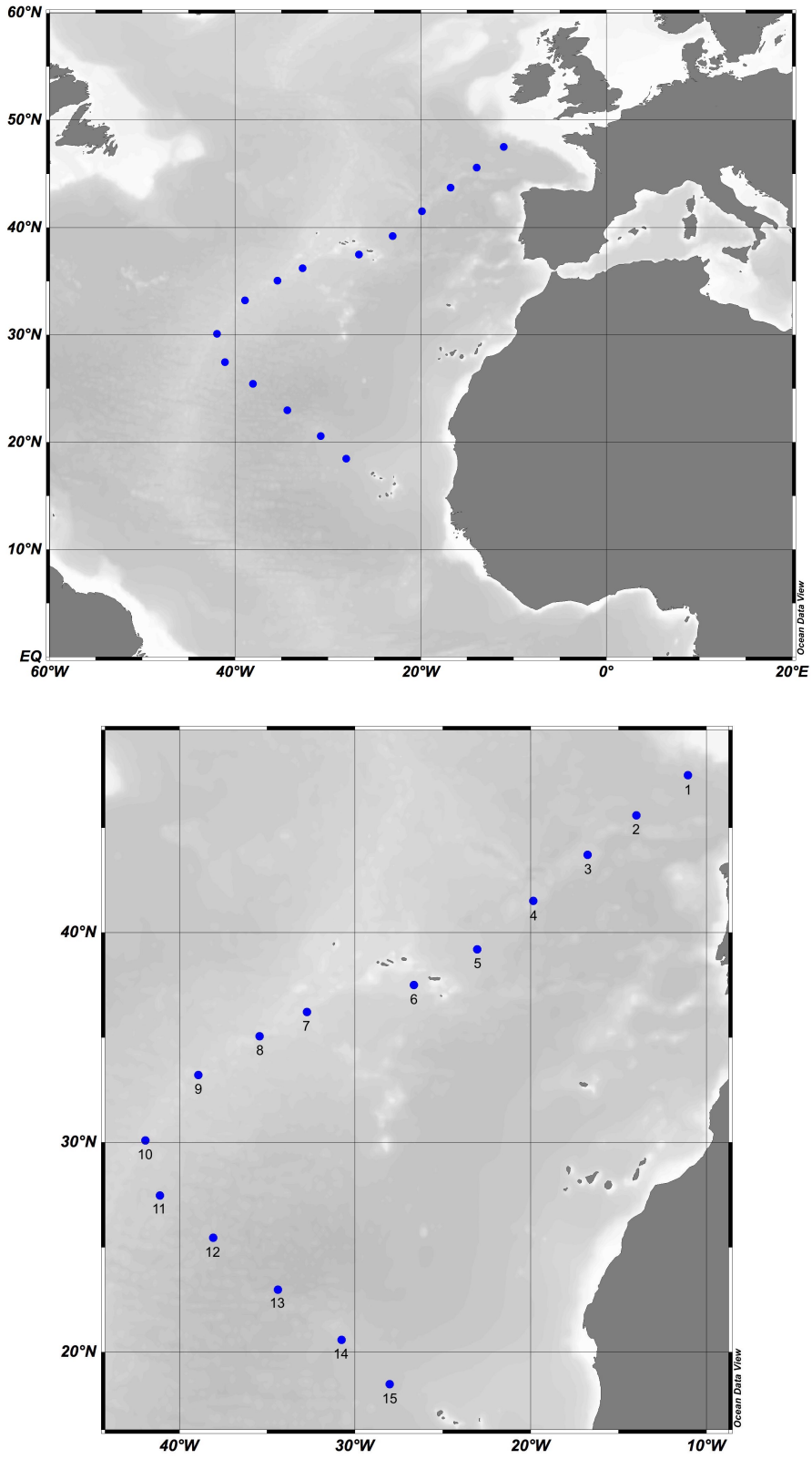

Figure 3.1: Location of sampling stations in the North Atlantic during AMT-25
Maps created using Ocean Data View Software 4.7.10 [181]
Top: Overview of cruise track in the North Atlantic
Bottom: Magnified view of station locations and IDs, details shown in Table 3.1

Table 3.1: Locations of sampling stations during AMT-25
Table shows co-ordinates of each sampling station, deployment time and station ID. Experiments conducted are highlighted in the final two columns, including nutrient addition experiments and the additional short term incubation. Stations deemed inside the NAG are highlighted in grey in the table.

Station ID	Date and Time (GMT)		Latitude	Longitude	Nutrient Addition Experiment?	Additional short term incubation?
1	19/09/15	14:06	47.51	-11.06		
2	20/09/15	13:15	45.59	-13.99		
3	21/09/15	13:16	43.71	-16.78		
4	22/09/15	13:06	41.52	-19.87	✓	✓
5	23/09/15	13:07	39.20	-23.05		
6	24/09/15	13:04	37.51	-26.66	✓	✓
7	27/09/15	14:25	36.22	-32.75	✓	✓
8	28/09/15	13:20	35.06	-35.44	✓	
9	29/09/15	13:24	33.22	-38.92	✓	✓
10	30/09/15	13:09	30.10	-41.94	✓	
11	01/10/15	13:24	27.47	-41.11	✓	✓
12	02/10/15	13:25	25.45	-38.07	✓	
13	03/10/15	13:12	22.99	-34.39	✓	
14	04/10/15	13:11	20.58	-30.77	✓	
15	05/10/15	13:18	18.48	-28.33	✓	

3.2.2 Nutrient addition experiments

Whilst working in a laminar flow hood, 200 mL seawater samples were collected from the Go Flo in acid-cleaned (~1 M, Chapter 2, Section 2.2.1) 250 mL high-density polyethylene narrow neck bottles (Nalgene). To each sample bottle, an inorganic nitrogen source (ammonium chloride, NH_4Cl (Sigma Aldrich, UK)) and/or an inorganic phosphorus source (sodium hydrogen phosphate, Na_2HPO_4 (Sigma Aldrich, UK)) was added to final

concentrations as outlined in Table 3.2. For ease, these additions will be referred to using the sample notation shown in Table 3.2, or simply as 'ammonium' or 'phosphate' from here on. These nutrient concentrations were selected based on the methods of previous studies [e.g. 123,128,131]. In addition, a sample was left without any nutrient additions to act as the control (Ctl).

Samples were then transferred to an adapted recirculating water-bath (Grant Instruments, UK), maintained within approximately 2ºC of the ambient underway temperature. A diode light array (Photon Systems Instruments) illuminated samples from below between the hours of sunrise and sunset, at an intensity of approximately 300 µE/m/s.

After 2-3.5 h (referred to as 'short-term incubation'), and ~48 h ('long term incubation', specifically between 47-51 h), a 50 mL aliquot was taken from each incubation and used for on-ship flow cytometric analysis of cell abundance and bacterioplankton characterization (Chapter 2, Section 2.3). Additionally, the aliquot was used to perform a simple Met uptake experiment (see Chapter 2, Section 2.4) to assess cellular metabolic activity. After sampling the short-term aliquots, the incubations were returned to the water bath; however, after sampling at 48 h, the remaining incubation was discarded. The empty bottle was cleaned by filling with ~1M hydrochloric acid (see Section 2.2.1) for approximately 24 h before re-use in a subsequent incubation. Bottles were rinsed three times with seawater from the Go Flo before a new incubation, and nutrient additions were only added to bottles that previously contained the same added nutrient (i.e. control bottles were never previously used for nutrient addition incubations).

Table 3.2: Final concentrations of ammonium/phosphorus added to seawater incubations
Please note the sample notation highlighted in this table.

Sample Notation	Final concentration of added nutrient (µM)	
	NH_4^+	PO_4^-
Ctl	0	0
+N	1	0
+P	0	0.1
+NP	1	0.1

3.2.3 Data analysis of nutrient addition experiments

To determine the effect of added macronutrients, the cell concentration and Met uptake rate for each +N, +P, or +NP incubation was compared against each respective control incubation. Met uptake was presented as a fraction of Met assimilated per cell per hour (Equation 3.1) in order to allow comparison between different experiments. Scatter plots visualised the differences at each station, and percentage change from the control allowed quantification (Equation 3.2).

Eq. 3.1 $$\frac{\textit{Uptake (CPM/h/cell)}}{\textit{Total CPM added to sample}} = \textit{Fraction of Met assimilated per hour per cell}$$

Eq. 3.2 $$\frac{(\textit{Nutrient Sample - Control Sample})}{\textit{Control Sample}} \times 100 = \textit{Percentage change}$$

Statistical significance between control and nutrient addition samples was calculated as described in Section 2.6, using the Student's paired t-test and the F-test. These tests allowed comparison of the entire dataset (i.e. the overall effect of nitrogen and/or phosphorus addition), and was also performed on station groups defined either inside or outside the gyre, allowing observation of statistical differences between these regions.

3.3 Results

3.3.1 Location of the North Atlantic gyre

Flow cytometry was used to determine bacterioplankton concentrations at each station (except Stations 11 and 13) (Table 3.1). Values were plotted against latitude to provide a cell concentration transect profile (Figure 3.2a), which shows a diminished cell concentration between 25ºN and 37ºN, indicating the centre of the gyre. Additionally, the proportion of major bacterioplankton groups to the total community was plotted against latitude (Figure 3.2b), showing *Prochlorococcus* and LNA bacteria dominated across the transect, making up 18-41% and 31-56% of all bacterioplankton, respectively.

Additionally, an initial Met bioassay was conducted at all stations (except Stations 8, 13, and 14) allowing calculation of the uptake rate, ambient concentration, and turnover time of Met. The uptake rate of Met by the bacterioplankton community decreased between approximately 27ºN and 35ºN (Figure 3.2c), again indicating the NAG centre. The average total community uptake rate of Met for all stations was 0.19 ± 0.13 nM/h (mean ± SD of all values). Inside the gyre this was 0.13 ± 0.11 nM/h, and outside the gyre this was 0.24 ± 0.13 nM/h. Figure 3.2d shows the time taken for the bacterioplankton community to turn over the ambient Met. The average turnover time for all stations was calculated as 78.7 ± 57.4 h. Inside the gyre this was 109 ± 70.7 h, and outside the gyre this was 53.1 ± 29.5 h. It is worth noting that the error bars for this parameter are larger within the gyre between approximately 27ºN to 33ºN. Finally, ambient Met concentration remained fairly consistent across the transect (0.42 ± 0.17 nM) (Figure 3.2e). Inside the gyre this was 0.40 ± 0.14 nM, and outside the gyre this was 0.43 ± 0.20 nM.

From this dataset, the location of the NAG was deemed to be between approximately 25ºN and 37ºN. Nutrient addition locations can be split into two groups: inside the NAG (Stations 7, 8, 9, 10, 11, 12) and outside the NAG (Stations 4, 6, 13, 14, 15).

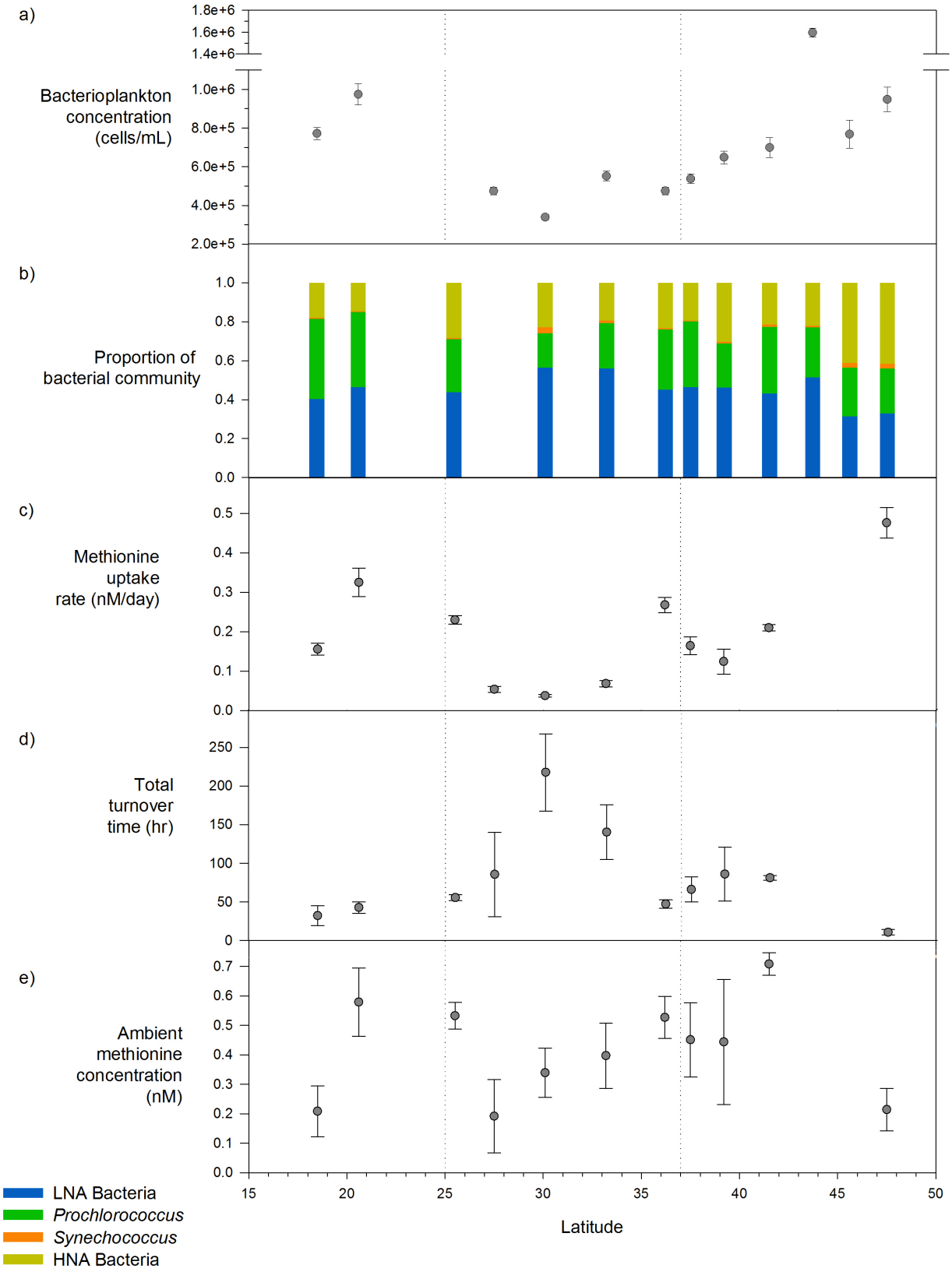

Figure 3.2: Bacterioplankton concentration and methionine bioassay data from initial samples taken in the North Atlantic during AMT-25
Samples indicated in Table 3.1 were assessed for bacterioplankton abundance (a), the proportion of each bacterial group (b), community Met uptake rate (c), total turnover time of ambient Met (d), and ambient Met concentration (e). Please note the scales on the y-axis. Dotted lines show gyre boundaries. For plot (b), Prochlorococcus, LNA bacteria, Synechococcus, and HNA bacteria are highlighted by green, blue, orange and yellow, respectively. Error bars for cells counts are described in Section 2.3.3, and for the methionine bioassay are described in Section 2.4.4.

3.3.2 Bacterioplankton responses to nutrient additions in short-term incubations

Figure 3.3 shows cell abundance/Met uptake rates of nutrient addition samples, plotted against their respective controls, whereby a unity line signified equal cell abundance/Met uptake rate in the control and nutrient addition sample. As this test was used to determine the effect of adding the synthetic chemicals on cells abundance and metabolic activity, stations do not need to be differentiated as inside or outside the NAG. The statistical significance/difference between each nutrient addition and its control was compared using the Students paired t-test and the F-test was employed to measure equality of variance (Section 2.6, Table 3.3).

Difference in cell abundance between the control and nutrient addition incubations were minimal, (Figure 3.3d-f), with error bars overlapping the unity line for most stations, and a fairly even spread of stations above and below the unity line for those with error bars that did not overlap. Most notably, there was no statistically significant difference in cell abundance (Table 3.3) between the control and nutrient addition incubation. The clear outlier is that of Station 4 upon addition of ammonium, which is highlighted on (Figure 3.3d). Met uptake rate showed slightly more variation (Figure 3.3a-c), although there was no clear trend, nor any statistically significant difference in uptake between the control and nutrient addition samples (Table 3.3).

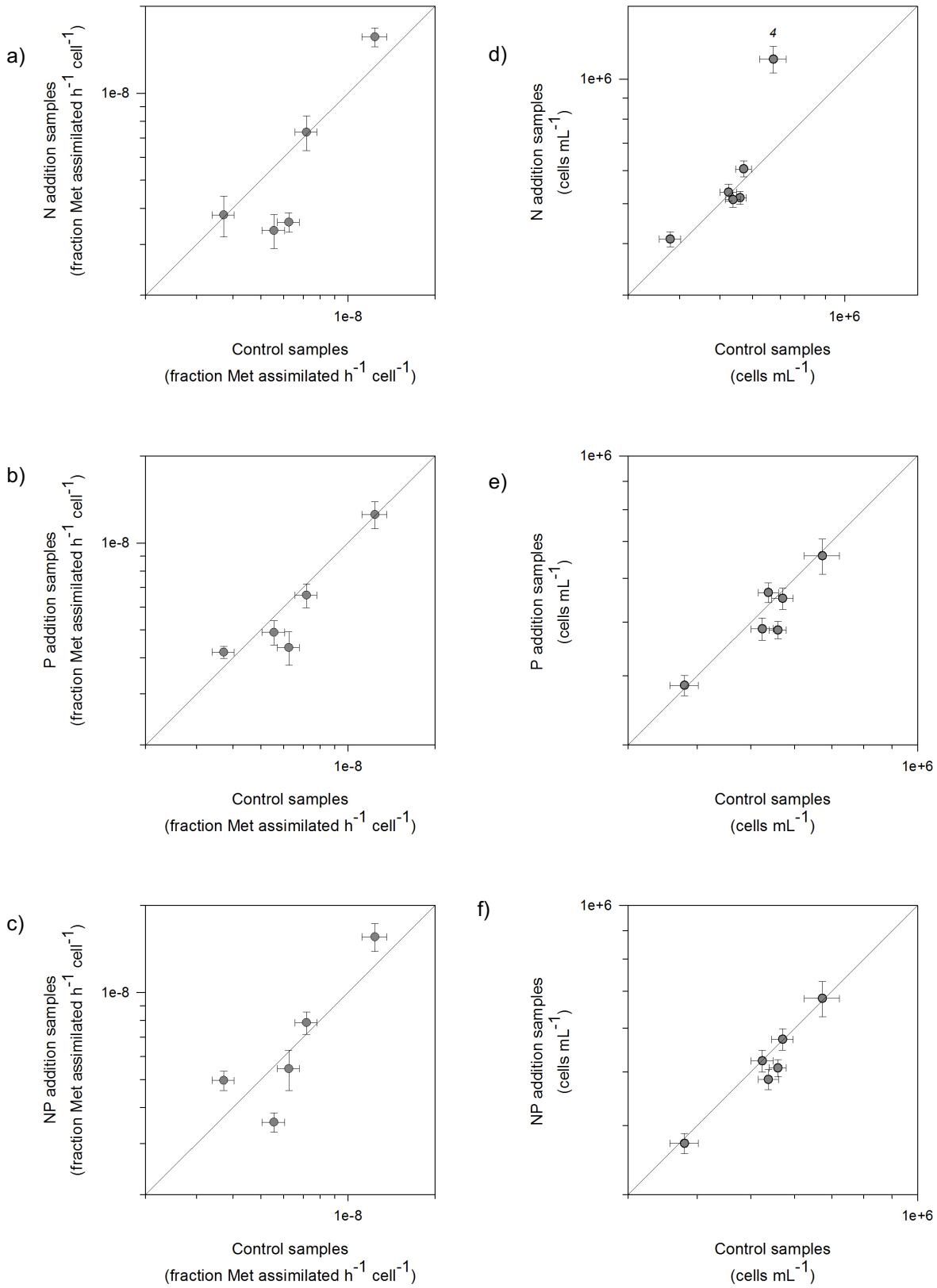

Figure 3.3: Changes in cell abundance and methionine uptake between control and ammonium/phosphorus addition samples after short-term incubation during AMT-25
Plots show changes in Met uptake rate (a, b, c) and cell abundance (d, e, f) from control samples upon addition of ammonium (a, d), phosphate (b, e) or both (c, f).
The notation used is outlined in Table 3.2. The diagonal line is the unity line, whereby values for the control sample and nutrient addition sample are equal. Stations of interest are highlighted with their station ID. Values for Met uptake: the fraction of Met taken up in one hour per cell, relative to the amount of Met added to the sample. Error bars show the error of propagation of cell concentration and amino acid uptake (Sections 2.3.3 and 2.4.4). Values for cell abundance: cells per millilitre. Error bars show uncertainty as described in Section 2.3.3). Note all axis are on a log scale.

Table 3.3: Statistical analysis (t-test) of the difference in cell abundance and methionine uptake upon addition of ammonium/phosphorus in short-term experiments
Each test shows the nutrient addition sample compared against the control sample. The number of samples in each group is shown in parentheses in the 'Parameter Analyzed' column. Samples with a p-value <0.05 are deemed to be statistically different from one another. The critical F value, is shown in parentheses in the 'Statistical Test' column. Values that show statistical significance are highlighted in bold italics. Samples that failed a normality test are highlighted with an asterisk, and instead show p values of a Wilcoxon signed rank test (see Section 2.6 for a more detailed description of the statistical analyses used).

Parameter analyzed	Statistical Test	+N	+P	+NP
Cell abundance (6)	T-test (p-value)	0.563*	0.249	0.313*
	F value (7.15)	7.11	1.04	1.14
Met Uptake Rate (5)	T test (p-value)	0.812	0.287	0.624
	F value (9.60)	2.59	1.15	2.15

3.3.3 Bacterioplankton responses to nutrient additions in long-term incubations

Figure 3.4 shows cell abundance and Met uptake after ~48 h incubation, with the nutrient addition samples plotted against their respective controls, and locations of interest highlighted with their station ID (Figure 3.4). Additionally, the percentage change from the control was calculated for each station (Figure 3.5). The Students paired t-test and F-test were used to determine statistical significance (Section 2.6, Table 3.4).

Addition of both nutrients

All stations (inside and outside the gyre) that received both nutrient additions were seen to be above the unity line, had a positive percentage increase and showed a statistically significant difference from the control for both cell abundance and Met uptake (Figures 3.4c, 3.4f, 3.5, and Table 3.4). The exception was that of Met uptake inside the gyre, which was not quite significant (Wilcoxon signed rank test, p= 0.063) (Table 3.4); although

all stations were above the unity line (Figure 3.4) and there was a large percentage increase in Met uptake at Stations 8, 9, and 10 (Figure 3.5).

Ammonium additions

Upon addition of ammonium alone, all stations located outside of the gyre showed an increase in cell abundance (except Station 13) and Met uptake (Figures 3.4a, 3.4d, and 3.5), although statistical difference from the control was only shown in Met uptake (Table 3.4). Inside the gyre, all ammonium supplemented stations showed no statistically significant increase from the control (Table 3.4). Stations of interest are: Station 7, which is located above the unity line (Figure 3.4a and 3.4d), and Station 4, which is clustered near to stations located inside the gyre (Figure 3.4d). It is interesting to note, that inside the gyre upon addition of ammonium there was a slight decrease in cell abundance (Figure 3.4d and Figure 3.5), although this was not shown to be statistically significant (Table 3.4).

Phosphate additions

Addition of only phosphate, showed no discernable trend, with all points distributed evenly across the unity line (Figures 3.4b and 3.4e), no major percentage change from control (Figure 3.5), and no statistically significant difference from the control (Table 3.4).

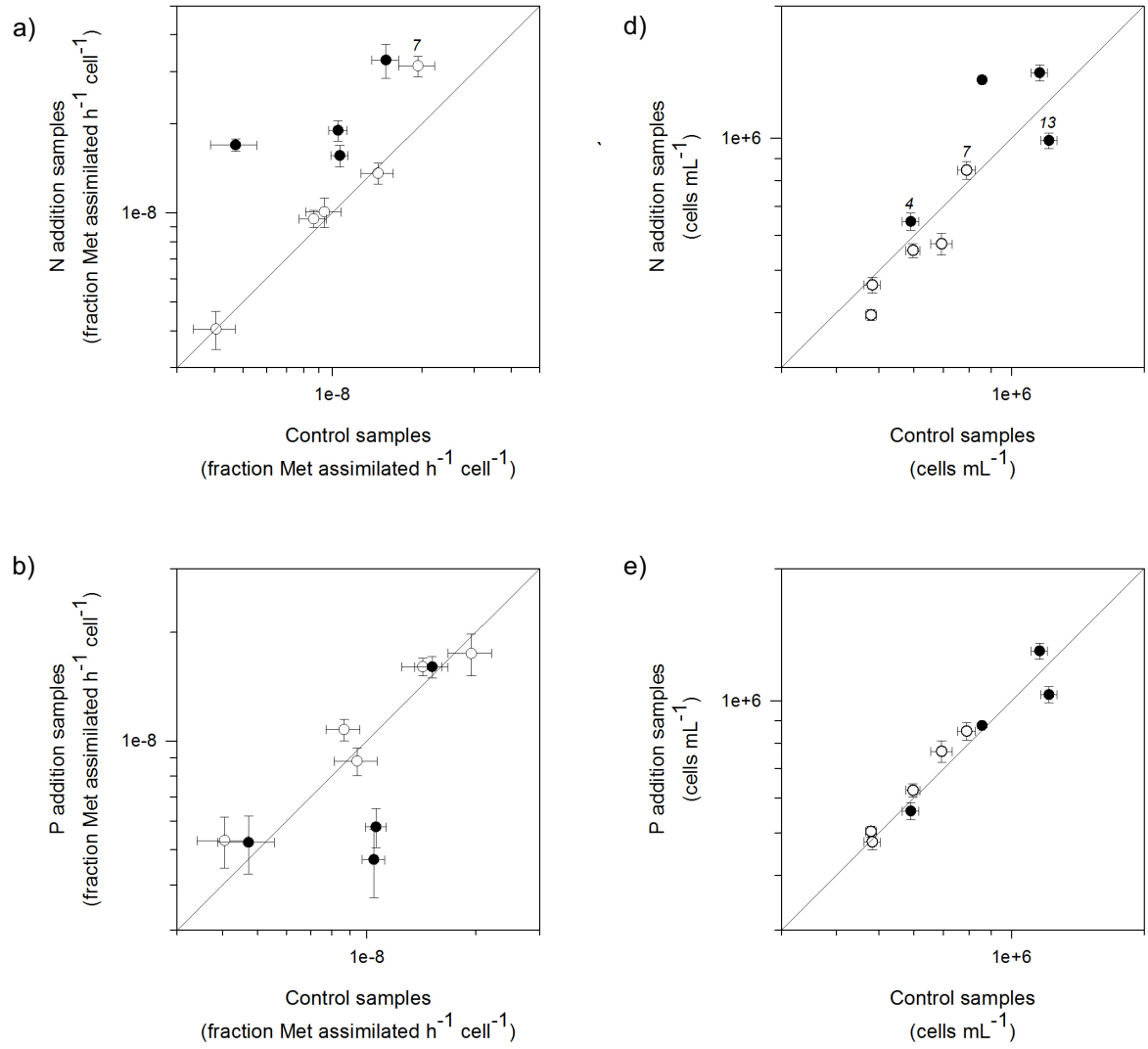

Figure 3.4: Changes in cell abundance and methionine uptake between control and ammonium/phosphorus addition samples after long-term incubation during AMT-25
Plots show changes in Met uptake rate (a, b, c) and cell abundance (d, e, f) from control samples upon addition of ammonium (a, d), phosphate (b, e) or both (c, f). Open and filled symbols are stations deemed inside and outside the gyre, respectively. The notation used is outlined in Table 3.2. The diagonal line is the unity line, whereby values for the control sample and nutrient addition sample are equal. Stations of interest are highlighted with their station ID. Values for Met uptake: the fraction of Met taken up in one hour per cell, relative to the amount of Met added to the sample. Error bars show the error of propagation of cell concentration and amino acid uptake (Sections 2.3.3 and 2.4.4). Values for cell abundance: cells per millilitre. Error bars show uncertainty as described in Section 2.3.3). Note all axis are on a log scale.

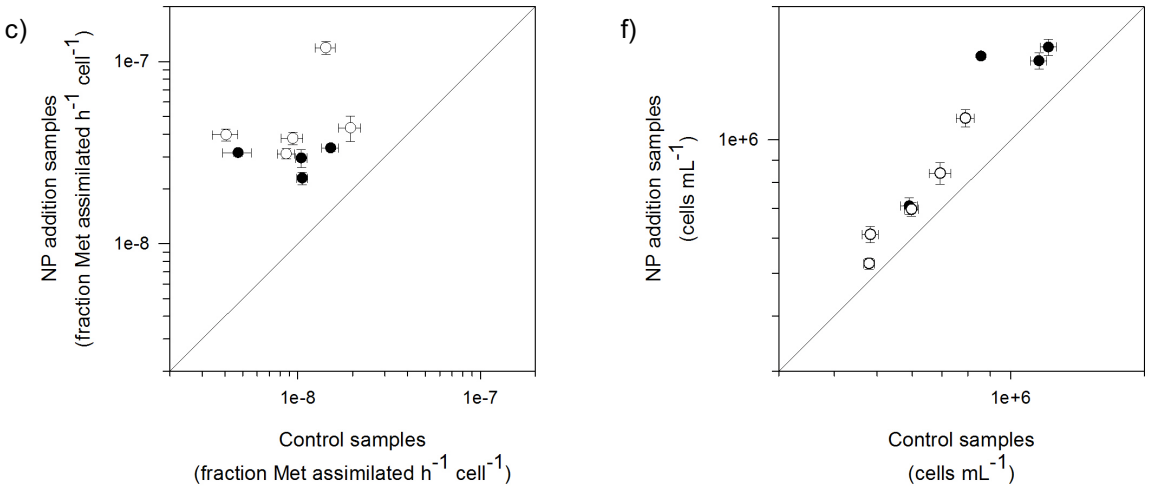

Figure 3.4: Changes in cell abundance and methionine uptake between control and ammonium/phosphorus addition samples after long-term incubation during AMT-25 *Continued*

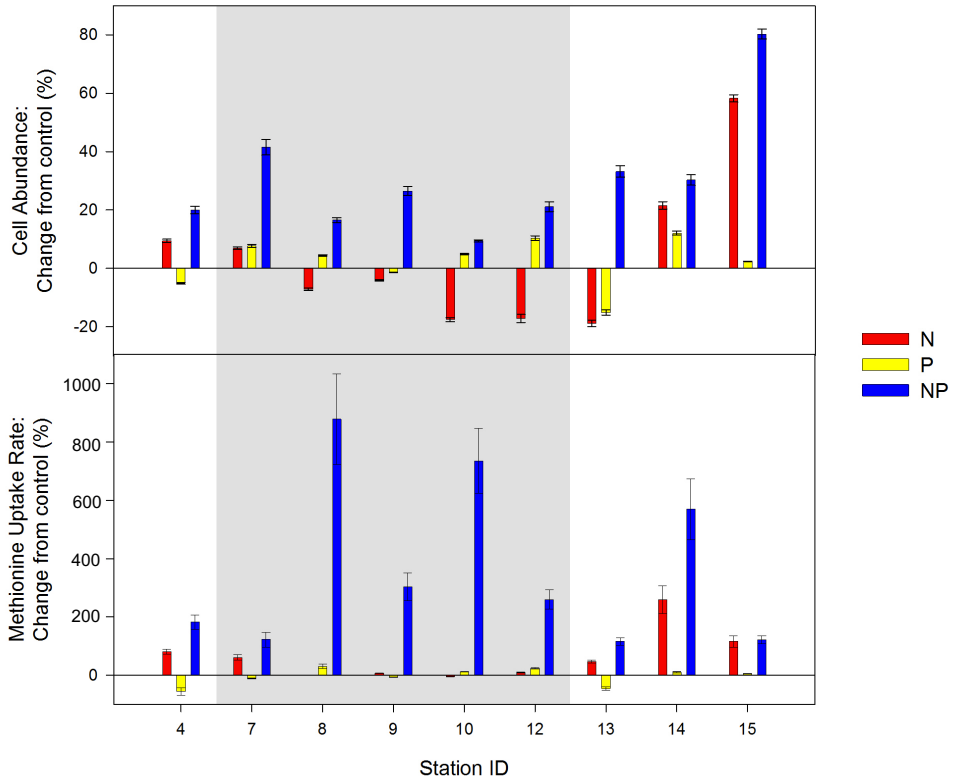

Figure 3.5: The percentage change in methionine uptake and cell abundance from control upon addition of ammonium/phosphorus during AMT-25 after long-term incubation
Plots show the percentage change in cell abundance and Met uptake rate from control for each nutrient addition sample. Red, yellow and blue bars represent ammonium, phosphate, and ammonium + phosphate additions, respectively. The grey shaded areas are those stations deemed to be located inside the NAG. Note the change in scales on the in y-axis.

Table 3.4: Statistical analysis (t-test) of the difference in cell abundance and methionine uptake upon addition of ammonium/phosphorus in long-term experiments
Each test shows the nutrient addition sample compared against the control sample. The number of samples in each group is shown in parentheses in the 'Parameter Analyzed' column. Samples with a p-value <0.05 are deemed to be statistically different from one another. The critical F value, whereby alpha is 0.025 (two tailed analysis, 0.05 significance divided by 2), is shown in parentheses in the 'Statistical Test' column. Values that show statistical significance are highlighted in bold italics. Samples that failed a normality test are highlighted with an asterisk, and instead show p values of a Wilcoxon signed rank test.

Area Analyzed	Statistical Test	Cell Abundance			Met Uptake		
		+N	+P	+NP	+N	+P	+NP
All Stations (9)	T test (p-value)	0.59	0.66	***<0.01***	***0.02***	0.47	***<0.01****
	F value (4.43)	1.91	1.01	2.59	3.83	1.14	***34.75***
Inside Gyre (5)	T test (p-value)	0.23	0.07	***0.04***	0.31*	0.54	0.06*
	F value (9.60)	1.62	1.46	2.98	3.16	1.35	***38.66***
Outside Gyre (4)	T test (p-value)	0.42	0.85	***0.05***	***0.03***	0.28	***<0.01***
	F value (15.44)	1.51	1.13	2.17	3.44	1.61	1.17

3.3.4 Response of key bacterial populations to nutrient additions in long-term incubations

In Figure 3.6, the cell abundances of key bacterioplankton groups for each nutrient addition sample was plotted against its respective control. Stations inside the gyre and outside the gyre are presented separately to allow direct comparison (Figure 3.6). Additionally, percentage change from the control is shown in Figure 3.7. Paired t-tests and F-tests allowed statistical significance to be calculated (Table 3.5, see Section 2.6).

Inside the gyre

Upon addition of ammonium, most cell groups showed an even spread along the unity line (Figure 3.6a and Table 3.5), indicating no difference between control and nutrient addition sample. The exception was *Prochlorococcus*, where a decrease in cell count occurred upon addition of ammonium alone, which was shown to be a statistically different from the

control incubation (Table 3.5). Conversely, addition of phosphate saw a statistically significant increase in *Synechococcus* abundance, whilst all other groups showed negligible difference (Figure 3.6b and 3.7, and Table 3.5). Addition of both nutrients saw a statistically significant decrease in *Synechococcus* abundance and a significant increase in *Prochlorococcus* (Figure 3.6c and Table 3.5). LNA bacteria show no statistically significant difference from the control (Table 3.5) and are found on both sides of the unity line in all nutrient amendments (Figure 3.6a-c), despite some percentage changes from the control samples (Figure 3.7).

HNA bacteria show an inconsistent trend, with the same nutrient additions showing a different result in different stations within the gyre. For example, Stations 7, 8, and 9 all showed an increase in cell abundance in +NP (and +P) samples, but Stations 10 and 12 saw a decrease upon addition of both nutrients (Figure 3.7). As a result, there was no overall statistical significant difference between cell abundance in the control and any nutrient addition samples in the HNA population (Table 3.5).

Outside the gyre

Both *Prochlorococcus* and LNA Bacteria increased in abundance upon addition of ammonium, bar Station 13 (Figure 3.6d and 3.7), although the difference was not considered statistically significant (Table 3.5). Sole ammonium additions did not increase the abundance of *Synechococcus*, except at Station 15, which is the most southerly experimental location (Figure 3.6d and Table 3.5). Addition of phosphate showed no statistically significant increase in cell abundance in any cell group (Figure 3.6e and Table 3.5). Finally, addition of both nutrients saw a statistically significant increase in cell abundance in all *Prochlorococcus* and LNA Bacteria samples (Figure 3.6f and 3.7 and Table 3.5). As shown on Figure 3.6f, an increase in *Synechococcus* abundance was only seen at Station 15 under these conditions.

As inside the gyre, HNA bacteria do not show any overall trend, with addition of the same nutrients causing a different response at different stations (Figure 3.6d-f and Table 3.5). Some stations showed a notable increase in cell abundance upon addition of both nutrients (Stations 13 and 15); however, at the other stations out of the gyre (Stations 4 and 14), there was a decrease in cell abundance in +NP samples. Interestingly, there was a slight increase in Stations 13, 14, and 15 upon addition of phosphate. Nevertheless, there was no statistically significant difference upon addition of any nutrient in comparison to the control sample (Table 3.5).

Table 3.5: Statistical analysis (t-test) of the difference in cell abundance upon addition of ammonium/phosphorus for different bacterioplankton populations
Each test shows the nutrient addition sample compared against the control sample. The number of samples in each group is shown in parentheses in the 'Parameter Analyzed' column. Samples with a p-value <0.05 are deemed to be statistically different from one another. The critical F value, whereby alpha is 0.025 (two tailed analysis, 0.05 significance divided by 2), is shown in parentheses in the 'Statistical Test' column. Values that show statistical significance are highlighted in bold italics. Samples that failed a normality test are highlighted with an asterisk, and instead show p values of a Wilcoxon signed rank test.

Area Analyzed	Statistical Test	*Prochlorococcus*			LNA Bacteria			*Synechococcus*			HNA bacteria		
		+N	+P	+NP	+N	+P	+NP	+N	+P	+NP	+N	+P	+NP
All Stations (9)	T test (p-value)	0.80	0.69	***<0.01***	0.19	0.77	0.07	0.82*	***0.03***	0.13*	0.86	0.09	0.08
	F value (4.43).	1.59	1.40	2.00	2.31	1.16	3.24	3.70	1.60	***6.60***	1.24	1.82	2.07
Inside Gyre (5)	T test (p-value)	***0.05***	0.33	***<0.01***	0.77	0.30	0.79	0.38	***0.03***	***<0.01***	0.81*	0.55	0.17
	F value (9.60).	1.23	1.22	1.93	4.26	2.00	8.20	1.18	2.14	1.08	2.32	1.14	1.34
Outside Gyre (4)	T test (p-value)	0.62	0.56	***0.04***	0.09	0.31	***0.03***	0.59	0.50	0.88*	0.65	0.12	0.27
	F value (15.44).	1.26	1.40	1.83	1.35	1.13	1.57	6.01	2.31	9.95	1.37	2.44	2.85

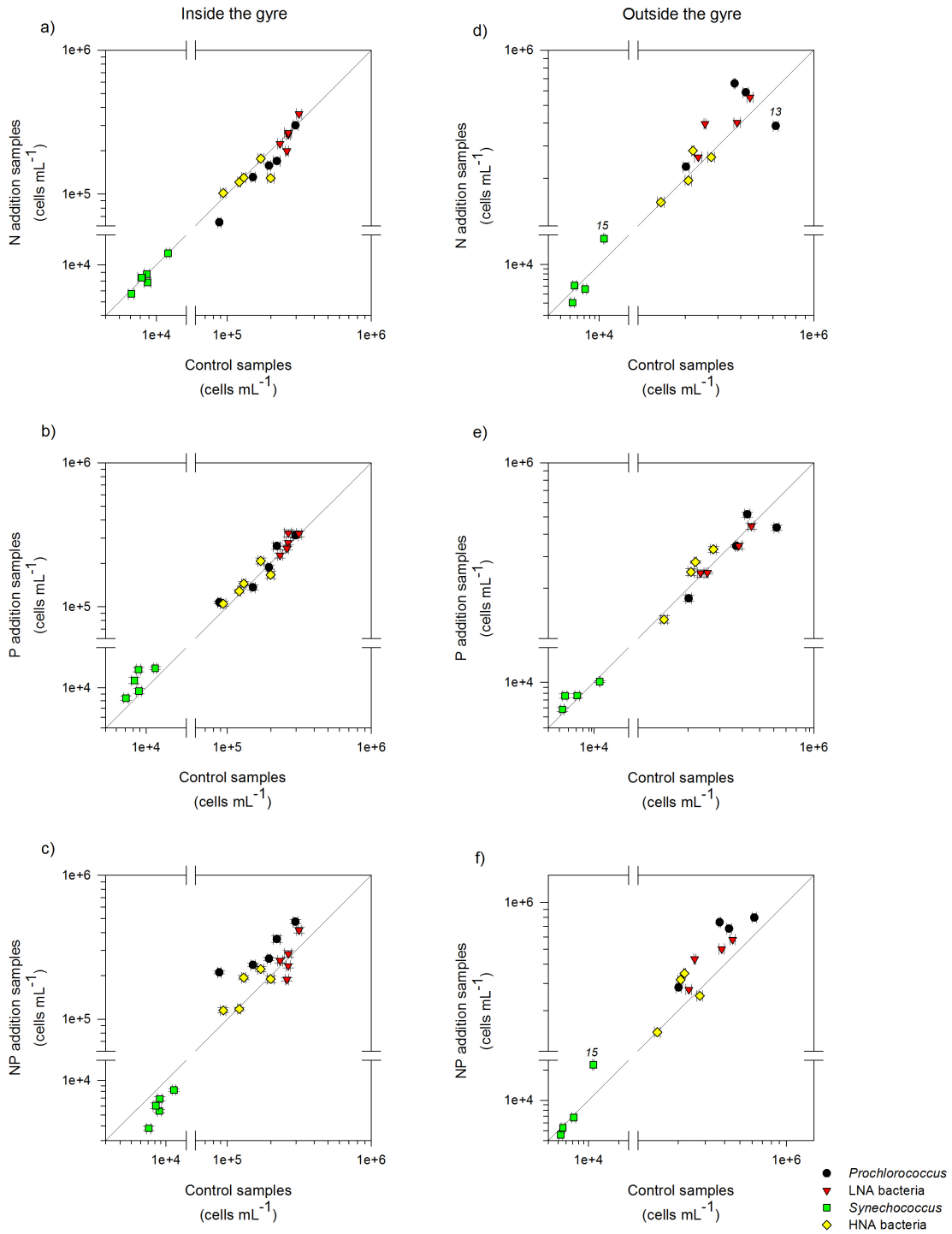

Figure 3.6: Changes in cell abundance between control and ammonium/phosphorus addition samples in key bacterioplankton populations during AMT-25 after long-term incubation

Plots show changes in cell abundance from control samples upon addition of nitrogen (a, d), phosphorus (b, e) or both nutrients (c, f) for stations located inside (a, b, c) and outside (d, e, f) the NAG. Prochlorococcus, LNA Bacteria, Synechococcus, and HNA bacteria are labelled with black, red, green, and yellow symbols, respectively. The notation used is outlined in Table 3.2. The diagonal line is the unity line, whereby values for the control sample and nutrient addition sample are equal. Stations of interest are highlighted with their station ID. Values for cell abundance: cells per millilitre. Error bars based on uncertainties as calculated in Section 2.3.3. Note all axes are on a logarithmic scale.

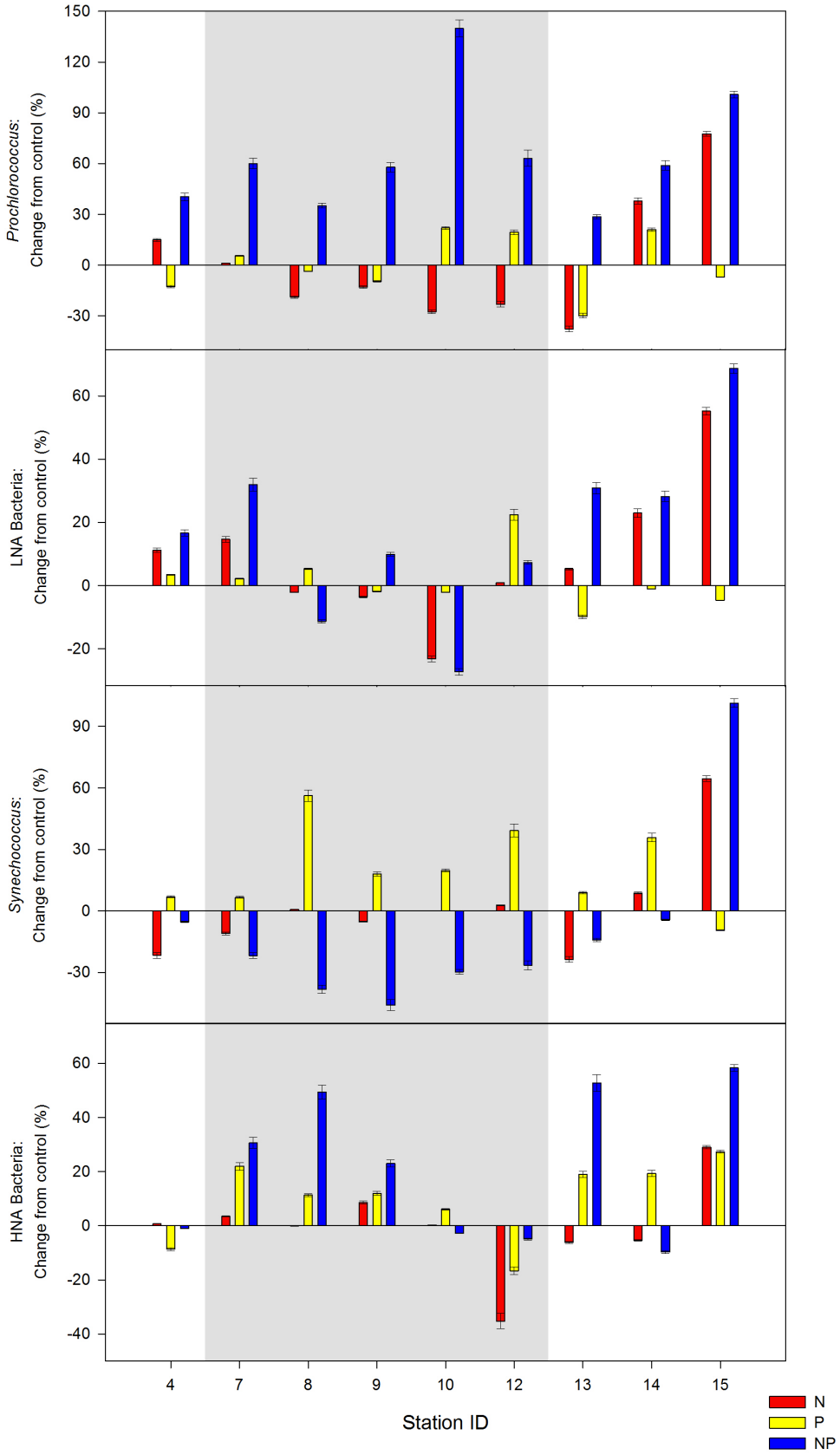

Figure 3.7: The percentage change in cell abundance from control upon addition of ammonium/phosphorus in key bacterioplankton populations after long-term incubation
Plots show the percentage change in cell abundance of Prochlorococcus, LNA Bacteria, Synechococcus, and HNA bacteria from their respective controls for each nutrient addition sample. Red, yellow and blue bars represent ammonium, phosphate, and ammonium + phosphate additions, respectively. The grey shaded areas are those stations deemed to be located inside the NAG. Note the change in scales on the in y-axis. Error bar based on cell concentration uncertainties (Section 2.3.3).

3.4 Discussion

The location of the NAG can be determined through initial Met bioassay and cell abundance measurements [198,226] and was shown to be between approximately 25ºN and 37ºN, matching previously observed locations [227]. Additional physical and chemical data from cruise AMT-25, provided by the British Oceanography Data Centre (contains data supplied by the Natural Environment Research Council), is shown Appendix C, supporting this location. It should be noted that temperature, salinity and chlorophyll all place the southern boundary of the NAG at approximately 20ºN (Appendix C); however, there were no stations analysed between 20.6 and 25.5ºN in the above data, thus 25ºN was used as the edge of the gyre in the subsequent discussion of these results. From these latitudinal boundaries, comparisons can be made between the responses of bacterioplankton inside and outside the NAG. It is important to note that these boundaries are not an absolute certainty. Stations where the expected trend is not followed are highlighted in Figure 3.4, and were located at the edges of the gyre (e.g. Station 7 and 13). Although the location of the NAG was shown to be between approximately 25 and 37ºN (Figure 3.2), the gyre boundaries determined by the initial measurements, are not an absolute certainty. For example, if the gyre location was based on Met uptake alone, then it would be located between 27 and 35ºN, and based upon turnover time alone the northern edge would be at ~33ºN. This is also seen in slight variations in gyre boundaries defined by temperature, salinity and chlorophyll (Appendix C). Thus, stations on the edge of the gyre may have behaved uncharacteristically, acting as either inside or outside the gyre. Indeed, in a study by Heywood *et al* (2006) some stations were omitted due to high dissimilarity to surrounding stations, many of which were located on the edges of gyres [226].

The dominance of *Prochlorococcus* and LNA bacteria seen in this study was also previously reported (e.g. 36±6% and 31% of bacterioplankton for LNA bacteria [142] and

Prochlorococcus [13]). Total cell counts are similar to those obtained on the previous AMT cruise (AMT-24), and cell counts of *Prochlorococcus* and *Synechococcus* inside the gyre are similar to a previous study by Heywood *et al* (2006) (~1 x10^5 and ~5 x 10^3, respectively) [226]. Cell counts in the gyre (~3.4 - 5.5 x10^5 cells/mL) are in agreement with bacterioplankton counts made by Priscila Lange (University of Oxford) during the same cruise (~3.4 - 5.2 x10^5 cells/mL, Appendix D). Finally, the values obtained for Met uptake rate, ambient Met concentration and turn over time matched previous measurements [198,200,201].

3.4.1 Bacterioplankton responses to nutrient additions in short-term incubations

Addition of ammonium and phosphate does not negatively affect cells, since after 2-3.5 h incubation no significant decrease in cell abundance or Met uptake was observed (Table 3.3). Equally, no increase was observed, which was predictable as cells predominantly replicate at night [154,228,229], which was significantly after the mid to late afternoon analysis of the short-term samples in this study. Although some stations showed slight increases or decreases relative to the control (particularly in Met uptake) (Figure 3.3), these are minor fluctuations and show no overall statistically significant difference (Table 3.3).

The exception was an unusually high cell concentration in an ammonium supplemented sample (Station 4, Figure 3.3d). However, as this increase (62%) was more than 3 standard deviations away from the mean increase for all other samples, it can be considered to be an outlier. Furthermore, upon performing a Grubb's test, Station 4 was shown to be an outlier, as the calculated Grubb's value (1.98) was higher than the critical value (1.89), using a significance level of 0.05.

Previous studies also did not observe a response during short incubations; for example, Grob *et al* (2015) incubated for 10-11 h, and witnessed no change in eukaryotic CO_2 fixation rate upon nutrient additions [177]. Additionally, Carlson and Ducklow (1996), did not note any measurable response (e.g. amino acid uptake) by bacterioplankton to nutrient additions within the first few hours of incubation [219].

Given that a response was observed upon addition of nutrients after the long-term incubation (see subsequent), detectable responses can be considered to fall between approximately 3.5 and 48 h. A more definitive time period cannot be conclusively drawn from this data set without further experimental time points; however, measurable changes in cell abundance, and consequently metabolic activity, are likely to appear within 24 h due to planktonic diel cycles [154,228,229]. Indeed, previous studies have observed the effects of nutrient additions after 24 h [e.g. 132,136] and even 12 h incubations [135].

3.4.2 Bacterioplankton responses to nutrient additions in long-term incubations

Inside the gyre

Inside the NAG, both ammonium and phosphate are required in order to stimulate an increase in cell abundance and Met uptake after 48 h. As can be seen from supplementary nutrient data (provided by the British Oceanography Data Centre, contains data supplied by the Natural Environment Research Council, Appendix B), concentrations of phosphate and nitrate + nitrite are minimal inside the NAG at 30 m (0.02 μM PO_4^{3+}, 0.02 μM NO_3^- + NO_2^-). Indeed, Mills *et al* (2008) and Moore *et al* (2008) noted increases in bacterial responses upon addition of nitrogen and phosphorus and concluded co-limitation of the two nutrients [123,124]. It is interesting to note that upon addition of ammonium alone, there was a general decrease in bacterioplankton abundance inside the gyre. Upon

analysis of individual bacterioplankton groups (Figures 3.6 and 3.7), this decrease appears to be primarily due to a decrease in *Prochlorococcus* abundance and is discussed in Section 3.4.3.

Outside the gyre

Moving out of the centre of the gyre and into more productive waters reduced the bacterial requirement for additional phosphate to a point where ammonium additions alone elicited a measurable response in cells (Figures 3.4a, 2,4d, 3.5 and Table 3.4). In this study, ammonium was required in order to observe a measurable increase in cell abundance and Met uptake. This reflects the very low nitrogen concentrations reported across the majority of the North Atlantic [e.g. 7,54]. Indeed, Mills *et al* (2004) observed nitrogen limitation with their east-west transect along approximately 4 to 12ºN [134], which matches the location of nitrogen-only stimulated responses seen in this study.

The change in bacterial responses from ammonium and phosphate, to ammonium alone can be clearly seen in the Met uptake rate moving from Station 013 to 015 (Figure 3.5). At Stations 013 and 014, the percentage increases seen in +N samples (~47% and ~260%) were approximately half of those seen in +NP samples (~120% and ~570%). However, at Station 015 the percentage increase was equal in +N and +NP samples (approximately 120%). This observation is in line with previously reported increases in ambient phosphorus moving out of the NAG [e.g. 176,216]; for example, Mather *et al* (2008) observed minimum concentrations of ~50nM dissolved organic phosphorus inside the NAG, with concentrations increasing to >100nM in surrounding waters out of the gyre [66]. This is further supported by data provided by the British Oceanography Data Centre (contains data supplied by the Natural Environment Research Council) that was generated during AMT-25. Near the gyre boundary (at 30 m depth), phosphate concentrations increase

(Appendix B, Figure S2b), whereby the concentration of phosphate at 26ºN (inside the gyre) was 0.02 µM, and at 19ºN (outside the gyre/edge of the gyre) was 0.15 µM.

It should be noted that, despite following the trend of increased cell abundance upon addition of ammonium, Station 4 has a lower cell abundance than its counterpart stations outside the gyre (Figure 3.4d). Here, cell counts in the control sample after 48 hours were approximately 16% lower than initial counts, implying the bottle incubations may have negatively affected cells at this station.

Phosphate

Addition of phosphate alone did not produce a measurable increase in total bacterioplankton abundance or methionine uptake from the control at any location (Figures 3.4b, 3.4e, 3.5, and Table 3.4), which is in agreement with some previous studies [123,124,136]. However, this is in contrast to other reports of increased cell growth and metabolism upon addition of phosphate [131,133,135]. A response was only seen when phosphate was added in combination with ammonium, which is indicative of co-limitation [53], as previously reported in the North Atlantic [123,124]. As addition of both nutrients was required to evoke a repose, neither ammonium or phosphate alone can be considered to be a primary limiting nutrient inside the NAG.

3.4.3 Response of key bacterial populations to nutrient additions in long-term incubations

Inside the gyre

Ammonium + phosphate additions

Prochlorococcus was the only bacterioplankton group that consistently and significantly increased in cell abundance upon addition of both nutrients (mirroring the results of the total community) (Figure 3.6c, 3.7 and Table 3.5). As assimilation of inorganic nutrients by both heterotrophs and autotrophs in the marine environment can lead to direct competition [124,230], *Prochlorococcus* could be considered to have outcompeted other bacterioplankton inside the NAG upon addition of both nutrients. Interestingly, Lui *et al* (1997) concluded that *Prochlorococcus* are not limited in oligotrophic waters of the North Pacific, as seen from high growth rates and abundance [154]. However, their study concluded that this was due to population control and nutrient supply from a high level of protozoan grazing [154], which may not have occurred in this study location. Indeed, a positive response of *Prochlorococcus* (e.g. an increase in chlorophyll concentration) to nutrient additions in the North Atlantic has been observed in previous studies [e.g. 123,136,221].

LNA bacteria showed a fairly mixed response to addition of ammonium and phosphorus, although overall there was no statistically significant difference to the control incubation. It is possible that LNA bacteria do not respond to enrichment experiments; for example, Mills *et al* (2008) noted minimal response of small LNA bacteria in their nutrient addition experiments [124]. Although the predominant group of bacteria in the LNA community is SAR-11 [65,142], the mixed responses seen (Figure 3.7) may also be the result of the difference in community structure in the remaining LNA population.

Alternatively, heterotrophic bacteria may have been subject to an alternative limiting factor in the centre of the gyre, such as carbon limitation. Due to their dependency on carbon

production by phytoplankton, Kirchman (1994) stated that ultimately heterotrophic bacteria are carbon limited [231], with Kirchman *et al* (1990) reporting carbon limitation of ammonium assimilation [232], and Carlson *et al* (2002) noting that once carbon limitation was relieved, then a secondary limitation (e.g. nitrogen) can be initiated [128]. For example, in this study, this may have been caused by moving out of the gyre, whereby LNA bacteria show an increase in cell abundance upon addition of ammonium (Figures 3.6d, 3.6f and 3.7). However, Pan *et al* (2014) measured higher dissolved organic carbon (DOC) concentrations in tropical and subtropical waters (70 - 90 μM) than in higher latitudes (50-55 μM in polar waters) of the upper Atlantic Ocean [130]. Furthermore, during their study of the North Atlantic, Carlson *et al* (2010) recorded their maximum DOC concentration in the surface waters (<100 m) of the upper NAG [129]. These reported high DOC concentrations imply that cells would not be carbon limited and, although some previous studies do support primary carbon limitation in the North Atlantic [e.g. 219], most other studies do not [e.g. 124,131-133].

Prochlorococcus: ammonium additions

Upon addition of ammonium inside the gyre, there is a slight decrease in cell abundance of *Prochlorococcus* (Table 3.5, Figures 3.6 and 3.7). *Prochlorococcus* may be subject to ammonium toxicity in these incubations; however, ammonium toxicity is unlikely in this study as a decreased *Prochlorococcus* abundance was not seen in incubations where ammonium was added in combination with phosphate. Instead, it is possible that the higher ammonium concentration affected the nutrient ratios (e.g. N:P) of *Prochlorococcus* negatively, causing stoichiometric deficiency [53], especially as the regulation of ammonium uptake pathways are minimised in *Prochlorococcus* [169,233].

Alternatively, elevated ammonium concentrations may have stimulated an increase in a predator, resulting in an increased level of *Prochlorococcus* grazing. Likewise, the

ammonium may have increased competition through stimulating the growth of an alternative competing plankton species.

Synechococcus: phosphate additions

Synechococcus are the only other group to respond consistently inside the centre of the gyre but, in contrast to the total community, showed an increase in abundance upon addition of phosphate (Figure 3.6b and 3.7). Conversely, a decrease in *Synechococcus* abundance was seen in +NP samples (figure 3.6c and 3.7), meaning cells may have been negatively affected by ammonium; however, if this was occurring, then a decrease in cell abundance may be expected in +N samples too, which was not observed (Figure 3.6a and Table 3.5). Furthermore, *Synechococcus* have been shown to survive at concentrations of ammonium higher than those used in this study [58,234]. Interestingly, Davey *et al* (2008) suggested that some strains of *Synechococcus* may become phosphorus (or iron) limited when nitrogen concentrations are sufficient, observing an increase in cell abundance and cellular fluorescence upon addition of phosphorus but not when in combination with nitrogen [221].

An alternative theory is that *Synechococcus* are simply phosphorus limited, especially considering they require more productive waters in comparison to *Prochlorococcus* [158], and are simply out-competed in +NP additions. Indeed, in the +NP incubations, another cell group may increase in growth and exhaust phosphorus (and/or other nutrients, such as DOC), ultimately limiting *Synechococcus*. At Station 15, furthest from the gyre, *Synechococcus* do not increase in cell numbers upon addition of phosphate, again indicating a departure from phosphate-limited waters [e.g. 176, Appendix B].

It should be noted that *Synechococcus* numbers are significantly lower than the other groups within the gyre (<3% of total bacterioplankton), so any minor changes in this population will have been amplified. Furthermore, Cavender-Bares *et al* (1999) noted that

changes in community structure may occur in nutrient addition experiments [235], which may have caused unusual growth of *Synechococcus* in the phosphate addition incubations.

Outside the gyre

Both *Prochlorococcus* and LNA Bacteria show an increase in cell abundance upon addition of ammonium (alone and in combination with phosphate), an observation that matches that of the total community. The exception is Station 13 (Figure 3.6d), which can be rationalized due to its location on the edge of the gyre (see previous). As both *Prochlorococcus* and LNA bacteria appear to contribute to the total community response, any competition/advantage seen between these two groups inside the gyre can be considered to be no longer relevant.

The most southerly station analyzed (Station 15), saw an increase in *Synechococcus* abundance upon addition of ammonium (alone or in combination, Figures 3.6d and 3.6f). As *Synechococcus* thrive in significantly more productive waters compared to *Prochlorococcus* [158], this increase in *Synechococcus* likely signifies a complete departure from phosphate poor waters.

HNA bacteria

HNA bacteria do not show any consistent trends, or statistically significant responses to any nutrient additions (Table 3.5). There are some differences in cell abundance (Figure 3.7), but no discernible trend for inside or outside the NAG can be concluded, even when considering stations located on the edge of the gyre. This is in contrast to Mills *et al* (2008) who reported that larger heterotrophic bacteria were responsible for observed increase in bacterial productivity upon the addition of nitrogen and phosphorus [124].

Results show a potential tendency towards an increase in cell concentration upon addition of phosphate. For example, +P incubation saw an increase in HNA bacterial abundance south of the gyre, indicating potential phosphate limitation. Furthermore, an increase in cell abundance was seen in the northern half of the gyre upon addition of phosphate, and more substantially when both nutrients are added, suggesting co-limitation at these stations, with phosphate being the primary limiting nutrient. Nevertheless, there was no overall trend upon addition of phosphate either inside the gyre, outside of the gyre, or when assessing all stations together (Table 3.5).

The inconsistent response from HNA bacteria in this study may come from the generic grouping of HNA bacteria. Each station may contain a different profile of bacteria [189,195], which will thus elicit a different response to nutrient additions. Flow cytometry alone cannot distinguish species within this group, and instead would require molecular identification techniques, such as fluorescent *in situ* hybridisation [189].

3.5 Conclusions

This study examined the response of bacterioplankton to the addition of ammonium and phosphate in a previously underrepresented region of the North Atlantic, thus expanding understanding of the impact from very low nutrient concentrations on North Atlantic bacterioplankton. Inside the NAG, total bacterioplankton populations were found to increase in cell abundance and metabolic activity upon addition of both nutrients. Conversely, out of the gyre the response of cells to phosphate additions was reduced, and ammonium alone was able to stimulate an increase in the measured parameters. These increases in cell growth and metabolic activity support the observed chemistry of very low concentrations of nitrogen and phosphorus in the North Atlantic, suggesting co-limitation [e.g. 7,53,54,66,216].

Upon analysis of individual bacterial groups, *Prochlorococcus* consistently showed a positive response to the addition of both ammonium and phosphate nutrients inside the gyre. Outside the gyre, both *Prochlorococcus* and LNA bacteria showed an increase in cell abundance when supplemented with ammonium (either alone or in combination). *Synechococcus* responded to phosphate additions, indicating that they may be phosphate-limited. And finally, HNA bacteria show a very mixed response with no clear trend, which is likely to be due to the huge species variation that exists within the HNA grouping. This shows that different cell populations respond differently to nutrient additions, and so to provide a full picture of the response of bacterioplankton, future nutrient enrichment experiments should consider analysis of individual cell groups in conjunction with the total community.

As the oligotrophic regions of the ocean continue to expand and global primary production decreases [e.g. 35,37], it is essential to understand the relationship plankton have with nutrients in these environments. An increase in the size of the NAG could result in increased nitrogen and phosphorus deficiency in the North Atlantic, and thus an increase in bacterioplankton limitation. Furthermore, as the NAG has been shown to be predominantly heterotrophic, gyre expansion would result in an increase in the heterotrophy of the global oceans [236]. Results such as those presented in this study, aid in contributing towards understanding bacterial nutrient interactions in the oligotrophic oceans, and the potential consequences of global gyre expansion on the marine ecosystem. As seen in this study, low concentrations of nitrogen and phosphorus impact bacterioplankton growth and metabolic activity, which could further contribute to the decline in global primary production [35], and consequently CO_2 drawdown from the atmosphere [237].

Chapter 4: The influence of iron additions on bacterioplankton abundance and metabolic activity in the South Atlantic

4.1 Introduction

Iron is a vital micronutrient for all living organisms, functioning as an essential protein cofactor in several key metabolic processes, including nitrogen fixation, photosynthesis and respiration [67,68]. However, despite being the fourth most abundant element in the earth's crust [87], in oxygenated seawater iron is largely biologically unavailable due to the rapid formation of ferric oxy-hydroxides that further crystallize to larger insoluble minerals [67,95]. This precipitation and consequent sinking of particulates, combined with high biological uptake and low input supply, results in very low concentrations of iron in large parts of the surface ocean, where the concentrations of dissolved iron (defined as being able to pass through a 0.2 µm or 0.4 µm filter [73,238]) are in the range of 0.02 - 1 nM [2,67,73,77,107].

High Nitrate Low Chlorophyll (HNLC) regions make up approximately 30% of the total global ocean (the subarctic Pacific, the equatorial Pacific, and the Southern Ocean) [53,56], and despite containing high levels of macronutrients (nitrogen and phosphorus), have reduced levels of phytoplankton due to iron limitation [218,239,240]. First observed by Martin and Fitzwater (1988) [239], this 'iron hypothesis' has been demonstrated throughout the HNLC regions of the world's oceans (see Boyd *et al* (2007) [180]) through a measured increase in phytoplankton growth and primary productivity after the addition of iron [e.g. 239-241]. This limitation of oceanic productivity by iron hinders ecosystem functioning and carbon export from the surface ocean, as approximately 50% of all global primary production occurs in the ocean [1]. Equally, as heterotrophic organisms rely on

phytoplankton for an organic carbon source [231], iron limitation affects the whole microbial community. For example, Cochlan (2001) showed that the heterotrophic bacterial population is iron limited in the equatorial Pacific [242].

Iron limitation is not restricted to HNLC regions, and has been observed in oligotrophic gyres (e.g. in the South Pacific gyre [178]) which are expanding as a result of climate change [35-38]. Notably, the surface waters of the oligotrophic South Atlantic Gyre (SAG) have been shown to have very low concentrations of iron [e.g. 115,126,127,176,243] with Moore *et al* (2009) reporting an average iron concentration of 0.03 ± 0.02 nM in the SAG [176], which is comparable with concentrations seen in HNLC regions [e.g. 244,245]. A major factor causing these low concentrations is reduced aerosol deposition (a key iron input source to the open ocean [71,218]) due to the intertropical convergence zone that hinders aerosol transfer from the northern hemisphere (e.g. from Saharan dust) [125], as well as Hadley cells that cause separation in atmospheric circulation at the equator [246]. Indeed, Shelley *et al* (2017) observed dissolved iron concentrations in the North and South Atlantic gyres of 0.68±0.28 nM and 0.26±0.06 nM, respectively [127].

Additionally, the SAG has very low concentrations of nitrogen [53], with Rees *et al* (2006) reporting a concentration of <0.01 μM nitrate in the gyre, compared to a maximum concentration of 33 μM in the productive Benguelan upwelling region [54]. However, despite the observed low concentrations of nitrogen and iron in the open ocean of the South Atlantic, studies examining the effect on microbial communities are rare.

It should be noted that the concentrations of phosphorus in the South Atlantic are not as low as those of the North Atlantic, with surface phosphate concentrations in the NAG and SAG being previously reported at 9 and 210 nM, respectively [66]. This is because the lower iron concentrations of the South Atlantic do not stimulate nitrogen fixation and subsequent phosphorus drawdown, as is seen in the North Atlantic gyre [66]. As such, phosphate enrichment experiments were not conducted in the South Atlantic during this study.

Nutrient enrichment experiments are a suitable approach for determining the effect of low nutrient concentrations on growth or production of the microbial community [122 and references therein][135 as an example study]. This study used this approach and examined the effect of iron and nitrogen additions on bacterioplankton abundance and metabolic activity across the South Atlantic. Bacterioplankton were selected for this study as they are the most abundant microorganism in the ocean [2], and have a higher iron requirement compared to eukaryotes [247,248], thus could produce a more notable response.

Seawater samples were incubated with iron and/or ammonium (as the preferred bacterial nitrogen source [3,249]) for 24-48 h [133] before on-ship analysis of changes in cell growth using flow cytometry [222] and metabolic activity via methionine (Met) uptake rate [197, e.g. 65,196,201]. Flow cytometry also allowed identification of key bacterioplankton groups and thus potential changes in community structure, and included *Prochlorococcus*, *Synechococcus*, low nucleic acid (LNA) heterotrophic bacteria, and high nucleic acid (HNA) heterotrophic bacteria [60,142,189]. As a second independent measure of potential iron limitation in the South Atlantic, iron uptake rates by the total microbial community were also assessed using radiolabelled iron. The iron uptake rate of iron-stressed cultures is higher than those of iron-replete cultures [206,250,251], thus measurements of iron assimilation may provide an additional indication of iron stress.

Through measurement of growth and metabolic activity, this study aimed to assess the responses of the bacterioplankton to additions of ammonium and iron in the South Atlantic. With the expansion of the oligotrophic gyres across the global ocean as a result of climate change [35-38], it is important to understand the effects of low nutrient concentrations on bacterial growth and metabolism. Previous studies in the South Atlantic are rare, with those that have conducted measurements only focussing on the phytoplankton community [176-179]. Therefore, this study is distinct as it monitors bacterioplankton, including the assessment of individual heterotrophic and autotrophic bacterial groups that dominate the oceans.

4.2 Methods

4.2.1 Seawater sampling

Nutrient addition studies were carried out in October 2015 during the 25th Atlantic Meridional Transect cruise (AMT-25). Uptake of iron by plankton was tested in October 2014 during the 24th Atlantic Meridional Transect cruise (AMT-24). Samples were collected from depths of 30 m (AMT-25) and 20 m (AMT-24) using an acid cleaned Go Flo sampler, as outlined in Chapter 2 (Section 2.2). Station locations and details are shown in Figure 4.1 and Table 4.1.

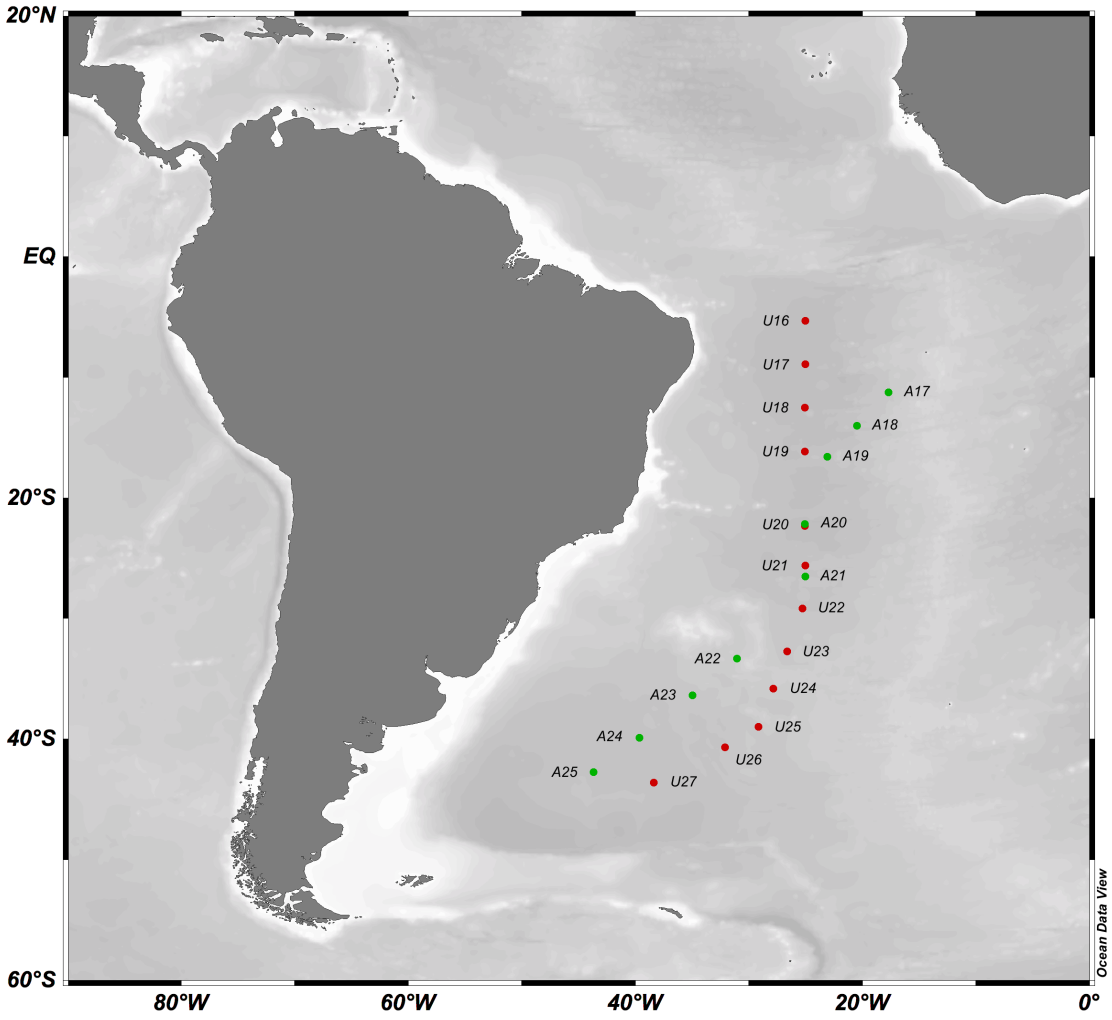

Figure 4.1: Locations of sampling stations during AMT-24 and AMT-25 used for iron uptake and ammonium/iron addition experiments
Stations with green dots were sampled during AMT-25 and represent the locations of nutrient enrichment studies. Stations with red dots were sampled during AMT-24 and represent iron uptake experiments. All stations are labelled with their ID as described in Table 4.1. Map created using Ocean Data View Software 4.7.10 [197].

Table 4.1: Locations of sampling stations during AMT-24 and AMT-25
Nutrient addition experiments conducted during AMT-25 are denoted with an 'A'. Iron uptake experiments conducted during AMT-24 are labelled with an 'U'. Nutrient addition or iron uptake experiments were not conducted at stations marked with an asterisk; however, initial measurements were still performed at these stations. Stations deemed to be inside the SAG are shaded in grey.

Station ID	Date and Time (GMT) of Sampling	Latitude (ºS)	Longitude (ºW)
A17 *	19-Oct-2015 13:13	11.23	17.69
A18 *	20-Oct-2015 14:05	14.02	20.50
A19 *	21-Oct-2015 14:08	16.57	23.10
A20	23-Oct-2015 14:04	22.16	25.09
A21	24-Oct-2015 14:04	26.50	25.04
A22	27-Oct-2015 14:15	33.33	31.07
A23	28-Oct-2015 15:07	36.36	34.98
A24 *	29-Oct-2015 15:06	39.87	39.66
A25	30-Oct-2015 15:25	42.72	43.70
U16	14-Oct-2014 14:07	05.32	25.03
U17	15-Oct-2014 14:13	08.91	25.04
U18	16-Oct-2014 14:08	12.49	25.07
U19	17-Oct-2014 14:07	16.13	25.08
U20	20-Oct-2014 14:08	22.32	25.06
U21	21-Oct-2014 14:08	25.59	25.04
U22	22-Oct-2014 14:07	29.15	25.28
U23	23-Oct-2014 15:05	32.72	26.63
U24	24-Oct-2014 15:07	35.80	27.87
U25	25-Oct-2014 15:11	38.96	29.17
U26	26-Oct-2014 15:09	40.69	32.10
U27 *	28-Oct-2014 15:05	43.59	38.39

4.2.2 Nutrient addition experiments

Four seawater samples (200 mL) were collected from the Go Flo sampler in a laminar flow hood and added to four separate acid cleaned (Chapter 2, Section 2.2.1) 250 mL high-density polyethylene (HDPE) narrow neck bottles (Nalgene). Aliquots of iron chloride ($FeCl_3$) and ammonium chloride (NH_4Cl) (Sigma Aldrich UK) were prepared fresh each day (Table 4.2), and thoroughly mixed via multiple inversions. To each sample bottle, ammonium chloride and/or iron chloride was added to final concentrations as shown in Table 4.3, which were based on concentrations used in previous studies [e.g. 123,134,178,252]. In addition, a sample was left without any nutrient additions to act as the control (Ctl). For ease, ammonium chloride will simply be referred to as 'ammonium' and iron chloride will be referred to as 'iron' from here on.

Samples were then transferred to an adapted recirculating water-bath (Grant Instruments, UK), maintained within approximately 3ºC of the ambient temperature of the sampled depths in the surface ocean, and illuminated from below using a diode array (Photon Systems Instruments, Czech Republic) between the hours of sunrise and sunset, at an intensity of approximately 300-700 µE/m/s. It should be noted that range in light intensity this represents inter-experimental variation and incubations within the same experiment were exposed to the same light intensity, for the same time period.

After approximately 24 h (range: 23.5 - 26.5 h) and 48 h (range: 48.5 - 51.5 h), a 50 mL aliquot was taken from each incubation, which was a sufficient volume for further experimental analysis. At 24 h, the incubation was returned to the water bath after sampling; however, at 48 h, the remaining incubation was discarded after sampling and the bottle was cleaned and re-used (as described in Section 3.2.2). The aliquot was used to measure changes in cell abundance and metabolic activity, using flow cytometry and Met uptake as described in Chapter 2 (Sections 2.3 and 2.4, respectively).

Table 4.2: Dilution steps for iron chloride and ammonium chloride stocks
All samples are diluted with deionized water, except the final sample where the previous stock is added directly to the seawater incubation (shown in italics). Note that hydrochloric acid is used to keep iron chloride in solution, with the resulting pH displayed in the right column. The final pH is based on if the solution was in deionized water and does not account for the additional buffering capacity of seawater in the final step.

Iron Chloride Stock: 0.66M in 6M hydrochloric acid

Dilution	Previous stock (µL)	Final volume (µL)	Iron (M)	HCl (M)	pH
1	40	1000	2.64×10^{-2}	2.40×10^{-1}	0.62
2	40	1000	1.06×10^{-3}	9.60×10^{-3}	2.02
3	40	1000	4.22×10^{-5}	3.84×10^{-4}	3.42
4	95	1000	4.01×10^{-6}	3.65×10^{-5}	4.44
Seawater Sample	*100*	*200100*	*2.01×10^{-9}*	*1.82×10^{-8}*	*7.74*

Ammonium Chloride Stock: 1M in deionized water

Dilution	Volume of previous stock (µL)	Final volume (µL)	Ammonium (M)
1	40	1000	4.00×10^{-2}
2	50	1000	2.00×10^{-3}
Seawater Sample	*100*	*200100*	*1.00×10^{-6}*

Table 4.3: Final concentrations of ammonium/iron added to seawater samples in nutrient addition experiments
Please note the sample notation highlighted in this table, and the concentration units for each nutrient.

Sample Notation	Final concentration of added nutrient	
	NH_4^+ (µM)	Fe^{3+} (nM)
Ctl	0	0
+N	1	0
+Fe	0	2
+NFe	1	2

Data analysis

Bacterioplankton cell concentrations were calculated as described in Chapter 2 (Section 2.3). The Met uptake rate per hour per cell for each sample was calculated using the uptake rate in CPM/min (calculated as described in Chapter 2, Section 2.4) and total cells

in the sample (Equation 4.1). Using this uptake rate, the fraction of Met assimilated (based on total Met added, Chapter 2, Section 2.4), was calculated using Equation 4.2.

Eq. 4.1 $$\frac{Uptake\ (CPM/min) \times 60}{Cells\ in\ sample} = Uptake\ (CPM/h/cell)$$

Eq. 4.2 $$\frac{(CPM/h/cell)}{Total\ CPM\ added} = Fraction\ of\ Met\ assimilated\ (per\ cell\ per\ h)$$

All Met uptake rates and cell concentrations of the nutrient addition incubations were compared against their respective controls. Unless stated otherwise, all statistical significances were determined through the Students t-test (two tailed), using a significance level of 0.05 and carried out using Sigma Plot 12.5 (Section 2.6). These analyses allowed comparison of a dataset (i.e. multiple stations), but do not allow comparison of incubations at individual stations. For individual station analysis, values of cell concentration or Met uptake rate for each nutrient addition sample was plotted against its associated control, and percentage change from the control was calculated as shown in Equation 4.3.

Eq. 4.3 $$\frac{(Value\ for\ Nutrient\ Addition\ Sample - Value\ for\ Control\ Sample)}{Value\ for\ Control\ Sample} \times 100 = Percentage\ change$$

4.2.3 Iron uptake experiments

$TiCl_3$ buffer

A titanium(III), citrate, and ethylenediaminetetraacetate (EDTA) buffer (termed $TiCl_3$ buffer from here on), developed by Hudson and Morel (1989) [253], was used to remove

extracellular iron from cell surfaces. From here on, the term 'washing' refers to the removal of extracellular iron from cells using the $TiCl_3$ buffer.

$TiCl_3$ buffer preparation was based on the method outlined in Hudson and Morel (1989) [253]. A stock solution of 0.05 M sodium citrate (Romil, UK) and 0.05 M sodium EDTA (Fisher Scientific, UK) (Solution A) was prepared in deionized water in an acid-cleaned polycarbonate (PC) bottle. Similarly, a 1 M potassium chloride (Sigma Aldrich, UK) stock solution (Solution B) was also prepared. The solutions were autoclaved (210047, Prestige Medical), inside a plastic autoclave bag to minimize iron contamination. Autoclaving was used to sterilize and de-gas the solutions. Once autoclaved, 50 mL of solution A and 0.5 mL of solution B were added to 0.6 g of sodium chloride (Sigma Aldrich, UK). Titanium chloride solution (Sigma Aldrich, UK) was added to a final concentration of ~0.6% $TiCl_3$. The pH was adjusted to pH 8 using 5 M sodium hydroxide solution (Tvr grade, Romil, UK). After approximately 30-60 min the buffer pH was re-adjusted to account for any drift in pH. Finally, the buffer was filtered through a 0.2 µm disposable filter (Minisart). Due to the instability of the buffer, the buffer was stored at 4ºC, in the dark, with minimal air exposure whenever possible [253,254].

Iron-55 incubation experiment

Upon recovery of the Go Flo sampler, 15-25 mL aliquots of seawater were collected in 30 mL Teflon bottles. To these seawater samples, radiolabeled iron chloride (^{55}Fe) was added and incubated up to a maximum period of approximately 24 hours. Two ^{55}Fe sources were used for these experiments (see Chapter 2, Section 2.4.5): source A (stored in 1 M hydrochloric acid) was used for stations U16-U23 and added to a final total iron concentration of Fe 0.2-0.3 nM (^{55}Fe, 0.003-0.006 nM); and source B (stored in 0.1M hydrochloric acid) was used for stations U24-U26 and added to a final total iron concentration of 0.04-0.07 nM (^{55}Fe, 0.005-0.008 nM).

A filtration unit (60104, Thermo Scientific, UK) was employed for filtration of cells for each incubation time point, and for the removal of extracellular iron using the $TiCl_3$ buffer (Figure 4.2). Two cellulose nitrate filters (≥0.45 µm, 25 mm diameter, Whatman) followed by a 0.2 µm polycarbonate (PC) membrane (25mm diameter, Whatman) (all wetted with deionized water) were placed in the filter holder (Figure 4.2). The filter funnel was screwed in place, and placed onto the plastic filtration manifold (Figure 4.2). A vacuum pump (FB70155, Fisherbrand) maintained the pressure at approximately 0.4 bar and at each incubation time point, unfixed cell samples were passed through the filter funnel, trapping cells in the 0.2 µm PC membrane (as performed by Zubkov *et al* (2007) [206]).

To remove extracellularly adsorbed ^{55}Fe, cells were washed with $TiCl_3$ buffer. Valves on the filtration unit were closed to prevent liquid passing through (Figure 4.2), after which 2 mL of $TiCl_3$ buffer was added to the funnels and incubated for 5 min. After incubation, the valves were reopened and the buffer was allowed to pass through into the waste, and filters were then rinsed with ~4 mL seawater from the Go Flo sampler.

Finally, all 0.2 µm PC filters were removed and placed in scintillation vials (20 mL, HDPE, Meridian), along with 5 mL of scintillation cocktail (Gold Star, Meridian). Samples were measured on a liquid scintillation counter (LSC) (Tri-Carb 2910, Perkin Elmer) using a counting window of 3-12 keV (based on the highest intensity decay energies of ^{55}Fe) and a count time of 2 min, which was deemed long enough to achieve a sufficient signal.

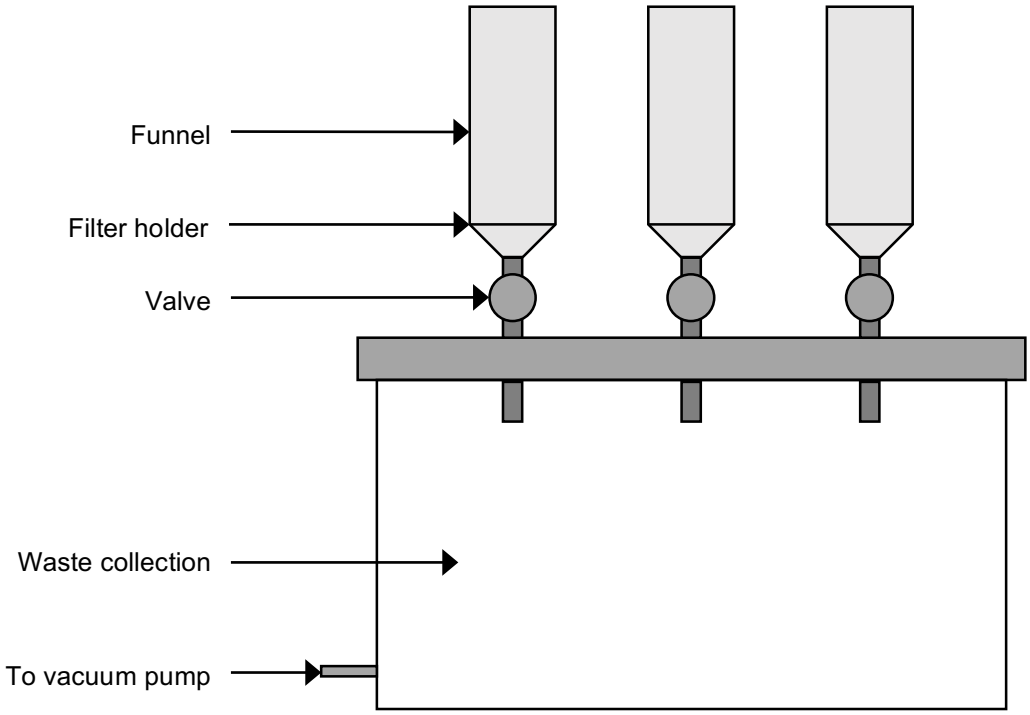

Figure 4.2: Diagrammatic representation of the filtration unit used for filtration of cell samples in iron experiments
Two cellulose nitrate filters (≥0.45 µm, 25 mm, Whatman) followed by a 0.2 µm PC membrane (25 mm, Whatman) (all wetted with deionized water) were placed in the plastic filter holder. Filtration funnels (plastic) were attached to the holders. A vacuum pump (FB70155, Fisherbrand) maintained pressure at 0.4 bar. Samples were passed over the filter, trapping cells in the 0.2 µm PC membrane, before being rinsed with ~4 mL of seawater collected from same the station. The filtration unit was from Thermo Scientific, UK (model 60104). Up to six samples can be filtered at any one time using this unit.

Data analysis

Intracellular radioactivity measurements (in CPM) of ^{55}Fe were converted to mole amounts of total iron added, which was based on the known concentrations of stable and radioactive iron in the source (Chapter 2, Section 2.4.5). Uptake rates were determined by plotting the amount of iron assimilated against time, with the gradient of linear regression providing an uptake rate in moles per hour (SI prefixes used where appropriate). Using this value, and the known amount of iron added to the sample, the percentage of iron taken up by the microbial community was calculated (Equations 4.4 and 4.5). All calculations were normalized based on the ^{55}Fe source used (Chapter 2, Section 2.4.5).

Eq. 4.4 *Uptake Rate (mol/h) × 24 = Iron assimilated (mol/day)*

Eq. 4.5 $\frac{\textit{Iron assimilated (mol/day)}}{\textit{Total iron added (mol)}} \times 100 = \textit{Iron assimilated per day (\%)}$

4.2.4 Initial measurements

In addition to the experiments outlined above, seawater samples were collected for initial analysis of cell abundance, amino acid uptake, and ambient amino acid concentration and turnover at all stations identified in Table 4.1. Cells were characterized using flow cytometry, allowing the bacterioplankton concentration at each station to be assessed, and major cell groups to be identified including *Prochlorococcus*, *Synechococcus*, heterotrophic low nucleic acid (LNA) and high nucleic acid (HNA) bacteria. Additionally, bacterioplankton metabolic activity was assessed using radiolabeled Met (^{35}S-Met, Perkin Elmer) and leucine (Leu) bioassays (^{3}H-Leu, Hartmann Analytic) (AMT-25 and AMT-24, respectively). The procedures for these analyses are discussed in detail in Chapter 2 (Section 2.4).

Ambient iron concentration (AMT-25)

Preparation of sample bottles

Seawater for determination of iron content was collected in trace metal cleaned low density polyethylene (LDPE) 60mL bottles (Nalgene). The cleaning procedure [255] was conducted prior to the cruise and was more extensive than the basic acid cleaning described in Chapter 2, Section 2.2.1. The initial cleaning step involved soaking in a dilute detergent solution (2% Decon 90, diluted with deionized water) for 1 week, followed by submersion in a ~6M HCl bath for 1 week, with thorough rinsing between each stage using deionized water [255]. Bottles were then filled with deionized water, to which 70µL of

concentrated hydrochloric acid (UpA grade, Romil) was added, and stored in plastic sample bags until required for use during AMT-25.

Sampling

Working in a laminar flow hood, 60 mL seawater samples were collected from the Go Flo sampler at each station identified in Table 4.1 (AMT-25 only). Note that the bottles were first rinsed with seawater three times before collection of the sample to remove traces of acid from the bottle. Two samples were collected for each station: total iron (unfiltered seawater) and dissolved iron. For the dissolved iron samples, seawater was filtered using a 0.2 µm Sartobran 300 Sterile Capsule (Sartorius Stedim) [e.g. 256]. Additionally, to ensure Ctl and +N nutrient addition samples were not contaminated with iron, unfiltered samples were collected for these incubations.

Measurement

The seawater samples were frozen until acidification using 70 µL concentrated hydrochloric acid (UpA grade, Romil). Samples were stored for approximately 6 months before analysis at the Marine Biogeochemistry Division at GEOMAR (Kiel, Germany), following a well-established mass spectrometry protocol, using isotope spiking and standard addition analysis [257] on an inductively coupled plasma mass spectrometer (Thermofisher Element XR). Sample preparation was performed with direction from Insa Rapp (GEOMAR, Kiel) [see 257]. Sample measurement (via mass spectrometry) and subsequent data analysis was conducted solely by Insa Rapp.

4.3 Results

4.3.1 Location of South Atlantic gyre: cruise AMT-25

Bacterioplankton abundance was measured at every station, except A25 and was plotted against latitude (Figure 4.3a). There was a slight decrease in cell abundance between 18º and 28ºS, with the lowest cell concentration at approximately 18ºS. However, it is interesting to note that the cell concentration decreased again between approximately 35ºS and the final station (~40ºS).

Analysis of bacterioplankton populations (Figure 4.3b), showed that LNA bacteria and *Prochlorococcus* were dominant across large parts of the AMT25 transect. However, south of ~30ºS *Prochlorococcus* populations started to decrease from 20-38% to 0-18% of total bacterioplankton, with no *Prochlorococcus* cells identified at the final station. The proportion of bacterioplankton that were *Synechococcus* was also different north and south of approximately 30ºS, with populations increasing from <1% north of 30ºS, compared to >1% south of 30ºS. Heterotrophic bacterioplankton (i.e. LNA and HNA bacteria) dominate the total bacterial population across the whole of the transect.

The Met uptake rate was lowest between approximately 10º and 27ºS (<0.1 nM/day); although, there was a further decrease in Met uptake rate between 36º and 40ºS (Figure 4.3c). Ambient Met concentrations ranged from approximately 0.1 - 0.3 nM, with the lowest concentration at ~22ºS (0.11 nM) (Figure 4.3d). Finally, between approximately 20º and 35ºS, the turnover time of ambient Met was <70 h (Figure 4.3e). Outside of this location, the turnover times were >100 h, aside from the most southerly station analysed (~23 h).

Based on the above analyses of the seawater samples, the location of the SAG (defined by cell abundance and amino acid uptake, Figure 4.3) was determined to be in the approximate latitudinal region of 13-28ºS. This distinguished stations A18-A21 as inside the SAG, and stations A17 and A22-25 as outside the gyre.

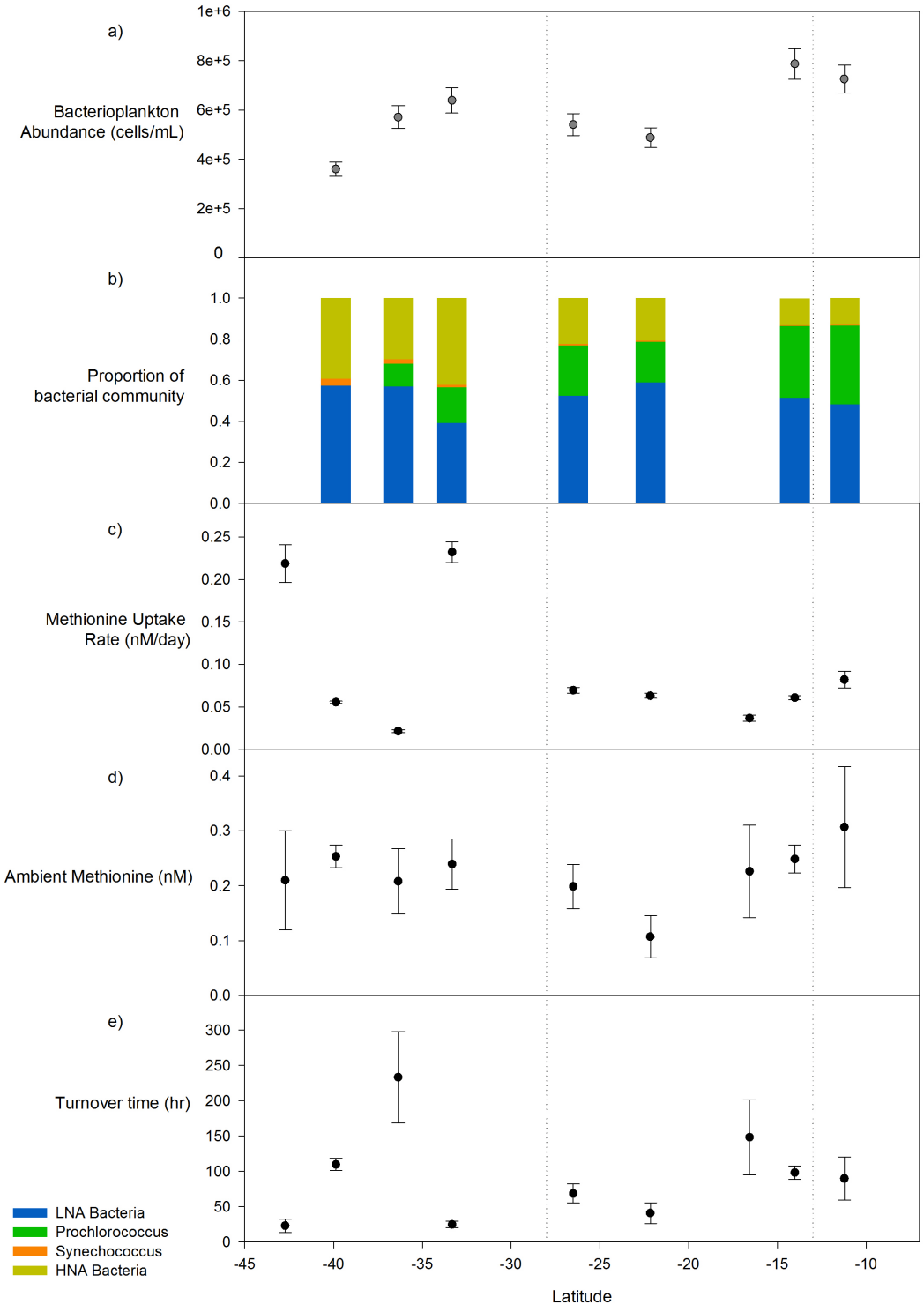

Figure 4.3: Bacterioplankton concentration and methionine bioassay data from initial samples taken in the South Atlantic during AMT-25
Plots shows (a) ambient bacterioplankton abundance, (b) proportion of major bacterioplankton groups, (c) Met uptake rate, (d) ambient Met, and (e) total turnover time of ambient Met, all plotted against latitude. The approximate location of the SAG is indicated using dotted lines. Calculation of error bars are described in Sections 2.3.3 and 2.4.4.

Ambient iron concentration

Dissolved and total iron concentrations were measured in water column samples from the AMT-25 transect, covering the North and South Atlantic (Figure 4.4), with sample measurement via mass spectrometry and subsequent data analysis conducted by Insa Rapp (GEOMAR, Kiel). Stations were omitted if the dissolved iron was higher than the total iron, as this should not occur and thus indicated an issue with the sample.

Total (unfiltered) iron concentrations in the North Atlantic ranged from 1.23 - 14.13 nM, and in the South Atlantic ranged from 0.39 - 1.35 nM. Dissolved (0.2 µm filtered) iron concentrations were 0.20 - 2.84 nM in the North Atlantic, and 0.17 - 0.52 nM in the South. It is interesting to note that there was no clear division in iron concentrations between inside the South Atlantic gyre (13-28ºS) and out of the gyre, although there were limited samples inside the gyre due to the omission of stations, as described above.

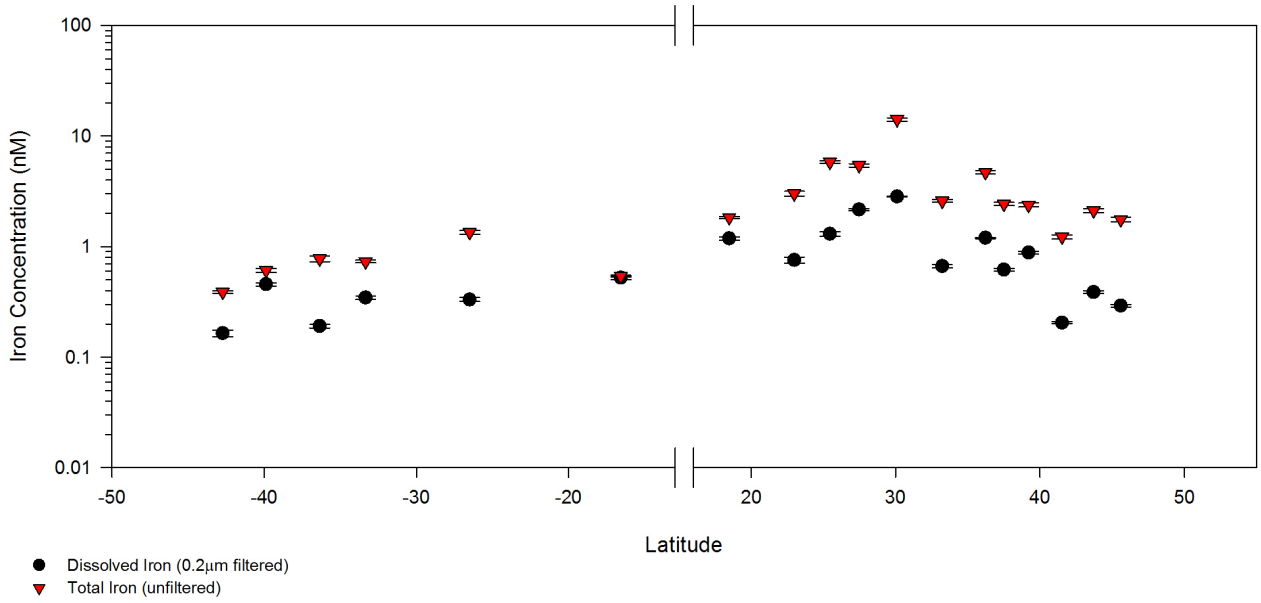

Figure 4.4: Concentration of total and dissolved iron in the initial samples taken in the South Atlantic during AMT-25
Dissolved (black circles) and total (red triangles) iron concentrations are plotted against latitude across the whole of the Atlantic transect, which was analysed during AMT-25. Separation between the two fractions was through a 0.2 µm filter. Error bars represent standard deviation, as calculated by Insa Rapp (GEOMAR, Kiel). Samples with a higher dissolved iron concentration compared to total iron, were omitted.

4.3.2 Location of South Atlantic gyre: cruise AMT-24

Figure 4.5 shows the cell abundance and Leu bioassay measurements at each station identified in Table 4.1. Bacterioplankton concentration, major bacterioplankton groups, Leu uptake rate, ambient Leu concentration, and total turnover time of ambient Leu were all plotted against latitude (Figure 4.5a-e, respectively).

The cell concentration between 0-35ºS falls within approximately 3.5 - 6.5 x10^5 cells/mL; however, south of 35ºS there was a significant increase in cell concentration to approximately 8.5 - 10.5 x10^5 cells/mL (Figure 4.5a). The lowest cell concentrations were observed between approximately 15º and 30ºS. The key difference when analyzing the proportions of major bacterioplankton groups (Figure 4.5b) was the appearance of *Synechococcus* south of 35ºS (2.5-6.5% of bacterioplankton). Prior to this, the proportion of *Synechococcus* within the bacterioplankton was <1%. Furthermore, *Prochlorococcus* were not present south of approximately 38ºS.

Leu uptake rate was <0.45 nM/day between approximately 10º and 35ºS, whereas out of this region, rates were >0.6 nM/day (Figure 4.5c). Ambient Leu was 0.092 ± 0.012 nM and remained relatively consistent across the transect (Figure 4.5d). Finally, total turnover time of ambient Leu was relatively consistent along the transect (1.8 - 5.4 h), except between approximately 16ºS and 22ºS, where it increased to 8.3-13.3 h, although there are larger uncertainties in these samples. The lowest turnover times were south of 35ºS (<3 h) (Figure 4.5e).

Therefore, based on analysis of all initial measurements, the location of the SAG (defined by cell abundance and amino acid uptake, Figure 4.5) was found between approximately 10º and 35ºS during AMT-24, with stations U18-U23 allocated as inside the gyre, and stations U16, U17 and U24-27 as outside the SAG.

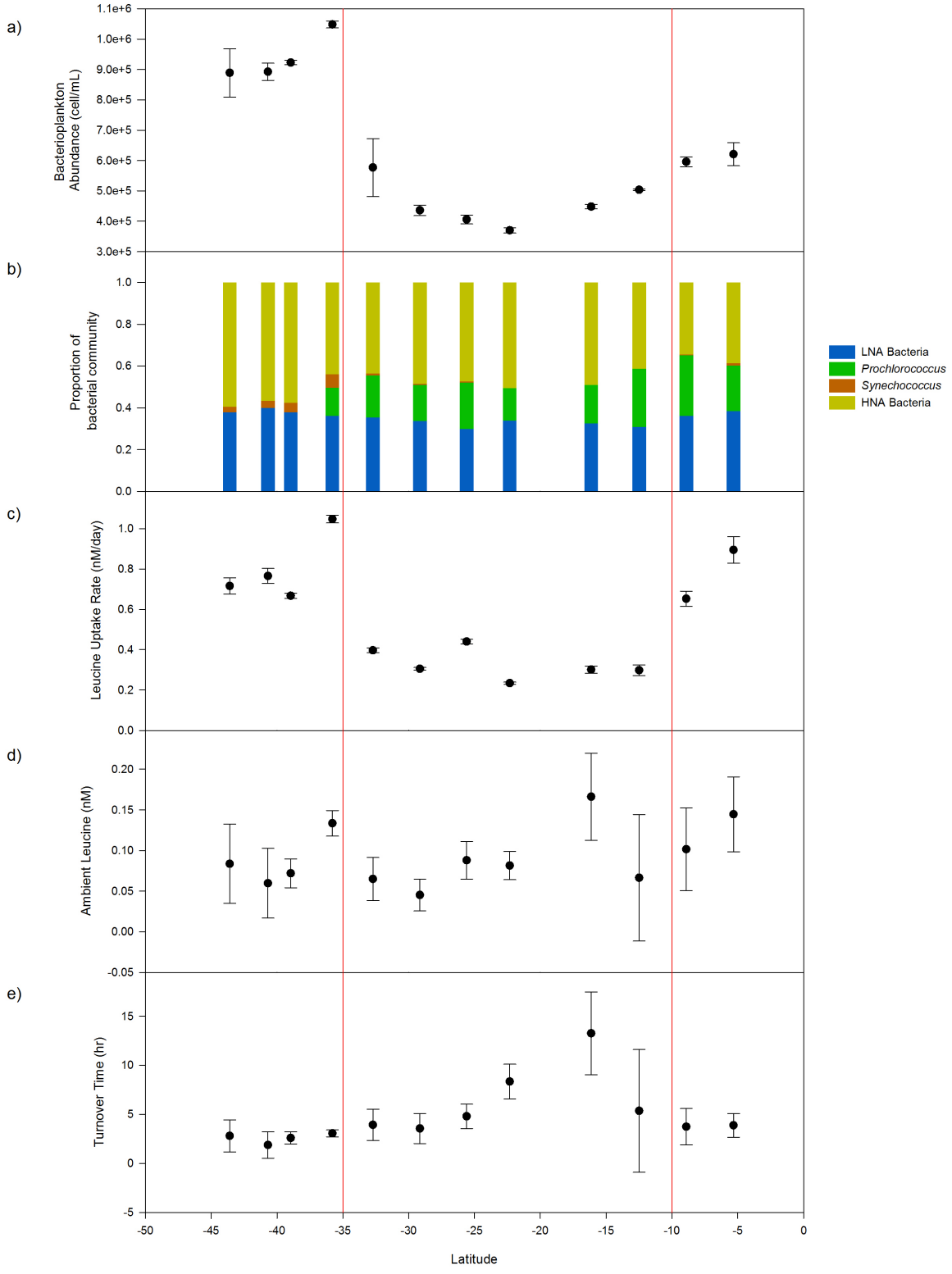

Figure 4.5: Bacterioplankton concentration and leucine bioassay data from initial samples taken in the South Atlantic during AMT-24

Plots showing (a) ambient bacterioplankton abundance, (b) proportion of major bacterioplankton groups, (c) Leu uptake rate, (d) ambient Leu, and (e) total turnover time of ambient Leu, all plotted against latitude. The approximate location of the SAG is highlighted using red lines. Error bars for uptake rate and turnover time show standard error, error bars for ambient Met show error of propagation, and error bars for cell counts show standard deviation (see Sections 2.3.3 and 2.4.4).

4.3.3 Nutrient addition experiments in the South Atlantic during AMT-25

Nutrient enrichment experiments were conducted at all stations highlighted in Table 4.1, with exceptions of 48 h incubations for A23, and 24 h incubations for A25, and Met analysis at 24 h for station A21 (as no samples were taken, or results were unreliable due to poor r^2 values).

To verify that samples were not contaminated, total iron was measured in the control (Ctl) and ammonium only (+N) incubations (Table 4.4). Iron concentration did not increase from the initial in any Ctl or +N incubation. Additionally, all Ctl incubations, +N incubations and initial samples had a total iron concentration below 1 nM (except A21, initial, which was below 1.4 nM), which is lower than the 2 nM iron added to +Fe and +NFe samples (Table 4.3). However, it is should be noted that in all instances, the initial iron concentration is higher than the concentrations in the incubations, which is unusual and may suggest inconsistencies in measurement or potential contamination.

Table 4.4 The concentration of iron in initial samples versus ammonium and control incubations
The iron concentration of control (Ctl) and ammonium only (+N) incubations was monitored for each station. Additionally, the initial ambient iron concentrations are shown. Concentrations show total iron from unfiltered samples. Note that all incubation samples were taken after 48 h, except station 23, which was sampled at 24 h.

Station ID	Initial Total Iron (nM)	Incubation Samples	
		Nutrient Additions	Total Iron Conc (nM)
A20	0.678 ± 0.015	Ctl	0.422 ± 0.023
		+N	0.631 ± 0.014
A21	1.350 ± 0.056	Ctl	0.387 ± 0.014
		+N	0.363 ± 0.011
A22	0.735 ± 0.021	Ctl	0.455 ± 0.010
		+N	0.543 ± 0.019
A23	0.777 ± 0.046	Ctl	0.688 ± 0.021
		+N	0.456 ± 0.016
A25	0.389 ± 0.010	Ctl	0.370 ± 0.017
		+N	0.282 ± 0.014

Cell concentration

Figure 4.6 shows the cell concentrations in samples with added nutrients plotted against the cell concentration of the controls. The percentage change of cell concentration was calculated as shown in Equation 4.3, and presented in Figure 4.7.

Ammonium

Upon addition of ammonium (Figure 4.6a) after 24 h incubation, all samples (except station A20) were found along the unity line, thus showed no change between control and nutrient addition. This can be seen in Figure 4.7, which showed that the incubation at station A20 was the only one with a large percentage increase from the control after 24 h. After 48 h, three out of the four incubations were found above the unity line, thus showing that cell concentrations were generally higher in ammonium supplemented samples after a two-day incubation (Figure 4.6a). The exception was A25, where no difference from the control was observed after 48 h (Figure 4.7).

Ammonium and iron

Addition of ammonium and iron together (+NFe) (Figure 4.6c) also stimulated an increase in cell concentration from the control after 48 h for three out of four incubations. As before, only station A20 showed an increase after 24 h, and A25 showed no increase after 48 h (Figures 4.6c and 4.7). Indeed, the trend observed upon addition of both nutrients (+NFe) was the same as adding ammonium alone (+N) (no statistical difference in cell concentration between +N and +NFe incubations: paired t-test $p = 0.314$ F-test value = 1.0, critical value = 5.0). However, it should be noted that upon addition of both nutrients (+NFe) at station A20 after 24 h, the cell abundance increase was more than doubled compared to addition of ammonium alone; although, this difference was reduced after 48 h (Figure 4.7).

Iron

Finally, the addition of iron only showed no increase in cell concentration at any station or time point (Figures 4.6b and 4.7).

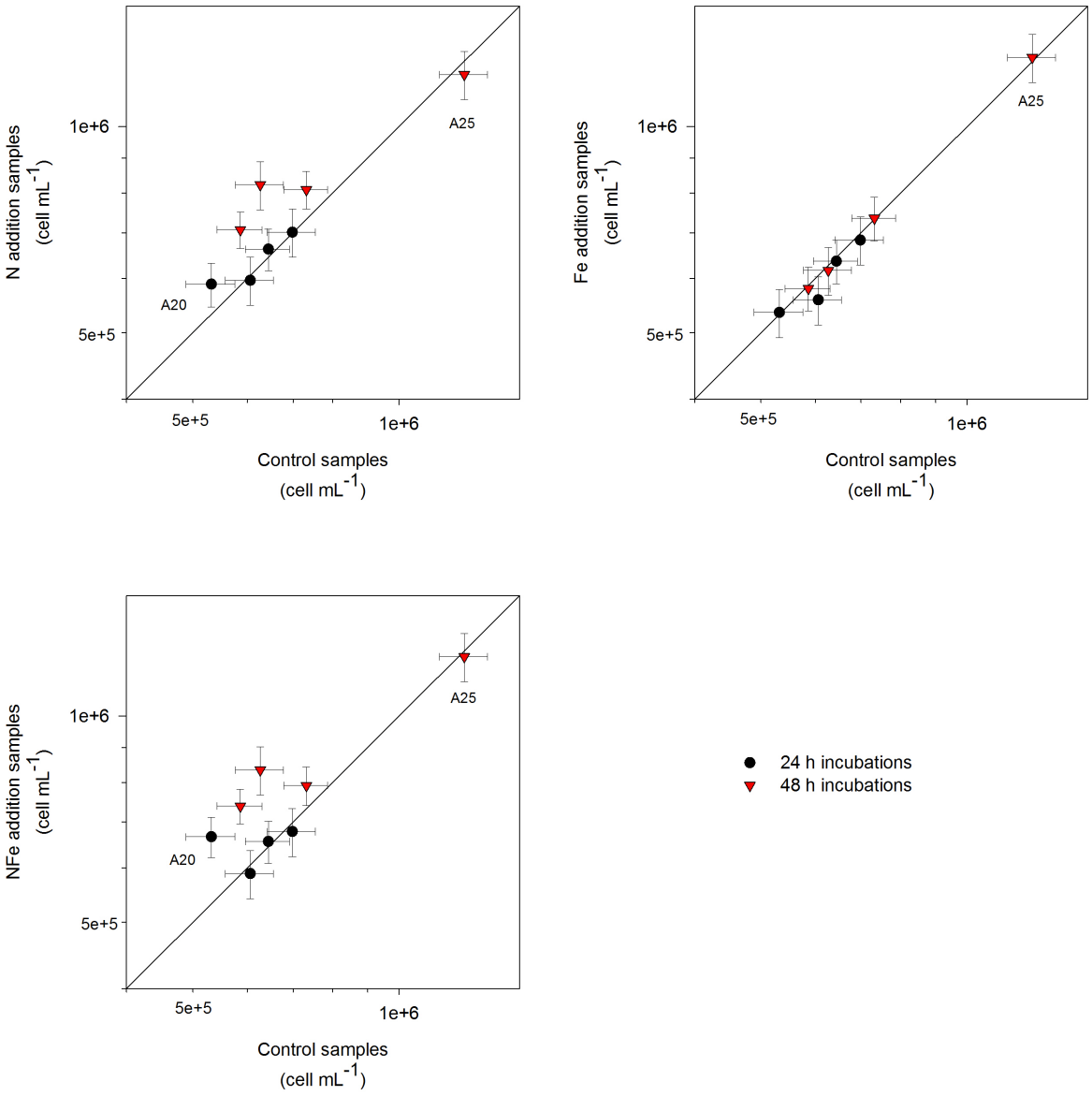

Figure 4.6: Changes in bacterioplankton concentration upon addition of ammonium/iron during AMT-25
Effect on cell concentration of addition of (a) ammonium, (b) iron, or (c) both nutrients. Black circles and red triangles represent samples incubated for 24 and 48 h, respectively. Units are cells/mL, error bars represent uncertainty in cell count (Section 2.3.3). The diagonal line is the unity line whereby cell concentration in the control and nutrient addition sample are equal.

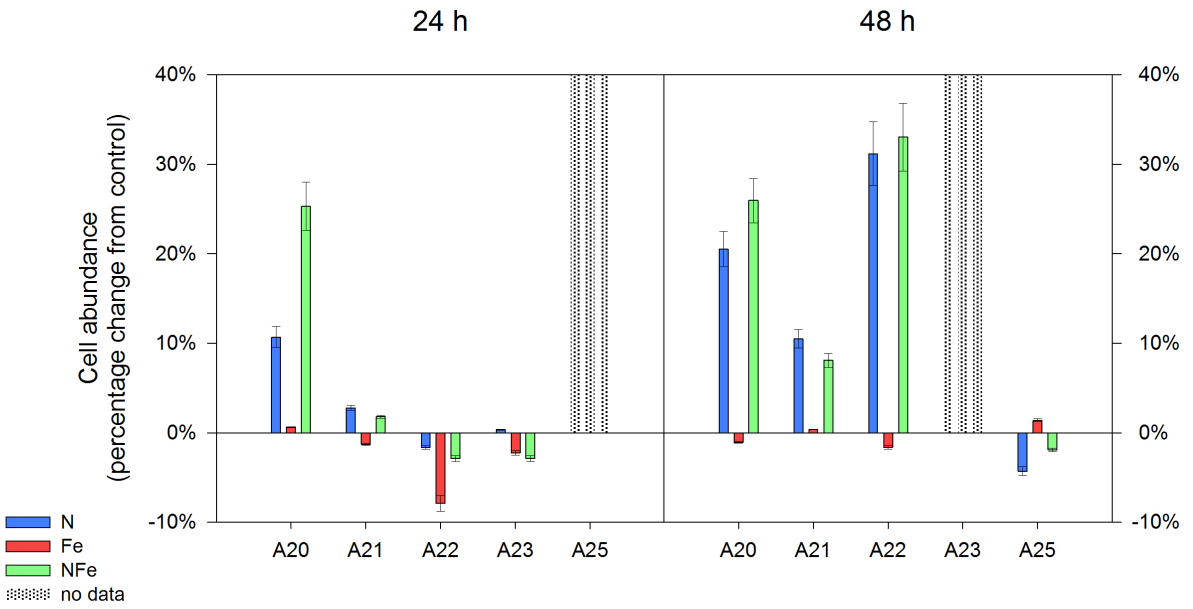

Figure 4.7: Percentage change in bacterioplankton concentration upon addition of ammonium/iron during AMT-25
Based on Equation 4.3 above, the percentage changes in cell concentration from the control sample upon nutrient addition are presented. Each cluster represents ammonium (blue), iron (red), or ammonium + iron (green) additions at each station. Bars in grey show stations without data. Error bars are based on the error of propagation of cell concentration uncertainties from control and nutrient addition samples.

Methionine uptake rate

Changes in Met uptake rate upon nutrient additions are shown in Figure 4.8, with percentage change from the control shown in Figure 4.9.

Ammonium

Upon addition of ammonium alone, all stations showed a notable increase in Met uptake, except station A23, 24 h incubation, which is very close to the unity line (Figure 4.8a). The highest percentage increase from the control was seen at station A20 after 48 h (~150% increase). The only incubation to show a slight decrease (~10%) from the control was A23 (24 h) (Figure 4.9). It should be noted that the error bars for station A20, 48 h, are large

due to an r^2 value of <0.7 in the control sample; however, this does not adversely affect the results as the error bars do not overlap the unity line (Figure 4.8a).

Ammonium and iron

All samples showed an increase in Met uptake when both nutrients were added (Figure 4.8c). The lowest change was seen at station A22, 24h (~17%), and the highest change at station A20, 24 h (~420%) (no data for 48 h at this station) (Figure 4.9). As was observed for changes in cell concentration, there was no statistical difference between adding ammonium alone (+N) or in combination with iron (+NFe) (paired t-test p = 0.152, F-test value of 1.6, critical value 9.6), although, as before, at station A20 (24 h) the increase in Met uptake was more than double upon addition of both nutrients compared to ammonium alone.

Iron

Addition of iron resulted in a slight increase in Met uptake in samples incubated for 24 h (Figure 4.8b, all 24 h stations located above the unity line); however, paired t-test analysis against the control samples showed no statistical difference between Met uptake in the control and iron addition sample (paired t-test p = 0.123, F-test value of 3.14, critical value 39 (24 h incubations only)). After 48 h, no change was observed (Figures 4.8b 4.9). It is interesting to note that at station A23, 24 h the +Fe and +NFe incubations saw a similar percentage change (44±11 and 61±9% increase, respectively), which was not seen when ammonium was added alone (Figure 4.9).

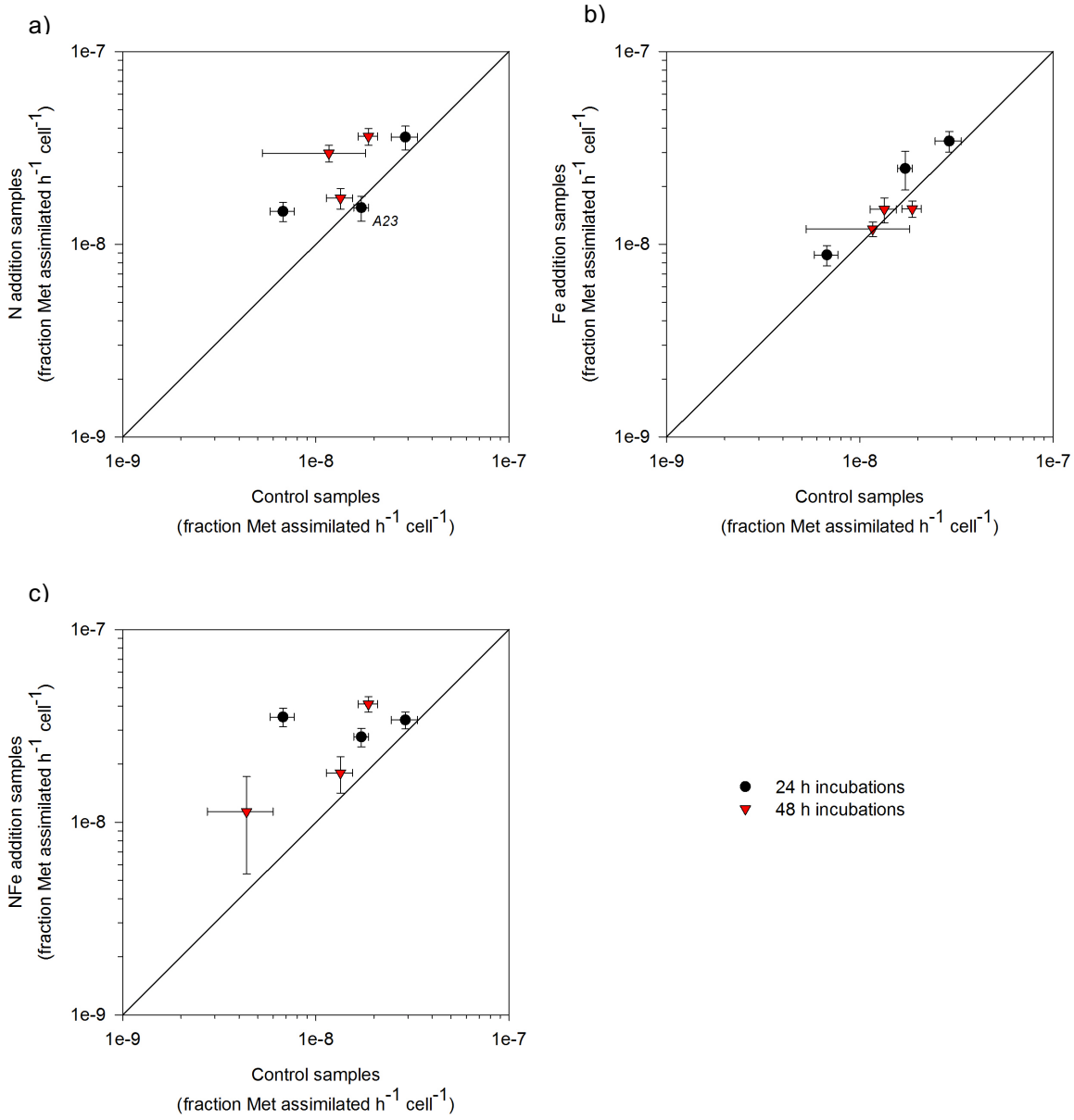

Figure 4.8: Changes in methionine uptake rate upon addition of ammonium/iron during AMT-25

Effect on Met uptake rate of addition of (a) ammonium, (b) iron, or (c) both nutrients. Black circles and red triangles represent 24 and 48 h samples, respectively. Units are fraction of Met assimilated (relative to the amount added) per cell per hour. The diagonal line is the unity line whereby cell concentration in the control and nutrient addition samples are equal. Highlighted are stations of interest. Error bars represent error of propagation of cell concentration (Section 2.3.3) and methionine uptake (Section 2.4.4)

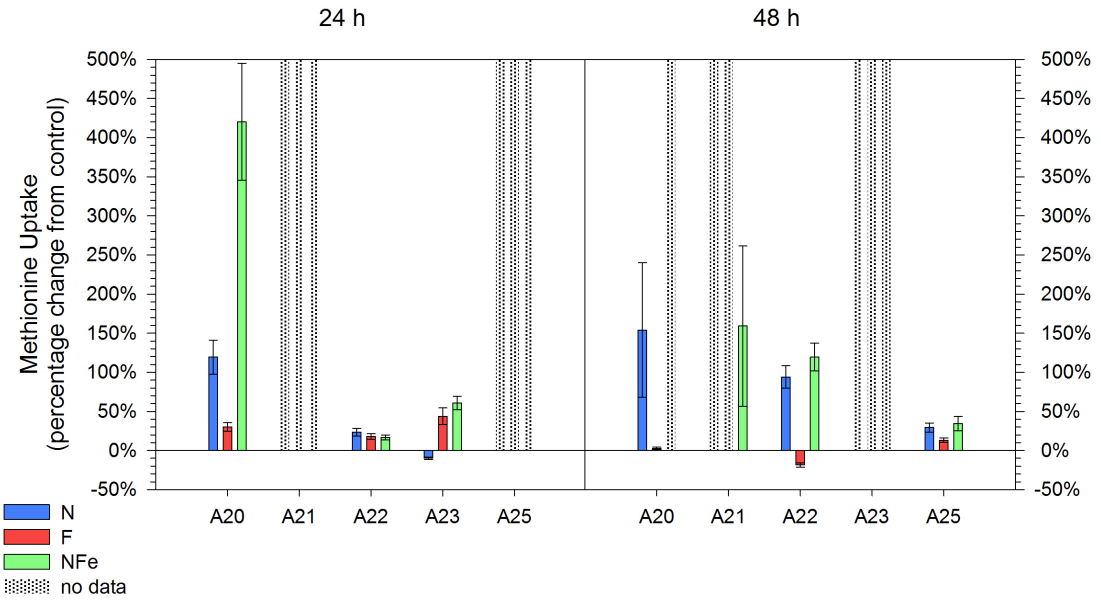

Figure 4.9: Percentage change in methionine uptake rate upon addition of ammonium/iron during AMT-25
The percentage changes in Met uptake rate from the control sample upon nutrient addition (Equation 4.3) are presented. Each cluster represents ammonium (blue), iron (red), or ammonium + iron (green) additions for each station. Bars in grey show stations without data. Error bars represent error of propagation from control and nutrient addition samples.

Individual bacterioplankton groups

Using flow cytometric identification, the effect of nutrient additions on the major bacterioplankton groups was assessed (Figure 4.10). Cyanobacteria (i.e. *Prochlorococcus* and *Synechococcus*) and LNA bacteria showed no increase in cell concentration upon addition of any nutrient (Figures 4.10a-i), except following addition of ammonium (alone or in combination) at stations A22 (LNA bacteria, *Synechococcus* and *Prochlorococcus*) and A20 (*Synechococcus* only) (Figures 4.10a, 4.10d, and 4.10g). Conversely, HNA bacteria showed a notable increase in cell concentration upon addition of ammonium alone (+N), and in combination with iron (+NFe) (Figures 4.10j, and 4.10l), at all stations, except station A25, and after 24 h for stations A22 and A23. There was no increase in any major bacterioplankton population following addition of iron alone (Figures 4.10b, 4.10e, 4.10h, and 4.10k). It is interesting to note that at most stations, *Prochlorococcus* showed a decrease in cell abundance upon the addition of +N or +NFe.

An additional large heterotrophic HNA bacterial population (termed L-HNA bacteria) was observed in nutrient addition samples (+N, +Fe, and +NFe) at station A20, and in all samples (including the initial sample taken before incubation) at station A21.

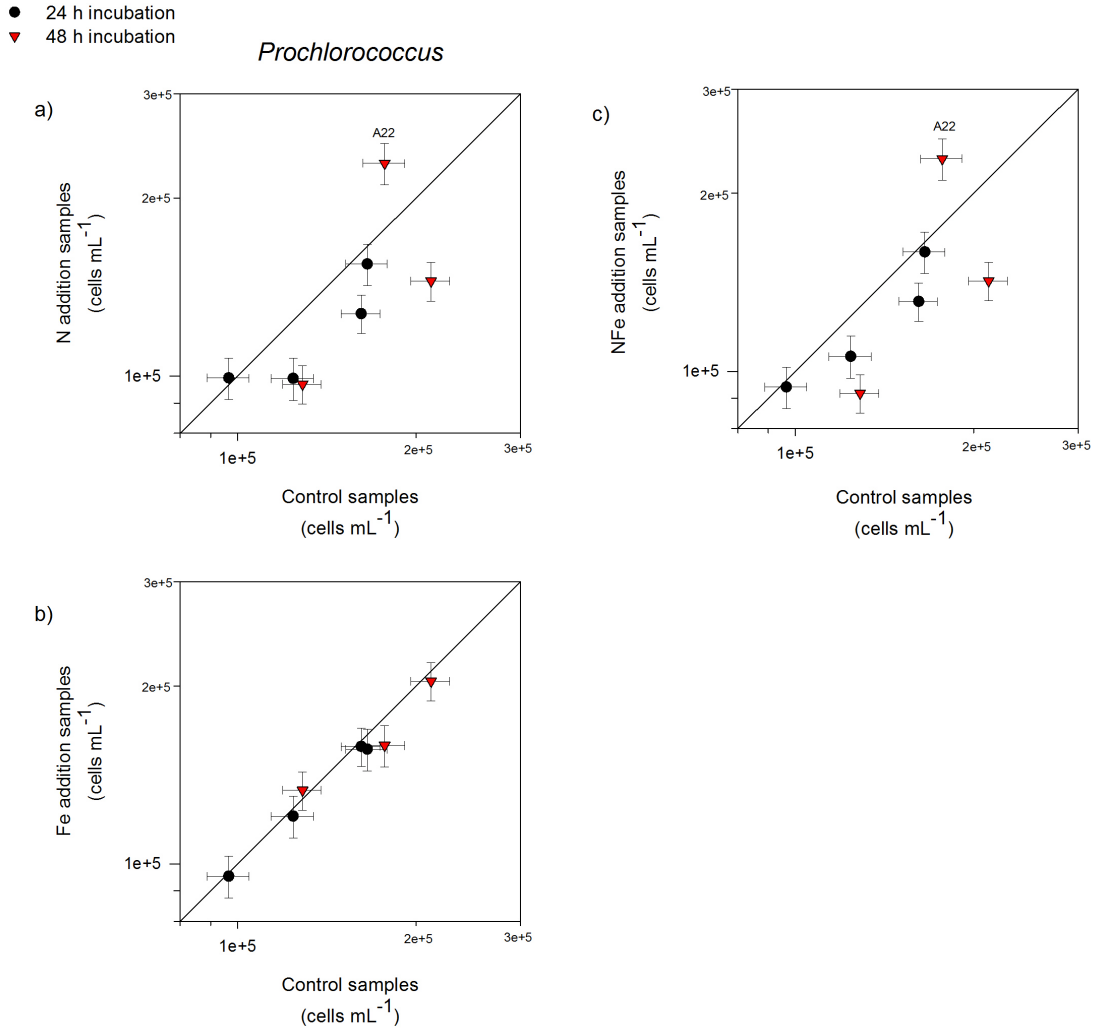

Figure 4.10: Changes in cell abundance of key bacterioplankton populations upon addition of ammonium/iron during AMT-25
Effect of addition of (a, d, g, j) ammonium, (b, e, h, k) iron, or (c, f, i, l) both nutrients on the cell abundance of (a-c) Prochlorococcus, (d-f) Synechococcus, (g-i) LNA Bacteria, or (j-l) HNA bacteria. Blue and black circles represent 24 and 48 h samples, respectively. Units are cells/mL. Error calculated as described in Section 2.3.3. The diagonal line is the unity line whereby cell concentration in the control and nutrient addition samples are equal. Highlighted are stations of interest.

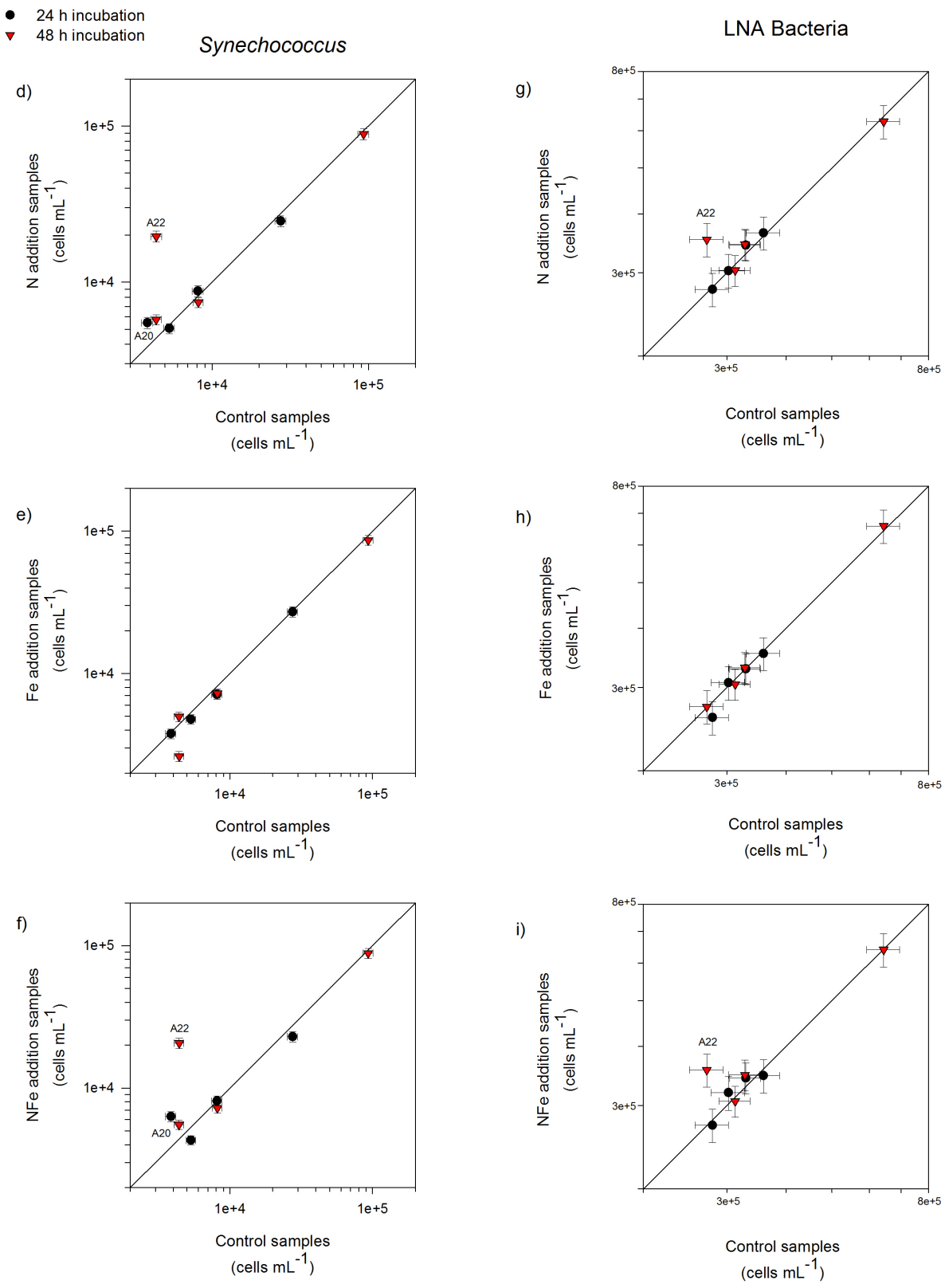

Figure 4.10: Changes in cell abundance of key bacterioplankton populations upon addition of ammonium/iron during AMT-25
Continued.

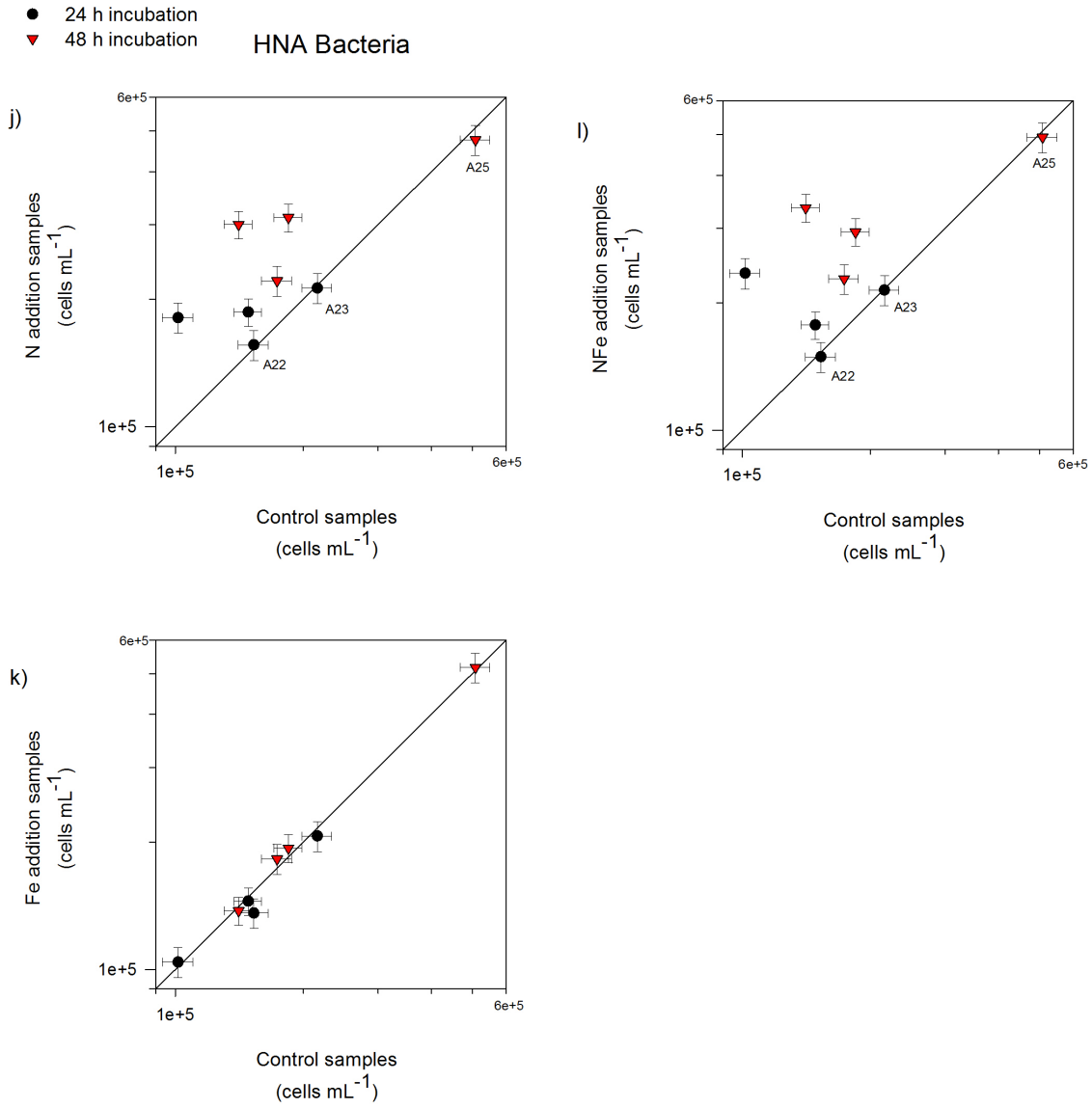

Figure 4.10: Changes in cell abundance of key bacterioplankton populations upon addition of ammonium/iron during AMT-25
Continued.

4.3.4 Iron uptake experiments

During cruise AMT-24, seawater samples were incubated with radiolabeled (^{55}Fe) iron chloride and monitored over a period of approximately 24 h at all stations identified in Table 4.1. To assess uptake of iron, the unassimilated extracellular iron was removed using the $TiCl_3$ buffer [253] allowing sole measurement of intracellular iron. Table 4.5 provides uptake rates at each station, and the calculated proportion of iron taken up by the microbial community after 1 day.

All experiments showed a very minimal amount of iron uptake per day in comparison to the amount of iron added to samples (≤0.21%), and many showed either negative or unreliable (poor r^2 value, or only 2 data points available) uptake rates (Table 4.5). The highest level of uptake was seen in sample U22 (2.14±0.54 x10^{-18} mol/h).

Table 4.5: Bacterioplankton iron uptake from AMT-24 experiments
Community uptake rate is based on the concentration of iron assimilated per hour. Using this value, the percentage of iron taken up in one day by the microbial community was calculated relative to the concentration of iron added to the sample (Equations 4.4 and 4.5).
Samples in red show no uptake due to a negative uptake rate. Samples in italics can be considered unreliable due to either a low r-squared (r^2) value, marked by a single asterisk, or experiments with only 2 data points, marked with a double asterisk.

Station ID	Community Uptake Rate (x10^{-19} mol Fe/h)	Fraction of iron assimilated (per day)
U16	-3.11 ± 1.2	-0.004 ± 0.002 %
U17 **	*13.7*	*0.017 %*
U18 **	*5.22*	*0.007 %*
U19	1.48±0.03	0.002 ± 0.00004 %
U20	-6.43±11.2	-0.006 ± 0.011 %
U21 *	*1.02±1.28*	*0.001 ± 0.002 %*
U22	21.4±5.39	0.21 ± 0.005 %
U23 *	*0.85±8.83*	*0.001 ± 0.007 %*
U24	5.98±1.10	0.033 ± 0.006 %
U25	1.59±0.07	0.009 ± 0.0004 %
U26	0.54±0.18	0.003 ± 0.001 %

4.4. Discussion

4.4.1 Gyre location and initial measurements

Identification of the exact location of the SAG for both cruises allowed a comparison between cellular responses inside the oligotrophic gyre, and the more productive non-gyre waters. The SAG was located between approximately 13-28ºS and 10-35ºS for the AMT-

25 and AMT-24 cruises, respectively. These locations were based on bacterial abundance as well as amino acid uptake rates, turnover time and ambient concentration. Additionally, increasing *Synechococcus* populations and decreasing *Prochlorococcus* populations were a good indicator of the transition into more productive waters [158], thus providing further data to determine the gyre boundaries. Supplementary temperature, salinity and chlorophyll concentration data (provided by the British Oceanography Data Centre (contains data supplied by the Natural Environment Research Council)) also supports these gyre locations (Appendix C and E). The locations of the SAG were in good agreement with literature reports [227], with slight variations likely to be due to inter-annual variations of gyre boundaries [33].

Values from Met/Leu bioassays in the SAG were similar to those of previous studies [e.g. 188,198,200]. Additionally, validation of cell counts can be seen through both AMT cruises producing similar bacterioplankton abundances (Figure 4.3 and 4.5). Additionally, cell counts of *Prochlorococcus* (1.4±0.9 and 0.9±0.3 $x10^5$ cells/mL, for AMT-25 and AMT-24) and *Synechococcus* (2.7±1.8 and 2.9±1.6 $x10^3$ cells/mL, for AMT-25 and AMT-24) matched those of Heywood *et al* (2006) in the SAG above the nitracline (1.2±0.1 $x10^5$ cells/mL and 1.9±0.3 $x10^3$ cells/mL for *Prochlorococcus* and *Synechococcus*, respectively) [226]. Finally, cell counts inside the SAG during AMT-25 (~4.9 - 7.9 $x10^5$ cells/mL) agree with measurement range observed by Priscila Lange (University of Oxford) during the same cruise (~6.3 - 9.9 $x10^5$ cells/mL, Appendix D).

It should be noted that the gyre locations highlighted above are not an absolute certainty, as different parameters may not always indicate the same gyre boundary. For example, using cell concentration alone would yield the northern edge of the SAG at approximately 18ºS during AMT-25, but when considering other parameters such as Met uptake, this is shifted north to ~13ºS. As such, stations located on the edges may behave as "inside" or "outside" the gyre, and will be highlighted in the discussion when relevant.

Ambient iron concentrations measured in the South Atlantic during AMT-25 were lower than the North Atlantic (Figure 4.4), in agreement with previous studies [e.g. 126,127,258]. As

dust is a major source of iron to the open surface ocean [71,126,218], the difference between the North and South Atlantic iron concentrations is primarily due to reduced dust deposition in the South Atlantic [e.g. 72].

Within the South Atlantic, there is no discernible difference between iron concentrations inside and outside of the SAG (Figure 4.4), despite previous studies noting an increase in dissolved iron out of the SAG centre, and moving closer to coastal waters [e.g. 126,182,243]. However, there were only two stations inside the gyre with reliable values, due to the omission of other stations that had implausible data (i.e. having a higher filtered iron concentration in comparison to unfiltered iron).

Elevated iron concentrations in the south western South Atlantic may be observed due to flux from the subtropical shelf [182,243], or Patagonian dust transport [72]. For example, Bowie *et al* (2002) noted increased total dissolvable iron concentrations south of the South Atlantic subtropical convergence zone (>1.5nM on ship analysis, versus 0.6nM between 5-30ºS) [182], and Rijkenberg *et al* (2014) noted elevated dissolved iron concentrations (up to 6.1nM) between 33-40ºS, due lateral transport from the shelf of South America [243]. As elevated concentrations were not observed in the more southerly stations of this study, it is possible that the cruise transect during October 2015 did not pass close enough to these areas to experience increased lateral, benthic or aerial iron inputs.

4.4.2 Bacterioplankton response to iron addition

Based on the results of two independent experiments, the low iron concentrations observed in the South Atlantic [115,126,127,176] do not appear to affect bacterioplankton abundance or metabolic activity.

The nutrient enrichment studies showed no increase in bacterial abundance or Met uptake rate upon addition of iron (Figures 4.6 - 4.9). This was true both inside and outside of the SAG. Even when combined with nitrogen, no significant response from iron additions was

observed. Furthermore, as Met uptake rates and cell abundance did not decrease upon addition of iron, cells were seen to not be harmed by the potentially toxic effects of high iron concentrations [89] (e.g. nanomolar concentration of iron saw DNA breakages in *E.coli* as a result of the Fenton reaction [259]).

Minimal intracellular uptake was observed upon incubation with radiolabelled iron (Table 4.5). Iron-limited cells have been shown to have a higher uptake rate (e.g. 0.12 nM Fe/day [206]) compared to iron-sufficient cells (e.g. 0.02 nM Fe/day [206]) [250,251]; thus, the very low uptake rates observed in this study (≤5.04 $x10^{-7}$ nM Fe/day), imply cells were not iron stressed. This is in agreement with M. Hartmann (unpublished) who reported no iron uptake in the South Atlantic. Equally, Maldonado and Price (2001) could not always detect iron uptake rates in an iron-replete marine diatom [250]. As a comparison, laboratory cultures of iron-starved *Synechococcus* were able to take up iron (M. Hartmann, unpublished data), and Zubkov *et al* (2007) observed high iron uptake in HNLC waters (uptake of 49±3% of initially added radiotracer) compared to minimal uptake in productive waters (6.3±0.1% of tracer) [206]. Furthermore, the negligible intracellular iron observed in this study was not due to cellular damage from the $TiCl_3$ buffer as indicated by previous studies [e.g. 253,260,261], as well as an independent laboratory experiment (Appendix G).

The results agree with the limited previous nutrient enrichment studies that have been conducted in the South Atlantic; for example, Behrenfeld and Kolber (1999) concluded that phytoplankton across the Atlantic were not iron limited [178]. Additionally, Grob *et al* (2015) and Moore *et al* (2009) noted that there was no increase in carbon fixation rate upon addition of iron [176,177]. Interestingly, Browning *et al* (2017) showed that co-limitation of phytoplankton growth by iron and nitrogen occurred inside the south-eastern South Atlantic gyre, but out of the gyre, nitrogen was the proximal limiting nutrient [179]. Laboratory studies conducted by Timmermans *et al* (2005) showed that growth rates of three species of phytoplankton were only effected at dissolved inorganic iron concentrations of <10 pM (with iron limiting concentrations only reached through addition of excess desferrioxamine-B, a chelating agent) [262], which is significantly lower than

some previous ambient iron concentrations measured in the South Atlantic [e.g. 182,243, this study].

Oceanic plankton have a number of adaptations for surviving in environments with a very low concentration of iron, such as a slower growth rate [88,170], and a large surface area:volume ratio, which provides a bigger area for iron (and indeed all nutrient) uptake [2,88]. Additionally, the cellular iron requirement for open ocean species is much lower than similar species found in more nutrient-rich coastal waters [88,263]. This reduced iron quota can be achieved through a number of cellular adaptations, including substitutions of iron-rich for iron-free proteins (e.g. replacement of ferredoxin with flavodoxin in phytoplankton [88 and references therein]); elimination of unnecessary iron-containing proteins (e.g. removal of ferredoxin from some clades of *Prochlorococcus* [264]); and reduction in the iron content of iron-containing molecular structures (e.g. a reduction in the iron:chlorophyll ratio in the photosystems of oceanic, compared to coastal phytoplankton [88]). The combination of all these adaptations help explain why bacterioplankton were not stressed, as demonstrated by no change in bacterioplankton abundance or Met uptake rate upon addition of iron, or the low intracellular iron uptake that was observed in this study.

Iron bioavailability

Due to the insolubility of iron in oxygenated seawaters [67,95], difficulties in working with iron are inevitable. This study followed several established procedures using an acidified stock to maintain iron in solution prior to addition to the incubation bottles [e.g. 136,239,245], although some studies do not state the form in which iron was added or stored [e.g. 123,124,134,221]. Precipitation of iron is inevitable and would have resulted in biologically unavailable iron. This would have been true for previous iron addition experiments; however, these studies still had sufficiently available iron to induce a biological response in microbial communities [e.g. 134,221]. Conversely, increasing iron solubility by lowering the pH through the addition of the acid in the iron stock could potentially harm plankton. Berge *et al* (2010) showed that

some phytoplankton can tolerate small changes in pH, although open ocean species are thought to be less well adapted [265 and references therein]. Therefore, a balance between solubility of iron and the pH of the experiment must be achieved in any biological iron experiment. Indeed, addition of a chelator such as EDTA could have assisted in this balance. However, this would have introduced an additional variable into the experiment; for example, Rudolf *et al* (2015) noted a decrease in iron uptake upon increasing EDTA concentrations in the cyanobacteria *Anabaena* sp. due to the unavailability of the Fe-EDTA complex to cells [266]. Weaker ligands, such as citrate or oxalate, could have been an alternative possibility; however, their influence on microbial respiration would require assessment, namely citrate as it is a component of the tricarboxylic acid cycle.

Precipitation of extracellular iron-55 is not a concern in the iron uptake experiment, as a control sample that incubated ^{55}Fe in deionized water saw that <1% of total iron was retained on the 0.2 µm filter, although this does not account for adhesion of iron to the wall of the sample tube, which may have reduced iron availability. With regards to an altered pH, independent measurements show that the pH of experimental samples was lowered by no more than ~0.5 upon addition of the acidified iron-55, with the majority of experiments showing a smaller change (Appendix F). Whilst the change in pH in this study was not ideal, it was only slightly larger than the change in pH observed by Fu *et al* (2007) that still allowed optimal growth in *Synechococcus* and *Prochlorococcus* (difference of 0.4, pH 7.8 - 8.2) [267], with Traving *et al* (2014) showing that only once at pH 7 was the growth of *Synechococcus* severely reduced [268]. Furthermore, as some minor intracellular assimilation of iron did occur during the experiment (most notably at station U22, Table 4.5) cells were considered to not have been negatively influenced by any potential change in pH. However, it should be noted that the negligible uptake (≤5.04 $x10^{-7}$ nM Fe/day) could have been a sign that cells were not viable or highly stressed during the incubations. As no corresponding assessment of cell health was made (e.g. amino acid uptake) cell viability cannot be ascertained. Alternatively, it could be that contamination of

samples with stable iron caused a dilution effect on the ^{55}Fe, which prevented measurement of radiolabelled iron uptake.

For the nutrient addition experiments, the pH was not an issue. Table 4.2 shows that in deionized water alone, the pH of the incubation would have been 7.7 so when including the buffering capacity of seawater (Appendix F), the pH change would have been minimal, as evidenced by the fact that cells were still metabolically active (Figures 4.8). With regards to precipitation in these incubations, trends in the data provide information on the bioavailability of iron. After 24 h, Met uptake rates increased slightly upon addition of iron alone, and addition of both nutrients elicited a greater increase in cell abundance and Met uptake than ammonium alone at station A20 (Figures 4.7 and 4.9). Finally, station A23, 24 h appears to have an increase in Met uptake only when iron is added (i.e. +Fe and +NFe incubations, Figure 4.9). As no other variable was changed in these incubations, the trends indicate a role of iron in enhancing cell abundance and Met uptake as a possible secondary limiting nutrient. These results also assume that the concentrations of iron in the Ctl and +N sample (Table 4.4) were correct, and that these incubations were not contaminated with iron. The results presented in Table 4.4 are unusual in that there was less iron in the Ctl and +N incubations compared to the initial sample, despite the initial water being used for the incubations.

The two independent experiments in this study showed no response to iron additions in the South Atlantic, in agreement with previous investigations that saw either no response to iron additions, or a secondary/co-limitation of iron [176-178 179]. Thus, assuming there was no iron contamination and that cells remained viable, iron precipitation or a lowered pH did not negatively affect the finding that there was no response to iron additions in the South Atlantic in this study.

4.4.3 Bacterioplankton response to nitrogen addition

Bacterioplankton inside the SAG responded to nitrogen additions. An increase in cell concentration and Met uptake rate was observed upon addition of ammonium, either alone or in combination with iron. This agrees with results from the study by Moore *et al* (2009), who observed plankton stimulation from a nitrogen source via an increase in carbon fixation in the South Atlantic [176].

Nitrogen limitation across the global ocean is a common feature [53], with Moore *et al* (2009) noting the same nitrogen concentrations in both Atlantic gyres (5 nM nitrate + nitrite, 17 nM ammonium, and 6 μM organic nitrogen) [176], and supplementary data (provided by the British Oceanography Data Centre (contains data supplied by the Natural Environment Research Council)) showing a concentration of approximately 0.02 μM NO_3^+ + NO_2^+ (AMT-25, 20-40 m depth) (Appendix B). Therefore, the response to ammonium additions seen in the South Atlantic in this study was expected, due to the same response being observed in the North Atlantic during AMT-25 (Chapter 3). Interestingly, in the NAG, cells also responded to additions of phosphate. Although concentrations of phosphate and dissolved organic phosphorus (DOP) in the SAG are low due to the oligotrophy of gyres [53] (~0.2 μM PO_4^- [127,176] and 150±70 nM DOP [66]), they are significantly higher than those of the North Atlantic Gyre (NAG) [66,176,216] (<0.05 μM PO_4^- [127,176] and 80±140 nM DOP [66]), and are deemed to be sufficient with respect to the required cellular N:P ratio [53,176].

Within the South Atlantic, differences between gyre (i.e. 13-28ºS) and non-gyre waters were apparent. The station furthest from the gyre (A25) did not show an increase in cell abundance upon addition of any nutrients, and the percentage increase in Met uptake is lowest at A25 compared to all other stations (except +N incubation, A23, 24 h) (Figures 4.8 and 4.9). These waters are likely to be more productive and have an increased nitrogen concentration, especially considering the disappearance of *Prochlorococcus* at A25 (Figure 4.3) that can act as an indicator of departure from oligotrophic waters [158]. Indeed, Rees *et al* (2006) noted a nitrate concentration of around 0.01 μM in the SAG but

concentrations of approximately 14.7 µM south of the gyre, with a similar profile being observed for ammonium [54]. Supplementary data supplied by the British Oceanography Data Centre (contains data supplied by the Natural Environment Research Council) showed that at approximately 36ºS the NO_3^+ + NO_2^+ concentration increased rapidly, and at 45ºS it was in excess of 10 µM (Appendix B). Despite no changes being observed in iron concentrations (Figure 4.4), at station A25 (which is furthest from the centre of the SAG) it is likely that the ambient nitrogen concentrations had increased sufficiently so as the addition of 1 µM ammonium had a minimal effect on total ambient nitrogen concentrations (note Appendix B shows NO_3^+ + NO_2^+ concentrations, which were approximately 6 µM at ~42ºS, ~30m); thus, less of a bacterial response is observed when compared to stations inside the SAG with lower ambient nitrogen concentrations.

Furthermore, stations located inside the SAG (A20 and A21) respond after just 24 h incubation, whereas stations located outside of the SAG did not show a large increase in cell abundance or Met uptake rate until after 48 h incubation (Figures 4.7 and 4.9). The difference in response time may indicate differences in the rate at which cells metabolise the ammonium (i.e. faster turnover time inside the SAG); although this is less likely, as cells adapted for oligotrophy have a slower growth rate [88,170]. Alternatively, cells may have different assimilation rates (i.e. uptake is faster inside the SAG); indeed, a faster assimilation rate may be an advantage stemming from the high adaptation of cells to oligotrophic waters, specifically a larger surface area:volume ratio to increase nutrient acquisition potential [88].

4.4.4 Response of heterotrophic HNA bacteria

As no increase in cell abundance was seen in any other cell group across the South Atlantic, results of the nutrient addition studies imply that the community cell increase was primarily due to heterotrophic HNA bacteria.

The highest increases in HNA bacteria abundance occurred at stations A20 and A21, which coincided with locations inside the SAG, as well as the appearance of an additional distinct population of L-HNA heterotrophic bacteria. This L-HNA group may be an opportunistic population of bacterioplankton [269 and references therein]. Indeed, Mills *et al* (2008) observed a response of HNA bacteria upon addition of inorganic nutrients in the North Atlantic and termed them "opportunistic" bacteria [124]. It is interesting to note that at station A22, which is located on the edge of the gyre, the L-HNA bacteria population disappeared and all other bacterioplankton groups increased in abundance after 48 h incubation with ammonium.

One possible reason for the minimal response of *Prochlorococcus*, *Synechococcus* and LNA bacteria could be because all three groups are primarily limited by an alternative nutrient, such as dissolved organic carbon (DOC). For example, Kirchman *et al* (1990) noted carbon limitation of ammonium assimilation [232], and Carlson *et al* (2002) observed that once carbon limitation of bacterioplankton was relieved (through addition of 10 μM glucose), the community became limited by a secondary nutrient [128]. However, in this scenario it is unlikely that HNA bacteria would not be limited by DOC (or an alternative nutrient) and other more specifically adapted oligotrophs (e.g. *Prochlorococcus* [138]) would have been limited. Indeed, Pan *et al* (2014) recorded higher DOC concentrations inside the Atlantic gyres (>70 μM), than in the more productive surrounding waters [130]. A number of possible alternative reasons for absent responses from these bacterioplankton populations are discussed subsequently; however, without further data and investigation no major conclusions can be drawn from these results.

Dominance by HNA bacteria in the South Atlantic is in contrast to the results of the North Atlantic study, where the main group to respond to nutrient additions was *Prochlorococcus* (Chapter 3). In the South Atlantic, HNA bacteria may have outcompeted *Prochlorococcus* in the assimilation of ammonium, as Mills *et al* (2008) concluded that heterotrophic HNA bacteria outcompeted autotrophs upon addition of inorganic nutrients in the North Atlantic [124]. Alternatively, it could be that *Prochlorococcus* were able to utilise a different nitrogen

source. Although ammonium is the preferential nitrogen source for *Prochlorococcus*, some strains have been shown to assimilate alternative sources such as nitrite, nitrate, urea, and even cyanate [58,59,93,233,270]. There is also evidence for the use of organic nitrogen sources such as amino acids [60].

LNA bacteria did not respond to nutrient additions, which matches the result seen in the centre of the NAG (Chapter 3). SAR-11 are the dominant bacteria within the LNA bacterial population [65,142], and as highly adapted oligotrophs [143,170], may not respond to nutrient additions. Indeed, Mills *et al* (2008) noted that LNA bacteria produced a minimal response to nutrient additions in the North Atlantic [124]. Furthermore, Sebastián and Gasol (2013), and Gifford *et al* (2012) all observed that SAR-11 did not respond to nutrient additions or environmental stimulations, respectively [271,272].

Interestingly, *Prochlorococcus* appeared to decrease in abundance upon addition of ammonium (either alone, or in combination with iron). This matches the negative response seen to ammonium additions in the North Atlantic (Chapter 3). It is possible that addition of ammonium initiates stoichiometric deficiency of an alternative element [53], or that a competing organism/predator is stimulated by this addition.

The response of *Synechococcus* to nutrient additions was also minimal. As noted in Chapter 3, Davey *et al* (2008) suggested *Synechococcus* may become phosphorus or iron limited when ample concentrations of nitrogen were available [221]. As no response was noted upon addition of iron, this could imply phosphorus limitation in *Synechococcus* is initiated when ammonium is added to the incubations. It is interesting to note that in the centre of the gyre, at station A20, there is a slight increase in cell abundance upon addition of ammonium. Perhaps at this station, the ambient concentration of ammonium was sufficiently low that when combined with the 1 μM supplemented ammonium, the overall concentration was not high enough to invoke phosphorus limitation. However, as phosphate enrichment was not conducted in the South Atlantic, *Synechococcus* phosphorus limitation cannot be determined. Furthermore, as discussed previously,

changes in *Synechococcus* concentration should be treated with caution as the cell counts are so low (<8% of total bacterioplankton), meaning minor changes are amplified.

4.5 Conclusions

Limitation of plankton across the ocean can affect global primary production and the carbon cycle, as the ocean contributes to approximately 50% of global primary production [1]. Therefore, understanding nutrient limitation of the bacterioplankton community is essential, especially due to changing ocean chemistry [e.g. 174,273] and expansion of oligotrophic waters [35-38] as a result of anthropogenically influenced climate change. Iron has been shown to limit the HNLC regions of the ocean [180 and references therein]; however, its potential limitation in the South Atlantic gyre has been scarcely studied.

Through the measurement of cell abundance, metabolic activity, and iron uptake rates, this study showed that bacterioplankton did not respond to iron additions across the South Atlantic. Based on these experiments, and using the definition of limitation previously set out (Chapter 1, Section 1.4) this could be inferred to imply that bacterioplankton were not limited by iron [122,247]. The results of this study agree with previous studies that also did not witness iron limitation in the South Atlantic [176-178, M. Hartmann (unpublished)]. However, this interpretation assumes the iron concentrations measured in the Ctl and +N samples were correct and there was no contamination of iron. It also assumes cells were viable in the iron uptake experiments, that there was no contamination of stable iron in uptake experiments, and that iron was bioavailable in the +Fe and +NFe incubations. Indeed, Browning *et al* (2017) concluded co-limitation of iron and nitrogen inside the south-eastern region of the SAG [179].

Bacterioplankton (specifically HNA bacteria) increased in cell abundance and Met uptake upon addition of ammonium (10±13% and 102±115% increase, average ± standard deviation of +N and +NFe incubations, for cell abundance and Met uptake, respectively).

Stimulation of cells was also observed in the North Atlantic when ammonium was added (Chapter 3), showing an Atlantic wide response to ammonium, which is in keeping with the very low concentrations of nitrogen reported across the global ocean [53].

Chapter 5: Comparison of microbial iron adsorption between oligotrophic and productive waters of the South Atlantic

5.1 Introduction

Iron is a key element for many essential metabolic processes such as photosynthesis and respiration [67,68]. Half of global primary production takes place in the oceans [1]; therefore, understanding the iron cycle is key for assessing the functioning of global marine ecosystems and the carbon cycle. Unchelated Fe(III) is a highly bioavailable form of iron for plankton assimilation [274]; however, as iron is highly insoluble in oxygenated seawater [67,95], and inputs to the open ocean can be minimal [e.g. 71,73,218], dissolved iron concentrations in the open ocean are very low, and usually in the range of 0.02 – 1 nM [7,67].

Biological processes play a significant role in the marine iron cycle [77,275-277]. Some plankton are able to utilise the redox conversions between ferrous and ferric iron to their metabolic advantage. Ferrous iron can be oxidised, using Fe(II) is an electron donor, with this process typically occurring under anoxic conditions where ferrous iron has a longer half-life [275,278]. Equally, ferric iron reduction can be used for microbial respiration (typically anaerobic) by using Fe(III) as a terminal electron acceptor [275,278]. Furthermore, to prevent rapid formation of insoluble iron oxyhydroxides [67,95], many microorganisms produce chelating molecules (siderophores) to maintain iron in solution [67]; indeed, over 99% of dissolved iron in the marine environment is bound by organic ligands (which includes, but are not exclusively, siderophores) [82]. Interestingly, siderophore production is not as wide-spread in phytoplankton [e.g. 97 and references therein], and is extremely rare in eukaryotic marine microorganisms [67,97-99]. Most *Synechococcus* species (especially in the open ocean) are

unable to produce siderophores [e.g. 279 and references therein], and the *Prochloroccus* genome lacks the required genes [93,279]. Furthermore, siderophore acquisition genes have not been identified in the oligotroph *Pelagibacter ubique* (SAR-11) [280], which is one of the most abundant bacterioplankton in the oceans [137]. Finally, microbes (e.g. zooplankton, viruses, heterotrophic bacteria [78]) can influence the iron cycle through remineralization and regeneration [77]. As iron inputs do not generally meet planktonic requirements, recycling of iron is an essential process in the oceans [71], for example via zooplankton grazing [74].

Export of iron from the ocean is chemically and biologically influenced, and may occur following biological uptake, formation of precipitates (iron oxyhydroxides) and adsorption (scavenging) of iron onto surfaces of biological cells, biological debris and lithogenic material [73,75-77]. This removal results in a short oceanic residence time of dissolved iron in the surface ocean (i.e. months-years [78,81]). Precipitation of iron by plankton can occur as a by-product of an alternative cellular reaction, such as release of a metabolic end product (e.g. OH^-, NH_3, H^+), which stimulates nucleation of iron minerals [277 and references therein]. Alternatively, ionized cell surfaces, specifically negatively charged sites such as amino or carboxyl groups and phospholipid heads of the cell envelope, promote the adsorption and nucleation of metal cations to the cell [175,275,277,281-283]. As scavenging can facilitate iron export from the marine surface waters [73,75-77], it is essential to expand the understanding of iron adsorption processes and the distribution of iron in the marine environment [175]. This is of even greater importance as anthropogenic influenced global change will affect iron biogeochemistry [273]. For example, it has been suggested that ocean acidification caused by increasing global CO_2 levels, may result in decreasing metal adsorption due to a decreasing pH that affects the charged surfaces of organic material [174,284,285].

Iron cycling in the South Atlantic is of particular interest because, despite low dissolved iron concentrations compared to other oceanic regions (e.g. the North Atlantic [126]), plankton are not primarily iron limited [Chapter 4 and references 176-178]. Interestingly, Browning *et al* (2017) observed co-limitation of phytoplankton growth by iron and nitrogen inside the

South Atlantic gyre, and secondary iron limitation (nitrogen as the primary) out of the gyre [179]. Furthermore, due to lowered iron inputs to the South Atlantic (such as low aerial dust deposition, and benthic and lateral transport from coastal and shelf areas [72,182,243]) dissolved iron concentrations are lower in the oligotrophic South Atlantic gyre (SAG) compared to the more productive and coastal waters of the South Atlantic [e.g. 115,126,243]; for example, Noble *et al* (2012) reported 0.05 nM in the gyre centre, and 3.03 nM by the Namibian coast [115]. As oligotrophic gyres make up approximately 40% of the world´s ocean [e.g. 33] (see Chapter 1, Section 1.2.3), with expansion of these regions shown to be occurring [35-38], it is important to assess capacity of microbial iron adsorption in these regions and the potential removal of iron from the surface ocean.

Despite this observation of low iron concentrations, cellular iron assimilation studies are rare in the South Atlantic. Thus, this study determined iron adsorption by the microbial community along a transect across the South Atlantic [73,75-77]. Microbial adsorption levels in the SAG were compared to levels out of the gyre. Additionally, adsorption levels were measured in two marine laboratory cultures to act as a comparison to field studies. The basic experimental setup incubated cell samples with radiolabelled iron (^{55}Fe or ^{59}Fe) before filtration through a 0.2 µm pore size filter to remove unbound iron, as iron below 0.2 µm can be considered to be dissolved [73,238]. Since biological iron assimilation includes both intracellular uptake and extracellular adsorption, it was important to determine intracellular iron uptake rates in order to calculate exact values for cell-surface iron adsorption. A buffer developed by Hudson and Morel (1989) containing titanium(III) chloride, citrate, and ethylenediaminetetraacetate buffer (referred to as $TiCl_3$ Buffer from here on) was used to remove extracellular iron and allowed differentiation between adsorption and uptake [253].

5.2 Methods

5.2.1 South Atlantic experiments

Samples were collected during the 24th Atlantic Meridional Transect cruise (AMT-24), on board the R.R.S. James Clark Ross (JCR) during October 2014 (Figure 5.1, Table 5.1). Each station is numbered and has a 'U' prefix, in line with station IDs used in Chapter 4. A 10 L acid cleaned (Analytical grade hydrochloric acid (HCl), diluted to ca. 1 M with deionized water, referred to as 10% HCl from here on) Go Flo sampler (Ocean Test Equipment) was used to collect seawater samples from a depth of 20 m, as described in Chapter 2 (Section 2.2), with cell counts made at each station using flow cytometry (Chapter 2, Section 2.3). Upon recovery of the Go Flo sampler, 15-25 mL aliquots of seawater were collected in 30 mL acid cleaned (10% HCl) Teflon bottles. Radiolabeled iron chloride (^{55}Fe, see Chapter 2, Section 2.4.5) was added to these seawater samples and incubated for several hours, up to a maximum period of approximately 24 h, which allowed consistent experimental routine on ship and was similar to the maximum incubation time used by Zubkov *et al* (2007) (19.5 h) [206]. Two sources were used for the incubation experiments (Chapter 2, Section 2.4.5). Source A, used for stations U16-U23, was stored in 1 M HCl and added to a final total iron concentration of Fe 0.2-0.3 nM (^{55}Fe, 0.003-0.006 nM). Source B, used for stations U24-U26, was stored in 0.1 M HCl acid and added to a final total iron concentration of 0.04-0.07 nM (^{55}Fe, 0.005-0.008 nM).

After each time point, unfixed cell samples were filtered onto a 0.2 µm polycarbonate (PC) filter (25mm, Whatman), using a filtration unit (60104, Thermo Scientific, UK) (Chapter 4, Figure 4.2) maintained at a pressure of approximately 0.4 bar [as described in 206]. Samples were washed with 4 mL of seawater (taken from the same station) before being placed in scintillation vials (20 mL, high density polyethylene (HDPE), Meridian), along with 5 mL of scintillation cocktail (Gold Star, Meridian). Samples were measured on a liquid scintillation counter (LSC) (Tri-Carb 2910, Perkin Elmer) using a counting window of 3-12 keV (based

on the decay energy of ^{55}Fe) and a count time of 2 min, which was deemed long enough to produce a sufficient signal (see Chapter 2, Section 2.4.3 for information on LSC measurement).

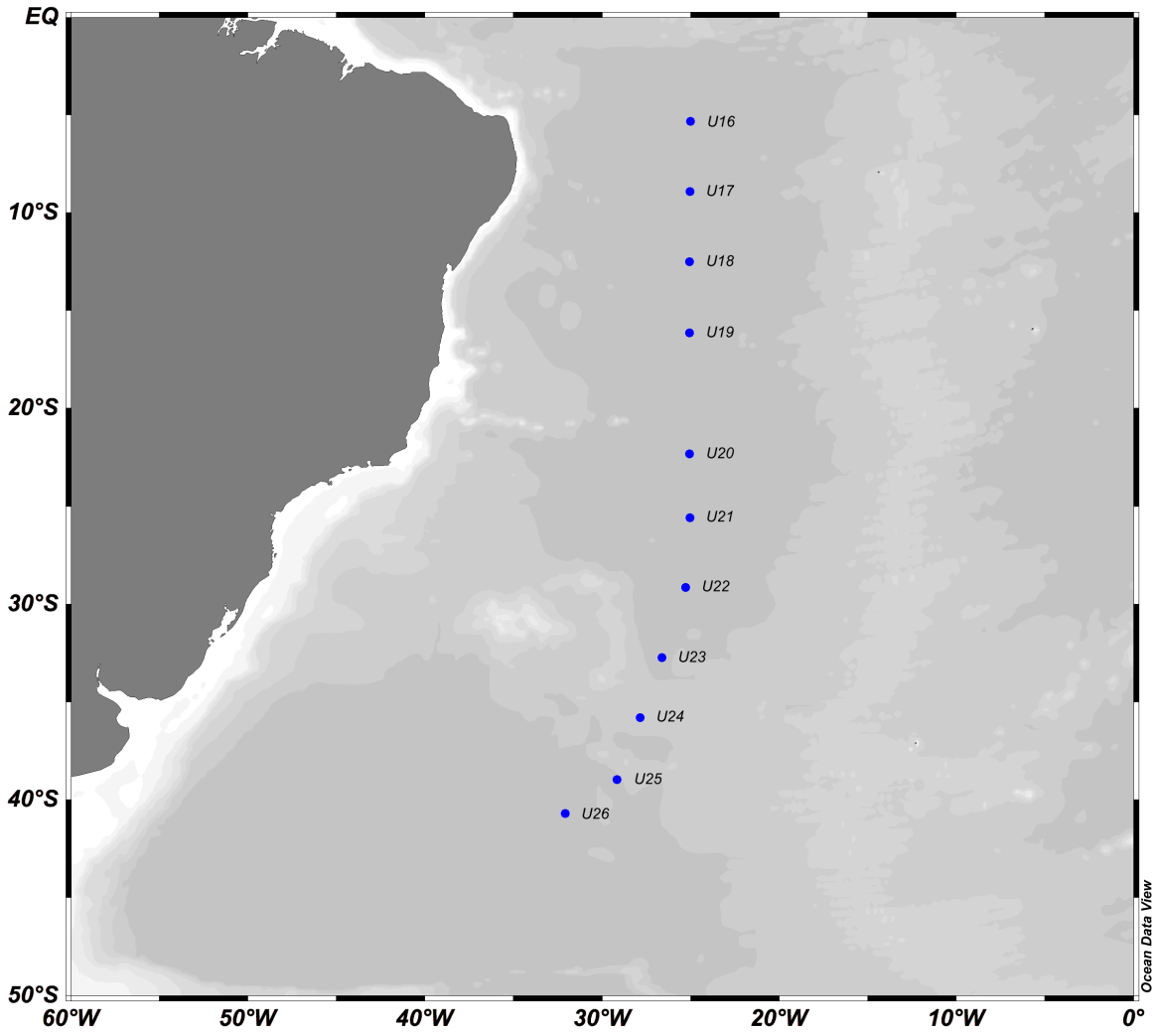

Figure 5.1: Station locations of iron adsorption experiments conducted during AMT-24
The location of stations sampled in the South Atlantic where iron adsorption experiments were conducted. Station are labelled with their IDs, and details of the stations are provided in Table 5.1. Map created using Ocean Data View Software 4.7.10 [197].

Table 5.1: Station locations of iron adsorption experiments conducted during AMT-24
The locations, date and time of stations sampled across the South Atlantic where iron adsorption experiments were conducted. The shaded area represents the stations defined as inside the SAG, as determined in Chapter 4. A map of the station locations is provided in Figure 5.1.

Station ID	Date and Time (GMT) of Sampling	Latitude (ºS)	Longitude (ºW)
U16	14-Oct-2014 14:07	5.32	25.03
U17	15-Oct-2014 14:13	8.91	25.04
U18	16-Oct-2014 14:08	12.49	25.07
U19	17-Oct-2014 14:07	16.13	25.08
U20	20-Oct-2014 14:08	22.32	25.06
U21	21-Oct-2014 14:08	25.59	25.04
U22	22-Oct-2014 14:07	29.15	25.28
U23	23-Oct-2014 15:05	32.72	26.63
U24	24-Oct-2014 15:07	35.80	27.87
U25	25-Oct-2014 15:11	38.96	29.17
U26	26-Oct-2014 15:09	40.69	32.10

5.2.2 Laboratory culture experiments

Laboratory adsorption experiments were conducted under a laminar flow hood (aerial contamination approximately ≤0.3ppb Fe (measured by Zilvinas Zacharauskas, GAU, using an Agilent 8800 mass spectrometer) using acid cleaned equipment (Chapter 2, Section 2.2.1). Cultures, grown under iron-replete conditions, of either *Halomonas sp. (Halo)* or *Aurantimonas sp. ATCC BAA-1229* (*Aur*) were prepared as outlined in Chapter 2 (Section 2.5), to a cell concentration between approximately 300,000 and 7,000,000 cells/mL, diluted in aged Atlantic seawater (AASW) (previously collected in the middle of the North Atlantic subtropical gyre during the cruise D369 in August-September 2011, by the Microbial Plankton Group, National Oceanography Centre). Multiple experiments were conducted, and individually labelled with an experiment number and a prefix of 'H' or 'A'

for *Halo* or *Aur* cultures, respectively (whereby H1 - H4 and A1 - A5 all denote separate experiments using either *Halo* (H) or *Aur* (A) cultures).

Radiolabelled iron (^{59}Fe) chloride (Perkin Elmer, stored in 0.5 M HCl) was added to 1.6 mL aliquots of cell cultures to a final total iron concentration of 35-38 nM (^{59}Fe, 0.04-0.05 nM) (in 0.5 M HCl) and incubated for several hours up to a maximum of approximately 24 h. Aliquots were fixed at regular time points using 80 µL 20% paraformaldehyde (PFA) (final concentration 1%) (Sigma Aldrich, UK). Separate aliquots were taken at specific time points for enumeration of cells, using flow cytometry as described in Chapter 2 (Section 2.3).

Once fixed, samples were filtered onto 0.2 µm PC filters (Whatman) and rinsed with 2x 3 mL deionized water, following the protocol outlined in Chapter 2 (Section 2.4). Filters were added to scintillation vials along with 5 mL scintillation cocktail (Gold Star, Meridian) for measurement on a LSC (Perkin Elmer). As ^{59}Fe is a gamma emitter and LSCs typically measure beta emissions, a wide counting window of 2-2000 keV and longer count time of 5 min was used to provide a higher counting efficiency and a detectable signal (see Chapter 2, Section 2.4.3).

Abiotic controls

Samples of AASW, without cell culture, were incubated with ^{55}Fe (final concentration of approximately 0.097 nM ^{55}Fe, in excess of that which was used in cell samples) for 60-90 min, before being filtered and measured on the LSC, as was performed on cell samples. Three abiotic samples were tested, from which an average signal was calculated. These samples acted as the experimental blank for Atlantic and laboratory experiments.

5.2.3 Extracellular iron determination and data analysis

Radioactivity measured in each sample (in counts per minute, CPM) was converted to moles of iron (SI unit prefixes used where appropriate) using the known concentration of iron initially added to a sample, as described in Chapter 2 (Section 2.4). Signals measured on the LSC included the total iron assimilated (extracellular adsorption and intracellular uptake), as well as any abiotic signal. Terminology describing these fractions is described in Table 5.2.

Table 5.2: Terminology used to determine iron adsorption, uptake and assimilation
The table presents terminology that will be used throughout the chapter relating to iron uptake, adsorption and assimilation, the use of the $TiCl_3$ buffer, and how the terms link together.

Term	Meaning
Original Signal Measured	*The original radioactivity measurement, directly obtained from the LSC, including abiotic signal*
Total Iron Assimilated	*Combined intracellular uptake and extracellular adsorption of iron by the cell. Does not include background signal.*
Intracellular Iron/Uptake	*Iron taken inside the cell which cannot be removed using the $TiCl_3$ buffer*
Extracellular Adsorption	*Iron associated/bound to the surface of a cell and can be calculated by subtracting intracellular uptake from total iron assimilation.*
Washed Cells	*Cells rinsed with the $TiCl_3$ buffer to remove extracellular iron, thus showing intracellular uptake*
Unwashed Cells	*Cells which have not been subject to rinsing with the $TiCl_3$ buffer and thus show total iron assimilation*
Abiotic control	*The amount of abiotically formed iron (in moles) in abiotic AASW samples that contained no cell culture*
Abiotic signal	*The measured signal (in CPM) in abiotic AASW samples that contained no cell culture*

Extracellularly adsorbed iron was calculated by subtracting the abiotic signal and intracellular uptake (if these values were notable, >10% of total signal) from the original measurement (Equation 5.1).

Eq. 5.1 *(Original Signal Measured) - (Abiotic control) - (Intracellular Iron) = Extracellular Iron*

Abiotic control

To determine the significance of abiotic precipitation in samples, the signal measured in abiotic AASW samples was compared to the total amount of radioactivity added to the sample (Equation 5.2).

Eq. 5.2 $$\frac{\text{Abiotic control (mol)}}{\text{Total iron added to sample (mol)}} \times 100 = \text{Proportion of added iron that becomes abiotic (\%)}$$

For the three controls, the percentage of abiotic signal in comparison to the total iron added was found to be 3.0 ± 0.9 % (average ± standard deviation). This percentage was then used to calculate the abiotic signal in all samples (Equation 5.3).

Eq. 5.3 *Total iron added to a sample (mol) x 3.0% = Abiotic signal in a sample (mol)*

A second calculation determined the proportion of the original signal (measured from a cell/seawater sample) that could be attributed to abiotic signal (Equation 5.4)

Eq. 5.4 $$\frac{\text{Abiotic control (mol)}_{\text{(Eq. 5.3)}}}{\text{Original signal measured (mol)}} \times 100 = \text{Contribution of abiotic signal to measured signal (\%)}$$

If the resulting contribution was more than 10%, it was deemed notable and was considered in the calculation of extracellular iron (Equation 5.5).

Eq. 5.5 *Original signal measured on LSC - abiotic control = Total iron assimilated*

Intracellular uptake

Intracellular iron, as a result of cellular uptake, was measured by incubating duplicate samples with radiolabelled iron and washing them with the $TiCl_3$ buffer [253] (method outlined in Chapter 4) to remove extracellular iron, before measurement on the LSC.

The contribution from intracellular iron to the original signal was calculated (Equation 5.6), and if it was more than 10%, then it was deemed notable and was considered in the calculation of extracellular iron (Equation 5.7).

Eq. 5.6 $$\frac{\textit{Intracellular iron}}{\textit{Original signal measured on LSC}} \times 100 = \textit{Contribution to measured signal (\%)}$$

Eq. 5.7 *Total iron assimilated - Intracellular uptake = Extracellular adsorption*

Adsorption per cell

Once extracellular adsorption was determined, accounting for background signal and intracellular uptake, iron values (in moles, SI unit prefixes used when relevant) were converted to per cell basis (mol/cell) using the cell concentration of the sample (previously determined by flow cytometry, Chapter 2, Section 2.3) (Equation 5.8).

Eq. 5.8 $$\frac{\textit{mol Fe adsorbed}}{\textit{cells in sample}} = \textit{iron adsorbed (mol/cell)}$$

Error of iron adsorption per cell was based on the combined uncertainties in cell count and iron adsorption. Cell concentration error was determined from the standard deviation of multiple replicate samples analysed by flow cytometry (as described in Chapter 2, Section

2.3). The error in the amount of iron adsorbed was based on multiple incubations within an experiment (e.g. 2, 4, 8, 22 h incubation time points from a single experiment).

5.2.4 Cell surface area calculations

In a study by Sunda and Huntsman (1995), adsorption of iron by phytoplankton was normalized to cell surface area, thereby accounting for differences in cell size [88]. The same calculations were performed in this study in order to account for differences in cell size between small Atlantic plankton and larger *Halo* and *Aur* cells. Cell surface areas of low nucleic acid (LNA) and high nucleic acid (HNA) bacteria, *Prochlorococcus*, *Synechococcus*, picoeukaryotes, *Halo* and *Aur* were obtained using values from the literature (Table 5.3). Total cell surface area was estimated using measured cell abundances, and the amount of iron adsorbed per μm^2 was calculated (Equations 5.9 and 5.10). It should be noted that these values are not quantitative and are only used as an estimation for cell surface area. For example, different studies provide different sizes for the same cell type (e.g. *Aur* [212,213]), eukaryotic cell counts were based on counts taken on an alternative cruise (AMT-25) and assumed the presence of only plastidic cells, and calculations presumed that cells are perfect spheres or cylinders.

Eq.5.9 Individual cell surface area (μm^2) × cell abundance (cells/mL) = Total surface area (μm^2/mL)

Eq. 5.10 $$\frac{\text{Iron adsorbed (nmol/mL)}}{\text{Total surface area } (\mu m^2/\text{mL})} = \text{Iron adsorbed (nmol}/\mu m^2)$$

Table 5.3: Calculations for the estimation of bacterioplankton cell surface area
Surface areas are based on the volume of a sphere or cylinder, using the cell dimensions obtained in the literature. Where a range is used, the approximate middle value was used for calculations.
LNA bacteria size is based on SAR-11 (most dominant LNA bacteria [65,142]).
HNA bacteria size is based on unstained Prochlorococcus cells, which are themselves HNA bacteria.
Picoeukaryotic cell counts were not measured during AMT-24, but proportions were based upon values obtained during AMT-25 (average of 0.3% of total cell population). Cell sizes were based on two key plastidic groups identified by Hartmann et al *(2014) [286], and assumes that no other eukaryotic groups were present.*
All cell sizes are rough estimates, and should not be considered truly quantitative.

Cell Group	Cell size (µm)	Cell shape	Surface area of a single cell (μm^2)	Reference
LNA Bacteria	0.37–0.89 long 0.12–0.20 diameter	cylinder	0.4	Rappé *et al* (2002) [140]
HNA bacteria and *Prochlorococcus*	0.63 diameter	sphere	1.3	Hartmann *et al* (2014) [286]
Synechococcus	0.95 diameter	sphere	2.8	Hartmann *et al* (2014) [286]
Picoeukaryotes	2.0-3.1 diameter	sphere	20.4	Hartmann *et al* (2014) [286]
Aurantimonas	1-2.5 long 0.5-1 diameter	cylinder	5	Denner *et al* (2003), and Anderson *et al* (2009) [212,213]
Halomonas	2-3 long 0.75-1.3 diameter	cylinder	9.7	Garcia *et al* (2004), Martinez-Checa *et al* (2005), and Jeong *et al* (2013) [287-289]

5.3 Results

5.3.1 Calculating extracellular iron adsorption

Influences from the abiotic signal and/or intracellular uptake were initially assessed to determine their contribution to the original signal measured, thus allowing calculation of only extracellularly adsorbed iron. If either factor was more than 10% of the measured signal, then it was considered to be notable and the final adsorption value was adjusted.

South Atlantic samples

Over the course of each experiment, no overall increase in total iron levels were noted with increasing incubation time (Section 5.3.2, Figure 5.2); therefore, an average ± standard deviation of all time points from within an experiment are presented, with no omission of outliers (i.e. those that are more than 3 standard deviations away from the mean).

In the South Atlantic samples, based on a 3% abiotic signal of total iron added (Section 5.2.3), the proportion of abiotic signal ranged from 4.8 - 31.4% (12.3 ± 10.1 %, average ± standard deviation) of the original signal measured. As this was >10%, abiotic signal was accounted for when calculating total assimilated iron (Equation 5.5) (Table 5.4).

Table 5.4: Determination of extracellular iron in Atlantic samples
For Atlantic samples. the contribution of the abiotic signal was >10%, and so was used in the calculation of total iron assimilated (Equation 5.5). Intracellular iron uptake provided a minimal contribution, and so did not need to be considered in the calculation of extracellularly absorbed iron. All values are presented as average ± standard deviation. As there was no clear increase or decrease in signal throughout the incubation period (Section 5.3.2), uncertainties presented were based on error of multiple time points (up to 24 h) within an experiment. Where appropriate, equations or previous chapters are referred to in the column headers. No outliers are omitted from this dataset.

Sample	Original signal measured (x10^{-12} mol)	Contribution of abiotic signal *(Eq. 5.4)*	Total iron assimilated *(Eq. 5.5)* (x10^{-12} mol)	Intracellular uptake *(Chapter 4)* (x10^{-14} mol)	Contribution of intracellular uptake *(Eq. 5.6)*	Extracellular iron (x10^{-12} mol)
U16	2.1±0.4	6.1±0.3%	2.2±0.1	0.94±0.32	0.4±0.2%	2.2±0.1
U17	1.6±0.4	8.0±0.3%	1.7±0.06	0.63±0.32	0.4±0.2%	1.7±0.06
U18	2.1±0.3	6.9±0.1%	1.9±0.02	0.68±0.6	0.3±0.3%	1.9±0.02
U19	2.8±0.4	4.8±0.1%	2.9±0.03	1.6±0.1	0.6±0.04%	2.9±0.03
U20	1.9±0.2	7.8±0.2%	1.7±0.05	1.7±1.2	1.0±0.7%	1.7±0.05
U21	1.9±0.8	5.0±0.2%	2.2±0.08	0.97±0.14	0.4±0.1%	2.2±0.08
U22	2.7±0.3	5.2±0.5%	2.6±0.2	2.0±1.7	0.8±0.7%	2.6±0.2
U23	1.9±0.4	8.4±0.9%	1.6±0.2	1.1±0.8	0.7±0.5%	1.6±0.2
U24	0.11±0.02	26.6±1.5%	0.07±0.004	0.32±0.13	4.4±1.8%	0.07±0.004
U25	0.14±0.05	25.6±9.4%	0.1±0.04	0.26±0.14	2.6±1.7%	0.1±0.04
U26	0.14±0.01	31.4±0.8%	0.1±0.002	0.25±0.05	2.6±0.5%	0.1±0.002

Intracellular uptake rates of iron were minimal (Chapter 4). As a proportion of total assimilated iron, intracellular iron was shown to only be 1.3 ± 1.3 % (average ± standard deviation) (Table 5.4). As this was less than 10%, the total assimilated iron in unwashed Atlantic samples was considered to equal extracellularly adsorbed iron.

Laboratory cultures

The majority of laboratory experiments showed no overall increase in total iron levels with an increasing incubation time (Section 5.3.3, Figure 5.4); therefore, an average ± standard deviation of all time points from within an experiment are presented, with no omission of outliers. The exceptions were two *Aur* experiments (A1 ad A3), which did see a linear increase; however, when accounting for cell concentration this increase was no longer linear. The other exception was a *Halo* experiment (H4); however, this experiment only had two data points. For these experiments, the average ± standard deviation of multiple time points was still calculated, matching treatment of all other experimental data.

In laboratory samples, the contribution of the abiotic signal to the original signal measured was notable, and seen to be 33.2 ± 12.5 % of the total iron added (average ± standard deviation), and thus a correction to the original measured signal was required to calculate the total iron assimilated (Equation 5.5).

Additionally, despite iron replete conditions, intracellular uptake in laboratory experiments ranged from 2.2 - 31.5 % of total iron assimilated (11.7 ± 10.6 % average ± standard deviation, Table 5.5). Due to the significant proportion of intracellular uptake (>10%) in some samples, total iron assimilated was corrected for intracellular uptake in all samples, in order to determine extracellularly adsorbed iron (Equation 5.7).

Table 5.5: Determination of extracellular iron in laboratory samples
H1-4 and A1-5 denote separate experiments using Halo *and* Aur *cultures, respectively. Both the abiotic signal and intracellular uptake provided a notable signal, and so the extracellular iron was calculated accordingly (Equations 5.5 and 5.7). Values are presented as an average and standard deviation of multiple time points. Almost all experiments show no linear increase over time (Section 5.3.3), with the exception of those highlighted with an asterisk; however, the average and standard deviation of the multiple incubation time points for these experiments are still used in order to match the treatment of other experimental data. No outliers are omitted from this dataset.*

Sample	Original signal measured (x10^{-12} mol)	Contribution of abiotic signal *(Eq. 5.4)*	Total iron assimilated *(Eq. 5.5)* (x10^{-12} mol)	Intracellular uptake (x10^{-13} mol)	Contribution of intracellular uptake *(Eq. 5.6)*	Extracellular iron *(Eq. 5.7)* (x10^{-12} mol)
H1	11.4±2.3	17.0±3.7%	9.5±2.3	29.9±20.0	31.5±22.4%	6.5±4.6
H2	5.8±1.5	33.3±7.2%	4.0±1.5	6.3±0.2	15.8±8.4%	3.3±1.8
H3	12.2±6.3	17.3±8.5%	10.5±6.3	2.5±1.5	2.4±2.0%	10.2±8.9
H4	5.9±4.2	40.6±24.5%	4.1±4.2	9.4±1.8	22.9±23.7%	3.2±3.3
A1*	8.1±3.8	26.5±11.6%	6.2±3.8	1.3±0.3	2.2±1.4%	6.1±4.0
A2	6.6±0.2	28.4±0.8%	4.7±0.2	1.7±0.9	3.7±2.0%	4.5±2.5
A3*	5.5±2.0	38.0±14.1%	3.6±2.0	1.6±0.8	4.4±3.3%	3.4±2.6
A4	4.4±0.4	42.2±4.2%	2.6±0.4	1.3±0.5	5.0±2.0%	2.4±0.1
A5	3.1±0.02	55.8±0.4%	1.4±0.02	2.3±0.3	17.1±2.2%	1.1±0.2

5.3.2 South Atlantic iron adsorption

Seawater samples collected along a north-south transect in the South Atlantic were incubated with radiolabeled iron (^{55}Fe). All individual data points were corrected for abiotic signal (Section 5.2.3) to determine extracellularly adsorbed iron, before being converted to a per cell basis. This allowed the changes in iron adsorption to be monitored throughout the course of an incubation. Over the course of each incubation, there was no significant increase or decrease in adsorbed iron, with first and final adsorption levels being similar (Figure 5.2a) (paired t-test p = 0.149, F value = 1.2, critical F value = 3.7) and no trend of increase over time (Figure 5.2b). This allowed an average extracellular iron amount to be calculated from all time points for each incubation.

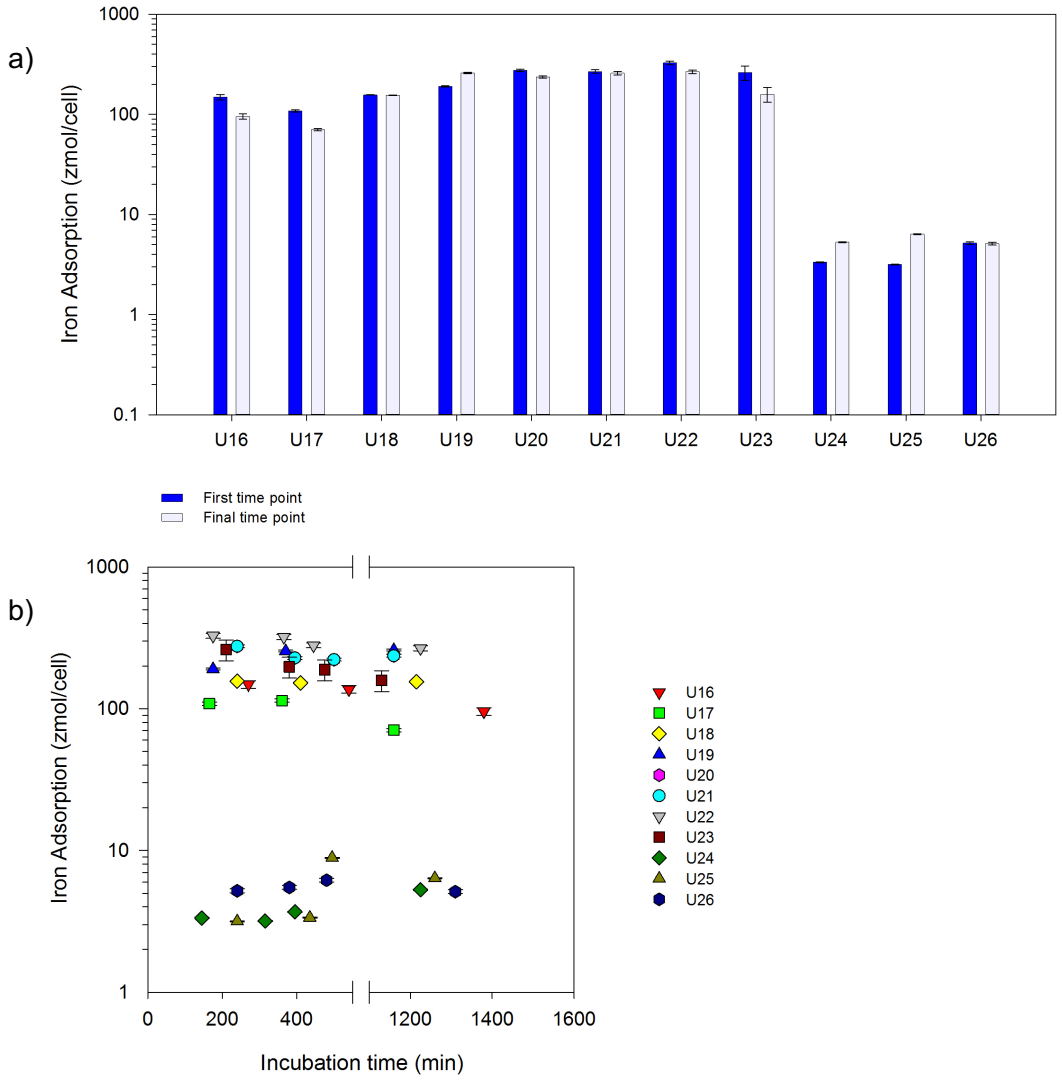

Figure 5.2: Differences in cellular iron adsorption throughout incubations conducted in the South Atlantic
a) Level of extracellular iron (presented as zmol/cell) in first and final time points of incubations for each experiment. Dark blue and light blue bars represent first and final time points, respectively.
b) Time course profile showing the amount of iron adsorbed in zmol/cell throughout the course of the whole incubation. Each symbol colour is a different station.
Note all axes are on a log scale. Error bars are based on standard deviation of cell counts. No outliers are omitted.

Average iron adsorbed at each station was then presented against latitude (Figure 5.3). There was a clear division between stations located south and north of approximately 35ºS. South of 35ºS, the amount of iron adsorbed was between 3.4-5.5 zmol/cell (3.4-5.5 $x10^{-21}$ mol/cell); however, north of this latitude the amount of iron adsorbed increased to between 111-299 zmol/cell (1.1-3.0 $x10^{-19}$ mol/cell) (statistically significant difference, Mann-Whitney rank sum test, $p = 0.012$).

Additionally, stations north of approximately 14ºS also had lower adsorption levels (111-155 zmol/cell, which is equivalent to 1.1-1.6 x10^{-19} mol/cell) than those between 14º and 35ºS (182-299 zmol/cell, which is equivalent to 1.8-3.0 x10^{-19} mol/cell); indeed, a Student's unpaired t-test shows high statistical difference ($p = 0.008$), with equality in population variances (F-test value = 3.8, critical F value = 39.3.

The difference between the two regions north of 14ºS and south of 35ºS is also statistically significant (unpaired t-test $p<0.001$) (unequal variances, F-test value = 392.2, critical F value = 39.0), with stations north of 14ºS (111-155 zmol/cell) showing higher adsorption than those south of 35ºS (3.4-5.5 zmol/cell).

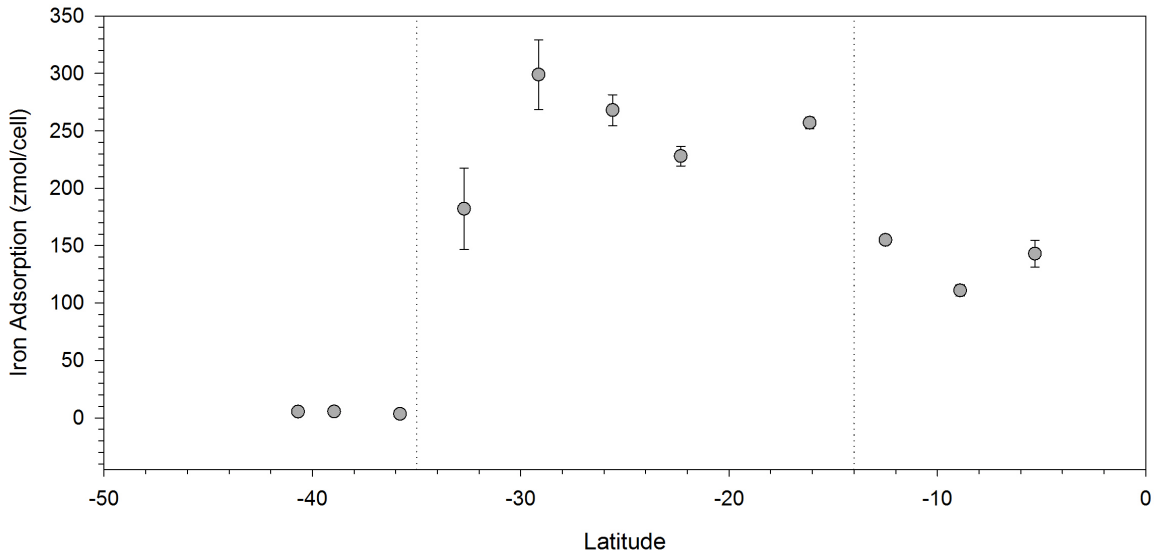

Figure 5.3: Relative cellular iron adsorption across the South Atlantic
The plot shows amount of iron adsorption per cell at each station relative to the latitude of sampling. Iron measured is that which did not pass through a 0.2 µm filter. Dotted lines represent statistically distinct groups of adsorption levels (see text). Error bars show error of propagation from cell counts and average of time points within each incubation.

5.3.3 Comparison to laboratory cultures

Laboratory samples of *Halo* and *Aur* were incubated with radiolabeled iron (^{59}Fe) up to a maximum of 16-26 h (exception of H3, up to 68 h, final time point not shown in Figure 5.4b). First and final extracellular iron adsorption values (calculated on a per cell basis)

were plotted for each experiment and showed no increase in the amount of iron between first and final time points, regardless of the culture (Figure 5.4), with paired t-tests showing no statistical difference between the two time points (*Halo:* p = 0.617, F-value = 4.84, critical F value = 15.44) (*Aur*: p = 0.494, F-value = 3.68, critical F-value = 9.60). Indeed, some experimental samples showed a decrease in iron adsorption (e.g. experiment H3, Figure 5.4b).

As a comparison to samples from the South Atlantic, all values from all experiments for *Halo* or *Aur* were grouped together and presented against all Atlantic values (Figure 5.5). There is an order of magnitude difference between the amount of iron adsorbed to laboratory cultures and seawater samples. *Halo* adsorbed between approximately 0.5-8.9 amol/cell (0.5-8.9 $x10^{-18}$ mol/cell), *Aur* adsorbed 0.7-5.9 amol/cell (0.7-5.9 $x10^{-18}$ mol/cell), and Atlantic seawater samples adsorbed 0.003-0.3 amol/cell (0.03-3 $x10^{-19}$ mol/cell). Whilst the laboratory cultures showed small variation in adsorbed iron between experiments, the Atlantic samples showed a wider range of adsorption due to the differences seen across the transect (Figure 5.3). Statistical analysis of the data sets shows there is a significant difference in the amount of iron adsorbed by *Halo* or *Aur* cultures and the amount adsorbed by the Atlantic samples (Mann-Whitney rank sum test, $p<0.001$). However, the difference in adsorbed iron between *Halo* and *Aur* samples is not statistically significant (Mann-Whitney rank sum test, p = 0.470).

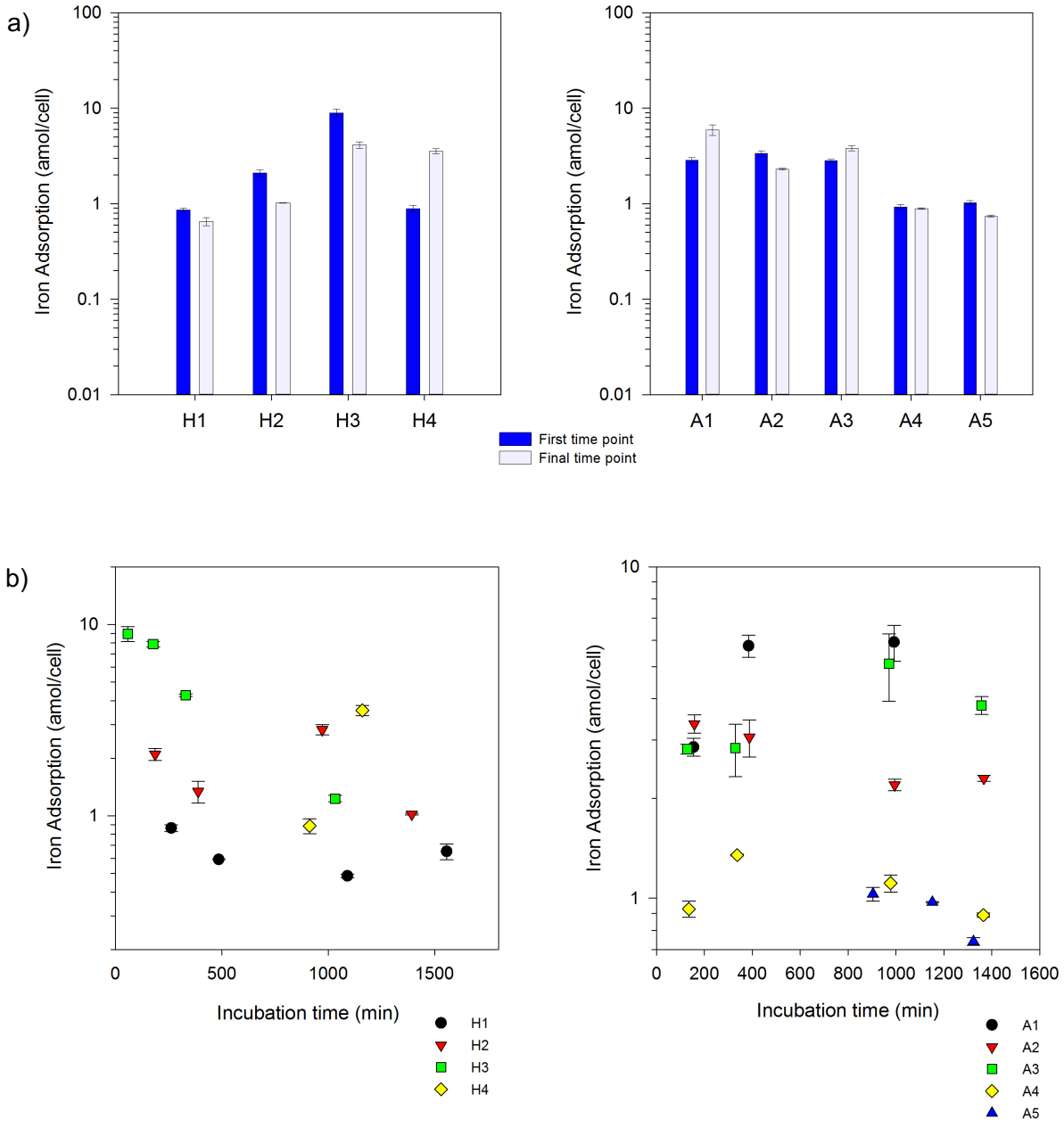

Figure 5.4: Differences in cellular iron adsorption throughout incubations conducted in the laboratory

a) Level of extracellular iron (presented as amol/cell) in first and final time points of incubations for each experiment for Halo (left) and Aur (right). Dark blue and light blue bars represent first and final time points, respectively.

b) Time course profile showing the amount of iron adsorbed in amol/cell throughout the course of the whole incubation for Halo (left) and Aur (right)

Note the axis are on a log scale. Error bars are based on error of propagation of cell counts and iron concentration.

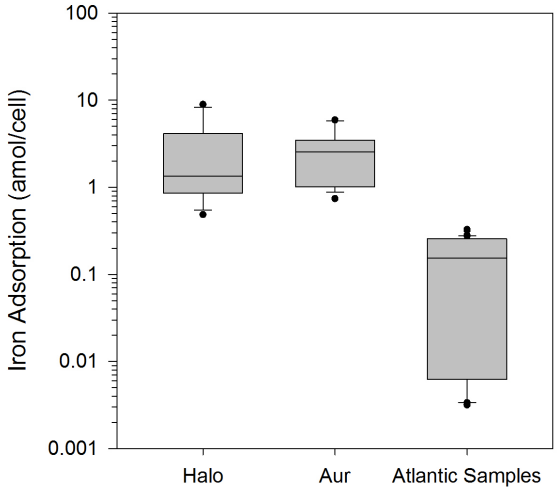

Figure 5.5: Comparison of total cellular iron adsorption in the incubations of Halomonas, Aurantimonas and South Atlantic samples
Extracellularly adsorbed iron based on a per cell basis were grouped together and values for Halo, Aur, and Atlantic samples were plotted against one another to allow direct comparison. All individual data points are plotted on a per cell basis, from each incubation time point. No outliers are omitted from the dataset. Data is displayed as a box and whisker plot, where the shaded box displays data between the upper and lower quartile, and the horizontal line shows the median. Error bars indicate upper and lower extremes and the dots signify outliers.

5.3.4 Cell surface area

Upon normalization of iron adsorption to cell surface area, samples from the South Atlantic provided values of 0.4-27.7 zmol Fe/μm^2 (0.4-27.7 x10^{-21} mol Fe/μm^2). The values were plotted against latitude (Figure 5.6), along with iron adsorption per cell, with the two parameters showing close correlation.

Iron adsorption based on surface area in *Halo* and *Aur* was similar (50-920 zmol Fe/μm^2 and 150-1020 zmol Fe/μm^2, which is equivalent to 0.5-9.2 x10^{-19} and 1.5-10.2 x10^{-19} mol Fe/μm^2, respectively), and were much higher than Atlantic samples (Figure 5.7).

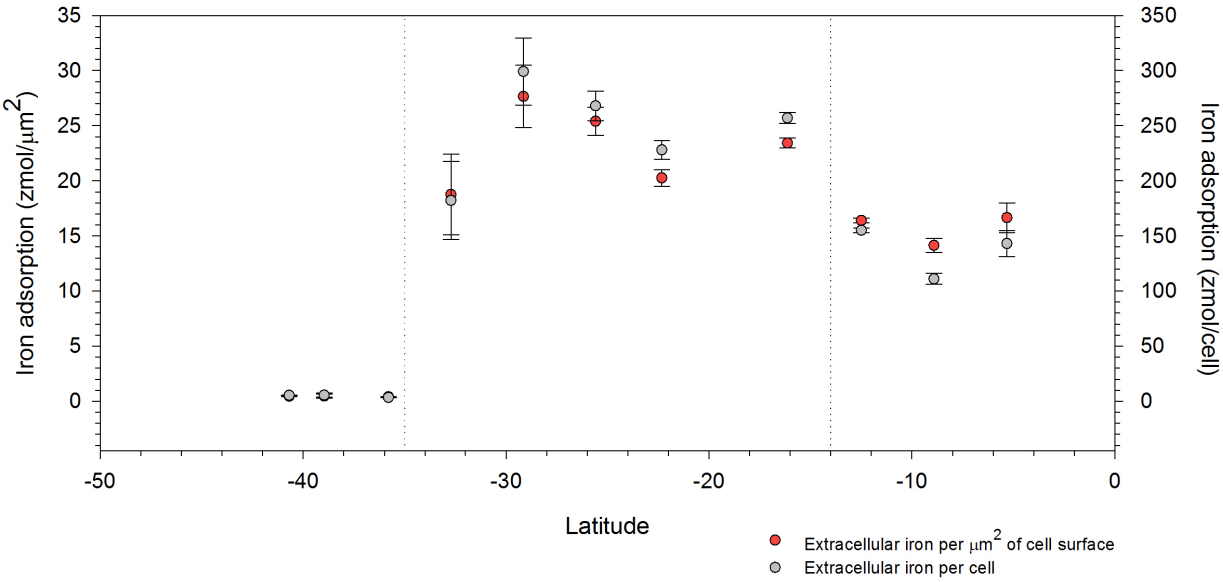

Figure 5.6: Comparison of cellular iron adsorption across the South Atlantic to relative to cell surface area
Iron adsorption is plotted against latitude on a per cell basis (grey) (same as Figure 5.3) and when normalized to cell surface area, μm^2 (red). No error bars are shown due to the high level of uncertainty that exists with cell surface area calculations.

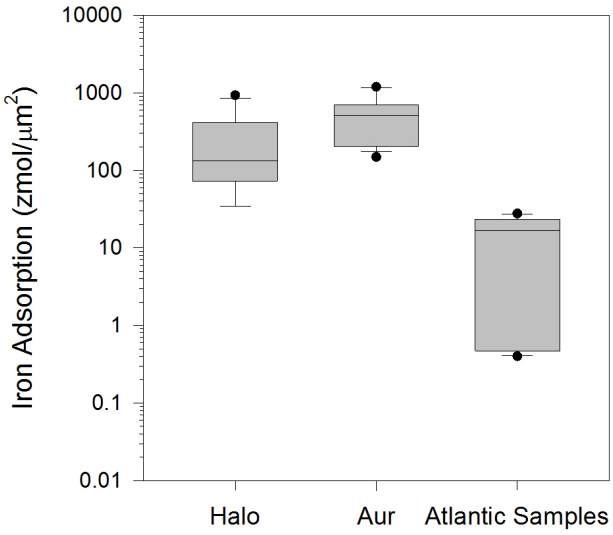

Figure 5.7: Comparison of iron adsorption normalized to cell surface area for Halomonas, Aurantimonas and Atlantic seawater samples
*Iron adsorption per μm^2 surface area is displayed for the three cell groups analysed: Halomonas (*Halo*), Aurantimonas (*Aur*) and Atlantic seawater samples. Individual data points from experiments are presented. Note the y-axis is on a log scale. Data is displayed as a box and whisker plot, where the shaded box displays data between the upper and lower quartile, and the horizontal line shows the median. Error bars indicate upper and lower extremes and the dots signify outliers.*

5.4 Discussion

5.4.1 Adsorption time profile

All cell samples saw a notable level of iron adsorption, which was quantified through the elimination of intracellular uptake, and contribution from blank samples. Adsorption occurred extremely quickly (e.g. within 1 hour, experiment H3), as evidenced by no increased adsorbed iron throughout the experimental time course (Figures 5.2b and 5.4b). This implies that equilibrium with cellular adsorption of iron was quickly reached. Previous studies have also witnessed no increase in adsorption of iron and other transition metals over time [e.g. 253,261], with rapid extracellular adsorption [261,290] but internalization occurring much more slowly [261 and references therein].

Extracellular loss is also much more likely than intracellular loss due to the labile nature of surface adsorbed iron [77]. This can be seen in some samples showing a loss in extracellular iron over time, such as experiment H3 (Figure 5.4). Furthermore, Beveridge and Murray (1976) witnessed some leaching of precipitated iron, which may also be a reason for a decrease in adsorbed iron seen in some samples, and Zubkov *et al* (2007) noted that adsorption of iron to particulates (including cells) was reversible [206,291]. Finally, this decrease may be the result of iron loss from inside the cell, as Miao and Wang (2006) noted significant iron efflux in their study on coastal diatoms [290].

5.4.2 Microbial iron adsorption in the South Atlantic

The location of the SAG was determined through cell counts and leucine bioassays, and validated through temperature, salinity and chlorophyll concentration (Appendix E), which is discussed in Chapter 4. Using these measurements, the gyre was seen to be located between approximately 10 and 35ºS.

Although there was no observed intracellular iron assimilation, extracellular association of iron with cells was substantial across the South Atlantic (10-65% of iron added to samples was adsorbed, calculated for mol Fe/cell). Adsorption per cell was strongly correlated with adsorption per μm^2 of cell surface area (Figure 5.6). As such, cell abundance and surface area can be considered to be closely linked in this scenario and do not change significantly across the transect, possibly indicating cell uniformity or a consistency in community structure.

There was a statistically higher iron adsorption level seen within the boundaries of the SAG. The division between high adsorption (1.1-3.0 $x10^{-19}$ mol/cell) and low sorption (3.4-5.5 $x10^{-21}$ mol/cell) at approximately 35ºS matched the southern boundary of the SAG. Furthermore, the division between high adsorption (1.8-3.0 $x10^{-19}$ mol/cell) and low adsorption (1.1-1.6 $x10^{-19}$ mol/cell) at ~14ºS was approximately the same location as the northern edge of the gyre (Figure 5.3). The slight difference in location of the northern boundary (SAG edge defined as 10ºS in Chapter 4) is likely to be due to variations seen at gyre edges (see Chapters 3 and 4).

Higher iron adsorption inside the SAG compared to out of the gyre could be explained by differences in ambient iron concentration. In the presence of elevated concentrations of an adsorptive solute, cell surfaces can become saturated, decreasing the rate of sorption [292]. Productive waters of the South Atlantic have higher iron concentrations than the gyre, which may be due to a number of factors including coastal and shelf sediment supplies, or aerial dust deposition [e.g. 72,115,126,218,243]. For example, Noble *et al* (2012), noted surface total iron concentrations in the SAG of 0.05 nM, compared to 3 nM along the Namibian coast [115], and Ussher *et al* (2013) reported minimum dissolved iron concentrations in the SAG (<0.4 nM), which was in contrast to values in the north equatorial Atlantic (0.8 - 1.6 nM) [126]. Additionally, Rijkenberg *et al* (2014), observed concentrations in the upper South Atlantic of <0.5 nM, but elevated concentrations at the subtropical shelf front near Brazil (>1 nM) [243]. Thus, it is likely that away from the centre of the SAG the higher ambient concentrations of iron resulted in more environmental iron absorption to cell surfaces,

saturating the cells and leaving less surface area for absorption of the radiolabeled iron. In comparison, there is less ambient iron in the centre of the SAG [e.g. 115,126,243], and although the levels are not primarily limiting to plankton growth and production [Chapter 4, 176-179], there may be a larger free surface area/more adsorption sites to which the ^{55}Fe can adsorb.

Indeed, the difference in adsorption north and south of the gyre (whereby adsorption is lower south of the gyre compared to north of the gyre) may be explained with the same hypothesis. Iron concentrations might be substantially higher south of the gyre due to large input from Patagonian dust and subtropical shelf transfer [72,182,243], compared to waters north of the gyre that may still face low concentrations of iron [293]. The transect likely crossed into the south subtropical convergence zone at around 35ºS, where a higher concentrations of ambient iron concentration have been observed [e.g. 126]. The drastic decline in iron adsorption at this location was also mirrored by a drop in seawater temperature and salinity, as well as an increase in chlorophyll concentration (Appendix E). It should be noted that two different ^{55}Fe sources were used between these regions; although, all values were normalized and corrected for the amount of known stable iron in each tracer (see Chapter 2, Section 2.4.5).

The relationship between free binding sites and adsorption capacity has been previously observed for other metals, including copper [294,295], and chromium [296], as well as iron [297]. Furthermore, after an approximate 10-hour incubation, Zubkov *et al* (2007) noted substantially higher iron adsorption in a high-nutrient-low-chlorophyll (HNLC) iron-limited region of the ocean, compared to more productive waters [206]. Conversely, Warren and Ferris (1998) noted that the binding of iron to a cell surface occurs via initial sorption and saturation of the cell surface, followed by additional accumulation and precipitation of iron as concentrations increase [175], implying no specific capacity for iron binding.

It is interesting to note that iron concentrations along a similar (although not identical, Figure 4.1) transect during the subsequent AMT cruise (AMT-25, October 2015) did not show any differences inside and outside of the SAG (Chapter 4); although, ambient iron concentrations were not measured during AMT-24 and there were a reduced number of

measurements inside the gyre during AMT-25. It could be that instead of differences in iron concentration, an alternative trace metal (e.g. Mg^{2+}, Mn^{3+}), could have been competing for iron binding sites [298]. However, most cells have a very high affinity for iron binding [e.g. 89,95,98], with cells at their physical limit of iron binding, restricted by available cell surface area [299 and references therein], thus competition from other metals is not as likely.

5.4.3 Laboratory vs Atlantic samples

There is a high level of iron adsorption in both South Atlantic and laboratory samples. However, when presented on a per cell basis, there was an order of magnitude higher adsorption in laboratory samples (Figure 5.5), despite *Halo* and *Aur* cultures being kept under iron replete conditions.

This observation may be due to the differences in cell size and thus available surface area for iron binding. For example, Lis *et al* (2015) noted a strong correlation between cell surface area and iron uptake rate in phytoplankton, irrespective of the species examined (i.e. cyanobacteria and eukaryotes) [299]. They proposed that uptake was limited by available space for iron binding, which is dictated by a number of factors, including cell surface area and space occupied by other membrane components [299]. Additionally, Sunda and Huntsman (1995) noted similar iron uptake rates in oceanic and coastal phytoplankton species, when normalised to cell surface area [88]. Indeed, phytoplankton are considered to be at the physical limit of iron uptake due to available free cell surface area [88,297,299].

Halo and *Aur* have differing cell surface areas but similar iron adsorption per μm^2, which is in agreement with previous studies [e.g. 88,299]. However, their iron adsorption levels are still much higher than those of Atlantic plankton in this study, even when normalized to cell surface area. This difference in adsorption per μm^2 between Atlantic and laboratory samples may be due to the fact that Lis *et al* (2015) only examined intracellular iron uptake, and Sunda and Huntsman (1995) noted a high level of intracellular uptake, which

was not observed in this study. Additionally, it may be because the previous studies only examined phytoplankton [88,299].

Differences in iron adsorption per cell between Atlantic and laboratory cultures may be an artefact of a reduced iron requirement by open ocean cells that have adapted for oligotrophy [88,263]. Indeed, whilst intracellular iron uptake was negligible in Atlantic samples (Chapter 4 and Table 5.4), it was more pronounced in some laboratory cultures, being as high as 31.5% (average from one *Halo* experiment) of total assimilated iron (Table 5.5), despite being grown under iron replete conditions and over a similar time period as the Atlantic samples (approximately 24 h).

Alternatively, higher adsorption in laboratory cultures may be due to the amount of iron added to samples [291], as laboratory cultures were spiked with a higher concentration of radiolabelled iron compared to Atlantic samples. However, the ratio of ambient stable iron relative to the amount of tracer iron should also be considered [77]. For example, although more iron was added to laboratory samples, the ambient stable iron in the *Halo* and *Aur* cultures will have been much higher than those of the Atlantic samples, due to culturing in iron-replete growth media (including the <0.3 ppb iron measured under the laminar flow hood (see Section 5.2.2)). Furthermore, the EDTA content of the ASW (*Halo* cultures, Section 2.5.2) used may have influenced the iron chemistry in these cultures. Therefore, whilst this the amount of radiolabelled iron is added is notable, it cannot be corrected for without knowledge of absolute concentrations of ambient iron in each sample.

5.5 Conclusion

Through measurement of the iron adsorption capacity of plankton, this study identified a clear distinction between the oligotrophic SAG and more productive waters of the South Atlantic. Iron adsorption per cell was shown to be significantly higher in the centre of the gyre, and decreased in more productive waters, especially towards Patagonia and the

southern subtropical convergence zone. Additionally, assessment of larger cells in laboratory cultures, showed a higher (an order of magnitude) level of iron adsorption per cell than in Atlantic samples. Thus, cellular iron adsorption was theorized to be linked to available binding sites on the cell surface, whereby in the gyre a lower ambient iron concentration resulted in a larger number of available binding sites.

Iron is a biologically essential micronutrient, thus processes affecting formation of particulate/insoluble species, including adsorption, are important in considering the cycling and removal of iron in the marine environment [73,75-77,175]. This is particularly important due to the changes in iron biogeochemistry as a result of climate change [273]; for example, adsorption rates have been predicted to decrease due to ocean acidification [174,284,285]. A decrease in bioavailability or a change in the chemistry of iron, can potentially affect plankton growth and consequently global primary production and carbon fluxes.

Chapter 6: Formation of particulate cobalt by the Mn-oxidizing bacteria *Aurantimonas* sp. (ATCC BAA-1229)

6.1 Introduction

Cobalt is an essential trace element that, when at deficient concentrations, has been shown to cause a reduction in growth rate of the key cyanobacteria, *Prochlorococcus* and *Synechococcus* [105,118,300], with Ho *et al* (2003) calculating an elemental ratio for phytoplankton of $(C_{124}N_{16}P_1)_{1000}Co_{0:19}$. The main cellular role of cobalt in cells is in the synthesis of vitamin B12, which is required for the functioning of a range of enzymes [101,102] (e.g. methionine synthesis [e.g. 301]) and has been observed to co-limit phytoplankton growth [103]. Due to the requirement for vitamin B12, phytoplankton that are unable to synthesise vitamin B12 must rely on bacterial supply through a symbiotic relationship [302]. Cobalt may also be involved in the formation of amides via the enzyme nitrile hydratase [303], as well as the acquisition of soluble phosphorus via alkaline phosphatase [104], with a clear linear relationship between Co and P concentrations in oceanic surface waters [e.g. 106,109]. Cobalt and zinc have also shown to be interchangeable in phytoplankton, with Co replacing Zn under conditions of Zn limitation, such as in the enzyme carbonic anhydrase [300,304-306]. Concentrations of cobalt in the ocean are found in the picomolar range [106,115,116,307], with phytoplankton typically requiring <0.2 mmol Co per mole of P [102,120]. As expected, concentrations of dissolved cobalt in the surface of the subtropical gyres are generally lower than in more productive waters [e.g. 106]; for example, Noble *et al* (2012) noted concentrations of 6 pM in the South Atlantic gyre, in comparison to 200 pM by the Namibian coast [115]. Additionally, Jakuba *et al* (2008) noted concentrations <10 pM in the open ocean of the Northwest Atlantic, but much higher concentrations (>50 pM) near the Massachusetts coast [104], and Shelley *et al* (2017) reported very low dissolved cobalt

concentrations in the North Atlantic subtropical gyre (23 ± 9 pM), compared to 59 ± 23 pM in the North Atlantic drift province (see Chapter 1, Figure 1.3)) [127]. Interestingly, Shelley *et al* (2017) noted a higher dissolved concentration in the South Atlantic gyre (55 ± 18 pM), and proposed the very low cobalt concentrations seen in the North Atlantic were a result of cyanobacterial uptake for use in alkaline phosphatase, which was upregulated due to the low phosphate concentrations of the North Atlantic [127 and references therein].

Manganese oxides

The distribution of cobalt (and indeed many other trace and toxic elements) can be highly influenced by the presence of manganese oxide, oxyhydroxide and hydroxide complexes (namely Mn(IV) species, but also including Mn(III)) (collectively termed MnOx from here on) due to their oxidative and sorptive properties [111,308-312, and 112 and references therein]; for example, the release of dissolved cobalt into a lake was seen to be closely related to MnOx dissolution [310].

Mn(II), the main soluble form of manganese (present as cationic species, e.g. Mn^{2+}, $MnOH^{+}$), is thermodynamically unfavourable under oxic conditions [112,215]. Dissolved manganese is present in the surface of the open ocean in concentrations of 0.08 - 5 nM, although these concentrations increase nearer to the coast due to riverine and continental influences [313]. Mn(II) may also be found in insoluble phosphates and carbonates, and as a minor component of larger insoluble complexes (including MnOx) [112,215]. However, the more favourably oxidised Mn(III)/Mn(IV) species form the insoluble MnOx complexes [112,215].

Manganese oxidation requires a high activation energy and as such generally occurs through the action of specific Mn-oxidising micro-organisms [112,215]. As a result, manganese oxidation in the marine environment is predominantly biological [112,215], with multicopper oxidase or haem peroxidase enzymes being implicated in the oxidation process [e.g. 214,314-316]. The biological benefit of Mn-oxidation is unknown; however, some

suggestions include chemolithotrophy or cellular protection [112]. Abiotic oxidation occurs much more slowly [112], with a half-life of 500 years for Mn(II) in seawater [317], although once the biogenic MnOx are formed autocatalytic abiotic oxidation of additional MnOx may occur [112,215]. Consequently, the cycling and formation of MnOx is a major factor in the distribution of manganese (and other trace metals) in the marine environment [312].

Oxidation and sorption by manganese oxides

MnOx are powerful oxidants [112,215]; for example, Cr(III) is rapidly oxidized to Cr(VI) in the presence of MnOx [318,319]. The process of oxidation by MnOx is not fully described yet, but may occur via a redox reaction using reduction of Mn(IV) or Mn(III) in the MnOx, which are subsequently re-oxidised [111 and references therein]. As well as direct oxidation by MnOx, many trace metals can be sorbed onto MnOx, being either adsorbed via negative charges present on the surface of the MnOx, or absorbed and incorporated into the mineral itself (e.g. through substitution of manganese) [312, 112 and references therein]; for example, Marcus (2004) showed the incorporation of zinc into vacant sites in MnOx from marine nodules. Biologically formed MnOx are more reactive than abiotic forms, with the presence of Mn-oxidising micro-organisms further enhancing oxidation rates [111,318], potentially due to the production of highly reactive MnOx compounds and their intermediates [112,114,319].

Cobalt and manganese oxidising bacteria

Cobalt is one such element that is influenced by the presence of MnOx and/or Mn-oxidising microorganisms, with abiotic cobalt oxidation rarely occurring in the marine environment [110]. Formation of insoluble and particulate cobalt (simply termed particulate cobalt from here on) (e.g. via sorption, or via oxidation from soluble Co(II) to insoluble Co(III)) has been linked to the presence of manganese-oxidising bacteria [e.g. 110,111,113,320], and may occur either as a direct result of cellular reactions by the Mn-oxidising

microorganisms (e.g. a cell-surface enzyme), or as an indirect consequence of the production of MnOx (as described above) [110,113].

Aurantimonas is a genus of gram-negative alpha-proteobacteria, of which some species are capable of Mn-oxidation [213]. *Aurantimonas* are globally distributed (although their abundance is not well studied [213]), with many isolates being identified in marine environments (e.g. Pacific Ocean, Sargasso Sea, the Mediterranean) [213], as well as in a number of diverse locations including the oxic/anoxic interface of a fjord, a diseased coral, and even on the surface of a deep sea hydrothermal tube worm [212,213,321]. In addition to Mn-oxidation, it has been suggested that *Aurantimonas* have the potential for autotrophy [321], thus could contribute to global primary production.

As *Aurantimonas* are able to survive at conditions that reflect the marine environment (e.g. growth between temperatures of 4 to 37ºC and salinities of 0 to 15%) [213], they are an ideal model organism to study marine Mn-oxidation by Gram-negative bacteria. Most previous microbial studies on the interactions between MnOx and cobalt were not performed on *Aurantimonas*, but instead assessed Gram-positive bacteria (i.e. *Bacillus* sp. and their spores [e.g. 110,114]), community water column samples [e.g. 113,310,320,322], or even fungi [e.g. 323]. Therefore, based on the importance of Mn-oxidising bacteria to cobalt distribution, and the lack of data on the role *Aurantimonas* play, this study examined the interactions between cobalt and *Aurantimonas* sp. (ATCC BAA-1229). Formation of particulate cobalt due to sorption or oxidation by the bacteria, or the biogenic MnOx, was measured through additions of radiolabelled cobalt to *Aurantimonas* sp. cultures. Varying concentrations of manganese were used to assess co-precipitation reactions of cobalt and manganese, and were compared to formation in non-Mn-oxidising bacteria (*Halomonas* sp.). Additionally, as metal competition for binding sites is known to occur [e.g. 298], this study examined the potential competition and effect on the formation of particulate cobalt from alternative trace metals. As noted by Churchill *et al* (1995), the general affinities of certain biosorbents for chromium, copper and nickel were all higher than that of cobalt [324]; therefore, these trace metals were investigated, with nickel and copper both serving

biological roles (e.g. they are found in the enzyme superoxide dismutase [102]), and with chromium as a potentially very toxic pollutant [e.g. 318,319,325].

6.2 Methods

6.2.1 Preparation of cultures

Aurantimonas sp. (ATCC BAA-1229)

Manganese-replete *Aurantimonas* sp. (ATCC BAA-1229) (*Aur*) were grown in approximately 50 mL of M-media [215] or ATCC® 2584 media (Appendix A) in autoclaved glass conical flasks (Fisherbrand), maintained at room temperature. For cells grown under Mn-limited conditions, altered M-media was used (Table 6.1), which lacked manganese chloride, peptone and yeast. Table 6.1 lists the terminology that will be used from here onwards to describe the media conditions. *Aur* cultures were grown and maintained by Manuela Hartmann (NOCS). Due to the facilities available, stock cultures were not grown under trace metal free conditions.

Table 6.1: Terminology used to describe manganese growth conditions of bacterial cultures

Term	Description
Mn-replete media	Standard unaltered M-media [215] or ATCC® 2584 media (Appendix A)
Mn-limited media	M-media lacking $MnCl_2$, peptone and yeast
Mn-replete cultures	Cells grown in Mn-replete media
Mn-limited cultures	Cells grown in Mn-limited media

Samples were taken from cultures after approximately 2 weeks. This interval was based on personal communication with Manuela Hartmann and allowed for the development of a brown residue, which indicated MnOx formation (brown MnOx crust after 11 d [213]).

Samples were filtered through a 1.0 µm polycarbonate (PC) filter (Whatman) in order to remove larger aggregates of cells and MnOx, thus creating a uniform cell suspension.

Cell concentration was estimated using a Nanodrop 1000 (Thermo Scientific) using a previously prepared calibration curve of cell concentration (accurately measured by flow cytometry) versus the optical density signal from the Nanodrop. This estimation of cell concentration was used to calculate the dilution of the culture to typically ~1 $x10^6$ cells/mL, using either M-replete or M-limited media. The Nanodrop allowed a fast estimation of cell number, and an accurate cell count was done subsequently using flow cytometry (Chapter 2, Section 2.3). Flow cytometric cell counts were done for at least the first and final incubation time point, and an average cell abundance for each experiment was calculated (unless there was a significant change in cell concentration throughout the incubation, or data for all time points was available, in which case individual cell counts were used for each time point). Uncertainty of cell concentration was based on the standard deviation of multiple samples/replicates (Section 2.3.3).

Halomonas sp.

Non Mn-oxidising *Halomonas* sp. (*Halo*) cultures were grown and harvested as described in Chapter 2 (Section 2.5). As above, cell cultures were diluted to approximately 1 $x10^6$ cells/mL (estimated using the Nanodrop 1000) using M-replete/limited media, and counted accurately using flow cytometry.

6.2.2 Cobalt incubation experiments

For incubation experiments, all plasticware was initially cleaned by soaking in a bath containing concentrated Analytical grade hydrochloric acid (HCl) (Sigma Aldrich UK or Fisher Scientific UK), diluted to ca. 1 M using deionized water (resistivity >18.2 MΩcm, Millipore) (Chapter 2, Section 2.2.1). Plasticware was then rinsed three times using

deionized water and allowed to dry under a laminar flow hood (Circulaire VLF650E, Monmouth Scientific), before being stored in sealed plastic sample bags.

Basic experimental setup

Nine main experiments were conducted and numbered 1-9, which tested a number of different variables (described in 'Experimental variables' below). The basis of each experiment involved adding 1.6 mL of cell culture to 10 µL radiolabelled cobalt chloride (^{57}Co) (in solution with 0.1 M HCl) in acid cleaned plastic vials (^{57}Co source stock: 312.02 GBq/mg, 3880.30 MBq/mL, Perkin Elmer) to a final cobalt concentration of 0.03 nM. At set time points, samples were fixed with paraformaldehyde (PFA) (1% final concentration) (Sigma Aldrich, UK) and immediately filtered onto 0.2 µm PC membrane (Whatman) using a vacuum filtration manifold (as described in Chapter 2, Section 2.4). Samples were washed with ~6 mL deionized water and filters placed into scintillation vials (20 mL, high-density polyethylene, HDPE, Meridian) along with 5 mL of scintillation cocktail (Gold Star, Meridian), before counting on a liquid scintillation counter (Tri-carb 3180, Perkin Elmer). Radioactivity (^{57}Co) retained on the 0.2 µm PC filter represented the particulate cobalt formed in the culture and included any precipitated, oxidised, sorbed or assimilated cobalt. Additionally, throughout the course of the experiment (most significantly, at the start and end of the incubation), 1.6 mL samples were taken, fixed with 1% PFA (final concentration) and stored at 4ºC for subsequent flow cytometric analysis to determine cell concentration (as described in Chapter 2 (Section 2.3).

Data Analysis

Replicate samples were used for each variable within an experiment. For the majority of experiments, four replicates were incubated for multiple time points at intervals of several hours, usually up to a maximum of approximately 3-5.5 h (except Experiment 1,

incubation up to ~24 h). However, for Experiments 4 and 8 multiple samples of increasing cell concentration were used, with only one incubation time (4 h and 3.25 h, respectively).

Radioactivity measurements (in counts per minute, CPM) were converted to mole values (SI unit prefixes used when required), as described in Chapter 2 (Section 2.4). After consideration of abiotic particulate cobalt formation, most values were presented on a mole per cell basis to allow comparison between experiments. Data was assessed using either all the individual replicates within each experiment and/or an average value of particulate cobalt formation for each experiment. Statistical analysis was performed on data, as described in Chapter 2, Section 2.6. Outliers were defined as those that deviated from the mean by more than 3 standard deviations and were omitted from calculations.

Experimental uncertainties were based on the uncertainties in cell counts (Section 2.3.3), amount of radioactivity added to the sample (Section 2.4.4), as well as sample replicates.

Experimental variables

Variations to the basic experiment were conducted within the nine experiments, aiming to monitor the effect of different variables on particulate cobalt formation. Variables examined were:

- Level of particulate cobalt formation in non Mn-oxidising bacterial cultures
- Comparison of particulate cobalt formation in Mn-replete vs Mn-limited cultures
- Change in particulate cobalt formation upon the addition of a Mn(II) source
- Level of particulate cobalt formation in dead *Aurantimonas* cultures
- Effect on particulate cobalt formation upon the addition of potentially competing metals (i.e. chromium, copper, or nickel).

All experiments followed the basic setup, with specific methodological alterations made according to the variable to be tested.

Non Mn-oxidising bacteria

Formation of particulate cobalt in bacterial cultures not capable of Mn-oxidation was assessed using cultures of *Halomonas*. This was performed in Experiments 1, 2 and 3 alongside *Aurantimonas* cultures.

Mn-replete vs Mn-limited cultures

Differences in formation of particulate cobalt between *Aurantimonas* cells grown in Mn-replete or Mn-limited media was assessed in Experiments 3, 4, 8, and 9, where Mn-replete and Mn-limited cultures were tested concurrently.

Addition of an additional Mn(II) source

Murray *et al* (2007) and Murray and Tebo (2007), noted that colloidal MnO_2 was much more reactive than aged crystalline MnOx in the formation of particulate cobalt/chromium [114,319]; therefore, Experiments 1 - 5 tested the effect of adding a Mn(II) source to samples, which acted as a fresh manganese source to the cells. Manganese chloride ($MnCl_2$) was added to sample tubes (prior to addition of cells) to a final concentration of 100 µM, which was based on the concentration used in M-media [215]. Cell samples with no extra $MnCl_2$ were incubated concurrently, and both Mn-replete (Experiments 1, 3, 4, and 5) and Mn-limited (Experiments 2, 3, and 4) cultures were tested. The percentage change in particulate cobalt formation upon addition of $MnCl_2$ was calculated using Equation 6.1.

Eq. 6.1 $$\frac{(\text{Metal addition sample} - \text{Control sample})}{\text{Control sample}} \times 100 = \text{Change in particulate cobalt upon addition of metal (\%)}$$

Dead Aurantimonas cultures

In Experiment 9, the level of particulate cobalt formation was compared in live and dead *Aurantimonas* cultures. This was done for both Mn-replete and Mn-limited cultures. Dead *Aurantimonas* cultures were prepared through the addition of paraformaldehyde (1% final concentration) prior to incubation with cobalt.

Addition of potentially competing metals

The effect of potentially competing metals on the formation of particulate cobalt was also examined in this study. Chromium, copper or nickel was added to samples (prior to introduction of *Aurantimonas* cultures), alongside a control sample with no extra metal additions (final concentrations shown in Table 6.2). Both Mn-replete (Experiments 6, 7, and 8) and Mn-limited (Experiment 8) cultures were assessed. The percentage change in particulate cobalt formation upon addition of chromium, copper or nickel was calculated using Equation 6.1.

Table 6.2: Final concentrations of additional trace metals added to bacterial cultures
Final concentrations of nickel, copper and chromium were based on average ambient concentrations found in the open ocean [326], all of which are in excess over the 0.03 nM cobalt.

Metal	Chemical Form	Final Concentration	Grade and company
Ni	Nickel (II) chloride	12.1 nM	GR analysis, Merck
Cu	Copper (II) sulphate	4.5 nM	Analytical reagent, Fisher Scientific
Cr	Chromium (III) nitrate	5.0 nM	Laboratory reagent, Fisher Scientific

Abiotic controls

In order to assess potential abiotic cobalt formation in the samples, aliquots of Mn-replete and/or Mn-limited media containing no cells were incubated with the radiolabelled cobalt, as described above for the basic experimental setup. This was done during Experiments 1, 4, and 8. Additionally, samples of media with additional $MnCl_2$ were tested in Experiments 1 and 4.

The proportion of abiotic signal in comparison to the total amount of radioactivity added to a sample was calculated (Equation 6.2). A percentage of <10% was considered to be an insignificant amount of abiotic particulate cobalt formation.

Eq. 6.2 $$\frac{\textit{Cobalt in abiotic control (mol)}}{\textit{Total cobalt added (mol)}} \times 100 = \textit{Percentage of cobalt added that becomes background signal}$$

Additionally, the abiotic signal was compared to the signal measured in cell samples, which provided an estimate of how much of a cell sample signal is attributed to the abiotic signal (Equation 6.3). As before, <10% was considered to be an insignificant amount of abiotic particulate cobalt formation in comparison to cell sample signals.

Eq. 6.3 $$\frac{\textit{Cobalt in abiotic control (mol)}}{\textit{Cobalt in cell sample (mol)}} \times 100 = \textit{Percentage of the cell sample signal that is background signal}$$

Time course assessment

In Experiments 1, 2, 3, 5, 6, 7, and 9, replicates were incubated for an increasing amount of time. This allowed the progression of particulate cobalt formation to be monitored over time in both Mn-replete and Mn-limited cultures. The percentage change in particulate cobalt was compared between the first and final time point of the incubation (Equation 6.4).

Eq. 6.4 $$\frac{\textit{(Final sample - First sample)}}{\textit{First sample}} \times 100 = \textit{Percentage change in amount of particulate cobalt from first}$$

Long term incubation

Finally, a tenth experiment (Experiment 10, also named Long Term Incubation) was conducted over the course of approximately 13 d. For this experiment, *Aur* cells were taken from a Mn-replete culture stock and added to 50 mL of Mn-replete or Mn-limited media, to a final cell concentration of approximately 5 x10^6 cells/mL. Radiolabelled cobalt (^{57}Co, final concentration ~0.03 nM) was added to two replicates of Mn-replete and Mn-limited cultures. Aliquots (1.6 mL) were taken at regular intervals, and 1.4 mL was filtered for measurement of ^{57}Co, as standard. The remaining sample volume (0.2 mL) was used to determine cell concentrations using flow cytometry (Chapter 2, Section 2.3).

6.3 Results

6.3.1 Manganese oxidation by *Aurantimonas*

Manganese oxidation by *Aur* in Mn-replete media was visible through the formation of a brown residue in the culture stocks, which did not occur in the absence of *Aur* (M. Hartmann, personal communication). Cultures grown in Mn-limited media did not have an obvious brown residue (M. Hartmann, personal communication).

6.3.2 Formation of particulate cobalt

Presentation of the following data includes individual data points of replicates (based on increasing incubation time or increasing cell concentration) within each experiment and/or an average value for each experiment. The use of individual points, or an average will be highlighted where relevant.

Abiotic controls

Formation of particulate cobalt was assessed in media blanks, which were used as abiotic controls (Experiments 1, 4, and 8). The average values from all blanks were shown to be negligible compared to the amount of cobalt added to the sample for both Mn-limited and Mn-replete media (≤0.13% of total added Co) (Equation 6.2).

These abiotic values were also compared to the amount of particulate cobalt in cell samples (Equation 6.3). When the cell concentration was less than 400,000 cells/mL, the blank signal contributed a noteworthy proportion of the total signal (11.5±2.9% and 23.6±5.3% in Mn-replete and Mn-limited media, respectively). However, in samples where the cell concentration was more than 400,000 cells/mL, then the blank signal was a minimal proportion (<10%) of the total signal (4.31±1.00% and 6.53±1.04% in Mn-replete and Mn-limited cultures, respectively). Therefore, in all experiments, cell concentrations of less than approximately 400,000 cells/mL were discounted.

Increasing Aur *concentration*

For Experiments 4 and 8, the amount of particulate cobalt formed (in fmol, whereby 1 fmol = 10^{-15} mol = 6 x10^{8} atoms of cobalt) was plotted against increasing cell concentration (Figure 6.1). Within each experiment, for both Mn-limited and Mn-replete media, there was a strong linear correlation between increasing cell concentration and increasing particulate cobalt. Additionally, Figure 6.1 shows two statistically distinct groups (Mann-Whitney rank sum test, p = 0.002), representing cells from either Mn-replete (black and green symbols) or Mn-limited (red and yellow symbols) media. Linear regression analysis of all Mn-replete or all Mn-limited data points in this plot produced slopes of 0.95±0.20 zmol/cell and 0.32±0.05 zmol/cell (note: 1 zmol = 10^{-21} mol = 600 atoms of cobalt) and y-axis intercepts of 0.5±1.1 fmol and 0.06±0.08 fmol, respectively.

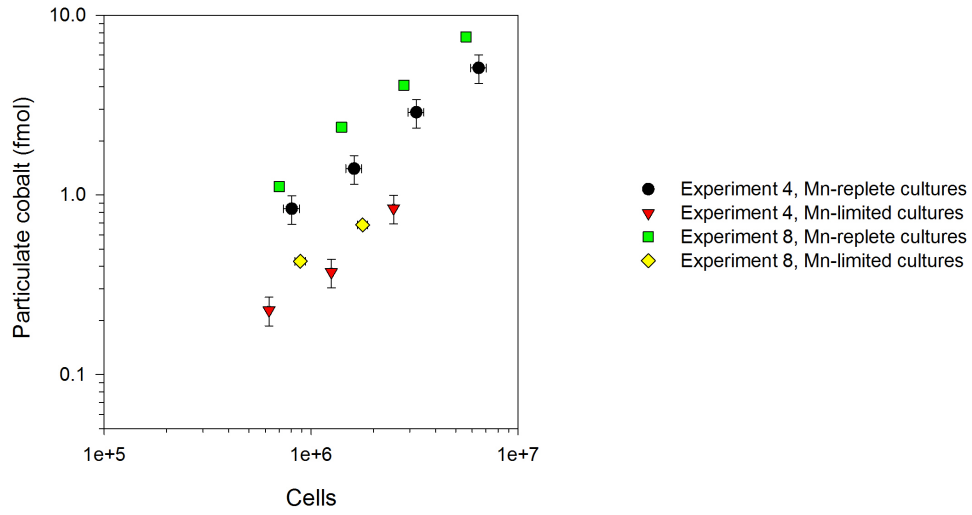

Figure 6.1: Amount of particulate cobalt for an increasing cell concentration
Individual data points for Experiments 4 and 8 are plotted as cell concentration versus the amount of particulate cobalt in fmol. Each colour represents a different experiment, with black and green symbols showing Mn-replete cultures, and red and yellow symbols showing Mn-limited cultures. Vertical error bars show the uncertainty in the amount of cobalt, based on calculations of the amount of cobalt added to the sample (Section 2.4.5). Horizontal error bars are based on standard deviation of cell counts. Note both axes are plotted on a log scale.

Time course

For Experiments 1, 2, 3, 5, 6, 7 and 9, the amount of particulate cobalt at the first and final incubation time points were compared and presented in Figure 6.2a, where a unity line represents equal particulate cobalt at the first and final time point. All experiments are distributed across the unity line, with statistical analysis of all experiments showing no significant difference (Wilcoxon signed rank Test, $p = 0.688$). Additionally, percentage change between first and final time points is shown in Figure 6.2b, with most experiments showing minimal (<27%) change in particulate cobalt. As there was generally no overall effect of time on the amount of particulate cobalt, incubation time was disregarded as an additional variable in Experiments 1-9.

Experiments 1 and 5 using Mn-replete media were the only notable outliers, showing an 81.7±0.2% decrease and an 86.2±14.7% increase (respectively) in amount of particulate cobalt from first to final time point (Figure 6.2b).

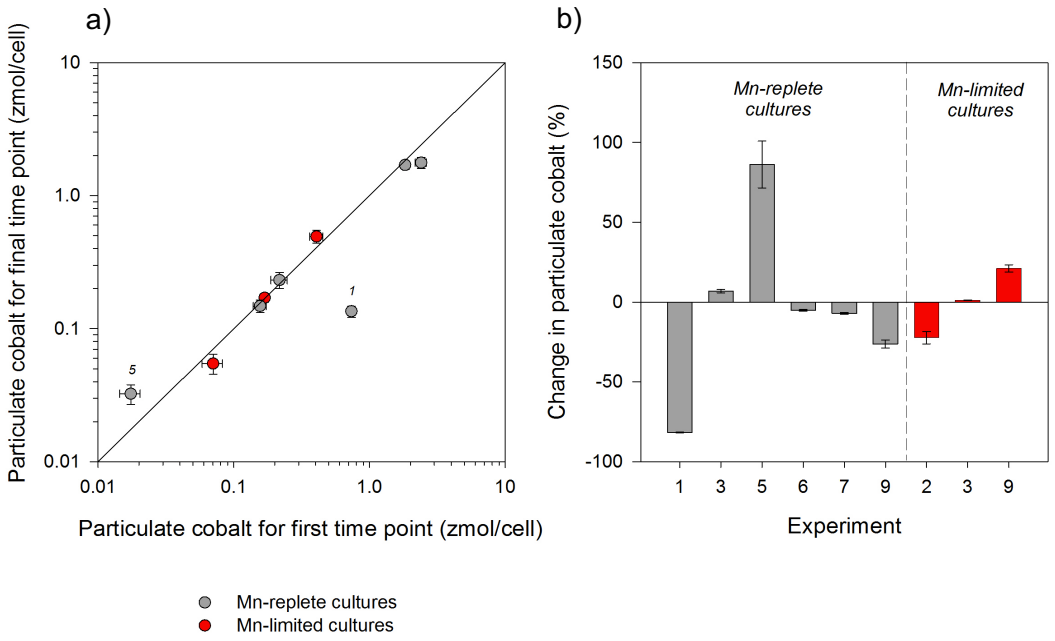

Figure 6.2: Comparison of particulate cobalt at the beginning and end of incubation experiments

a) *The amount of particulate cobalt (zmol/cell) in the first and final incubation points of Experiments 1, 2, 3, 5, 6, 7, and 9 are directly compared against one another. A unity line indicates equal particulate cobalt in the two time-points. Symbols in grey and red indicate experiments that used Mn-replete and Mn-limited media, respectively. Experiments of interest are labelled with their experimental number. Error bars represent error of propagation from cell counts and amount of cobalt added to sample. Note both axes are on a log scale.*

b) The change in particulate cobalt between the first and final time points is presented as a percentage, where a negative value indicates a decrease in particulate cobalt over time, and a positive value indicates an increase. Bars shaded in grey and red used Mn-replete and Mn-limited media, respectively. Error bars represent combined uncertainty of the errors calculated in the first and final values (Figure 6.2a).

Upon comparison of first and final values of particulate cobalt in the Long-Term experiment (Experiment 10), samples in Mn-replete media showed a decrease in particulate cobalt formation between the first and final time points by 27.4±3.4% and 61.5±0.0%. Conversely, samples in the Mn-limited media increased in particulate cobalt by 6.5±1.3% and 712.5±178.9% (figure 6.3a). The most substantial change occurred in one of the replicates from the Mn-limited culture. Plotting the amount of particulate cobalt formed in this incubation against time shows a linear increase until approximately 190 h when the formation of particulate cobalt plateaued (Figure 6.3b). Also, shown in Figure 6.3b as a comparison, is the time course profile for the other Mn-limited culture replicate, which remains relatively constant throughout the experiment.

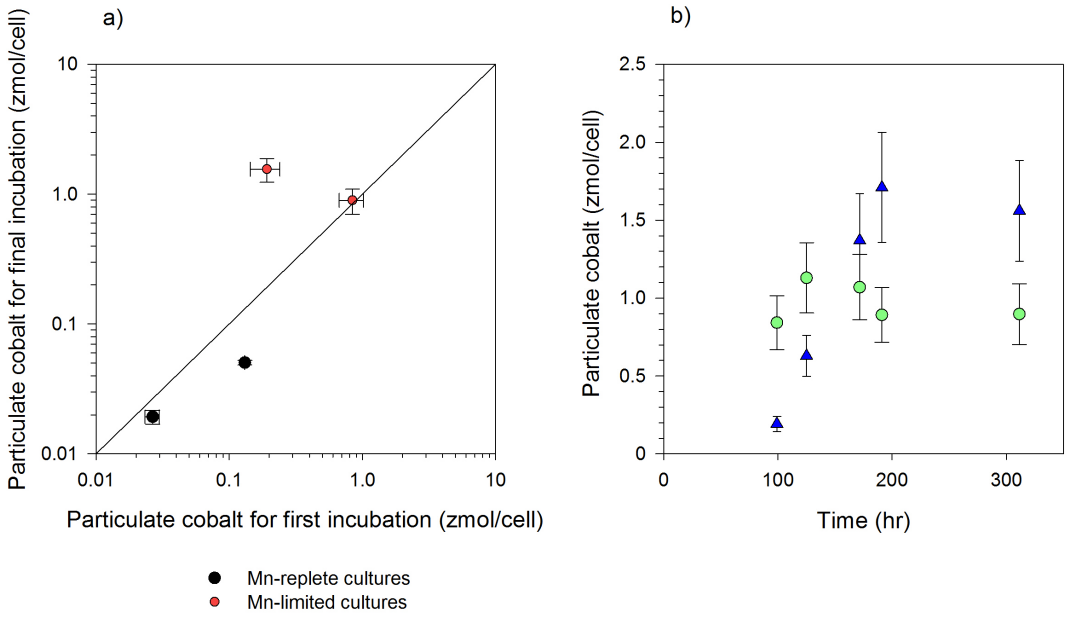

Figure 6.3: Comparison of particulate cobalt at the beginning and end of long term incubation experiments

a) *The amount of particulate cobalt (zmol/cell) in the first and final incubation points of experiment 10 are directly compared against one another, where a unity line indicates equal particulate cobalt in the two time-points. Symbols in black and red indicate experiments that used Mn-replete and Mn-limited media, respectively. Error bars represent error of propagation from cell counts and cobalt added to sample. Note both axes are on a log scale.*

b) *Individual data points from Mn-limited cultures are plotted as incubation time versus the amount of particulate cobalt. Blue triangles and green circles represent the two different replicate cultures. Error bars represent error of propagation from cell counts and cobalt added to sample.*

Mn-limited vs Mn-replete media

Figure 6.4 shows a direct comparison of particulate cobalt (in zmol/cell) in Mn-replete and Mn-limited cultures from four separate experiments (Experiments 3, 4, 8, and 9), where a unity line represents equal amounts of particulate cobalt in Mn-replete and Mn-limited cultures. In all experiments, there was a higher amount of particulate cobalt in Mn-replete cultures, with differences between the two media types ranging from 32.6±4.5% (Experiment 3) to 365.7±35.1% (Experiment 9) and statistically significant differences between the two media types within each experiment (paired t-test, $p<0.03$ for each experiment).

Conversely, in the long-term incubations (Experiment 10) (Figure 6.5), there was significantly more cobalt in Mn-limited media (0.19 - 1.71 zmol/cell) compared to Mn-replete media (0.02 - 0.13 zmol/cell).

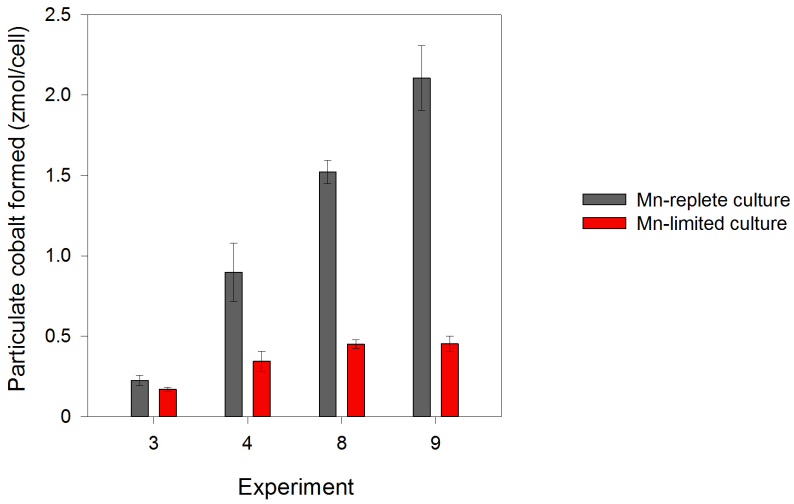

Figure 6.4: Comparison of particulate cobalt in Mn-replete and Mn-limited cultures
The average amount of particulate cobalt (zmol/cell) for Mn-replete and Mn-limited cultures for Experiments 3, 4, 8 and 9 are directly compared. Mn-replete cultures are plotted in grey, and Mn-limited in red. Cultures measured during the same experiment are clustered together. Error bars represent the averaged error from individual data points within an experiment.

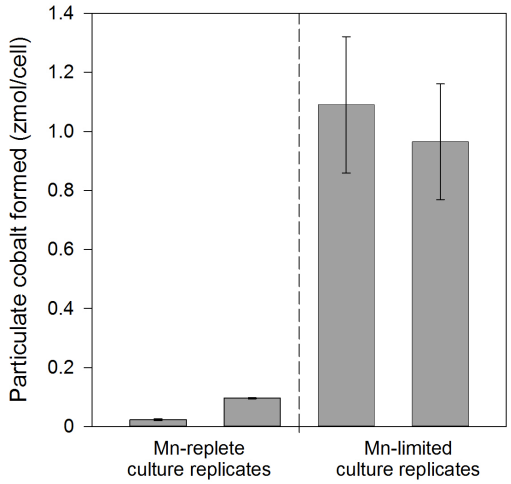

Figure 6.5: Comparison of particulate cobalt in Mn-replete and Mn-limited cultures from long-term incubations in replicate experiments
The average amount of particulate cobalt formed in the four incubations from Experiment 10 is presented as zmol of Co per cell. Replicate cultures of Mn-replete and Mn-limited media are presented, with error bars representing the averaged error from individual data points.

Halomonas

Halo cultures were incubated alongside *Aur* in Experiments 1, 2 and 3. The average level of cobalt in *Halo* cultures tested was 0.04±0.03 zmol/cell, which was an order of magnitude lower than values seen in Mn-replete and Mn-limited cultures of *Aur* that were concurrently incubated (0.36±0.26 zmol/cell and 0.12±0.06 zmol/cell, respectively). Figure 6.6 shows the distribution of the data (which used the individual replicates within each experiment), with the lowest group being those of *Halo*. Statistical analysis of the experiments showed Mn-replete *Aur* and *Halo* to be significantly different (Wilcoxon signed rank Test p = 0.016), but the difference between Mn-limited *Aur* and *Halo* to be not quite significant (Wilcoxon signed rank Test, p= 0.063).

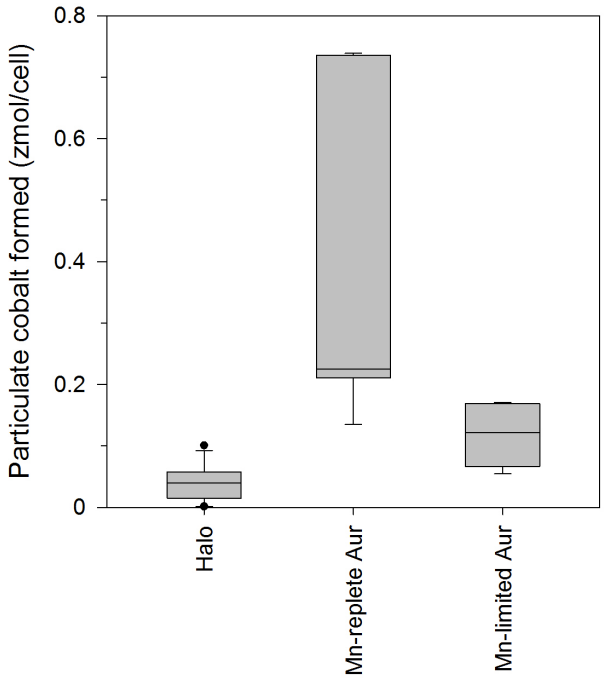

Figure 6.6: Comparison of particulate cobalt in Halomonas, Mn-replete Aurantimonas and Mn-limited Aurantimonas
The amount of particulate cobalt is presented as zmol of Co per cell, with Halo and Aur cultures displayed against each other to allow for direct comparison. All individual data points (i.e. from each incubation time point, omitting outliers) from Experiments 1, 2 and 3 are grouped together for each culture. Individual time points showing changes in particulate cobalt throughout the course of the incubation are not shown, as this plot is used to indicate differences between difference cell cultures, encompassing all measurements throughout an incubation. Data is displayed as a box and whisker plot, where the shaded box displays data between the upper and lower quartile, and the horizontal line showing the median. Error bars indicate upper and lower extremes and the dots signify outliers.

Dead Aur cultures

The formation of particulate cobalt in PFA-killed *Aur* was compared to live *Aur* in Experiment 9 (Figure 6.7). Dead cells showed significantly lower amounts of particulate cobalt compared to live *Aur*, regardless of the media used for the experiment (Wilcoxon signed test of all individual data points, $p = 0.008$). The levels of particulate cobalt seen in dead *Aur* cells (0.02 - 0.21 zmol/cell) was comparable to the level seen in live *Halo* cultures (0.002 - 0.1 zmol/cell) (Mann-Whitney rank sum test of all individual data points, $p = 0.148$). There was also a notable difference between experiments in the two types of media: dead cells in Mn-limited media had 34-45% of the cobalt found in live cultures, whereas dead cells in Mn-replete media had <2% of the cobalt found in live cultures.

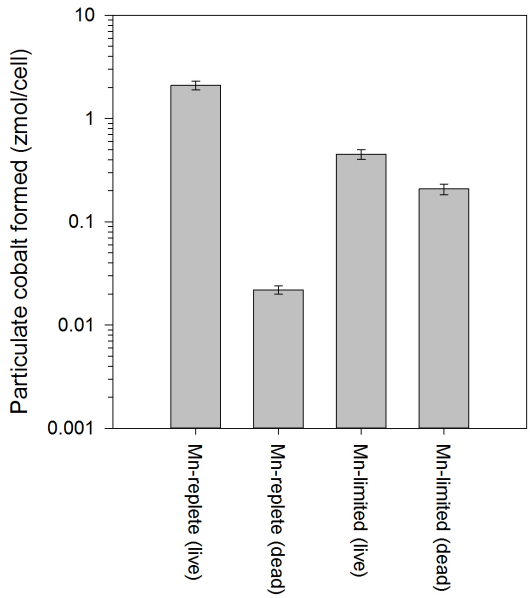

Figure 6.7: Comparison of particulate cobalt in PFA-killed and live Aurantimonas (Experiment 9)
The average amounts of particulate cobalt for live and dead cells in Mn-replete and Mn-limited media are displayed adjacently. Error bars represent the average error from each individual data point within the incubation. Note the y-axis is on a log scale.

6.3.3 Addition of metals

Manganese

Manganese ($MnCl_2$) (100 μM) was added to *Aur* cultures in Experiments 1-5 and the average amount of particulate cobalt formed per cell (zmol/cell) was plotted against the respective control sample, which had no additions (Figure 6.8a). Also presented is the percentage change in particulate cobalt levels upon addition of $MnCl_2$ (Figure 6.8b). In samples that used Mn-replete media, there was no overall trend of an increase in particulate cobalt formation upon addition of $MnCl_2$, with a slight tendency towards a decrease in Experiments 3, 4 and 5. There was no statistical difference shown between particulate cobalt formation in Mn-replete cultures with or without additional $MnCl_2$ (Table 6.3).

Conversely, in Mn-limited cultures, there appeared to be an increase (approximately 13-60%) in particulate cobalt formation upon addition of $MnCl_2$, with Experiment 2 showing the smallest increase, and Experiment 4 showing the largest increase. However, a statistically significant difference between particulate cobalt formation was only seen in Experiment 3 (Table 6.3). Nevertheless, it should be noted that Experiment 4 (using Mn-limited media), only has two data pairs due to the elimination of data because in some samples cell concentration was less than 400,000 cells/mL (see below) or values were more than three standard deviations away from the mean. Including these eliminated values results in a statistically significant difference (i.e. $p<0.05$) upon addition of $MnCl_2$. between the amount of particulate cobalt formed in $MnCl_2$ supplemented and control incubations.

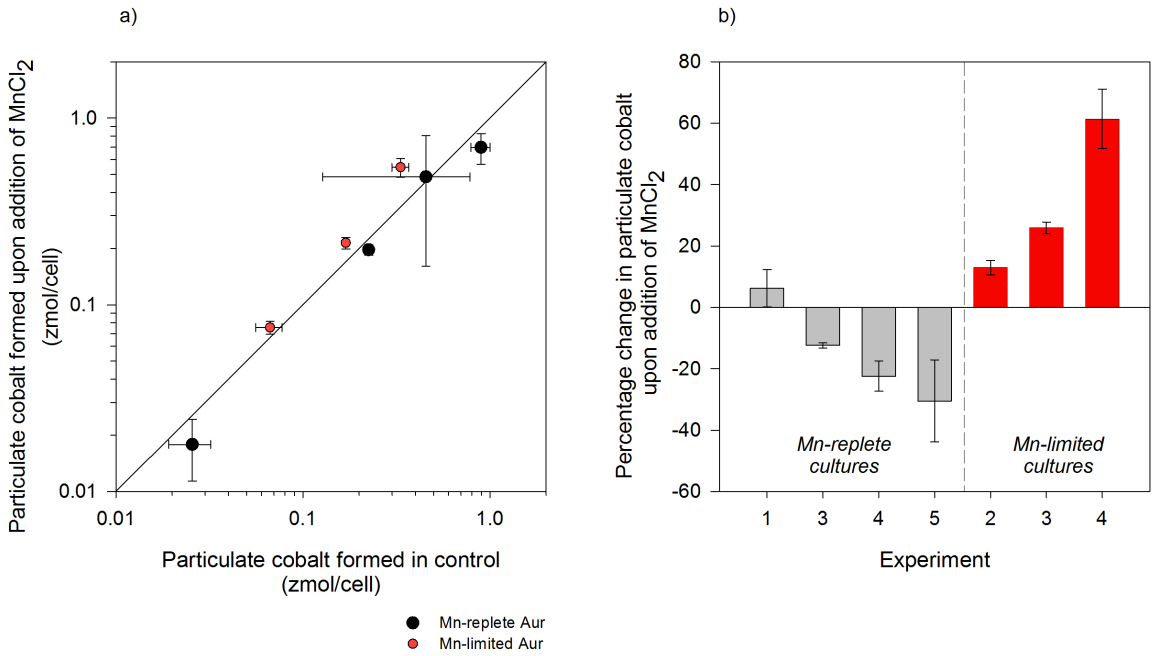

Figure 6.8: Comparison of particulate cobalt in experiments with/without $MnCl_2$ supplements

a) The average amount of particulate cobalt in Experiments 1-5 is compared between incubations that did/did not have additions of $MnCl_2$. The unity line indicates equal particulate cobalt in incubations supplemented with $MnCl_2$ and control incubations. Incubations using Mn-replete and Mn-limited media are indicated with black and red symbols, respectively. Data points are based on the average of multiple time points, with the error bars showing standard deviation. Note both axes are on a log scale.

b) The change in particulate cobalt between the control and $MnCl_2$ supplemented incubations (using averaged values from each experiment) is presented as a percentage, where a negative value indicates a decrease in particulate cobalt upon addition of $MnCl_2$, and a positive value indicates an increase. Bars shaded in grey and red used Mn-replete and Mn-limited media, respectively. Error bars represent error of propagation of the standard deviation with and without $MnCl_2$.

Table 6.3: Statistical analysis of particulate cobalt in experiments with/without $MnCl_2$ supplements

Statistical tests (Student's paired t-test and F-test, see Section 2.6) were based on individual data points within each experiment. A p-value of less than 0.050 was deemed to show statistical significance between control and $MnCl_2$ additions, and are highlighted in bold. Experiments highlighted with an asterisk indicates that the data failed a normality test and that a Wilcoxon signed rank test was performed. An F-value less than the critical value show equality of variance between of data groups, with those that show unequal variance highlighted in italics. The value in brackets is the number of data pairs.

Media	Experiment	P-value	F-value
Mn-replete	1	0.255*	1.0 (4)
	3	0.083*	1.8 (3)
	4	0.057*	1.5 (4)
	5	0.125*	1.0 (4)
Mn-limited	2	0.446*	5.3 (3)
	3	0.046*	*101.9 (3)*
	4	0.144*	1.6 (2)

Chromium, copper and nickel

Additionally, chromium, copper and nickel were added to samples in Experiments 6, 7, and 8, and the level of particulate cobalt formed was assessed. Metal addition samples were paired with their respective control samples that had no additions (based on the same incubation time in Experiments 6 and 7, or the same cell concentration in Experiment 8) for all individual data points (Figure 6.9). A unity line represents equal particulate cobalt in control and metal addition samples.

The amount of particulate cobalt did not change upon addition of chromium as evidenced by minimal deviation from the unity line as well as no statistical difference from the control (Table 6.4). Copper caused a slight decrease in particulate cobalt formation, as two of the three copper addition experiments fell slightly below the unity line (Figure 6.9), although were not statistically different from the control (Table 6.4). Upon addition of nickel there is also a slight decrease in the amount of particulate cobalt formed (Figure 6.9). Indeed, collective analysis of all individual data points within each experiment showed that this difference was statistically significant (Table 6.4). However, this was not the case when individual experiments were assessed (Table 6.4).

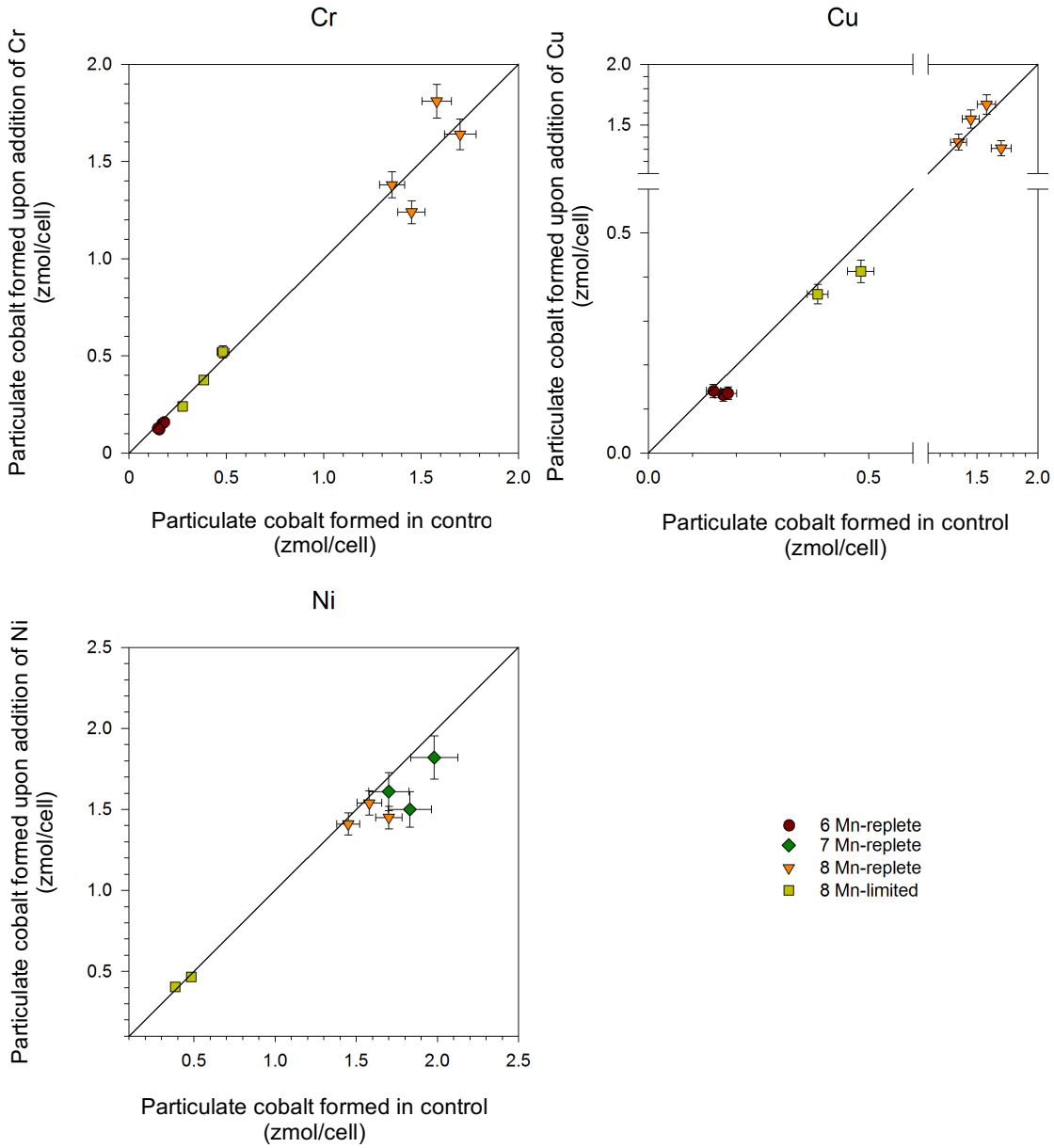

Figure 6.9: Comparison of particulate cobalt in experiments with/without Cr, Cu or Ni supplements

The amount of particulate cobalt (zmol/cell) formed upon addition of supplementary chromium, copper or nickel supplements are compared against control incubations without additions for Experiments 6, 7, and 8. The unity line indicates equal particulate cobalt in control and supplemented incubations. Presented are individual data points from each experiment, paired based on a shared incubation time (Experiments 6 and 7) or a shared cell concentration (Experiment 8). The legend identifies the experimental number and the media used. Error bars for individual data points represent error of propagation of cell counts and amount of cobalt added.

Table 6.4: Statistical analysis of particulate cobalt in experiments with/without chromium, copper or nickel supplements
Statistical tests (Student's paired t-test and F-test, see Section 2.6) were based on (a) individual data points within each experiment, (b) all data points for all experiments. A p-value of less than 0.050 was deemed to show statistical significance between control and Ni additions (highlighted in bold). The experiment with an asterisk indicates that the data failed a normality test and a Wilcoxon signed rank test was performed. An F-value less than the critical value show equality of variance between data groups. The value in brackets is the critical F-value.

Metal Addition	Dataset	paired t-test	F-value
Cr	a) Experiment 6 (Mn-replete)	0.125*	1.5 (15.4)
	a) Experiment 8 (Mn-replete)	0.980	2.8 (5.0)
	a) Experiment 8 (Mn-limited)	0.978	1.8 (39.0)
	b) All individual data points	0.465*	1.1 (3.7)
Cu	a) Experiment 6 (Mn-replete)	0.124	13.9 (39.0)
	a) Experiment 8 (Mn-replete)	0.875*	1.2 (15.4)
	a) Experiment 8 (Mn-limited)	0.295	3.6 (647.3)
	b) All individual data points	0.570*	1.0 (4.3)
Ni	a) Experiment 7 (Mn-replete)	0.113	1.3 (39.0)
	a) Experiment 8 (Mn-replete)	0.250*	3.5 (39.0)
	a) Experiment 8 (Mn-limited)	0.930	2.5 (647.3)
	b) All individual data points	**0.035**	1.3 (5.0)

6.4 Discussion

6.4.1 Particulate cobalt formation (Experiments 1-9)

The formation of particulate cobalt was influenced by the presence of live *Aur* cells. This is shown by the clear relationship between an increase in cell concentration leading to an increase in particulate cobalt (Figure 6.1). This is in agreement with previous studies that also observed an increase in particulate cobalt formation in the presence of Mn-oxidising microorganisms [e.g. 110,111]. Furthermore, in the absence of *Aur*, there was reduced particulate cobalt formation, specifically in cultures containing the non-Mn-oxidising *Halo* (Figure 6.6) and abiotic controls (media blanks) where a negligible signal was obtained (≤0.13% of total cobalt added). Any minor signal in the media blank may have been the result of surface adhesion of cobalt to the filter. This observation is to be expected as

abiotic cobalt precipitation rarely occurs in the marine environment [110], where biological uptake is a more significant cobalt export factor than particulate settling [106].

The majority of the particulate cobalt formed in this study seemingly occurred outside of the cell (i.e. it was not intracellular). Cell-surface association occurs rapidly and generally does not show an increase with time [e.g. 261], as was observed in Experiments 1, 2, 3, 5, 6, 7, 9 (Figure 6.2). No intracellular uptake was noted in this study, which is typically demonstrated by an increase in radioactivity over time, such as for amino acid uptake [e.g. 188,198]. Interestingly, Moffett and Ho (1996) noted a lag period (~2-3 h) before they could accurately measure cobalt uptake in seawater samples from Waquoit Bay [113], which may explain why no intracellular uptake was observed in this study. However, this is in contrast to Lee and Tebo (1994) who noted a linear increase in cobalt binding in *Bacillus* sp. strain SG-1 during the first 6 h of their experiment [110].

Some experiments (specifically Experiment 1, using Mn-replete media, Figure 6.2b) saw a decrease in particulate cobalt between the first and final time points, which is indicative of metal desorption from particulates/cells, as seen in iron [e.g. Chapter 5, and reference 77]. The most notable exception in this study was that of Experiment 5, using Mn-replete media, which saw an increase in particulate cobalt formation throughout the course of the incubation; however, this experiment used a cell stock that had a cell concentration that was an order of magnitude higher (ca. 1.6 x10^7 cells/mL) than all other experiments, which may explain the deviation from the trend.

It should be noted that these results assume that addition of 10 µL ^{57}Co in 0.1 M HCl to a 1600 µL sample was not harmful to cells and that the culture media provided suitable buffering capacity (see Appendix F). It is likely cells were still viable, as upon deliberate killing of cells (Experiment 9, addition of PFA, Figure 6.7) a marked decrease in particulate cobalt formation was observed. Additionally, both *Halomonas* and *Aurantimonas* have a wide pH tolerance for growth (pH 5 - 9 [208] and pH 5.5 - 9.5 [213], respectively, strain dependent). Additionally, most incubations saw no change in cell count between first and final incubation (i.e. counts were within 1 standard deviation of each

other), with some even showing an increase (e.g. Experiment 1), thus indicating cells were not harmed. In three incubations (Experiment 3 Mn-limited culture, Experiment 6, Experiment 9 Mn-limited culture), a slight decrease in cell concentration was seen during the experiment; however this was a small decrease (approximately 7.6 - 17.5%) between first and final time points, and did not affect inferences drawn from the data.

Is formation of particulate cobalt due to cells or MnOx?

Particulate cobalt formation is either a direct result of *Aur* cells or an indirect result of the MnOx produced by *Aur* [110,113]. In this study, upon killing of cells using PFA, particulate cobalt formation was severely reduced, especially in Mn-replete cultures (Figure 6.7). This is in agreement with previous studies that saw a reduction in Co(II) binding in azide-killed cultures [113,322]. As PFA would not have changed the concentration of MnOx in the sample, this result implies that particulate cobalt formation is the result of a direct microbial pathway, not the presence of MnOx. Indeed, Moffett & Ho (1996) suggested that Co(II) and Mn(II) were directly oxidised by a shared catalytic pathway, which led to the incorporation of cobalt into MnOx [113]. Additionally, Lee and Fisher (1993) concluded that cobalt oxidation was a direct result of microbial activity, rather than adsorption to or oxidation by MnOx, and that Mn and Co oxidation pathways were independent [320].

However, Murray *et al* (2007) claimed that the results seen by Moffett and Ho (1996) were a result of manganese contamination, and that Co(II) oxidation actually occurs indirectly by MnOx, specifically by a highly reactive colloidal MnO_2 [114]. Indeed, one proposed mechanism for particulate cobalt formation is that Co(II) is adsorbed to MnOx, oxidised to Co(III) and subsequently incorporated into the MnOx (although, it should be noted that this study examined sediment samples, so may not reflect marine ecosystems) [111 and references therein]. Results from this study support the presence of MnOx stimulating particulate cobalt formation, as formation was higher in Mn-replete cultures (Figure 6.4), which is likely due to the presence of more pre-formed MnOx, observed as a brown residue in Mn-replete

culture stocks (M. Hartmann, personal communication) (residue also previously observed by Anderson *et al* (2009) [213]).

Addition of $MnCl_2$ to Mn-limited cultures saw a trend of increasing particulate cobalt formation (Figure 6.8), again showing manganese had an influence on particulate cobalt formation. This was not always a major increase in particulate cobalt formation (i.e. Experiment 2, Mn-limited media); however, this may have been a result of incubation time, as Murray *et al* (2007) indicated that 3 h was an optimal time period to ensure cells were linearly oxidising manganese [114], but Mn-limited cultures in this study were only incubated up to a maximum of approximately 5.5 h. Thus, upon $MnCl_2$ addition, longer incubation times may have seen more of a dramatic change in particulate cobalt formation in Mn-limited cultures.

Conversely, Mn-replete incubations did not see a significant change in particulate cobalt formation upon addition of $MnCl_2$, with many even showing a decrease in particulate cobalt, which may have been the result of desorption [77,206,291] (Figure 6.8). This may have been because 100 µM of $MnCl_2$ was not a substantially high enough concentration to cause a dramatic change in the concentration of manganese already in the solution (i.e. as pre-formed MnOx), as Mn-replete media had 100 µM $MnCl_2$ originally added upon preparation (Appendix A). This result is in agreement with Lee and Tebo (1993), who did not observe any change in particulate cobalt formation upon addition of $Mn(NO_3)_2$ [320]. Moreover, some studies have shown that, despite the need for manganese to oxidise cobalt [114], elevated concentrations of manganese actually hindered particulate cobalt formation [e.g. 113,114,322].

Interestingly, the results of this study appeared to indicate that both MnOx and *Aur* cells could be implicated in the formation of particulate cobalt (i.e. manganese additions and PFA-killed cells, respectively). Lee and Tebo (1994) suggested that Co(II) oxidation occurs as a direct result of cellular activity, but in natural environments indirect oxidation also contributes to the formation of oxidised cobalt, especially in suboxic conditions [110]. Indeed, previous studies do not have a unified agreement on the formation of particulate

cobalt, with some studies favouring direct microbial action [e.g. 113,320], and some arguing the indirect action of MnOx [e.g. 114]; therefore, it is possible that particulate cobalt formation may have been due to both the direct action of the *Aur* cells, and an indirect result of biologically formed MnOx.

6.4.2 Long-term incubation (Experiment 10)

In the long-term experiment, Mn-limited cultures had a significantly higher level of particulate cobalt than their Mn-replete counterparts (Figure 6.5), which is in contrast to the results of shorter term (<24 h) incubations (Experiments 3, 4, 8, 9) (Figure 6.4). One possible explanation for this difference is that as long-term incubations did not use acid-cleaned glassware, there may have been contamination of manganese (which was previously implied as a risk by Murray *et al* (2007) [114]). The contaminated manganese could have initiated the production of fresh MnOx in the Mn-limited cultures. Murray *et al* (2007), suggested that freshly formed colloidal manganese oxides are much more reactive than their aged counterparts [114], which would have causing a higher rate of particulate cobalt formation in Mn-limited cultures. The same response was not seen in Mn-replete cultures, potentially because any fresh MnOx in the Mn-replete cultures may have suffered a dilution affect from the older MnOx already formed in these cultures. This is also reflected in this study through the addition of $MnCl_2$ to *Aurantimonas* cultures, whereby a higher increase in particulate cobalt formation was observed in Mn-limited cultures, compared to Mn-replete (Figure 6.8).

Nevertheless, this experiment showed contradictory results to the rest of the study. Indeed, within the experiment itself replicate cultures do not agree, with one replicate of a Mn-limited culture showing a time course profile that was indicative of intracellular uptake (e.g. amino acid uptake [188,198]) and the other Mn-limited replicate indicating only sorption (Figure 6.3b).

6.4.3 Effect of chromium, copper and nickel on the formation of particulate cobalt

Despite Churchill *et al* (1995) noting that chromium was the most reactive metal in the reactivity series of Cr>Cu>Ni>Co [324], chromium did not cause a significant increase or decrease in particulate cobalt formation. This suggests that chromium did not compete with the mechanism which formed particulate cobalt. Chromium is rapidly oxidised (Cr(III) to Cr(VI) in the presence of biogenic MnOx, with the process enhanced by Mn-oxidising microorganisms [319]. However, as chromium is soluble when oxidised [112,319], it is likely that its solubility limited any potential influence on binding and particulate cobalt formation. It should be noted that only a small concentration of chromium was added to these experiments (Table 6.2). It is possible that a more significant response would be observed upon addition of a higher concentration of chromium.

Copper and nickel additions did cause a small decrease in particulate cobalt formation (Figure 6.9) (although this was not always significant, Table 6.4). This may have been because copper and nickel hindered either direct particulate cobalt formation or MnOx formation (and thus subsequent particulate cobalt formation). Copper has been shown to competitively inhibit manganese uptake in *Chlamydomonas* [327], and inhibits Mn^{2+} binding in *Arthrobacter* sp., even causing desorption [328]. Equally, nickel has been shown to competitively inhibit Mn(II) binding sites [111]. This suggests that in this study copper and nickel may have caused a slight inhibition of particulate cobalt formation, potentially due to competition for manganese binding sites [111,298,327,328], which may either also bind cobalt [e.g. 113] or stunt the production of MnOx. As with chromium, only a small concentration of copper or nickel was added to these experiments (Table 6.2), and a more notable response may be observed with higher concentrations of these potentially competing metals.

6.5 Conclusions

This study shows that particulate cobalt formation is greatly enhanced by the presence of Mn-oxidising bacteria (*Aurantimonas*) and that formation is generally elevated by the presence of manganese (either as MnOx or $MnCl_2$). However, data cannot conclusively indicate how the particulate cobalt formation occurs due to the conflicting results that were seen both within this study and in previous investigations [e.g. 113,114], implying both a direct cellular role and/or an indirect biogenic MnOx role. This suggests that a highly complex mechanism is involved in formation of particulate cobalt, which is greatly affected by a number of variables. Additionally, supplementation of chromium, copper and nickel showed that some metals have a potential trend towards inhibition of particulate cobalt formation, possibly through competition with a manganese binding site; however, further experiments that use a higher concentration of copper or nickel (or indeed chromium) would be required in order to provide a more definitive conclusion.

The cycling of cobalt in the marine environment is linked to the presence of biogenic MnOx and the associated Mn-oxidising bacteria [112] (i.e. *Aurantimonas*, found in marine environments such as the Pacific Ocean, the Sargasso Sea, and the Mediterranean [213]). Cobalt is an important nutrient for plankton [e.g. 101,102,105] and as plankton are a major influence on the oceanic ecosystem and global carbon cycling [1], it is essential to understand influences on cobalt's distribution in the water column. Several previous studies have attempted to examine the interactions of cobalt and MnOx, with no unifying conclusions about the mechanism of particulate cobalt formation [e.g. 113,114]; thus, any additional data provided by this study will help contribute to formulating a full picture of cobalt and manganese cycling in the marine environment. This, in turn, will assist in understanding bioavailability of nutrients to plankton, which is especially important due to potential changes to ocean biogeochemistry as a result of anthropogenic activities [e.g. 174,284,285].

Chapter 7: Conclusions and future work

7.1 Conclusions

7.1.1 Rationale

Bacteria dominate the microbial communities of the global surface ocean [2,13], playing a key role in the microbial loop [10,11] and recycling nutrients for utilisation by phytoplankton and other microorganisms [2,3] (Chapter 1). As such, bacterioplankton (i.e. oceanic bacteria) play a key role in surface ocean ecosystems and are critical to carbon fluxes and global primary production, of which approximately half is carried out by oceanic autotrophs [1]. Large regions of the global surface ocean are deemed oligotrophic, including the subtropical gyres, and have low levels of productivity [4]. Increasing sea surface temperature as a result of climate change leads to a deeper pycnocline, increased stratification, and expansion of these oligotrophic regions [35-38]; hence, investigations into gyre productivity, microbial processes and carbon export are important.

All plankton require a range of nutrients for optimal growth and metabolism. Low concentrations of biologically available nutrients can result in plankton growth limitation, which will affect the whole marine ecosystem. Therefore, this study examined nutrient bioavailability by measuring the effects of low nutrient concentrations on bacterioplankton growth and metabolism in the Atlantic, as well as the formation of particulate/insoluble micronutrient species (i.e. iron and cobalt). In Chapters 3 and 4, nutrient enrichment experiments were conducted across the Atlantic to examine the effect of low concentrations of nitrogen and phosphorus/iron on bacterioplankton growth and metabolism. In Chapter 5, iron adsorption to cell surfaces was monitored across the South Atlantic, with comparisons made between the oligotrophic gyre and more productive waters. Finally, formation of particulate/insoluble cobalt (termed simply particulate cobalt)

was investigated under differing concentrations of manganese and potentially competing trace metals.

7.1.2 Findings and implications

Upon addition of ammonium in both the North and South Atlantic, bacterioplankton abundance and metabolic activity increased, which aptly reflects the low concentrations of nitrogen that have been previously reported across the Atlantic [e.g. 53,54]. However, inside the North Atlantic gyre (NAG), a response was only observed upon addition of both ammonium and phosphate, which highlights the localised low concentrations of phosphorus seen in the NAG as a result of iron inputs (from Saharan dust) that stimulates diazotrophy and consequent phosphate drawdown [e.g. 66]. In the South Atlantic, previously reported low concentrations of iron [e.g. 126,127,243] did not negatively affect cell growth or metabolic activity, with negligible increases upon iron addition. This implies that the iron concentrations available in the South Atlantic are deemed sufficient to support bacterioplankton growth and metabolic activity; thus, poor nitrogen concentrations are the primary constraint on growth in the South Atlantic. However, this conclusion assumes that during the study in the South Atlantic, there was no contamination of iron in samples, that cells remained viable throughout the experiment and that iron was freely available for biological uptake.

Overall, addition of nitrogen in the South Atlantic subtropical gyre, and phosphorus and nitrogen in the North Atlantic subtropical gyre, stimulated an increase in amino acid uptake and cell abundance in bacterioplankton in this study. Based on the definition of limitation previously set out in Chapter 1, Section 1.4, the very low ambient concentrations of these nutrients are limiting bacterioplankton in the gyre, by restricting optimal growth and metabolism. This is of particular importance considering the expansion of the subtropical gyres as a result of climate change [35-38]. An increase in the size of oligotrophic gyres, and a further decrease in biologically essential nutrient concentrations,

will decrease bacterioplankton growth and metabolism, ultimately affecting surface ocean ecology and reducing primary production. This has significant implications, with the effects being transferred to higher trophic levels (e.g. zooplankton, fish and whales) due to a reduction in prey [329], which in turn, could reduce the catch of fisheries [329]. Additionally, carbon flux will be affected by a reduction in ocean primary productivity, as atmospheric carbon dioxide drawdown will be reduced, creating a positive feedback loop that will further accentuate climate change [e.g. 330].

It should be noted that different bacterioplankton groups dominated responses to nutrient additions in the NAG (i.e. *Prochlorococcus*) and South Atlantic (i.e. high nucleic acid bacteria). This suggests that climate-change induced alterations to ocean biogeochemistry could lead to significant variation in responses across the global ocean. For example, *Prochlorococcus* and *Synechococcus* have been predicted to shift towards the poles [151], and although their abundances are expected to rise with increasing temperatures [151], the potential implications of this on the marine ecosystem are unknown [156].

In addition to investigating nutrient limitation, the formation of particulate/insoluble micronutrient species was examined, specifically iron and cobalt, which are essential co-factors for a range of enzymes and metabolic processes. Cellular iron adsorption was measured across the South Atlantic, with iron sorption per cell being highest in oligotrophic regions, and decreasing in more productive oceanic waters. This was proposed to be linked to ambient iron concentrations and free cell surface area. Upon analysis of particulate cobalt formation, despite an inconclusive mechanism of formation, levels were elevated in the presence of *Aurantimonas* cultures. Additionally, different trace metals were shown to affect particulate cobalt formation, with manganese generally increasing production, and nickel and copper showing a tendency towards competitive inhibition (although this result requires further investigation with higher concentrations of competing metals).

Formation of particulate/insoluble metal species may affect micronutrient distributions in the marine environment, potentially reducing bioavailability through particle sinking from the surface ocean and beneath the euphotic zone [e.g. 75,326]. Furthermore, ocean acidification has been linked to decreased metal adsorption and release of metals from cell binding sites [174,284,285], as well as a change in the chemistry of ligand binding [173]. This can influence micronutrient bioavailability; for example, decreasing free inorganic iron [331], a highly bioavailable form of iron [274]. Decreased bioavailability of micronutrients could potentially limit plankton growth and metabolism, and thus have a knock-on effect on ocean productivity, as described above. Thus, understanding the formation and distribution of particulate/insoluble species in the marine environment will allow more informed predictions of changing ocean chemistry and metal bioavailability that may result from climate change.

The results obtained in this thesis improve understanding of nutrient bioavailability in the marine environment. An increase in bacterioplankton abundance and metabolic activity was observed upon addition of nutrients that are found at very low concentrations in oligotrophic waters. Formation of particulate/insoluble trace elements is influenced by ambient metal concentrations. Anthropogenic influences are resulting in ocean acidification and an increase in sea surface temperature, which will likely cause an increase in the oligotrophy of the oceans [35-38], and changes to trace metal biogeochemistry [e.g., 174,273], potentially increasing plankton nutrient limitation. Studies such as presented in this thesis all aid in providing a better understanding of marine processes affecting ocean productivity and global carbon flux, thus can help predict any ecological changes that may arise from climate change.

7.2 Future work

7.2.1 Flow cytometric sorting

An interesting aspect of the nutrient enrichment studies was the analysis of individual bacterioplankton groups in order to assess changes in community structure or potential dominance of a particular group. During the study, only changes in cell abundance could be measured for individual populations. However, future studies should consider the use of radioactive sorting, which allows determination of proportions of radiolabelled nutrient assimilated by different plankton groups [e.g. 60]. Flow cytometric sorting separates a specific cell population from a sample through the application of a charge to the cells of interest, which have been identified using their characteristic fluorescence/side scatter [e.g. 332]. Thus, this method would build a stronger picture of potential group dominance (e.g. *Prochlorococcus* in the NAG, and high nucleic acid bacteria in the South Atlantic) by using an effective technique that has not been widely utilised in previous nutrient enrichment studies. Furthermore, molecular based techniques, such as fluorescent in situ hybridisation [e.g. 189] would allow specific identification of bacterial groups, especially in categories such as high and low nucleic acid (HNA, LNA) bacteria, where populations can be varied [e.g. 189,195].

7.2.2 Nutrient enrichment studies

The South Atlantic

Although this project does provide data for an under-represented region of the global ocean, the transect covered is only one small area of the ocean and only two specific nutrients (i.e. ammonium and iron) were measured. Therefore, the South Atlantic would benefit from further nutrient enrichment studies to provide a wider wealth of data. This could include investigation of other nutrients; for example, Noble *et al* (2012) noted very

low concentrations of cobalt in the South Atlantic gyre (SAG) [115]. Alternative cruise transects (e.g. west to east) could also be undertaken, in order to provide data for a larger portion of the South Atlantic.

Organic nutrients

Enrichment studies conducted in this study only investigated one nutrient source for each element tested; for example, nitrate is also a key nitrogen source [e.g. 7] but was not analysed. Furthermore, only inorganic nutrients were investigated, yet bacterioplankton are capable of utilising a wide range of nutrient sources, including dissolved organic nitrogen (DON) and dissolved organic phosphorus (DOP) sources [e.g. 6]. Future work could expand upon this study by investigating the addition of DON and DOP across the Atlantic, and comparing the results to those of inorganic nutrient enrichment. In addition, enrichment experiments could investigate responses of bacterioplankton to addition of a dissolved organic carbon (DOC) source. DOC is a huge and essential carbon source in the oceans [e.g. 2] and as such potential limitation of bacterioplankton in the Atlantic should be assessed.

Previous organic enrichment studies in the Atlantic Ocean have primarily investigated the addition of organic carbon (namely glucose) [e.g. 124,128,131-133,135]. The majority of these studies were conducted in the northwest Atlantic, leaving a significant area of the Atlantic underrepresented, thus providing potential scope for future enrichment experiments. Carlson and Ducklow (1996) also focussed on DOC additions in the northwest Atlantic, but used a wider variety of sources including dissolved free amino acids (a potential DON source) and algal lysate [219]. As few studies investigating DON and DOP enrichment are available, there are multiple opportunities for future analysis of organic nutrient utilization and nutrient limitation in the Atlantic Ocean.

7.2.3 Iron uptake

As cells require small amounts of iron, uptake rates are low. This presents a problem when measuring uptake using radiolabelled iron, as the tracer will be diluted by any contaminating stable iron present in the spike, potentially reducing cellular assimilation of radiolabelled iron to below detection limits. Trace metal clean techniques allow the preparation of iron-clean reagents; however, they do not account for iron adsorbed to cell surfaces. Therefore, removal of extracellular iron is required in order to create truly iron clean conditions for measurement of radiotracer uptake. This would also allow iron deficient oceans to be mimicked in a laboratory setting.

Hudson and Morel (1989) developed the $TiCl_3$ buffer (Chapters 4 and 5), which was shown to remove ≥97% of all extracellular iron [253,254,260] via a reductive mechanism [253,260]. The buffer is also suitable for such an experiment due to the minimal damage inflicted upon cells after washing (Appendix G) [253,260], although it should be noted that Sunda and Huntsman (1995) did note membrane damage upon use of the $TiCl_3$ buffer [88].

Although the buffer has been shown to remove iron without harm to the cells, it also leaves stable iron contamination, with preliminary experiments conducted during this project showing a high level of iron precipitation after washing with $TiCl_3$ buffer (Appendix H). Theoretically, the buffer itself should keep this contamination in solution [253], and sufficient washes would allow removal of such contamination [260]; although, the salt solution (NaCl) recommended by Tang and Morel (2006) to do this second wash was shown to only remove 35% of iron when used alone [260]. Tovar-Sanchez *et al* (2003) suggested that the stable iron contamination rendered the $TiCl_3$ buffer only suitable for radiotracer experiments [254], which does not solve the initial issue set out of creating trace metal clean conditions. Tovar-Sanchez *et al* (2003) proposed an alternative oxalate wash buffer, which removes iron via a ligand mediated process [260], and can be made trace-metal clean using a meticulous and complex protocol [254]. No cellular damage was observed from the oxalate wash, with an iron removal efficiency of 97% [254]; however, Tang and Morel (2006), claimed the oxalate reagent only removed 90% of extracellular

iron compared to a 99.6% removal efficiency by the $TiCl_3$ Buffer [260]. Overall, the removal of extracellular iron in a trace-metal clean manner without damage to the cell is a difficult process and would require further investigation; however, once achieved it would open up a significant number of opportunities for trace metal experimentation, including biological uptake of other micronutrients such as cobalt and manganese and trace metal sorption studies.

The ability to remove ambient iron from cell surfaces prior to experimentation potentially restricted some experiments within this study. Specifically, in Chapter 5, *Halomonas* and *Aurantimonas* cultures had an unknown concentration of ambient iron adsorbed; removal of this iron before addition of radiolabelled iron would have allowed iron adsorption levels to be more quantitatively defined. Additionally, removal of ambient adsorbed iron would have added valuable insight and strengthened conclusions drawn from adsorption experiments of Atlantic samples (Chapter 5), whereby adsorption levels were theorised to be linked to free cell surface area available.

7.2.4 Formation of particulate cobalt

The final scientific chapter of this thesis (Chapter 6), highlighted a number of potential opportunities for further investigation into the formation of particulate cobalt. Due to the large number of factors that could potentially influence formation (e.g. culture conditions, trace metal concentrations), this study was limited by the practicality of investigating all variables. Some potential future investigations and experiments are discussed subsequently.

Time course

Results showed a disagreement between trends seen in long-term and short-term experiments. More particulate cobalt was formed in manganese-replete media for the

short-term incubations (Experiments 3, 4, 8, 9), but more particulate cobalt was formed in manganese-limited media for the long-term experiment (Experiment 10). Future incubation experiments should cover a more extensive incubation period, covering the time period between the final time point of short term experiments (<24 h) and the first time point of the long-term incubation (~100 h), during which a change in the biogeochemical interactions of manganese, cobalt and *Aurantimonas* presumably occurred. Most previous experiments have conducted short-term (hours) experiments, but have neglected long-term (days) sampling [e.g. 110,113,322]. Equally, some experiments use long term incubations, but omit shorter experiments [e.g. 320]. By covering a wider timescale, and using trace metal clean techniques to avoid contamination, this potential future experiment would provide valuable insight into particulate cobalt formation.

Cobalt uptake

Intracellular uptake was not recognised in short-term experiments as there was no increase in cell-associated ^{57}Co over time (Figures 6.2 and 6.3); however, long-term experiments suggested intracellular uptake in one replicate. Future analysis could utilise the method developed to measure intracellular iron uptake (Chapter 4) and apply the technique to remove extracellularly associated cobalt (via the $TiCl_3$ buffer developed by Hudson and Morel (1989) [253]) and provide data on intracellular cobalt uptake rates. This could offer information on cellular cobalt requirements, and also the contribution of intracellular assimilation to particulate cobalt formation in the marine environment. Furthermore, experiments could alter the concentration of ambient cobalt, thereby allowing the influence of environmental cobalt on intracellular uptake and particulate cobalt formation to be assessed.

Dual labelling

A key unknown factor concerning the formation of particulate cobalt is whether oxidation or sorption is the mechanism responsible for the formation process [112], and if a direct microbial pathway or an indirect influence from biogenic manganese oxides is the cause of formation [113]. The results of this study do not confirm a mechanism; however, a method that uses radiolabelling of manganese (e.g. ^{54}Mn) and cobalt (e.g. ^{57}Co) could provide some insight into formation. For example, if manganese oxides are responsible for particulate cobalt formation through sorption, then cobalt and manganese will be associated, which will be reflected in a strong correlation between ^{54}Mn and ^{57}Co signals. Conversely, if cells are directly responsible there should be no correlation between the two nuclides. Previous studies that have used dual-labelling include Duhamel *et al* (2006) [333] who used dual labelling to assess simultaneous carbon and phosphorus uptake by plankton, and Mary *et al* (2008) [199] who used the method to monitor uptake of two different amino acids by bacterioplankton.

Appendix

Appendix A: Components of media used for growth of *Aurantimonas*

All media were prepared by Manuela Hartmann (NOCS). Unless otherwise stated, all chemicals used were either from Sigma Aldrich UK, or Fisher Scientific UK.

M-medium (termed Mn-replete in this study) was prepared following the protocol as outlined in Tebo *et al* (2007) [215]. To natural seawater chemicals were added to the final concentration as follows: 15 g/L Noble Agar, 0.05 g/L yeast extract, 0.05 g/L peptone, 20 mM HEPES (pH 7.8), 2 mM potassium bicarbonate, 100 µM manganese chloride tetrahydrate, 0.3 µg/mL ferric ammonium citrate (MP Biomedicals), 10 mM glycerol, and 10 mM sodium formate.

Mn-limited media was made as above; however, manganese chloride, peptone and yeast were omitted.

ATCC® 2584 media was prepared in deionized water, with the following chemicals added to a final concentration of: 4.77 g/L HEPES (pH 7.7-7.8), 27.75 mL/L natural seawater (adapted by M. Hartmann from the original protocol that used Instant Ocean 75%), 0.05 g/L yeast extract, 0.05 g/L peptone, 0.2 g/L potassium bicarbonate, and 0.02 g/L manganese chloride tetrahydrate.

Appendix B: Supporting nutrient data for AMT-25

During AMT-25, ambient nutrient data was generated by other researchers (cruise report available online [334]). Data was provided by the British Oceanographic Data Centre (BODC) (www.bodc.ac.uk) (contains data supplied by the Natural Environment Research Council). These data are presented and act to provide more information for the nutrient enrichment experiments conducted during this study.

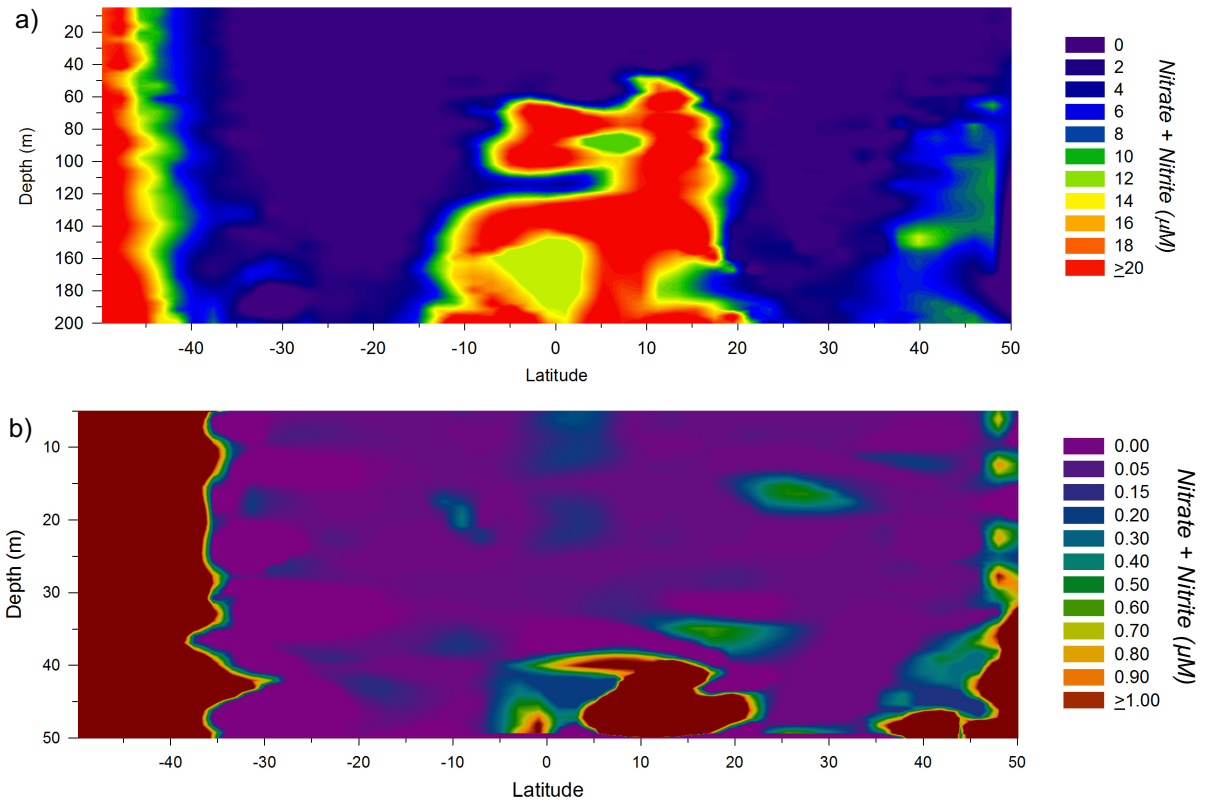

Figure S1: Nitrate + nitrite concentration measured during AMT-25, supplied by BODC

Contains data supplied by the Natural Environment Research Council.

Data provided by the British Oceanographic Data Centre (BODC) (www.bodc.ac.uk) (Natural Environment Research Council). Please note, this data, has not yet had metadata checked against the files on record (Joana Beja, email communication).

Upper 200 m (a) and 50 m (b). Note change in scale. At the sampling depth (30 m), elevated concentrations are seen south of approximately 35ºS, and north of approximately 45ºN.

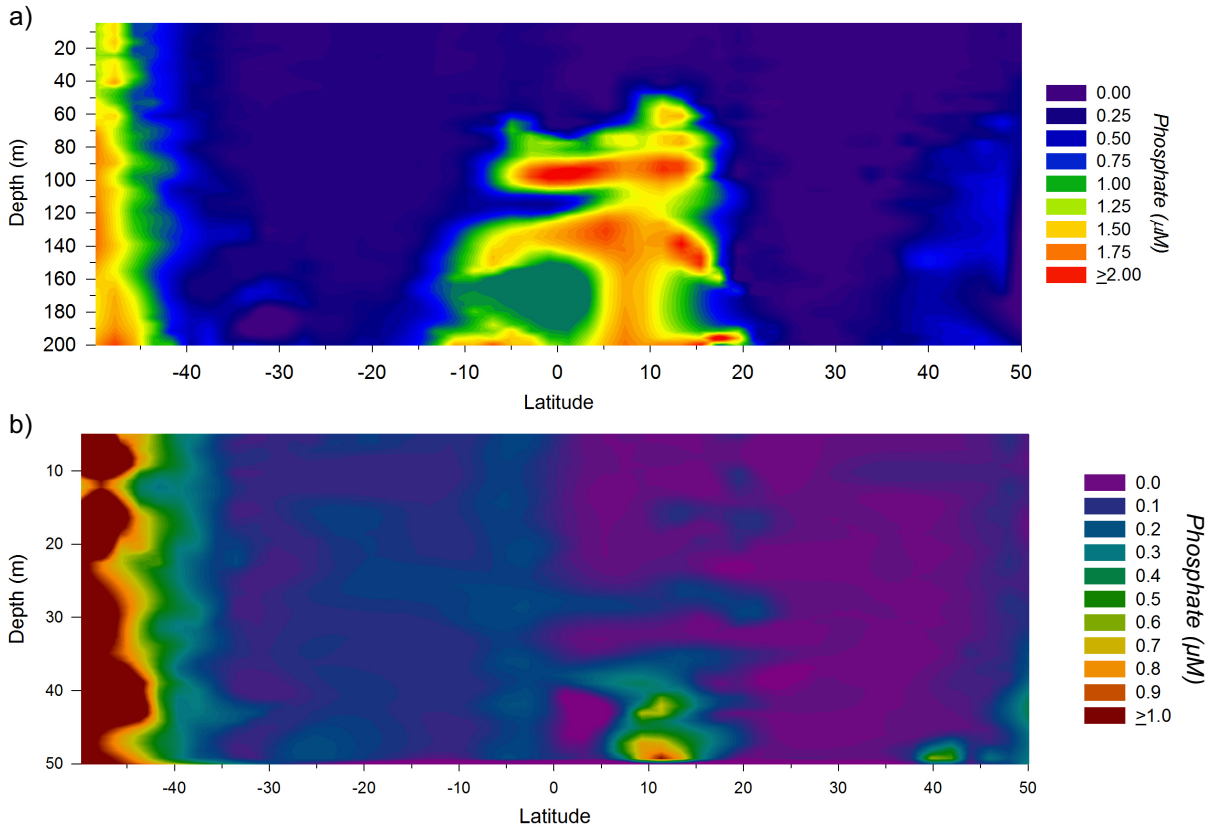

Figure S2: Phosphate concentration measured during AMT-25, supplied by BODC

Contains data supplied by the Natural Environment Research Council.

Data provided by the British Oceanographic Data Centre (BODC) (www.bodc.ac.uk) (Natural Environment Research Council) via email communication. Please note, this data, has not yet had metadata checked against the files on record (Joana Beja, email communication).

Upper 200 m (a) and 50 m (b). Note change in scale. At the sampling depth (30 m), elevated concentrations are seen south of approximately 40ºS. A higher concentration is seen in the South Atlantic, compared to the North Atlantic. The average concentration in the upper 100 m was 0.14 ± 0.27 µM in the North Atlantic, and 0.36 ± 0.42 µM in the South Atlantic (average ± standard deviation).

Appendix C: Supporting data for AMT-25

During AMT-25, additional chemical and physical data was generated by other researchers (cruise report available online [334]). Data was provided by the British Oceanographic Data Centre (BODC) (www.bodc.ac.uk) (contains data supplied by the Natural Environment Research Council). These data are presented, and act to support the biologically defined locations of the oligotrophic gyres noted in this study, namely between approximately 25-37ºN for the North Atlantic gyre (Chapter 3), and 13-28ºS for the South Atlantic gyre (Chapter 4).

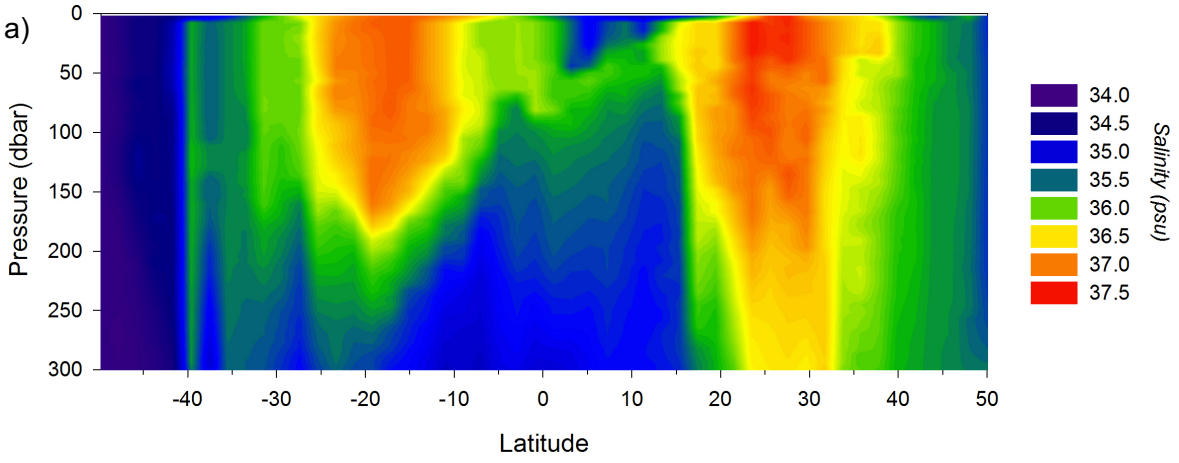

Figure S3: Seawater temperature, salinity and chlorophyll concentration measured in the upper 300 m during AMT-25, supplied by BODC

Contains data supplied by Natural Environment Research Council.

Data provided by the British Oceanographic Data Centre (BODC) (www.bodc.ac.uk) (Natural Environment Research Council). Please note that erroneous data spikes were not screened for in this dataset (Arwen Bargery, email communication).

a) Temperature: The increased temperatures between approximately 20-35ºN, and 10-30ºS indicates the locations of the oligotrophic gyres. Based on an average value of two measurements.

b) Salinity: The increased salinity between approximately 15-35ºN, and 10-30ºS, indicate the oligotrophic gyres. Based on an average value of two measurements.

c) Chlorophyll concentration: The depth at which the highest chlorophyll concentration is found, increases between 20-37ºN, and 10-35ºS, indicating the oligotrophic gyres.

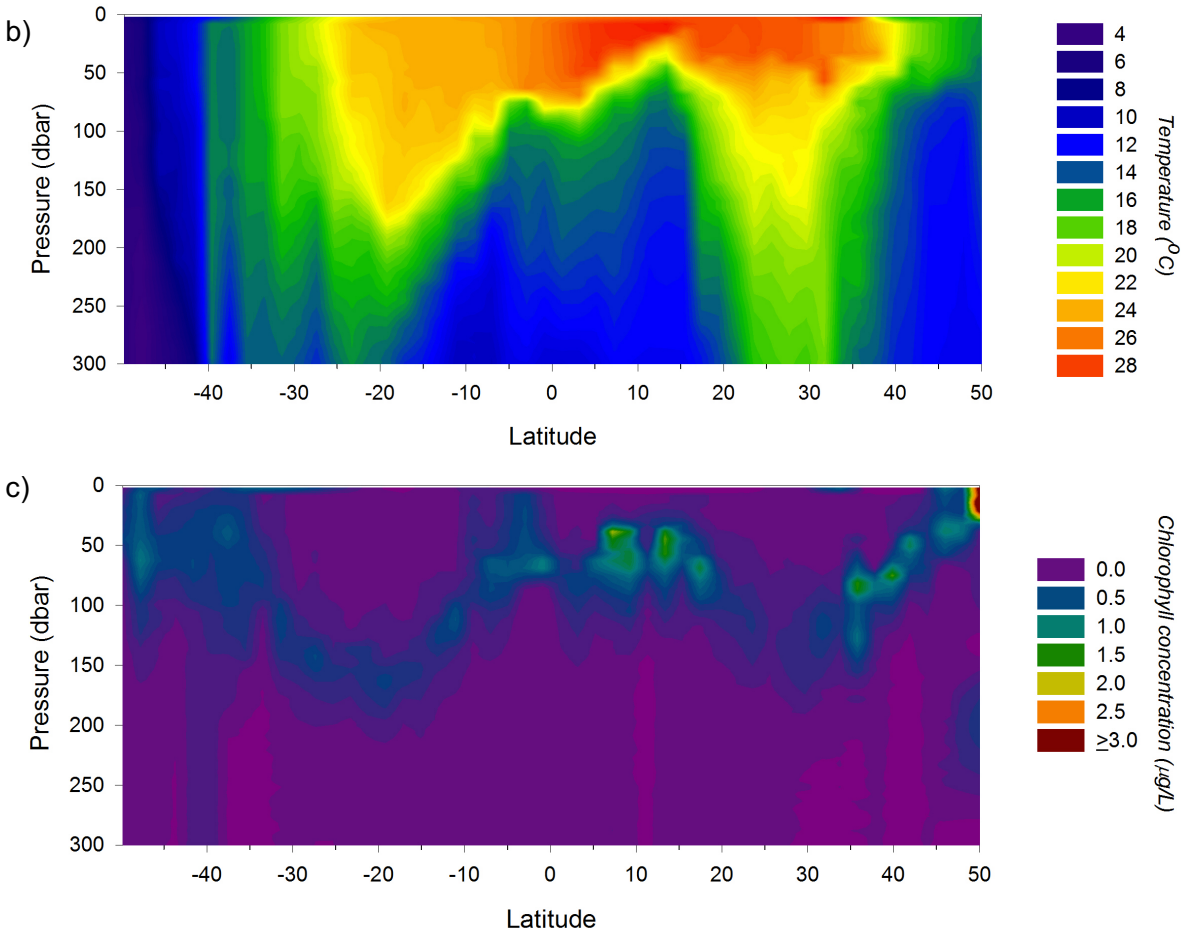

Figure S3: Seawater temperature, salinity and chlorophyll concentration measured in the upper 300 m during AMT-25, supplied by BODC

Continued

Appendix D: Supporting data for AMT-25 cell abundance

Additional bacterioplankton counts generated by Priscila Lange (University of Oxford) are presented in Figure S4. Priscila Lange collected and measured these samples during AMT-25 and kindly provided her analysed data, which allowed comparison to the bacterioplankton counts seen in this study (Chapters 3 and 4).

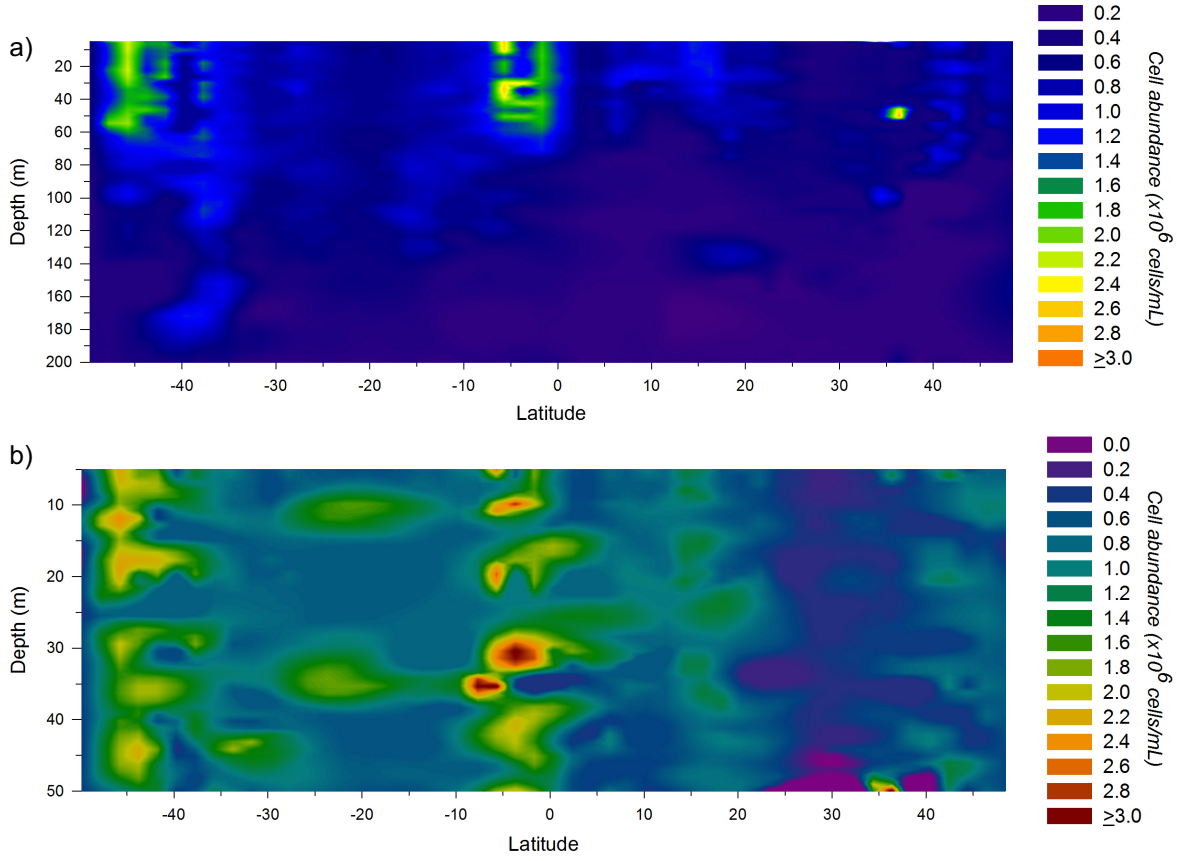

Figure S4: Supporting bacterioplankton cell counts, measured during AMT-25, supplied by Priscila Lange

This data was sampled, measured, analysed and provided by Priscila Lange (University of Oxford).

Upper 200 m (a) and 50 m (b). Note scale is measured in x10^6 cells/mL and is different on each graph. Cell concentrations in the North Atlantic decrease between approximately 25 - 35ºN, ranging between ~3.4 - 5.2 x10^5 cells/mL (at approximately 30m). In the South Atlantic, there is a lower cell count between approximately 10 - 35ºS (~6.3 - 9.9 x10^5 cells/mL, at approximately 30m). It is interesting to note two pockets of higher cell concentrations in the South Atlantic gyre at ~10m and ~35m.

Appendix E: Supporting data for AMT-24

During AMT-24, additional chemical and physical data was generated by other researchers (cruise report available online [335]). Data was provided by the British Oceanographic Data Centre (BODC) (www.bodc.ac.uk) (contains data supplied by the Natural Environment Research Council) and is presented below. This data acts to support the biological location of the South Atlantic gyre noted in this study, namely between 10-35ºS (Chapter 4). Also, shown in this data is the location of the North Atlantic gyre (approximately 20-35ºN).

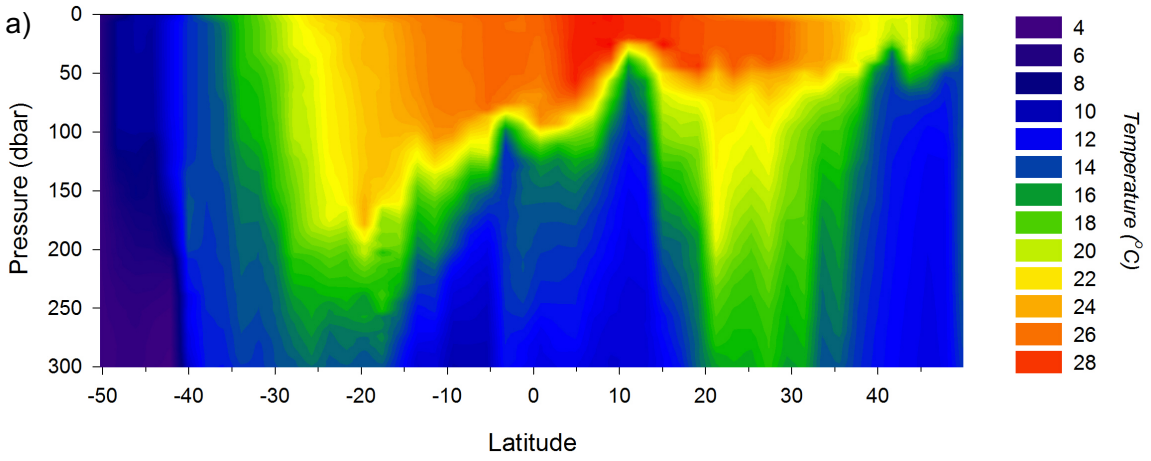

Figure S5: Seawater temperature, salinity and chlorophyll concentration measured in the upper 300 m during AMT-24, supplied by BODC

Contains data supplied by Natural Environment Research Council.

Data provided by the British Oceanographic Data Centre (BODC) (www.bodc.ac.uk) (Natural Environment Research Council). Please note that erroneous data spikes were not screened for in this dataset (Arwen Bargery, email communication).

a) Temperature: The increased temperatures between approximately 20-35ºN, indicates the North Atlantic oligotrophic gyre. The edges of the South Atlantic gyre are defined by a sharp decrease in temperature at 30-35ºS (southern edge), and a change at approximately 5-10ºS (northern edge). Based on an average value of two measurements.

b) Salinity: The increased salinity between approximately 20-35ºN, indicates the North Atlantic oligotrophic gyre. The edges of the South Atlantic gyre are defined by a sharp decrease in salinity at ~30ºS (southern edge) and approximately 10ºS (northern edge). Based on an average value of two measurements.

c) Chlorophyll concentration: The depth at which the highest chlorophyll concentration is found, increases between approximately 20-35ºN and 10-35ºS, indicating the oligotrophic gyres. Based on an average value of two measurements.

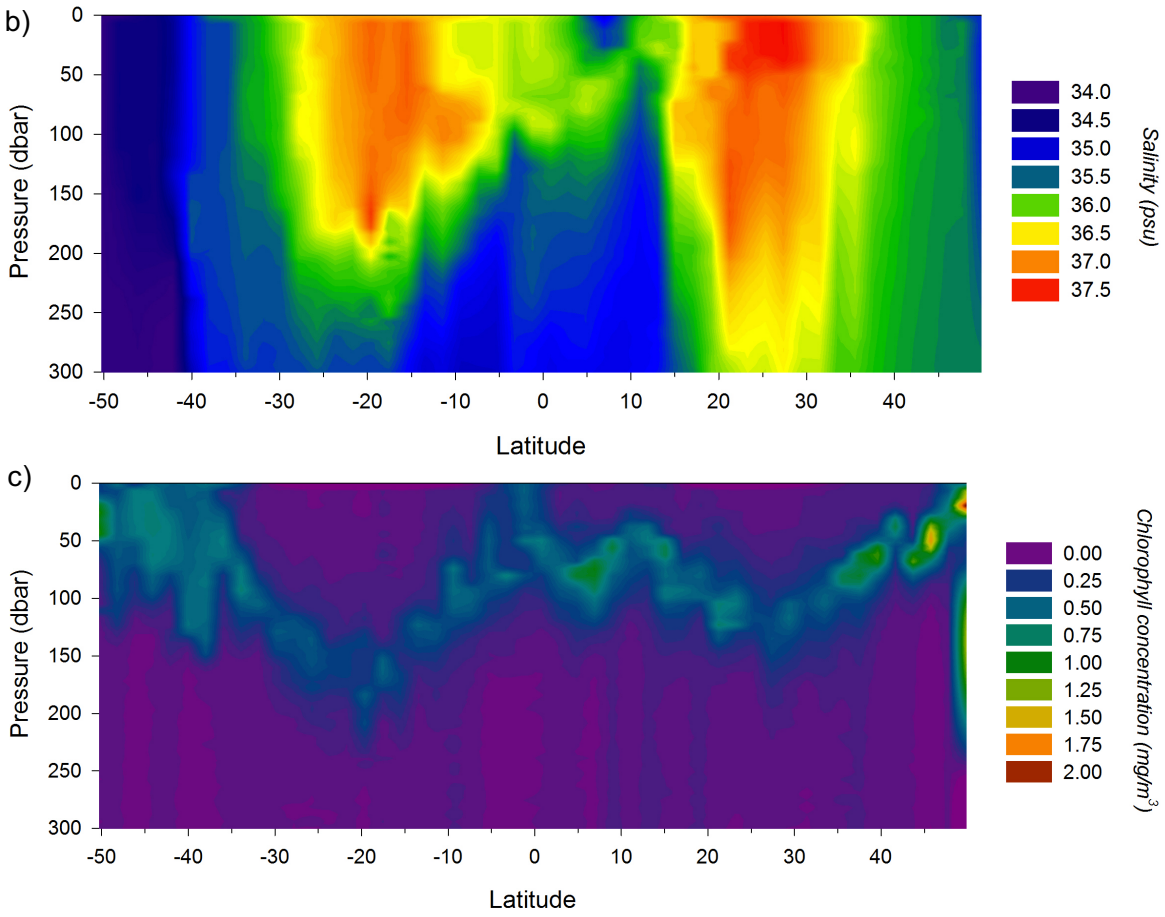

Figure S5: Seawater temperature, salinity and chlorophyll concentration measured in the upper 300 m during AMT-24, supplied by BODC

Continued.

Appendix F: Changing the pH of seawater

An independent assessment of pH was conducted to determine the effect of adding an acidified iron chloride (^{55}Fe) stock to seawater samples during the iron uptake experiments of AMT-24 (Chapter 4). The largest volume of acid (5 µL, 1 M HCl) in the lowest volume of seawater (15 mL) was the most acidic sample for this set of experiments, giving a final concentration of hydrochloric acid of 3.3×10^{-4} M, which gave a theoretical pH of 3.5 (calculated assuming complete disassociation in deionized water).

These conditions were mimicked in the lab by adding 5 µL of 1 M HCl to 15 mL of aged Atlantic seawater. Measurement upon addition of the acid found the pH changing from 8.9 to 8.6, and 8.2 to 7.7 in two different seawater stocks. The reduced pH is significantly higher than the theoretical pH calculated above in deionized water, thus the seawater carbonate has acted to minimize the effect of the acid.

As this test recreated the most acidic conditions used in Chapter 4, the pH changes observed would be the largest change experienced in the study, that is all pH changes would be no more than 0.5, with the majority of experiments having a lesser change due to dilution from using a smaller volume of acidified iron stock or a larger volume of seawater.

Appendix G: Effect of $TiCl_3$ buffer on membrane integrity

A ~10^6 cells/mL culture of *Halomonas* sp. was prepared as described in Chapter 2 (Section 2.5). Aliquots (1.6 mL) were incubated with ~3 kBq of tritium-labelled Leu, fixed with paraformaldehyde (PFA) (final concentration 1%) (Sigma Aldrich, UK) after 15-60 min, and stored for approximately 24 h. Cells were then filtered onto 0.2 µm PC filters (Whatman) and either subjected to a wash using $TiCl_3$ buffer or left as unwashed controls. Filters were placed in scintillation vials along with 5 mL scintillation cocktail (Gold Star, Meridian) and counted on an LSC using a counting window of 4-18.6 keV (based on decay energy of ^3H) and a counting time of 2 min.

Figure S6 shows the intracellular ^3H-Leu activity (CPM) versus each time point of the incubation for both washed and unwashed cells. The slopes of linear regression (see Chapter 2, Section 2.4.4), which represents the uptake rate (CPM/min), are similar: 36.5 ± 4.8 CPM/min and 26.1 ± 7.1 CPM/min for unwashed and washed cells, respectively (note that omission of the final data point for washed cells provides a slope of 35.7±2.5 CPM/min), showing no intracellular loss of ^3H-Leu and thus no cell rupture. The difference in y-axis intercept is likely to be attributed to background adsorbed ^3H-Leu in unwashed samples, that is removed by the $TiCl_3$ buffer in washed cells. Indeed, adsorption of ^3H-Leu may actually be occurring on the PC filter [336].

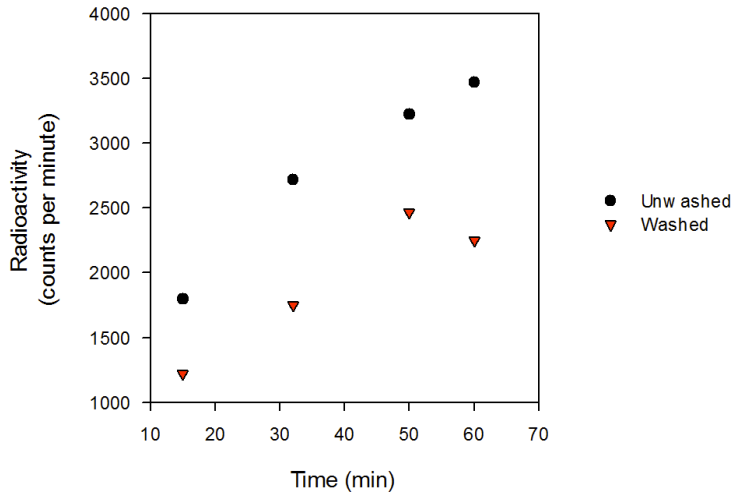

Figure S6: Cell integrity following a $TiCl_3$ buffer wash
Halomonas sp. cultures were incubated with ^3H-Leu before either being subjected to a $TiCl_3$ wash, or left as unwashed controls. Slopes of the graph represent uptake rate. The y-axis intercept represents background signal.

Appendix H: $TiCl_3$ buffer contamination

Working with acid-cleaned (10% HCl) equipment to remove environmental iron contamination, 2 mL of freshly prepared $TiCl_3$ buffer was passed over a 0.2 µm PC filter, incubated for 5 min, and rinsed with approximately 10 mL of aged Atlantic seawater. The filter was placed into 50 mL of aged Atlantic seawater, where it was agitated by pipetting and incubated for approximately 1 h. Aliquots of this seawater were incubated with ~230 Bq of iron chloride (^{55}Fe) for a further hour before filtration onto a new 0.2 µm PC membrane. Alongside, blanks of aged Atlantic seawater were incubated with radiolabelled iron before filtration. Samples were measured as standard using an LSC.

As shown in Table S1, there is a significant amount of iron adsorbed to the filter in the $TiCl_3$ buffer treated samples indicating substantial iron precipitation, which is likely to be due to iron contamination from the $TiCl_3$ buffer or may have been introduced from the filter or resuspension method.

Table S1: $TiCl_3$ buffer contamination controls
Blank samples of aged Atlantic seawater were subjected to a pre-wash using $TiCl_3$ buffer, before incubation with radiolabelled iron. The amount of precipitated iron was measured and compared to the amount of iron initially added to samples to be presented as a percentage.

Sample	Percentage of radiolabelled iron adsorbed
Aged Atlantic Seawater (blank)	2.0%
Aged Atlantic Seawater (blank)	3.7%
TiCl3 Buffer Washed Filter	40.1%
TiCl3 Buffer Washed Filter	48.8%

References

1 Field, C. B., Behrenfeld, M. J., Randerson, J. T. & Falkowski, P. Primary production of the biosphere: integrating terrestrial and oceanic components. *Science* **281**, 237-240 (1998).

2 Kirchman, D. Introduction and Overview. In *Microbial Ecology of the Oceans, Second Edition* (ed D. Kirchman) **1**. *1-26* (John Wiley & Sons, 2008).

3 Kirchman, D. Uptake and Regeneration of Inorganic Nutrients by Marine Heterotrophic Bacteria. In *Microbial Ecology of the Oceans, First Edition* (ed D. Kirchman) **9**. (Wiley-Liss Inc., 2000).

4 Sarmiento, J. L. & Gruber, N. Organic Matter Production. In *Ocean Biogeochemical Dynamics* **4**. (Prinston University Press, 2006).

5 Azam, F. & Malfatti, F. Microbial structuring of marine ecosystems. *Nature Reviews Microbiology* **5**, 782-791 (2007).

6 Nagata, T. Organic matter-bacteria interactions in seawater. In *Microbial Ecology of the Oceans, Second Edition* (ed D. Kirchman) **7**. *207-241* (John Wiley & Sons Inc., 2008).

7 Church, M. J. Resource control of bacterial dynamics in the sea. In *Microbial Ecology of the Oceans, Second Edition* (ed D. Kirchman) **10**. *335-382* (John Wiley & Sons, 2008).

8 Hansell, D. A. Recalcitrant Dissolved Organic Carbon Fractions. *Annual Review of Marine Science* **5**, 421-445, doi:10.1146/annurev-marine-120710-100757 (2013).

9 Jiao, N. *et al.* Microbial production of recalcitrant dissolved organic matter: long-term carbon storage in the global ocean. *Nature Reviews Microbiology* **8**, 593-599 (2010).

10 Ducklow, H. W. Production and fate of bacteria in the oceans. *BioScience* **33**, 494-501 (1983).

11 Azam, F. *et al.* The ecological role of water-column microbes in the sea. *Marine Ecology Progress Series* **10**, 257-263 (1983).

12 Buchan, A., LeCleir, G. R., Gulvik, C. A. & González, J. M. Master recyclers: features and functions of bacteria associated with phytoplankton blooms. *Nature Reviews Microbiology* **12**, 686-698 (2014).

13 Campbell, L. & Nolla, H. A. The importance of *Prochlorococcus* to community structure in the central North Pacific Ocean. *Limnology and Oceanography* **39**, 954-961 (1994).

14 Zhang, C. L., Xie, W., Martin-Cuadrado, A. B. & Rodriguez-Valera, F. Marine Group II Archaea, potentially important players in the global ocean carbon cycle. *Front Microbiol* **6**, 1108, doi:10.3389/fmicb.2015.01108 (2015).

15 DeLong, E. F. Archaea in coastal marine environments. *Ecology* **89**, 5685-5689 (1992).

16 Fuhrman, J. A. & Hagström, Å. Bacterial and Archaeal community structure and its patterns. In *Microbial Ecology of the Oceans, Second Edition* (ed D. Kirchman) **3**. (John Wiley & Sons, 2008).

17 Fuhrman, J. A., McCallum, K. & Davis, A. A. Novel major archaebacterial group from marine plankton. *Nature* **356**, 148-149 (1992).

18 Kirchman, D. L. Marine archaea take a short cut in the nitrogen cycle. *Proc Natl Acad Sci U S A* **109**, 17732-17733, doi:10.1073/pnas.1215654109 (2012).

19 Sarmiento, J. & Gruber, N. Tracer Conservation and Ocean Transport. In *Ocean Biogeochemical Dynamics* **2**. (2006).

20 Thorpe, S. A. Turbulence, Heat and Waves. In *An Introduction to Ocean Turbulence* **1**. (Cambridge University Press, 2007).

21 Marshall, J. & Plumb, R. A. The wind-driven circulation. In *Atmosphere, Ocean and Climate Dynamics* **10**. (2008).

22 Sigman, D. M. & Hain, M. P. The biological productivity of the ocean. *Nature Education* **3** (2012).

23 Marshall, J. & Plumb, R. A. The ocean and its circulation. In *Atmosphere, Ocean and Climate Dynamics* **9**. (Elsevier, 2008).

24 Talley, L. D., Pickard, G. L., Emery, W. J. & Swift, J. H. Physical Properties of Seawater. In *Descriptive Physical Oceanography* Vol. 6 **3**. (Elsevier, 2011).

25 Locarnini, R. A. *et al.* World Ocean Atlas 2009, Volume 1: Temperature. (U.S. Government Printing Office, Washington, D.C., 2010).

26 Antonov, J. I. *et al.* World Ocean Atlas 2009, Volume 2: Salinity. (U.S. Government Printing Office, Washington, D.C., 2010).

27 Monterey, G. I. & deWitt, L. M. (ed United States Department of Commerce NOAA) (2000).

28 Siegel, D. A., Doney, S. C. & Yoder, J. A. The North Atlantic spring phytoplankton bloom and Sverdrup's critical depth hypothesis. *Science* **296**, 730-733 (2002).

29 Sverdrup, H. U. On conditions for the vernal blooming of phytoplankton. *Journal du Conseil Permanent International pour l'Exploration de la Mer* **18**, 287-295 (1953).

30 Behrenfeld, M. Abandoning Sverdrup's Critical Depth Hypothesis on phytoplankton blooms. *Ecology* **91**, 977-989 (2010).

31 Boss, E. & Behrenfeld, M. In situ evaluation of the initiation of the North Atlantic phytoplankton bloom. *Geophysical Research Letters* **37**, n/a-n/a, doi:10.1029/2010gl044174 (2010).

32 Stewart, R. H. The Equations of Motion. In *Introduction to Physical Oceanography* **7**. (2008).

33 McClain, C. R., Signorini, S. R. & Christian, J. R. Subtropical gyre variability observed by ocean-colour satellites. *Deep-Sea Research II* **51**, 281-301 (2004).

34 Brown, E. *et al.* Ocean Currents. In *Ocean Circulation, Second Edition* **3**. (2001).

35 Gregg, W. W., Conkright, M. E., Ginoux, P., O'Reilly, J. E. & Casey, N. W. Ocean primary production and climate: Global decadal change. *Geophysical Research Letters* **30** (2003).

36 Hoegh-Guldberg, O. & Bruno, J. F. The Impact of Climate Change on the World's Marine Ecosystems. *Science* **328**, 1523-1528 (2010).

37 Polovina, J. J., Howell, E. A. & Abecassis, M. Ocean's least productive waters are expanding. *Geophysical Research Letters* **35**, doi:10.1029/2007GL031745 (2008).

38 Irwin, A. J. & Oliver, M. J. Are ocean deserts getting larger? *Geophysical Research Letters* **36** (2009).

39 Imagery produced by the Earth Observatory Group in coordination with Gene Feldman and Norman Kuring of NASA Goddard Ocean Color Group. ; '*Chlorophyll concentration (1 month - AQUA/MODIS)*'; from NASA Earth Observations (neo.sci.gsfc.nasa.gov/, accessed 11/07/2018) (Images are freely available for use by the public.)

40 Barton, E. D. Canary and Portugal Currents. *Encyclopedia of Ocean Sciences*, doi:10.1006/rwos.2001.0360 (2001).

41 Boltovskoy, D., Gibbons, M. J., Hutchings, L. & Binet, D. General bioloigcal features of the South Atlantic. In *South Atlantic Zooplankton* Vol. 1 (ed D. Boltovskoy) **1**. (Backhuys Publishers, 1999).

42 Stramma, L. & England, M. On the water masses and mean circulation of the South Atlantic Ocean. *Journal of Geophysical Research* **104** (1999).

43 Atlantic Meridional Transect (http://www.amt-uk.org/). (Co-ordinated and led by Plymouth Marine Laboratory in collaboration with the National Oceanography Centre).

44 Claus S., De Hauwere N., Vanhoorne B., Souza Dias F., Oset García P., Schepers L., Hernandez F., and Mees J. (Flanders Marine Institute) (2018). '*VLIZ (2009). Longhurst Provinces.*'; from Available online at http://www.marineregions.org/. Consulted on 2018-07-09.

45 Redfield, A. C. On the proportions of organic derivatives in sea water and their relation to the composition of plankton. *Liverpool, UK; University Press of Liverpool* (1934).

46 Redfield, A. C. The Biological Control of Chemical Factors in the Environment. *American Scientist* **46**, 205-221 (1958).

47 Madigan, M. T. & Martinko, J. M. In *Brock Biology of Microorganisms, Eleventh Edition*. (Pearson Prentice Hall, 2006).

48 Berges, J. A. & Mulholland, M. R. Enzymes and Nitrogen Cycling. In *Nitrogen in the Marine Environment, Second Edition* (eds D. G. Capone, D. A. Bronk, M. R. Mulholland, & E. J. Carpenter) **32**. (New York: Academic Press, 2008).

49 Gruber, N. The Marine Nitrogen Cycle: Overview and Challenges. In *Nitrogen in the Marine Environment, Second Edition* (eds D. G. Capone, D. A. Bronk, M. R. Mulholland, & E. J. Carpenter) **1**. (Elsevier Inc., 2008).

50 Zehr, J. P. & Ward, B. B. Nitrogen Cycling in the Ocean: New Perspectives on Process and Paradigms. *Applied and Environmental Microbiology* **68**, 1015-1024 (2002).

51 Cabello, P., Roldán, M. D., Castillo, F. & Moreno-Vivián, C. Nitrogen Cycle. In *Encyclopedia of Microbiology (Third Edition)* Vol. 3 (ed M. Schaechter). *299-321* (2009).

52 Capone, D. G. The Marine Microbial Nitrogen Cycle. In *Microbial Ecology of the Oceans, First Edition* (ed D. Kirchman) **15**. (Wiley-Liss Inc, 2000).

53 Moore, C. M. *et al.* Processes and patterns of oceanic nutrient limitation. *Nature Geoscience* **6**, 701-710 (2013).

54 Rees, A. P., Woodward, E. M. S. & Joint, I. Concentrations and uptake of nitrate and ammonium in the Atlantic Ocean between 60ºN and 50ºS. *Deep-Sea Research II* **53** (2006).

55 Garcia, H. E. *et al.* World Ocean Atlas 2009, Volume 4: Nutrients. (U.S. Government Printing Office, Washington, D.C., 2010).

56 Watson, A. J. Iron limitation in the oceans. In *The Biogeochemistry of Iron in Seawater* Vol. 7 (eds D. R. Turner & K. A. Hunter) **2**. *9-40* (John Wiley and Sons, 2001).

57 Woodward, E. M. S. & Rees, A. P. Nutrient distributions in an anticyclonic eddy in the northeast Atlantic Ocean, with reference to nanomolar ammonium concentrations. *Deep-Sea Research II* **48**, 775-793 (2001).

58 Moore, L. R., Post, A. F., Rocap, G. & Chisholm, S. W. Utilization of different nitrogen sources by the marine cyanobacteria *Prochlorococcus* and *Synechococcus*. *Limnology and Oceanography* **47**, 989-996 (2002).

59 Berube, P. M. *et al.* Physiology and evolution of nitrate acquisition in *Prochlorococcus*. *The ISME Journal* **9**, 1195-1207 (2015).

60 Zubkov, M. V., Fuchs, B. M., Tarran, G. A., Burkill, P. H. & Amann, R. High rate of uptake of organic nitrogen compunds by *Prochlorococcus* cyanobacteria as a key to their dominance in oligotrophic oceanic waters. *Applied and Environmental Microbiology* **69**, 1299-1304 (2003).

61 Arrigo, K. R. Marine microorganisms and global nutrient cycles. *Nature* **437**, 349-455 (2005).

62 Paytan, A. & McLaughlin, K. The Oceanic Phosphorus Cycle. *Chemical Reviews* **107**, 563-576 (2007).

63 Benitez-Nelson, C. R. The Biogeochemical Cycling of Phosphorus in Marine Systems. *Earth-Science Reviews* **51**, 109-135 (2000).

64 Lin, S., Litaker, R. W. & Sunda, W. Phosphorus Physiological Ecology and Molecular Mechanisms in Marine Phytoplankton. *Journal of Phycology* **52**, 10-36 (2016).

65 Gómez-Pereira, P. R. *et al.* Comparable light stimulation of organic nutrient uptake by SAR11 and *Prochlorococcus* in the North Atlantic subtropical gyre. *The ISME Journal*, 1-12 (2012).

66 Mather, R. L. *et al.* Phosphorus cycling in the North and South Atlantic Ocean subtropical gyres. *Nature Geoscience* **1**, 439-443 (2008).

67 Sunda, W. Bioavailability and bioaccumulation of iron in the sea. In *The Biogeochemistry of Iron in Seawater* Vol. 7 (eds D. R. Turner & K. A. Hunter) **3**. *41-78* (John Wiley and Sons Ltd, 2001).

68 Wilson, C. J., Apiyo, D. & Wittung-Stafshede, P. Role of cofactors in metalloprotein folding. *Quaterly Reviews of Biophysics* **37**, 285-314 (2004).

69 Tortell, P. D., Maldonado, M. T., Granger, J. & Price, N. M. Marine bacteria and biogeochemical cycling of iron in the oceans. *FEMS Microbiology Ecology* **29**, 1-11 (1999).

70 Archibald, F. *Lactobacillus plantarum*, an organism not requiring iron. *FEMS Microbiology Letters* **19**, 29-32 (1983).

71 Fung, I. Y. *et al.* Iron supply and demand in the upper ocean. *Global Biogeochemical Cycles* **14**, 281-295 (2000).

72 Baker, A. R. & Jickells, T. D. Atmospheric deposition of soluble trace elements along the Atlantic Meridional Transect (AMT). *Progress in Oceanography* (2016).

73 de Baar, H. J. W. & de Jong, J. T. M. Distributions, sources and sinks of iron in seawater. In *The Biogeochemistry of Iron in Seawater* Vol. 7 (eds D. R. Turner & K. A. Hunter) **5**. *123-253* (John Wiley and Sons Ltd, 2001).

74 Giering, S. L. C., Steigenberger, S., Achterberg, E. P., Sanders, R. & Mayor, D. J. Elevated iron to nitrogen recycling by mesozooplankton in the Northeast Atlantic Ocean. *Geophysical Research Letters* **39**, doi:10.1029/2012gl051776 (2012).

75 Wangersky, P. J. Biological control of trace metal residence time and speciation: a review and synthesis. *Marine Chemistry* **18**, 269-297 (1986).

76 Landing, W. & Bruland, K. W. The contrasting biogeochemistry of iron and manganese in the Pacific Ocean. *Geochimica et Cosmochimica Acta* **51**, 29-43 (1987).

77 Hutchins, D. A., DiTullio, G. R. & Bruland, K. W. Iron and regeneration production: Evidence for biological iron recycling in two marine environments. *Limnology and Oceanography* **38**, 1242-1255 (1993).

78 Boyd, P. W. & Ellwood, M. J. The biogeochemical cycle of iron in the ocean. *Nature Geoscience* **3**, 675-682, doi:10.1038/ngeo964 (2010).

79 Moffett, J. W. Transformations among different forms of iron in the ocean. In *The Biogeochemistry of Iron in Seawater* (eds D. R. Turner & K. A. Hunter) **8**. *343-372* (John Wiley and Sons Ltd, 2001).

80 Waite, T. D. Thermodynamics of the Iron System in Seawater. In *The Biogeochemistry of Iron in Seawater* (eds D. R. Turner & K. A. Hunter) **7**. *291-342* (John Wiley and Sons Ltd, 2001).

81 Bergquist, B. A., Wu, J. & Boyle, E. A. Variability in oceanic dissolved iron is dominated by the colloidal fraction. *Geochimica et Cosmochimica Acta* **71**, 2960-2974, doi:10.1016/j.gca.2007.03.013 (2007).

82 Gledhill, M. & Buck, K. N. The organic complexation of iron in the marine environment: a review. *Frontiers in Microbiology* **3**, doi:10.3389/fmicb.2012.00069 (2012).

83 Derenne, S. *et al.* Molecular evidence for life in the 3.5 billion year old Warrawoona chert. *Earth and Planetary Science Letters* **272**, 476-480 (2008).

84 Schidlowski, M. A 3,800-million-year isotopic record of life from carbon in sedimentary rocks. *Nature* **333**, 313-318 (1988).

85 Turner, D. R., Hunter, K. A. & de Barr, H. J. W. Introduction. In *The Biogeochemistry of Iron in Seawater* Vol. 7 (eds D.R. Turner & K.A. Hunter) **1**. *1-7* (John Wiley and Sons Ltd, 2001).

86 de Barr, H. J. W. & La Roche, J. Trace Metals in the Oceans: Evolution, Biology and Global Change. In *Marine Science Frontiers for Europe*. *79-105* (Springer Berlin Heidelberg, 2003).

87 Crichton, R. *Inorganic Biochemistry of Iron Metabolism: From Molecuar Mechanisms to Clinical Consequences*. (John Wiley and Sons Ltd, 2001).

88 Sunda, W. G. & Huntsman, S. A. Iron uptake and growth limitation in oceanic and coastal phytoplankton. *Marine Chemistry* **50**, 189-206 (1995).

89 Andrews, S. C., Robinson, A. K. & Rodríguez-Quiñones, F. Bacterial iron homostatsis. *FEMS Microbiology Reviews* **27**, 215-237 (2003).

90 Neilands, J. B. Iron absorption and transport in microorganisms. *Annual Reviews of Nutrition* **1**, 27-46 (1981).

91 Sandy, M. & Butler, A. Microbial Iron Acquisition: Marine and Terrestrial Siderophores. *Chemical Reviews* **109**, 4580-4595 (2009).

92 Ghassemian, M. & Straus, N. A. Fur regulates the expression of iron-stress genes in the cyanobacterium Synechococcus sp. strain PCC 7942. *Microbiology* **142**, 1469-1476 (1996).

93 Rocap, G. *et al.* Genome divergence in two *Prochlorococcus* ecotypes reflects oceanic niche differentiation. *Nature* **424**, 1042-1047 (2003).

94 Butler, A. Marine siderophores and microbial mobilization. *BioMetals* **18**, 369-374 (2005).

95 Guerinot, M. L. Microbial iron transport. *Annual Review of Microbiology* **48**, 743-772 (1994).

96 Morel, F. M. M., Rueter, J. G. & Price, N. M. Iron nutrition of phytoplankton and its possible importance in the ecology of ocean regions with high nutrient and low biomass. *Oceanography* **4**, 56-61 (1991).

97 Hopkinson, B. M. & Morel, F. M. M. The role of siderophores in iron acquisition by photosynthetic marine microorganisms. *Biometals* **22**, 659-669 (2009).

98 Kranzler, C., Lis, H., Shaked, Y. & Keren, N. The role of reduction in iron uptake processes in a unicellular, planktonic cyanobacterium. *Environmental Microbiology* **13**, 2990-2999 (2011).

99 Ehrenreich, I. M., Waterbury, J. & Webb, E. A. Distribution and Diversity of Natural Product Genes in Marine and Freshwater Cyanobacterial Cultures and Genomes. *Applied and Environmental Microbiology* **71**, 7401-7413 (2005).

100 Granger, J. & Price, N. M. The importance of siderophores in iron nutrition of heterotrophic marine bacteria. *Limnology and Oceanography* **44**, 541-555 (1999).

101 Panzeca, C. *et al.* Potential cobalt limitation of vitamin B12 synthesis in the North Atlantic Ocean. *Global Biogeochemical Cycles* **22**, GB2029 (2008).

102 Twining, B. S. & Baines, S. B. The Trace Metal Composition of Marine Phytoplankton. *Annual Review of Marine Science* **5**, 191-215 (2013).

103 Bertrand, E. M. *et al.* Vitamin B12 and iron colimitation of phytoplankton growth in the Ross Sea. *Limnology and Oceanography* **52**, 1079-1093 (2007).

104 Jakuba, R. W., Moffett, J. W. & Dyhrman, S. T. Evidence for the linked biogeochemical cycling of zinc, cobalt, and phosphorus in the western North Atlantic Ocean. *Global Biogeochemical Cycles* **22** (2008).

105 Saito, M. A., Moffett, J. W., Chisholm, S. W. & Waterbury, J. Cobalt limitation and uptake in *Prochlorococcus*. *Limnology and Oceanography* **47**, 1629-1636 (2002).

106 Dulaquais, G. *et al.* Contrasting Biogeochemical Cycles. *Global Biogeochemical Cycles* **28**, doi:10.1002/ (2014).

107 Vraspir, J. M. & Butler, A. Chemistry of marine ligands and siderophores. *Annual Review of Marine Science* **1**, 43-63 (2009).

108 Saito, M. A., Moffett, J. W. & DiTullio, G. R. Cobalt and nickel in the Peru upwelling region: A major flux of labile cobalt utilized as a micronutrient. *Global Biogeochemical Cycles* **18**, GB4030 (2004).

109 Bown, J. *et al.* The biogeochemical cycle of dissolved cobalt in the Atlantic and the Southern Ocean south off the coast of South Africa. *Marine Chemistry* **126**, 193-206, doi:10.1016/j.marchem.2011.03.008 (2011).

110 Lee, Y. & Tebo, B. M. Cobalt(II) Oxidation by the Marine Manganese(II)-Oxidizing Bacillus sp. Strain SG-1. *Applied and Environmental Microbiology* **60**, 2949-2957 (1994).

111 Kay, J. T., Conklin, M. H., Fuller, C. C. & O'Day, P. A. Processes of Nickel and Cobalt Uptake by a Manganese Oxide Forming Sediment in Pinal Creek, Globe Mining District, Arizona. *Environmental Science and Technology* **35**, 4719-4725 (2001).

112 Tebo, B. M. *et al.* Biogenic Manganese Oxides: Properties and Mechanisms of Formation. *Annual Review of Earth and Planetary Sciences* **32**, 287-328 (2004).

113 Moffett, J. W. & Ho, J. Oxidation of cobalt and manganese in seawater via a common microbially catalyzed pathway. *Geochimica et Cosmochimica Acta* **60**, 3415-3424 (1996).

114 Murray, K. J., Webb, S. M., Bargar, J. R. & Tebo, B. M. Indirect Oxidation of Co(II) in the Presence of the Marine Mn(II)-Oxidizing Bacterium Bacillus sp. Strain SG-1. *Applied and Environmental Microbiology* **73**, 6905-6909 (2007).

115 Noble, A. E. *et al.* Basin-scale inputs of cobalt, iron and manganese from the Benguela-Angola front to the South Atlantic Ocean. *Limnology and Oceanography* **57**, 989–1010 (2012).

116 Saito, M. A. & Moffett, J. W. Temporal and spatial variability of cobalt in the Atlantic Ocean. *Geochimica et Cosmochimica Acta* **66**, 1943-1953 (2002).

117 Ellwood, M. J. *et al.* Organic complexation of cobalt across the Antarctic Polar Front in the Southern Ocean. *Marine and Freshwater Research* **56**, 1069, doi:10.1071/mf05097 (2005).

118 Saito, M. A., Rocap, G. & Moffett, J. W. Production of cobalt binding ligands in a *Synechococcus* feature at the Costa Rica upwelling dome. *Limnology and Oceanography* **50**, 279-290 (2005).

119 Geider, R. J. & La Roche, J. Redfield revisited: variability of C:N:P in marine microalgae and its biochemical basis. *European Journal of Phycology* **37**, 1-17 (2002).

120 Ho, T. *et al.* The elemental composition of some marine phytoplankton. *Journal of Phycology* **39**, 1145-1159 (2003).

121 Twining, B. S., Baines, S. B. & Fisher, N. S. Element stoichiometries of individual plankton cells collected during the Southern Ocean Iron Experiment (SOFeX). *Limnology and Oceanography* **49**, 2115-2128 (2004).

122 Howarth, R. W. Nutrient limitation of net primary production in marine ecosystems. *Annual Review of Ecology and Systematics* **19**, 89-110 (1988).

123 Moore, C. M. *et al.* Relative influence of nitrogen and phosphorus availability on phytoplankton physiology and productivity in the oligotrophic sub-tropical North Atlantic Ocean. *Limnology and Oceanography* **53**, 291-305 (2008).

124 Mills, M. M. *et al.* Nitrogen and phosphorus co-limitation of bacterial productivity and growth in the oligotrophic subtropical North Atlantic. *Limnology and Oceanography* **53**, 824-834 (2008).

125 Schlosser, C. *et al.* Seasonal ITCZ migration dynamically controls the location of the (sub)tropical Atlantic biogeochemical divide. *Proceedings of the National Academy of Sciences* **111**, 1438-1442 (2014).

126 Ussher, S. J. *et al.* Impact of atmospheric deposition on the contrasting iron biogeochemistry of the North and South Atlantic Ocean. *Global Biogeochemical Cycles* **27**, 1096-1107 (2013).

127 Shelley, R. U. *et al.* A tale of two gyres: Contrasting distributions of dissolved cobalt and iron in the Atlantic Ocean during an Atlantic Meridional Transect (AMT-19). *Progress in Oceanography*, doi:https://doi.org/10.1016/j.pocean.2016.10.013 (2017).

128 Carlson, C. A. *et al.* Effect of nutrient amendments on bacterioplankton production, community structure, and DOC utilization in the northwestern Sargasso Sea. *Aquatic Microbial Ecology* **30**, 19-36 (2002).

129 Carlson, C. A. *et al.* Dissolved organic carbon export and subsequent remineralization in the mesopelagic and bathypelagic realms of the North Atlantic basin. *Deep Sea Research Part II: Topical Studies in Oceanography* **57**, 1433-1445, doi:10.1016/j.dsr2.2010.02.013 (2010).

130 Pan, X. *et al.* Dissolved organic carbon and apparent oxygen utilization in the Atlantic Ocean. *Deep Sea Research Part I: Oceanographic Research Papers* **85**, 80-87, doi:10.1016/j.dsr.2013.12.003 (2014).

131 Obernosterer, I., Kawasaki, N. & Benner, R. P-limitation of respiration in the Sargasso Sea and uncoupling of bacteria from P-regeneration in size-fractionation experiments. *Aquatic Microbial Ecology* **32**, 229-237 (2003).

132 Caron, D. A., Lim, E. L., Sanders, R. W., Dennett, M. R. & Berninger, U. Responses of bacterioplankton and phytoplankton to organic carbon and inorganic nutrient additions in contrasting oceanic ecosystems. *Aquatic Microbial Ecology* **22**, 175-184 (2000).

133 Cotner, J. B., Ammerman, J. W., Peele, E. R. & Bentzen, E. Phosphorus-limited bacterioplankton growth in the Sargasso Sea. *Aquatic Microbial Ecology* **13**, 141-149 (1997).

134 Mills, M. M., Ridame, C., Davey, M., La Roche, J. & Geider, R. J. Iron and phosphorus co-limit nitrogen fixation in the eastern tropical North Atlantic. *Nature* **429**, 292-232 (2004).

135 Rivkin, R. B. & Anderson, M. R. Inorganic nutrient limitation of oceanic bacterioplankton. *Limnology and Oceanography* **42**, 730-740 (1997).

136 Graziano, L. M., Geider, R. J., Li, W. K. W. & Olaizola, M. Nitrogen limitation of North Atlantic phytoplankton: analysis of physiological condition in nutrient enrichment experiments. *Aquatic Microbial Ecology* **11**, 53-64 (1996).

137 Morris, R. M. *et al.* SAR11 clade dominates ocean surface bacterioplankton communities. *Nature* **420**, 806-810 (2002).

138 Partensky, F., Hess, W. R. & Vaulot, D. *Prochlorococcus*, a marine photosynthetic prokaryote of global significance. *Microbiology and Molecular Biology Reviews* **63** (1999).

139 Giovannoni, S. J., Britschgi, T. B., Moyer, C. L. & Field, K. G. Genetic diversity in Sargasso Sea bacterioplankton. *Nature* **345**, 60-63 (1990).

140 Rappé, M. S., Connon, S. A., Vergin, K. L. & Giovannoni, S. J. Cultivation of the ubiquitous SAR11 marine bacterioplankton clade. *Nature* **418**, 630-633 (2002).

141 Lebaron, P., Servais, P., Agogue, H., Courties, C. & Joux, F. Does the high nucleic acid content of individual bacterial cells allow us to discriminate between active cells and inactive cells in aquatic systems? *Appl Environ Microbiol* **67**, 1775-1782, doi:10.1128/AEM.67.4.1775-1782.2001 (2001).

142 Mary, I. *et al.* SAR11 dominance among metabolically active low nucleic acid bacterioplankton in surface waters along an Atlantic meridonal transect. *Aquatic Microbial Ecology* **45**, 107-113 (2006).

143 Giovannoni, S. J. *et al.* Genome streamlining in a cosmopolitan oceanic bacterium. *Science* **309**, 1242-1245 (2005).

144 Alonson, C. & Pernthaler, J. *Roseobacter* and SAR11 dominate microbial glucose uptake in coastal North Sea waters. *Environmental Microbiology* **8**, 2022-2030 (2006).

145 Malmstrom, R. R., Cottrell, M. T., Elifantz, H. & Kirchman, D. Biomass production and assimilation of dissolved organic matter by SAR11 bacteria in the Northwest Atlantic Ocean. *Applied and Environmental Microbiology* **71**, 2979-2986 (2005).

146 Johnson, P. W. & Sieburth, J. Chroococcoid cyanobacteria in the sea: A ubiquitous and diverse phototrophic biomass. *Limnology and Oceanography* **24**, 928-935 (1979).

147 Chisholm, S. W. *et al.* A novel free-living prochlorophyte abundant in the oceanic euphotic zone. *Nature* **334**, 340-343 (1988).

148 Chisholm, S. W. *et al.* Prochlorococcus marinus nov. gen. nov. sp.: an oxyphototrophic marine prokaryote containing divinyl chlorophyll a and b. *Archives of Microbiology* **157**, 2997-2300 (1992).

149 Zubkov, M. V., Sleigh, M. A. & Burkill, P. H. Assaying picoplankton distribution by flow cytometry of underway samples collected along a meridional transect across the Atlantic Ocean. *Aquatic Microbial Ecology* **21**, 13-20 (2000).

150 Zubkov, M. V., Sleigh, M. A., Tarran, G. A., Burkill, P. H. & Leakey, J. G. Picoplanktonic community structure on an Atlantic transect from 50°N to 50°S. *Deep-Sea Research II* **45**, 1339-1355 (1998).

151 Flombaum, P. *et al.* Present and future global distributions of the marine cyanobacteria *Prochlorococcus* and *Synechococcus*. *Proceedings of the National Academy of Sciences* **110**, 9824-9829 (2013).

152 Vaulot, D., Marie, D., Olson, R. J. & Chisholm, S. W. Growth of *Prochlorococcus*, a photosynthetic prokaryote, in the equatorial Pacific Ocean. *Science* **268**, 1480-1482 (1995).

153 DuRand, M. D., Olson, R. J. & Chisholm, S. W. Phytoplankton population dynamics at the Bermuda Atlantic Time-series station in the Sargasso Sea. *Deep-Sea Research II* **48**, 1983-2003 (2001).

154 Liu, H., Nolla, H. A. & Campbell, L. *Prochlorococcus* growth rate and contribution to primary production in the equatorial and subtropical North Pacific Ocean. *Aquatic Microbial Ecology* **12**, 39-47 (1997).

155 Moore, L. R., Rocap, G. & Chisholm, S. W. Physiology and molecular phylogeny of coexisting *Prochlorococcus* ecotypes. *Nature* **393**, 464-467 (1998).

156 Biller, S. J., Berube, P. M., Lindell, D. & Chisholm, S. W. *Prochlorococcus*: the structure and function of collective diversity. *Nature Reviews Microbiology* **13**, 13-27 (2015).

157 Waterbury, J., Watson, S. W., Guillard, R. R. L. & Brand, L. E. Widespread occurence of a unicellular, marine, planktonic, cyanobacterium. *Nature* **277**, 293-294 (1979).

158 Partensky, F., Blanchot, J. & Vaulot, D. Differential distribution and ecology of *Prochlorococcus* and *Synechococcus* in oceanic waters: a review. *Bulletin de l'Institut Océanographique de Monaco* **19**, 457-475 (1999).

159 Li, W. K. W. Composition of ultraphytoplankton in the central North Atlantic. *Marine Ecology Progress Series* **122**, 1-8 (1995).

160 Morel, A., Ahn, Y., Partensky, F., Vaulot, D. & Claustre, H. *Prochlorococcus* and *Synechococcus*: A comparative study of their optical properties in relation to their size and pigmentation. *Journal of Marine Research* **51**, 617-649 (1993).

161 Chisholm, S. W. Phytoplankton size. In *Primary productivity and biogeochemical cycles in the sea* (eds P. Falkowski & A. D. Woodhead). *213-237* (Plenum Press, 1992).

162 Dufresne, A., Garczarek, L. & Partensky, F. Accelerated evolution associated with genome reduction in a free-living prokaryote. *Genome Biology* **6**, R14 (2005).

163 Sun, J. *et al.* One carbon metabolism in SAR11 pelagic marine bacteria. *PLoS One* **6**, e23973 (2011).

164 Zubkov, M. V., Martin, A. P., Hartmann, M., Grob, C. & Scanlan, D. J. Dominant oceanic bacteria secure phosphate using a large extracellular buffer. *Nature Communications* **22**, 7878-7885 (2015).

165 Grob, C. *et al.* Elemental composition of natural population of key microbial groups in Atlantic waters. *Environmental Microbiology* **15**, 3054-3064 (2013).

166 Bertilsson, S., Berglund, O., Karl, D. M. & Chisholm, S. W. Elemental composition of marine Prochlorococcus and Synechococcus: Implications for the ecological stoichiometry of the sea. *Limnology and Oceanography* **48** (2003).

167 Van Mooy, B. A. S., Rocap, G., Fredricks, H. F., Evans, C. T. & Devol, A. H. Sulfolipids dramatically decrease phosphorus demand by picocyanobacteria in oligotrophic marine environments. *Proceedings of the National Academy of Sciences* **103**, 8607-8612 (2006).

168 García-Fernández, J. M., Tandeau de Marsac, N. & Diez, J. Streamlined Regulation and Gene Loss as Adaptive Mechanisms in *Prochlorococcus* for Optimized Nitrogen Utilization in Oligotrophic Environments. *Microbiology and Molecular Biology Reviews* **68**, 630-638 (2004).

169 Lindell, D. *et al.* Nitrogen stress response of *Prochlorococcus* strain PCC 9511 (Oxyphotobacteria) involves contrasting regulation of ntcA and amt1. *Journal of Phycology* **38**, 1113-1124 (2002).

170 Giovannoni, S. J. SAR11: The most abundant plankton in the oceans. *Annual Review of Marine Science* **9**, 231-255 (2017).

171 Giovannoni, S. J. *et al.* Proteorhodopsin in the ubiquitous marine bacterium SAR-11. *Nature Letters* **438**, 82-85 (2005).

172 Scanlan, D. J. Physiological diversity and niche adaptation in marine *Synechococcus*. In *Advances in Microbial Physiology (Volume 47)* (ed R. K. Poole). (Elsevier Science Ltd, 2003).

173 Shi, D., Xu, Y., Hopkinson, B. M. & Morel, F. M. M. Effect of ocean acidification on iron availability to marine phytoplankton. *Science* **327**, 676-679 (2010).

174 Millero, F. J., Woosley, R., Ditrolio, B. & Waters, J. Effect of ocean acidifcation on the speciation of metals in seawater. *Oceanography* **22** (2009).

175 Warren, L. A. & Ferris, F. G. Continuum between sorption and precipitation of Fe(III) on microbial surfaces. *Environmental Science and Technology* **32**, 2331-2337 (1998).

176 Moore, C. M. *et al.* Large-scale distribution of Atlantic nitrogen fixation controlled by iron availability. *Nature Geoscience* **2**, 867-871 (2009).

177 Grob, C. *et al.* Cell-specific CO2 fixation rates of two distinct groups of plastidic protists in the Atlantic Ocean remain unchanged after nutrient addition. *Environmental Microbiology Reports* **7**, 211-218 (2015).

178 Behrenfeld, M. J. & Kolber, Z. Widespread Iron Limitation of Phytoplankton in the South Pacific Ocean. *Science* **283**, 840-843 (1999).

179 Browning, T. J. *et al.* Nutrient co-limitation at the boundary of an oceanic gyre. *Nature*, doi:10.1038/nature24063 (2017).

180 Boyd, P. W. *et al.* Mesoscale Iron Enrichment Experiments 1993-2005: Synthesis and Future Directions. *Science* **315**, 612-617 (2007).

181 Schlitzer, R. Ocean Data View http://odv.awi.de/. (2017).

182 Bowie, A. R., Whitworth, D. J., Achterberg, E. P., Mantoura, R. F. C. & Worsfold, P. J. Biogeochemistry of Fe and other trace elements (Al, Co, Ni) in the upper Atlantic Ocean. *Deep-Sea Research I* **49**, 605-636 (2002).

183 Brown, M. & Wittwer, C. Flow Cytometry: Principles and Clinical Applications in Hematology. *Clinical Chemistry* **46**, 1221-1229 (2000).

184 Olson, R. J., Zettler, E. R. & DuRand, M. D. Phytoplankton analysis using flow cytometry. In *Handbook of Methods in Aquatic Microbial Ecology* (eds P. F. Kemp, B. F. Sherr, E. B. Sherr, & J. J. Cole) **22**. *175-186* (Lewis Publishers, 1993).

185 Johnsen, G., Bricaud, A., Nelson, N., Prézelin, B. B. & Bidigare, R. R. *In vivo* bio-optical properties of phytoplankton pigments. In *Phytoplankton Pigements: Characterization, Chemotaxonomy and Applications in Oceanography* (eds S. Roy, C. A. Llewellyn, E. S. Egeland, & G. Johnsen) **13**. (Cambridge University Press, 2011).

186 Bolhàr-Nordenkampf, H. R. & Oquist, G. O. Chlorophyll fluorescence as a tool in photosynthesis research. In *Photosynthesis and Production in a Changing*

Environment (eds D. O. Hall *et al.*) **12**. (Springer Science + Business Media, 1993).

187 Marie, D., Partensky, F., Jacquet, S. & Vaulot, D. Enumeration and cell cycle analysis of natural populations of marine picoplankton by flow cytometry using the nucleic acid stain SYBR Green I. *Applied and Environmental Microbiology* **63**, 168-193 (1997).

188 Zubkov, M. V., Tarran, G. A., Mary, I. & Fuchs, B. M. Differential microbial uptake of dissolved amino acids and amino sugars in surface waters of the Atlantic Ocean. *Journal of Plankton Research* **30**, 211-220 (2008).

189 Fuchs, B. M., Woebken, D., Zubkov, M. V., Burkill, P. & Amann, R. Molecular identification of picoplankton populations in contrasting waters of the Arabian Sea. *Aquatic Microbial Ecology* **39**, 145-157 (2005).

190 Zubkov, M. V. & Burkill, P. Syringe pumped high speed flow cytometry of oceanic phytoplankton. *Cytometry Part A* **69**, 1010-1019 (2006).

191 Zubkov, M. V., Sleigh, M. A., Burkill, P. & Leakey, R. J. G. Picoplankton community structure on the Atlantic Meridional Transect: a comparison between seasons. *Progress in Oceanography* **45**, 369-386 (2000).

192 Payet, J. P. & Suttle, C. A. Physical and biological correlates of virus dynamics in the southern Beaufort Sea and Amundsen Gulf. *Journal of Marine Systems* **74**, 933-945 (2008).

193 Zubkov, M. V., Fuchs, B. M., Eilers, H., Burkill, P. H. & Amann, R. Determination of total protein content of bacterial cells by SYPRO staining and flow cytometry. *Applied and Environmental Microbiology* **65**, 3251-3257 (1999).

194 Zubkov, M. V., Tarran, G. A. & Burkill, P. Bacterioplankton of low and high DNA content in the suboxic waters of the Arabian Sea and the Gulf of Oman: abundance and amino acid uptake. *Aquatic Microbial Ecology* **43**, 23-32 (2006).

195 Fuhrman, J. A., McCallum, K. & Davis, A. A. Phylogenetic Diversity of Subsurface Marine Microbial Communities from the Atlantic and Pacific Oceans. *Applied and Environmental Microbiology* **59**, 1294-1302 (1993).

196 Zubkov, M. V. & Tarran, G. A. High bacterivory by the smallest phytoplankton in the North Atlantic Ocean. *Nature Letters* **455**, 224-227 (2008).

197 Kirchman, D., K'nees, E. & Hodson, R. Leucine incorporation and its potential as a measure of protein synthesis by bacteria in natural aquatic systems. *Applied and Environmental Microbiology* **49**, 599-607 (1985).

198 Hill, P. G., Mary, I., Purdie, D. A. & Zubkov, M. V. Similarity in microbial amino acid uptake in surface waters of the North and South Atlantic (sub-)tropical gyres. *Progress in Oceanography* **91**, 437-446 (2011).

199 Mary, I. *et al.* Light enhanced amino acid uptake by dominant bacterioplankton groups in surface waters of the Atlantic Ocean. *FEMS Microbiology Ecology* **63**, 36-45 (2008).

200 Zubkov, M. V. & Tarran, G. A. Amino acid uptake of *Prochlorococcus* spp. in surface waters across the South Atlantic Subtropical Front. *Aquatic Microbial Ecology* **40**, 241-249 (2005).

201 Zubkov, M. V., Tarran, G. A. & Fuchs, B. M. Depth related amino acid uptake by *Prochlorococcus* cyanobacteria in the Southern Atlantic tropical gyre. *FEMS Microbiology Ecology* **50**, 153-161 (2004).

202 Wright, R. R. & Hobbie, J. E. Use of Glucose and Acetate by Bacteria and Algae in Aquatic Ecosystems. *Ecology* **47**, 447-464 (1966).

203 Neidhardt, F. C., Ingraham, J. L. & Schaechter, M. Assembly and polymerization: The bacterial interior. In *Physiology of the Bacterial Cell: A Molecular Approach*. (Sinauer Associates Inc, 1990).

204 Tripp, H. J. *et al.* SAR11 marine bacteria require exogenous reduced sulphur for growth. *Nature Letters* **452**, 741-744 (2008).

205 Berg, J. M., Tymoczko, J. L. & Stryer, L. DNA. RNA, and the flow of genetic information. In *Biochemistry, Sixth Edition* **4**. (W. H. Freeman and Company, 2007).

206 Zubkov, M. V., Holland, R. J., Burkill, P. H., Croudace, I. W. & Warwick, P. E. Microbial abundance, activity and iron uptake in vicinity of the Crozet Isles in November 2004-January 2005. *Deep-Sea Research II* **54**, 2126-2137 (2007).

207 PerkinElmer. *Liquid scintillation counting theory*, available: http://www.perkinelmer.com/ (accessed 09-09-18).

208 Vreeland, R. H., Litchfield, C. D., Martin, E. L. & Elliot, E. Halomonas elongata, a new genus and species of extremely salt-tolerant bacteria. *International Journal of Systematic Bacteriology* **30**, 485-495 (1980).

209 Mata, J. M., Martínez-Cánovas, J., Quesada, E. & Béjar, V. A Detailed Phenotypic Characterisation of the Type Strains of *Halomonas* Species. *Systematic and Applied Microbiology* **25**, 360-375 (2002).

210 Levitus, S., Burgett, R. & Boyer, T. P. World Ocean Atlas 1994 Volume 3: Salinity. (National Oceanic and Atmospheric Administration, United States).

211 National Oceanic and Atmospheric Administration & Office of Satellite and Product Operations. *Sea Surface Temperature (SST) Contour Charts*, available: http://www.ospo.noaa.gov/Products/ocean/sst/contour/ (2013).

212 Denner, E. B. M. *et al.* Aurantimonas coralicida gen. nov., sp. nov., the causative agent of white plague type II on Caribbean scleractinian corals. *International Journal of Sysematic and Evolutionary Microbiology* **53**, 1115-1122 (2003).

213 Anderson, C. R. *et al. Aurantimonas manganoxydans*, sp. nov. and *Aurantimonas litoralis*, sp. nov.: Mn(II) oxidizing representatives of a globally distributed clade of alpha-*Proteobacteria* from the order *Rhizobiales*. *Geomicrobiology Journal* **26**, 189-198 (2009).

214 Anderson, C. R. *et al.* Mn(II) Oxidation Is Catalyzed by Heme Peroxidases in *"Aurantimonas manganoxydans"* Strain SI85-9A1 and Erythrobacter sp. Strain SD-21. *Applied and Environmental Microbiology* **75**, 4130-4138 (2009).

215 Tebo, B. M., Clement, B. G. & Dick, G. J. Biotransformations of manganese. In *Manual of Environmental Microbiology, Third Edition* (eds C. J. Hurst *et al.*). *1223-1238* (ASM Press, 2007).

216 Wu, J., Sunda, W., Boyle, E. A. & Karl, D. M. Phosphate depletion in the Western North Atlantic Ocean. *Science* **289**, 759-762 (2000).

217 Ammerman, J. W., Hood, R. R., Case, D. A. & Cotner, J. B. Phosphorus deficiency in the Atlantic: An Emerging Paradigm in Oceanography. *Eos* **84** (2003).

218 Jickels, T. D. *et al.* Global iron connections between desert dust, ocean biogeochemisty, and climate. *Science* **308**, 67-71 (2005).

219 Carlson, C. A. & Ducklow, H. W. Growth of bacterioplankton and consumption of dissolved organic carbon in the Sargasso Sea. *Aquatic Microbial Ecology* **10**, 69-85 (1996).

220 Mann, K. H. & Lazier, J. R. N. Vertical structure of the open ocean: biology of the mixed layer. In *Dynamics of Marine Ecosystems, Third Edition* **3**. (2006).

221 Davey, M. *et al.* Nutrient limitation of picophytoplankton photosynthesis and growth in the tropical North Atlantic. *Limnology and Oceanography* **53**, 1722-1733 (2008).

222 Olson, R. J., Vaulot, D. & Chisholm, S. W. Marine phytoplankton distributions measured using shipboard flow cytometry. *Deep-Sea Research Part A, Oceanographic Research Papers* **32**, 1273-1280 (1985).

223 Wheeler, P. A. & Kirchman, D. Utilization of inorganic and organic nitrogen by bacteria in marine systems. *Limnology and Oceanography* **31**, 998-1009 (1986).

224 Kirchman, D. & Williams, P. J. l. B. Introduction. In *Microbial Ecology of the Oceans, First Edition* (ed D. Kirchman) **1**. (2000).

225 Cotner, J. B. & Wetzel, R. G. Uptake of dissolved inorganic and organic phosphorus compounds by phytoplankton and bacterioplankton. *Limnology and Oceanography* **37**, 232-243 (1992).

226 Heywood, J. L., Zubkov, M. V., Tarran, G. A., Fuchs, B. M. & Hollingan, P. M. Prokaryoplankton standing stocks in oligotrophic gyre and equatorial provinces of the Atlantic Ocean: Evalulation of inter-annual variability. *Deep-Sea Research II* **53**, 1530-1547 (2006).

227 Robinson, C. *et al.* The Atlantic Meridonal Transect (AMT) Programme: A contextual view 1995-2005. *Deep-Sea Research II* **53**, 1485-1515 (2006).

228 Kuipers, B., van Noort, G. J., Vosjan, J. & Herndl, G. J. Diel periodicity of bacterioplankton in the euphotic zone of the subtropical Atlantic Ocean. *Marine Ecology Progress Series* **201**, 13-25 (2000).

229 Mary, I. *et al.* Diel rhythmicity in amino acid uptake by *Prochlorococcus*. *Environmental Microbiology* **10**, 2124-2131 (2008).

230 Zubkov, M. V. *et al.* Microbial control of phosphate in the nutrient-depleted North Atlantic subtropical gyre. *Environmental Microbiology* **9**, 2079-2089 (2007).

231 Kirchman, D. The uptake of inorganic nutrients by heterotrophic bacteria. *Microbial Ecology* **28**, 255-271 (1994).

232 Kirchman, D., Keil, R. G. & Wheeler, P. A. Carbon limitation of ammonium uptake by heterotrophic bacteria in the subarctic Pacific. *Limnology and Oceanography* **35**, 1258-1266 (1990).

233 García-Fernández, J. M. & Diez, J. Adaptive mechanisms of nitrogen and carbon assimilatory pathways in the marine cyanobacteria *Prochlorococcus*. *Research in Microbiology* **155**, 795-802 (2004).

234 Dai, G., Deblois, C. P., Liu, S., Juneau, P. & Qui, B. Differential sensitivity of five cyanobacterial strains to ammonium toxicity and its inhibitory mechanism on the

photosynthesis of rice-field cyanobacterium Ge-Xian-Mi (Nostoc). *Aquatic Toxicology* **89**, 113-121 (2008).

235 Cavender-Bares, K. K., Mann, E. L., Chisholm, S. W., Ondrusek, M. E. & Bidigare, R. R. Differential response of equatorial Pacific phytoplankton to iron fertilization. *Limnology and Oceanography* **44**, 237-246 (1999).

236 Serret, P. *et al.* Both respiration and photosynthesis determine the scaling of plankton metabolism in the oligotrophic ocean. *Nat Commun* **6**, 6961, doi:10.1038/ncomms7961 (2015).

237 Mann, K. H. & Lazier, J. R. N. The oceans and global climate change: physical and biological aspects. In *Dynamics of Marine Ecosystems, Third Edition* **10**. *390-422* (2006).

238 Wu, J. & Luther, G. W. Size-fractionated iron concentrations in the water column of the western North Atlantic Ocean. *Limnology and Oceanography* **39**, 1119-1129 (1994).

239 Martin, J. H. & Fitzwater, S. E. Iron deficiency limits phytoplankton growth in the north-east Pacific subarctic. *Nature* **331**, 341-343 (1988).

240 Martin, J. H., Gordon, R. M. & Fitzwater, S. E. Iron in Antarctic waters. *Nature* **345**, 156-158 (1990).

241 Coale, K. H. *et al.* IronEx-I, an *in situ* iron-enrichment experiment: Experimental design, implementation and results. *Deep-Sea Research II* **45**, 919-945 (1998).

242 Cochlan, W. P. The heterotrophic bacterial response during a mesoscale iron enrichment experiment (IronEx II) in the eastern equatorial Pacific Ocean. *Limnology and Oceanography* **46**, 428-435 (2001).

243 Rijkenberg, M. J. *et al.* The distribution of dissolved iron in the West Atlantic Ocean. *PLoS One* **9**, e101323, doi:10.1371/journal.pone.0101323 (2014).

244 Coale, K. H., Fitzwater, S. E., Gordon, R. M., Johnson, K. S. & Barber, R. Control of community growth and export production by upwelled iron in the equatorial Pacific Ocean. *Nature* **379**, 621-624 (1996).

245 Boyd, P. W. & Law, C. S. The Southern Ocean Iron RElease Experiment (SOIREE) - introduction and summary. *Deep-Sea Research II* **48**, 2425-2438 (2001).

246 Marshall, J. & Plumb, R. A. The general circulation of the atmosphere. In *Atmosphere, Ocean and Climate Dynamics* **8**. (Elsevier, 2008).

247 Maldonado, M. T. & Price, N. M. Utilization of iron bound to strong organic ligands by plankton communities in the subarctice Pacific Ocean. *Deep-Sea Research II* **46**, 2447-2473 (1999).

248 Wilhelm, S. W. Ecology of iron-limited cyanobacteria: a review of physiological responses and implications for aquatic systems. *Aquatic Microbial Ecology* **9**, 295-303 (1995).

249 Kirchman, D. & Wheeler, P. A. Uptake of ammonium and nitrate by heterotrophic bacteria and phytoplankton in the sub-Arctic Pacific. *Deep-Sea Research I* **45**, 347-365 (1998).

250 Maldonado, M. T. & Price, N. M. Reduction and transport of organically bound iron by *Thalassiosira oceanica* (bacillariophyceae). *Journal of Phycology* **37**, 298-309 (2001).

251 Harrison, G. I. & Morel, F. M. M. Response of the marine diatom *Thalassiosira weissflogii* to iron stress. *Limnology and Oceanography* **31**, 989-997 (1986).

252 Moore, C. M. *et al.* Iron limits primary production during spring bloom development in the central North Atlantic. *Global Change Biology* **12**, 626-634 (2006).

253 Hudson, R. J. M. & Morel, F. M. M. Distinguishing between extra- and intracellular iron in marine phytoplankton. *Limnology and Oceanography* **34**, 1113-1120 (1989).

254 Tovar-Sanchez, A. *et al.* A trace metal celan reagent to remove surface-bound iron from marine phytoplankton. *Marine Chemistry* **82**, 91-99 (2003).

255 Achterberg, E. P., Holland, T. W., Bowie, A. R., Mantoura, R. F. C. & Worsfold, P. J. Determination of iron in seawater. *Analytica Chimica Acta* **442**, 1-14 (2001).

256 Boye, M. *et al.* Distributions of dissolved trace metals (Cd, Cu, Mn, Pb, Ag) in the southeastern Atlantic and the Southern Ocean. *Biogeosciences* **9**, 3231-3246 (2012).

257 Rapp, I., Schlosser, C., Rusiecka, D., Gledhill, M. & Achterberg, E. P. Automated preconcentration of Fe, Zn, Cu, Ni, Cd, Pb, Co and Mn in seawater with analysis using high-resolution sector field inductively-coupled plasma mass spectrometry. *Analytica Chimica Acta* **976**, 1-13 (2017).

258 Bergquist, B. A. & Boyle, E. A. Dissolved iron in the tropical and subtropical Atlantic Ocean. *Global Biogeochemical Cycles* **20**, doi:10.1029/2005gb002505 (2006).

259 Imlay, J. A., Chin, S. M. & Linn, S. Toxic DNA damage by hydrogen peroxide through the Fenton Reaction in vivo and in vitro. *Science* **240**, 640-642 (1988).

260 Tang, D. & Morel, F. M. M. Distinguishing between cellular and Fe-oxide-associated trace elements in phytoplankton. *Marine Chemistry* **98**, 18-30 (2006).

261 Hassler, C. S., Slaveykova, V. I. & Wilkinson, K. J. Discrimination between intra- and extracellular metals using chemical extractions. *Limnology and Oceanography*, 237-347 (2004).

262 Timmermans, K. R., van der Wagt, B., Veldhuis, M. J. W., Maatman, A. & de Baar, H. J. W. Physiological responses of three species of marine pico-phytoplankton to ammonium, phosphate, iron and light limitation. *Journal of Sea Research* **53**, 109-120 (2005).

263 Sunda, W. Low iron requirement for growth in oceanic phytoplankton. *Nature* **351**, 55-57 (1991).

264 Rusch, D. B., Martiny, A. C., Dupont, C. L., Halpern, A. L. & Venter, J. C. Characterization of *Prochlorococcus* clades from iron-depleted oceanic regions. *Proceedings of the National Academy of Sciences* **107**, 16184-16189 (2010).

265 Berge, T., Daugbjerg, N., Andersen, B. B. & Hansen, P. J. Effect of lowered pH on marine phytoplankton growth rates. *Marine Ecology Progress Series* **416**, 79-91 (2010).

266 Rudolf, M. *et al.* Multiple modes of iron uptake by the filamentous, siderophore-producing cyanobacterium, *Anabaena* sp. PCC 7120. *Molecular Microbiology* **97**, 577-588 (2015).

267 Fu, F., Warner, M. E., Zhang, Y., Feng, Y. & Hutchins, D. A. Effects of increased temperature and CO2 on photosynthesis, growth, and elemental ratios in marine

Synechococcus and *Prochlorococcus* (cyanobacteria). *Journal of Phycology* **43**, 485-496 (2007).

268 Traving, S. J., Clokie, M. R. J. & Middelboe, M. Increased acidification has a profound effect on the interactions between the cyanobacterium *Synechococcus* sp. WH7803 and its viruses. *FEMS Microbiology Ecology* **87**, 133-141 (2014).

269 Yooseph, S. *et al.* Genomic and functional adaptation in surface ocean planktonic prokaryotes. *Nature* **468**, 60-67 (2010).

270 Rippka, R. *et al.* Prochlorococcus marinus Chisholm et al. 1992 subsp. pastoris subsp. nov. strain PCC 9511, the first axenic chlorophyll a2/b2-containing cyanobacterium (Oxyphotobacteria). *International Journal of Systematic and Evolutionary Microbiology* **50**, 1833-1847 (2000).

271 Sebastián, M. & Gasol, J. M. Heterogeneity in the nutrient limitation of different bacterioplankton groups in the Eastern Mediterranean Sea. *The ISME Journal* **7**, 1665-1668 (2013).

272 Gifford, S. M., Sharma, S., Booth, M. & Moran, M. A. Expression patterns reveal niche diversification in a marine microbial assemblage. *The ISME Journal* **7**, 281-298 (2013).

273 Hutchins, D. A. & Boyd, P. W. Marine phytoplankton and the changing ocean iron cycle. *Nature Climate Change* **6**, 1072-1079 (2016).

274 Morel, F. M. M., Kustka, A. B. & Shaked, Y. The role of unchelated Fe in the iron nutrition of phytoplankton. *Limnology and Oceanography* **53**, 400-404 (2008).

275 Kappler, A., Emerson, D., Gralnick, J. A., Roden, E. E. & Muehe, E. M. Geomicrobiology of Iron. In *Ehrlich's Geomicrobiology, Sixth Edition* (eds H. L. Ehrlich, D. K. Newman, & A. Kappler) **17**. (2015).

276 Gadd, G. M. Metals, minerals and microbes: geomicrobiology and bioremediation. *Microbiology* **156**, 609-643, doi:10.1099/mic.0.037143-0 (2010).

277 Konhauser, K. O. Bacterial iron biomineralisation in nature. *FEMS Microbiology Ecology* **20**, 315-326 (1997).

278 Melton, E. D., Swanner, E. D., Behrens, S., Schmidt, C. & Kappler, A. The interplay of microbially mediated and abiotic reactions in the biogeochemical Fe cycle. *Nat Rev Microbiol* **12**, 797-808, doi:10.1038/nrmicro3347 (2014).

279 Morrissey, J. & Bowler, C. Iron utilization in marine cyanobacteria and eukaryotic algae. *Frontiers in Microbiology* **3**, 1-13 (2012).

280 Hogle, S. L., Thrash, J. C., Dupont, C. L. & Barbeau, K. Trace metal acquisition by marine heterotrophic bacterioplankton with contrasting trophic strategies. *Applied and Environmental Microbiology* **82**, 1613-1624 (2016).

281 Beveridge, T. J. & Koval, S. F. Binding of metals to cell envelopes of *Escherichia coli* K-12. *Applied and Environmental Microbiology* **42**, 325-335 (1981).

282 Beveridge, T. J. Role of cellular design in bacterial metal accumulation and mineralization. *Annual Review of Microbiology* **43**, 147-171 (1989).

283 Balistrieri, L., Brewer, P. G. & Murray, J. W. Scavenging residence times of trace metals and surface chemistry of sinking particles in the deep ocean. *Deep-Sea Research Part A, Oceanographic Research Papers* **28A**, 101-121 (1981).

284 Wilde, K. L., Stauber, J. L., Markich, S. J., Franklin, N. M. & Brown, P. L. The effect of pH on the uptake and toxicity of copper and zinc in a tropical freshwater alga (Chlorella sp.). *Arch Environ Contam Toxicol* **51**, 174-185, doi:10.1007/s00244-004-0256-0 (2006).

285 Crist, R. H., Oberholser, K., Schwartz, D., Marzoff, J. & Ryder, D. Interactions of metals and protons with algae. *Environmental Science and Technology* **22**, 755-760 (1988).

286 Hartmann, M. *et al.* Efficient CO2 fixation by surface Prochlorococcus in the Atlantic Ocean. *ISME J* **8**, 2280-2289, doi:10.1038/ismej.2014.56 (2014).

287 Garcia, M. T., Mellado, E., Ostos, J. C. & Ventosa, A. Halomonas organivorans sp. nov., a moderate halophile able to degrade aromatic compounds. *Int J Syst Evol Microbiol* **54**, 1723-1728, doi:10.1099/ijs.0.63114-0 (2004).

288 Martinez-Checa, F., Bejar, V., Martinez-Canovas, M. J., Llamas, I. & Quesada, E. Halomonas almeriensis sp. nov., a moderately halophilic, exopolysaccharide-producing bacterium from Cabo de Gata, Almeria, south-east Spain. *Int J Syst Evol Microbiol* **55**, 2007-2011, doi:10.1099/ijs.0.63676-0 (2005).

289 Jeong, S. H. *et al. Halomonas cibimaris* sp. nov., isolated from *jeotgal*, a traditional Korean fermented seafood. *Antonie van Leeuwenhoek* **103**, 503-512, doi:10.1007/s10482-012-9832-x) (2013).

290 Miao, A. & Wang, W. Fulfilling iron requirements of a coastal diatom under different temperatures and irradiances. *Limnology and Oceanography* **51**, 925-935 (2006).

291 Beveridge, T. J. & Murray, R. G. E. Uptake and retention of metals by cell walls of *Bacillus subtilis*. *Journal of Bacteriology* **127**, 1502-1518 (1976).

292 Vijayaraghavan, K. & Yun, Y. Bacterial biosorbents and biosorption. *Biotechnology Advances* **26**, 266-291 (2008).

293 Vink, S. & Measures, C. I. The role of dust deposition in determining surface water distributions of Al and Fe in the South West Atlantic. *Deep-Sea Research II* **48**, 2787-2809 (2001).

294 Al-Homaidan, A. A., Al-Houri, H. J., Al-Hazzani, A. A., Elgaaly, G. & Moubayed, N. M. S. Biosorption of copper ions from aqueous solutions by *Spirulina platensis* biomass. *Arabian Journal of Chemistry* **7**, 57-62 (2014).

295 Ozturk, A., Artan, T. & Ayar, A. Biosorption of nickel(II) and copper(II) ions from aqueous solution by Streptomyces coelicolor A3(2). *Colloids Surf B Biointerfaces* **34**, 105-111, doi:10.1016/j.colsurfb.2003.11.008 (2004).

296 Bai, R. S. & Abraham, E. R. Biosorption of Cr (VI) from aqueous solution by Rhizopus nigricans. *Bioresource Technology* **79**, 73-81 (2001).

297 Hudson, R. J. M. & Morel, F. M. M. Iron transport in marine phytoplankton: Kinetics of cellular and medium coordination reactions. *Limnology and Oceanography* **35**, 1002-1020 (1990).

298 Sunda, W. & Huntsman, S. A. Processes regulating cellular metal accumulation and physiological effects: Phytoplankton as model systems. *The Science of the Total Environment* **219**, 165-181 (1998).

299 Lis, H., Shaked, Y., Kranzler, C., Keren, N. & Morel, F. M. Iron bioavailability to phytoplankton: an empirical approach. *ISME J* **9**, 1003-1013, doi:10.1038/ismej.2014.199 (2015).

300 Sunda, W. & Huntsman, S. A. Cobalt and zinc interreplacement in marine phytoplankton: biological and geochemical implications. *Limnology and Oceanography* **40**, 1404-1417 (1995).

301 Bertrand, E. M. *et al.* Methionine synthase interreplacement in diatom cultures and communities: Implications for the persistence of B12 use by eukaryotic phytoplankton. *Limnology and Oceanography* **58**, 1431-1450, doi:10.4319/lo.2013.58.4.1431 (2013).

302 Croft, M. T., Lawrence, A. D., Raux-Deery, E., Warren, M. J. & Smith, A. G. Algae acquire vitamin B12 through a symbiotic relationship with bacteria. *Nature* **438**, 90-93, doi:10.1038/nature04056 (2005).

303 Marron, A. O., Akam, M. & Walker, G. Nitrile hydratase genes are present in multiple eukaryotic supergroups. *PLoS One* **7**, e32867, doi:10.1371/ (2012).

304 Yee, D. & Morel, F. M. M. In vivo substitution of zinc by cobalt in carbonic anhydrase of a marine diatom. *Limnology and Oceanography* **41**, 573-577 (1996).

305 Price, N. M. & Morel, F. M. M. Cadmium and cobalt substitution for zinc in a marine diatom. *Nature* **344**, 658-660 (1990).

306 Xu, Y., Tang, D., Shaked, Y. & Morel, F. M. M. Zinc, cadmium, and cobalt interreplacement and relative use efficiencies in the coccolithophore *Emiliania huxleyi*. *Limnology and Oceanography* **52**, 2294-2305 (2007).

307 Noble, A. E., Saito, M. A., Maiti, K. & Benitez-Nelson, C. R. Cobalt, manganese, and iron near the Hawaiian Islands: A potential concentrating mechanism for cobalt within a cyclonic eddy and implications for the hybrid-type trace metals. *Deep Sea Research Part II: Topical Studies in Oceanography* **55**, 1473-1490, doi:10.1016/j.dsr2.2008.02.010 (2008).

308 Zwolsman, J. J. G. & van Eck, G. T. M. Geochemistry of major elements and trace metals in suspended matter of the Scheldt estuary, southwest Netherlands. *Marine Chemistry* **66**, 91-111 (1999).

309 McLaren, R. G., Lawson, D. M. & Swift, R. S. The forms of cobalt in some Scottish soils as determined by extraction and isotopic exchange. *Journal of Soil Science* **37**, 223-234 (1986).

310 Taillefert, M. *et al.* Evidence for a dynamic cycle between Mn and Co in the water column of a stratified lake. *Environmental Science and Technology* **36**, 468-476 (2002).

311 Fuller, C. C. & Harvey, J. W. Reactive Uptake of Trace Metals in the Hyporheic Zone of a Mining-Contaminated Stream, Pinal Creek, Arizona. *Environmental Science and Technology* **34**, 1150-1155 (2000).

312 Tebo, B. M., Johnson, H. A., McCarthy, J. K. & Templeton, A. S. Geomicrobiology of manganese(II) oxidation. *Trends Microbiol* **13**, 421-428, doi:10.1016/j.tim.2005.07.009 (2005).

313 Sunda, W. Trace metal interactions with marine phytoplankton. *Biological Oceanography* **6**, 411-442, doi:10.1080/01965581.1988.10749543 (1989).

314 Ridge, J. P. *et al.* A multicopper oxidase is essential for manganese oxidation and laccase-like activity in Pedomicrobium sp. ACM 3067. *Environ Microbiol* **9**, 944-953, doi:10.1111/j.1462-2920.2006.01216.x (2007).

315 Andeer, P. F., Learman, D. R., McIlvin, M., Dunn, J. A. & Hansel, C. M. Extracellular haem peroxidases mediate Mn(II) oxidation in a marine Roseobacter bacterium via superoxide production. *Environ Microbiol* **17**, 3925-3936, doi:10.1111/1462-2920.12893 (2015).

316 Dick, G. J., Torpey, J. W., Beveridge, T. J. & Tebo, B. M. Direct identification of a bacterial manganese(II) oxidase, the multicopper oxidase MnxG, from spores of several different marine Bacillus species. *Appl Environ Microbiol* **74**, 1527-1534, doi:10.1128/AEM.01240-07 (2008).

317 Morgan, J. J. Chemical equilibria and kinetic properties of manganese in natural waters. In *Principles and applications of water chemistry* (eds S. D. Faust & J. V. Hunter). *561-620* (John Wiley & Sons, 1967).

318 He, J.-Z., Meng, Y.-T., Zheng, Y.-M. & Zhang, L.-M. Cr(III) oxidation coupled with Mn(II) bacterial oxidation in the environment. *Journal of Soils and Sediments* **10**, 767-773, doi:10.1007/s11368-009-0139-0 (2010).

319 Murray, K. J. & Tebo, B. M. Cr(III) is indirectly oxidized by the Mn(II)-oxidizing bacterium *Bacillus* sp. strain SG-1. *Environmental Science and Technology* **41**, 528-533 (2007).

320 Lee, B. & Fisher, N. S. Microbially mediated cobalt oxidation in seawater revealed by radiotracer experiments. *Limnology and Oceanography* **38** (1993).

321 Dick, G. J. *et al.* Genomic insights in Mn(II) oxidation by the marine alphaproteobacterium *Aurantimonas* sp. strain SI85-9A1. *Applied and Environmental Microbiology* **74**, 2646-2658 (2008).

322 Tebo, B. M., Nealson, K. H., Emerson, S. & Jacobs, L. Microbial mediation of Mn(II) and Co(II) precipitation at the O2/H2S interfaces in two anoxic fjords. *Limnology and Oceanography* **29**, 1247-1258 (1984).

323 Souren, A. W. M. G. Comment on "Oxidation of cobalt and manganese in seawater via a common microbially catalyzed pathway" by J. W. Moffett and J. Ho. *Geochimica et Cosmochimica Acta* **62**, 351-355 (1998).

324 Churchill, S. A., Walters, J. V., Member ASCE & Churchill, P. F. Sorption of heavy metals by prepared bacterial cell surfaces. *Journal of Environmental Engineering* **121**, 706-711 (1995).

325 Sathicq, M. B. & Gomez, N. Effects of hexavalent chromium on phytoplankton and bacterioplankton of the Rio de la Plata estuary: an ex-situ assay. *Environ Monit Assess* **190**, 229, doi:10.1007/s10661-018-6619-1 (2018).

326 Bruland, K. W. & Lohan, M. C. Controls of Trace Metals in Seawater. In *Treatise on Geochemistry: The Oceans and Marine Geochemistry* Vol. 6 (ed H. Elderfield) **6.02**. *23-47* (Elsevier Pergamon, 2004).

327 Sunda, W. & Huntsman, S. A. Interactions among Cu2+, Zn2+, and Mn2+ in controlling cellular Mn, Zn, and growth rate in the coastal alga *Chlamydomonas*. *Limnology and Oceanography* **43**, 1055-1064 (1998).

328 Bromfield, S. M. & David, D. J. Sorption and oxidation of manganous ions and reduction of manganese oxide by cell suspensions of a manganese oxidising bacterium. *Soil Biology and Biochemistry* **8**, 37-43 (1976).

329 Hays, G. C., Richardson, A. J. & Robinson, C. Climate change and marine plankton. *Trends Ecol Evol* **20**, 337-344, doi:10.1016/j.tree.2005.03.004 (2005).

330 López-Urrutia, Á., San Martin, E., Harris, R. P. & Irigoien, X. Scaling the metabolic balance of the oceans. *Proceedings of the National Academy of Sciences* **103**, 8739-8744 (2006).

331 Sunda, W. Iron and the carbon pump. *Science* **327**, 654-655 (2010).

332 Givan, A. L. Flow Cytometry: An Introduction. In *Flow Cytometry Protocols, Third Edition* (eds T. S. Hawley & R. G. Hawley) **1**. (Humana Press, 2011).

333 Duhamel, S., Zeman, F. & Moutin, T. A dual-labelling method for the simultaneous measurement of dissolved inorganic carbon and phosphate uptake by marine planktonic species. *Limnology and Oceanography: Methods* **4**, 416-425 (2006).

334 Smyth, T. *et al.* AMT25 (JR15001) Cruise Report. (Available online: http://www.amt-uk.org/Cruises/AMT25, 2015).

335 Smyth, T. *et al.* AMT24 Cruise Report. (Available online: http://www.amt-uk.org/Cruises/AMT24, 2014).

336 Thomaz, S. M. & Wetzel, R. G. [3H]Leucine incorporation methodology to estimate epiphytic bacterial biomass production. *Microbial Ecology* **29**, 63-70 (1995).